Novel Halide Containing Bioactive Glasses

By

Xiaojing Chen

A thesis submitted in fulfilment of the requirements for the degree of Doctor of Philosophy in Institute of Dentistry, Queen Mary University of London

Institute of Dentistry, Bart's and the London School of Medicine and Dentistry,

Queen Mary University of London

2015

DECLARATION

I, Xiaojing Chen, confirm that the research included within this thesis is my own work or that where it has been carried out in collaboration with, or supported by others, that this is duly acknowledged below and my contribution indicated. Previously published material is also acknowledged below.

I attest that I have exercised reasonable care to ensure that the work is original, and does not to the best of my knowledge break any UK law, infringe any third party's copyright or other Intellectual Property Right, or contain any confidential material.

I accept that the College has the right to use plagiarism detection software to check the electronic version of the thesis.

I confirm that this thesis has not been previously submitted for the award of a degree by this or any other university.

Signature:

Date: 16/06/2015

ABSTRACT

Bioactive glasses (BG) are widely used in dentistry and medicine due to the ability to form a hydroxyapatite layer to bond to bone. Fluoride has been introduced into BG to provide additional effects, such as inhibition at enamel and dentine demineralisation, reduction of glass melting temperature and facilitating an acid durable fluorapatite formation etc.. Therefore, fluoride containing BG are attractive for remineralising toothpaste application. However, excessive fluoride is problematic.

Chlorine is thought to behave like fluorine in terms of glass structure and properties. As the chloride ion is larger than fluoride ion, the incorporation of chloride could expand the glass volume that might result in a more open structure and a more degradable glass. These glasses are of interest for resorbable bone grafts and remineralising toothpastes. In this thesis, the investigation of chloride as an alternative to fluoride in the silicate BG was carried out for the first time.

Sodium free BG based on SiO_2-P_2O_5-CaO-CaF_2/$CaCl_2$ or SiO_2-CaO-CaF_2/$CaCl_2$ with varying calcium halide content were synthesised via a melt-derived route and characterised by various advanced techniques. The glass bioactivity was estimated in Tris and SBF. Ion release measurements were carried out by using ICP-OES and ion selective electrodes. The apatite formation was characterised by FTIR, XRD and MAS-NMR. The crystallisation events of the glasses were explored by heat treatment.

This study reveals that the majority of chloride is successfully retained in the Q^2 type silicate BG. Glass transition temperature and density decrease with increasing halide content. The studied high phosphate containing BG are highly dissolvable and formed apatite-like phases within 3h in Tris. The glass dissolution rate was found to increase with $CaCl_2$ content but not with CaF_2. On heat treatment, fluorapatite or chlorapatite is the main crystalline phase in phosphate containing glasses, while CaF_2/$CaCl_2$ is likely the one for the glasses without phosphate. This is the first time to our knowledge that chlorapatite has been shown to crystallise from a glass.

ACKNOWLEDGEMENTS

I would like to first thank my supervisors Prof. Robert Hill and Dr. Natalia Karpukhina for their first rate supervision and inspiration, without their selfless advices, guidance and constant feedbacks and discussions, this PhD would not be achieved. Without their tremendous help and encouragement, four papers would not be published and different grants and prizes would not be awarded. I am particularly grateful to Prof. Robert Hill for supporting and covering my attendances to different conferences. An especially thankful is expressed to Dr Natalia Karpukhina for her massive supports and advices besides the research.

I would like to acknowledge Prof. Dr. Delia Brauer for offering me the opportunity to carry out a short-term research project at Otto Schott Institute, University of Jena, helping me with a DAAD grant application and sharing her knowledge of bioactive glasses and glass-ceramics. I am also grateful to Prof. Dr. Delia Brauer for spending a lot time on showing me around in Jena. It is a valuable experience.

I am very grateful to my sister Dr. Xiaohui Chen for first bringing me into the academic career, for selfless supports and many motivating discussions on my PhD project, for giving me so many happiness and beautiful memories all the time.

I am very thankful to Dr Rory Wilson for collecting all the X-ray diffraction data, Dr Harold Toms, NMR facility manager at QMUL for setting up the NMR experiments and sharing his knowledge and expertise of NMR and Dr Laura Shobolt and Mr Simon Dobinson for running samples with ICP-OES. I am also grateful to the staffs and colleagues in the Dental Physical Sciences Unit for cultivating a friendly research environment and offering all the help.

Queen Mary University of London and China Scholarship Council are thanked for awarding me the Joint PhD Scholarship. British Federation of Women Graduates is

appreciated for awarding me the Margaret KB Day Scholarship. Barts and The London School of Medicine and Dentistry QMUL, Queen Mary University of London, Society of Chemistry Industry and Armourers and Brasiers' Gauntlet Trust are acknowledged for sponsoring travel grants to me to attend different conferences.

Last but not least, I would like to thank my parents for their loves and unconditional support, my nephew Aaron Cao for all the happiness that he brings to me and my fiancé Yun Zhou for his love, encouragement and endless care, which all make me motivated, confident and strong.

TABLE OF CONTENTS

LIST OF FIGURES

1 Introduction

Bioactive glass can degrade in a physiological environment and form a hydroxycarbonate apatite (HCA, $Ca_{10}(PO_4)_6CO_3$)) layer, which can bond to bone and induce bone regeneration [1-3]. This type of material is extensively used for dental and medical applications. Incorporation of various elements can alter glass properties, for example, sodium is able to reduce the glass melting temperature, glass transition temperature and therefore probably glass hardness.

Addition of fluoride (CaF_2) to a silicate glass also reduces the melting temperature and glass transition temperature, probably glass hardness. The fluoride containing bioactive glasses investigated recently [4, 5] favour formation of fluoride substituted apatite (FAP, $Ca_{10}(PO_4)_6F_2$) which has a better capacity for acid resistance and is less soluble in acidic conditions than HCA and is, furthermore, easier to form at a neutral or acidic pH. Thus, fluoride containing bioactive glasses are particularly attractive for remineralising toothpaste applications.

In theory, the more fluoride is present in the glass the softer the glass is [6, 7]. However, an excess of fluoride in the bioactive glass will result in the formation of crystalline calcium fluoride (*fluorite*) instead of FAP. Additionally, there is a restriction on the fluoride content for over the counter toothpastes and the regulatory authorities set a restriction on the fluoride content in toothpaste at 1500 ppm in Europe, since the extra fluoride may lead to dental fluorosis and uncontrolled fluorite formation rather than FAP. Therefore the perception of “the more the better” is not suitable for fluoride. It is of critical importance to find the optimal concentration of fluoride addition to a bioactive glass composition – or to look for an alternative to fluoride.

Chlorine is assumed to have similar effects on the property and structure of bioactive glasses as fluorine, such as reducing the melting and glass transition temperatures. It is also proposed that the structural role of fluoride and chloride in glasses are similar,

and that both associate in the glass structure with cations, e.g. forming F-Ca(n) and Cl-Ca(n). Owing to the presence of halide ions (F^-, Cl^-) and phosphate in the glass, the oxyhalide bioactive glasses can form apatite either upon crystallisation (during heat treatment of the glasses) or as a result of reaction with body fluids (*e.g*. saliva or blood plasma).

Similar to fluoride containing bioactive glasses, which crystallise to fluorapatite, chloride containing glasses are likely to produce a chlorapatite (ClAP, $Ca_{10}(PO_4)_6Cl_2$) glass-ceramic upon crystallisation; this is of great interest for biomedical application and a number of other applications. In addition, since the chloride ion is larger than the hydroxyl and fluoride ions, chlorapatite is less stable and should be more resorbable than fluorapatite or hydroxyapatite (HAP, $Ca_{10}(PO_4)_6(OH)_2$). In solution, ClAP converts to hydroxyapatite [8]. Moreover, chloride is naturally present in the human body; there is no restriction on chloride content in toothpastes and biomedical materials unlike with fluoride.

Because of the larger size of the chloride ion compared to the oxygen ion, the introduction of chloride would be expected to expand the glass volume leading to a more expanded open glass structure. The chloride containing bioactive glasses are therefore likely to be softer, less abrasive, degrade faster and form apatite more rapidly. Chloride or mixed fluoride and chloride containing bioactive glasses will be innovative and promising for medical and dental applications, especially for remineralising toothpaste and cutting dental cavities or polishing using air abrasion [6].

Novel sodium-free oxyhalide silicate bioactive glasses could eliminate the potential disadvantages causing by the presence of sodium, such as, glass phase hygroscopicity resulting in an uncontrollable degradation and high initial pH surge, which is undesirable for homeostasis. Surprisingly, a fluoride containing bioactive glass without sodium also presents high bioactivity, even forming fluorapatite within 6 hours in Tris buffer solution [9].

Owing to the high volatilisation of chloride (normally as sodium chloride) during glass melting, chloride has been used as a refining additive used to remove bubbles from silicate glass melts. The difficulty of retaining chloride in glasses has resulted in a very limited literature available on chloride containing glasses, and no reports exist on chloride containing bioactive glasses. To our knowledge, the novel chloride containing bioactive glasses that are prepared and studied in this PhD thesis represent the first set of chloride containing bioactive glasses ever studied. Moreover, the chlorapatite glass-ceramics that are achieved upon heat treatment are the first ever made bioactive chlorapatite glass-ceramics.

2 Literature Review

2.1 Bioactive Glass

Bioactive glasses are well known for their bone regenerative properties [10, 11]. When immersed in physiological solutions, they can form an integrated bond with living bone via formation of an apatite layer on their surface. Recently, they have also drawn great attention for the application in soft tissue repair, due to their ability of promoting angiogenesis (formation of blood vessels) [12-14]. The bioactive glass (Bioglass® 45S5 composition) was first developed by Larry Hench in late 1960's for bone repairs. Since then, many new bioactive glass compositions have been developed. Strontium [15, 16], zinc [17, 18], cobalt [19], fluoride [20, 21] or magnesium [22] were incorporated into bioactive glass to combine therapeutic ion release and apatite formation with tailored glass properties for different applications.

2.1.1 The First Bioactive Glass, Bioglass® 45S5

The first bioactive glass, Bioglass® 45S5 was developed in response to the requirement to inhibit interfacial mobility in implanted bio-inert materials and form a bond between living tissue and the implant surface [23]. Bioglass® demonstrates a relatively high bioactivity and has a capacity to bond to living tissues. It is the most extensively investigated bioactive glass, which is composed of 46.1 mol% SiO_2, 26.9 mol% CaO, 24.4 mol% Na_2O, 2.6 mol% P_2O_5. It has been in clinical use since 1985 [1] and is currently used in a range of applications including orthopaedic (e.g. NovaBone®), periodontal (PerioGlas®) and toothpastes (NovaMin®). In addition, a small concentration of 45S5 bioactive glass is able to stimulate angiogenesis [12, 14].

The bioactivity for 45S5 bioactive glasses had been investigated in buffer solutions. Research has shown that 45S5 could form hydroxyapatite after immersing in Tris

buffer for 24 hours, while it took 3 days in Simulated Body Fluid (SBF) [12, 24]. Therefore, 45S5 presents favourable healing ability in many clinical programs. However, this glass exhibits some defects, the uncontrollably high dissolution rate is one of the primary problems [25], which is mainly caused by its high content of alkali (Na_2O). Although, the presence of high alkali content is beneficial in reducing the melting temperature, the high dissolution rate may lead to an imbalance of natural bone remodelling and a gap between living tissue and the implanted materials [26]. The polymer composites incorporated with high alkali containing glass 45S5 are apt to uptake water by osmosis, leading to the swelling and cracking of the composites, hereby, accelerating the degradation of the materials [25]. Moreover, the relatively high hardness is the other shortcoming. The bioactive glass 45S5 is currently used in commercial toothpaste (as Novamin™) for reminalisation of teeth. It has a hardness of 4.68 GPa, while enamel is about 3.50 GPa [27], consequentially, the enamel undergoes the potential risk of being worn away. Thus, the design of new bioactive glasses based on 45S5 in order to modify and avoid the deficiencies of 45S5 is highly desirable.

2.2 General Glass Concept

2.2.1 Definition of Glass

Glass is well accepted as an optically transparent, brittle and chemically inert non-crystalline solid material. It has been widely used for windows, drinking vessels and containers that can even store corrosive liquids for centuries. Bioactive glass does not fulfil completely this definition of glass as bioactive glass is not an inert material. However, various other glass definitions were proposed by scientists. The American Society for Testing Materials proposed that glasses are “inorganic products of fusion that have been cooled to a rigid condition without crystallising” [28]. McMillan [29] suggested that a glass is a transparent or translucent material with features of rigidity, brittleness and hardness. According to Doremus [30], glass is an amorphous solid

without long-range order; however, it exhibits a region of glass transition. This latter definition is perhaps the most general as it outlines the two special characteristics of glass, bioactive glass as well, the lack of a periodic arrangement in the glass network and a time-dependent glass transformation behaviour [31]. All the definitions above describe glass from different aspects, covering glass processing, physical and chemical properties. Indeed, any amorphous materials with a glass transition temperature independent of synthesis route can be defined as a glass. Glass differs from the crystalline solids in many aspects. For example, a single-phase crystalline solid melts at a well-defined melting temperature and converts into liquid, while the glass solid “ease” into a viscous liquid rather than melt at a well-defined temperature. In addition, when cooling down the melt from a high temperature, crystalline solids demonstrate an abrupt volume change at the solidification temperature. Conversely, glass changes from a liquid to a supercooled liquid and a continuous volume change is present during the whole process, which was described as the liquid-like nature of glass according to McMillan [32]. Moreover, crystalline solids show a fixed structure with long-range order while the atoms in the glass are in a random arrangement without the structural periodicity and a fixed long-range order. In general, glass looks like a liquid, however, behaves like a solid.

Glass and crystalline materials have different structures therefore different chemical and mechanical properties are presented. Their structural difference could be distinguished using a variety of techniques, such as X-Ray Diffraction (XRD), Raman Spectroscopy, Fourier Transform Infrared Spectroscopy (FTIR) and Solid State Magic Angle Spinning Nuclear Magnetic Resonance (MAS-NMR).

2.2.2 Glass Transition

Glass can be synthesised by the quenching of molten liquid. Rapid cooling is generally used to prevent crystallisation, as rapid cooling limits the available time for atomic

rearrangement to occur and the development of the long-range order associated with the crystal.

As illustrated in the volume-temperature curve in Figure 2.2.1, when slowly cooling a molten liquid from high temperature, the melt will yield a drastic volume change at the solidification temperature and lead to the formation of crystalline phases. This could easily happen when the molten glass has a similar stoichiometry to a crystalline material. Turnbull [33] advocated that crystallisation could be avoided if the cooling is sufficiently fast. During rapid cooling, glass has a continuous decrease in volume with an increase in viscosity. At a relatively lower temperature, the glass viscosity drops to 10^{12} Pa.s, where the melt starts to behave as a rigid glass, in addition, the slope of the volume-temperature curve changed similarly to the crystalline solid [34-36]. This temperature is defined as glass transition temperature (T_g). However, it is different from the melting temperature, the glass transition temperature is not a fixed temperature, it is cooling rate dependent and thus covers a wide range of temperatures [37]. Basically, the glass is an elastic solid below glass transition temperature and a viscous liquid above the temperature [38]. A fast cooling rate results in the T_g shifting to a higher temperature and the glass has a larger volume, higher conductivity and lower viscosity [39]. In contrast, a slow cooling rate leads to a lower T_g and volume but higher viscosity. The glass transition temperature is normally characterised by different techniques including Differential Scanning Calorimetry (DSC) and Dilatometry.

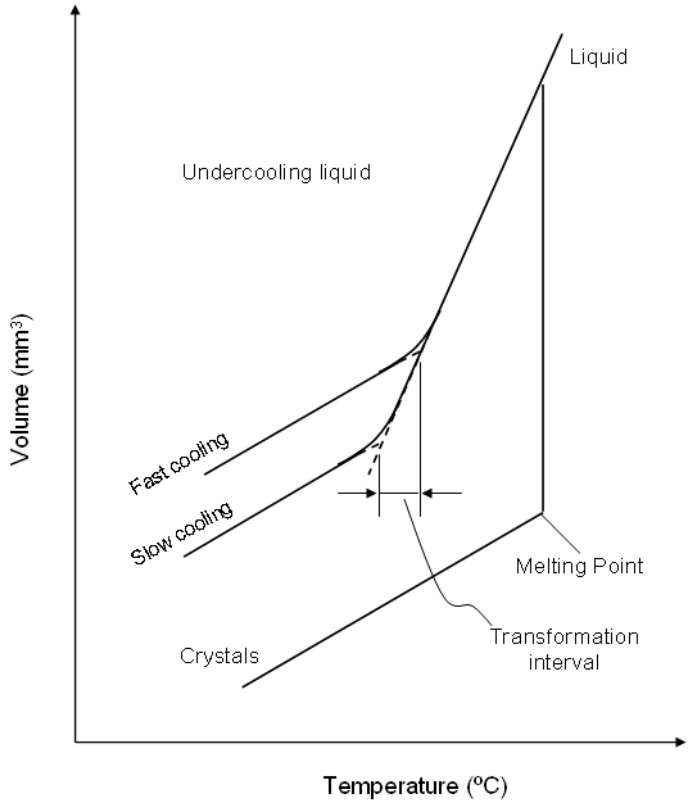

Figure 2.2.1 Glass transition temperature (T_g) and its relationship with cooling rate adapted from Jones [40].

The glass transition temperature is an important parameter for investigating glass properties. Relationships between the glass composition, glass transition temperature, glass structure and glass properties have been extensively studied. According to O'Donnell [41], "the glass transition temperature can be calculated from molar compositions of bioactive glasses up to seven components". However, determining T_g regardless of glass structure makes his approach oversimplified and not suitable for multi-component bioactive glass systems beyond certain compositional restrictions, such as those containing MgO and CaF_2 [42]. Thus, when predicting T_g, both glass composition and structure should be taken into consideration.

2.2.3 Glass Structure Theory

The random network theory proposed by Zachariasen is the foundation of the most commonly used models for glass structure [31]. Zachariasen provided an approach

which describes a structural model for glass based on a three dimensional structure. In order for a glass to form, long range order should be broken down that leads to a network distortion.

Warren and co-workers advocated a model based on spectroscopy to justify the trends observed in the properties of glass with simple binary compositions. This model can effectively be used to investigate the local structure and even somewhat for intermediate range of order, but is not suitable for the properties other than those controlled by structure at the short to intermediate range atomistic order. Thus, the comprehensive understanding of the structural model for glass is of particular importance before we accept the model.

Shelby [31] has proposed that 'no model can be considered to be valid unless that model can explain all of the available data' as known 'the Fundamental Law of Structural Models' to evaluate any proposed model.

2.2.4 Glass Forming Unit in Silicate Glass

The understanding of the glass structure is extremely vital to the design of glass compositions and the tailoring them to specific applications. A glass is a network of atoms (silicon, phosphorus, boron etc.) bonded to each other through covalent bonds with oxygen atoms. The basic and most well-known glass structure is a continuous, three dimensional network based on a SiO_4 tetrahedron. The silicon atom sits in the centre of the tetrahedron; four oxygens occupy the four corners as shown in Figure 2.2.2. In a silicate glass, each oxygen atom is shared between two silicons or one silicon and another non-silicon species. When directly connecting to two silicons, the oxygen is defined as a bridging oxygen (*BO*), while sharing with one silicon and the other species, the oxygen is named a non-bridging oxygen (*NBO*). Bridging oxygens are indispensable to the framework of a glass network, as the silicon atoms are connected by them to form the glass network. In contrast, non-bridging oxygens interact with network modifier cations to form ionic bonds, which are much weaker

than Si-O bonds. Therefore, the formation of NBOs effectively breaks up the glass network structure and results in a more disrupted glass network.

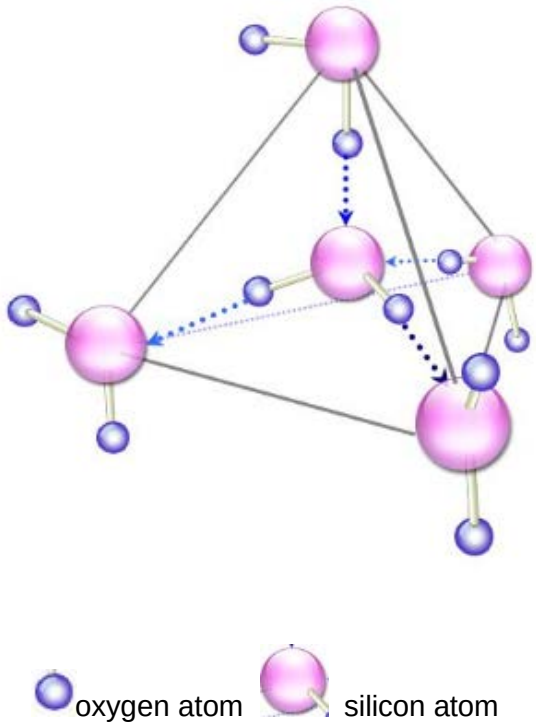

Figure 2.2.2 Diagram presenting the tetrahedral structure unit of silica

2.2.5 Typical Components of the Silicate Bioactive Glasses

In terms of how oxides affect glass formation and glass structure, the oxides are divided into three groups based on the electro negativity and their ability to form a glass [31].

2.2.5.1 Network formers

Cations such as silicon, phosphorus, boron and germanium which form bonds with oxygen with a fractional ionic character near covalent (> 50%) work as network formers. Network formers can form a cross-link network of the chemical bonds. In other words, they can form triangles or tetrahedra connected via bridging oxygens

(BO). These oxides have an ability to form glass on their own if rapidly cooled from the melt.

2.2.5.2 Intermediates

Intermediates have slightly lower electro negativities. This includes elements like titanium, aluminium, zirconium, beryllium, magnesium, and zinc. They are not capable of forming a glass network by themselves. However, they can either enhance the network or weaken the network depending on the glass composition.

2.2.5.3 Network modifiers

Cations with low electronegativities are termed as network modifiers. These cations can not build up a network. Instead, they are able to form highly ionic-bonds, modify the network structure, the cations adjacent to non-bridging oxygen result in breaking Si-O covalent bond. Thus, they modify or disrupt the main network. Examples of such cations include sodium, calcium, potassium, and lithium. However, the monovalent cations (Na^{+}) show more efficient network disruption compared with the divalent cations (Ca^{2+}). This can be explained by an additional ionic bond forming between two non-bridging oxygens and the M^{2+} cation. The schematic is presented in Figure 2.2.3.

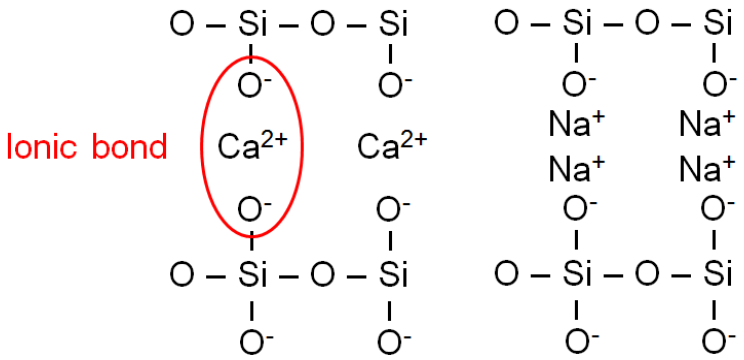

Figure 2.2.3 Network modifiers in the glass structure

2.3 Bioactive Glass Structure and Bioactivity

2.3.1 Q^n notation and Network Connectivity (NC)

A common nomenclature system known as "Q^n" structures can be used to present the proportion of bridging oxygens per tetrahedron by different n values. The value of n is equal to the number of bridging oxygens per tetrahedron unit. Moreover, Q^n is associated with the values of network connectivity. "The average number of bridging oxygen per network forming element" was defined as network connectivity (*NC*) [43]. It is a very important parameter for the understanding of bioactive glass structure. Glasses of low network connectivity are expected to have a highly disrupted glass network.

A pure silica glass with the BO average number of 4 would correspond to a NC of 4 and the Q structure would correspond to Q^4, while an isolated tetrahedron with no BO is described as Q^0 unit, as orthosilicate species. A glass represented as a linear Si-O-Si chain would have an average number of 2 BOs per tetrahedron which corresponds to a NC of 2 and Q structure equal to Q^2.

The NC can be used to predict the bioactivity of glasses and glass properties [44]. However, the prediction ability is reduced for more complicated glass compositions [43]. This is because NC is used to measure the average number of bridging oxygen per each silica tetrahedron, so we are assuming that the glass has homogenous structure. In general, the network connectivity of glasses could be calculated using [43, 45]:

$$NC = 2 + \frac{BO - NBO}{G} \tag{2.3.1}$$

Where "*BO*" is the total fractional number of bridging oxygens per network forming ion, "*NBO*" is the total fractional number of the non-bridging oxygen per network modifier ion and "*G*" is the total fractional number of glass forming units.

It is important to know the structural role of the glass component in order to used NC concept for the prediction of glass bioactivity. In this thesis, phosphate is assumed to be present as orthophosphate units (PO_4^{3-}) which require modifier ions (Ca^{2+} and Na^+) to charge balance itself instead of forming a part of the network. Thus, the equation for NC calculation can be written as following [44],

$$NC = \frac{4[SiO_2] - 2[M_2^I O + M^{II} O] + 6[P_2O_5]}{[SiO_2]} \quad (2.3.2)$$

Where $M_2^I O$ (Na^+, K^+) and $M^{II} O$ (Ca^{2+}) are network modifiers.

In the case of the GPF, GPCl and GPFCl glass series:

$$NC = \frac{4[SiO_2] - 2[CaO] + 6[P_2O_5]}{[SiO_2]} = 2.08. \quad (2.3.3)$$

In the case of the GF and GCl glass series:

$$NC = \frac{4[SiO_2] - 2[CaO]}{[SiO_2]} = 2.0 \quad (2.3.4)$$

2.3.2 Definition of Bioactivity

A bioactive material is a material that produces a bone-like apatite layer on its surface in the living body [46]. When such a material is immersed in physiological solution, it degrades and forms an apatite-like phase, which can act as an intimate bond between the material and living bone. This ability of degradation and forming apatite-like phase is often defined as bioactivity.

In general, the bioactivity of a glass depends on the rate of glass degradation and apatite formation in a biological medium. Fast degradation and rapid apatite formation corresponds to a high bioactivity.

Strnad [47] predicted glass bioactivity using Stevel's parameter (Y), where Y represents the mean number of bridging oxygen ions per polyhedron in the glass structure. According to the model, glasses show bioactivity when Y is less than 3 and are relatively bio-inert when Y exceeds 3. An optimum bioactivity is obtained when Y is equal to 2. However, this model failed to explain the hydrolysable phosphorus-oxygen bonds [48] and also neglects the structural role of phosphate in the glass network [49]. Hill and Brauer [44] used network connectivity which is considered as a useful tool to predict glass bioactivity and degradability. Nevertheless, for glasses with more than four components, the prediction is not as accurate as for simple glass compositions [43]. O'Donnell *et al*. focused on the positive influence of phosphorus content on the bioactivity of bioactive glasses that a higher P_2O_5 content in the glasses leads to a faster apatite formation [50]. Edén put forward the split network model to evaluate the bioactivity assuming the phosphorus in the glass remains predominantly as Q^0 orthophosphate tetrahedra and the average silicate network-polymerisation is 'favorable' [49]; However, Edén did not define "favourable" when the NC beyond the value of 2.6, while Hill defined it as a network connectivity close to 2.0 but less than 2.4.

Hill describes the relationship between bioactivity and the glass network connectivity, as shown in Figure 2.3.1. The theoretical relationship was illustrated by the sharp cut off profile, as given in the figure.

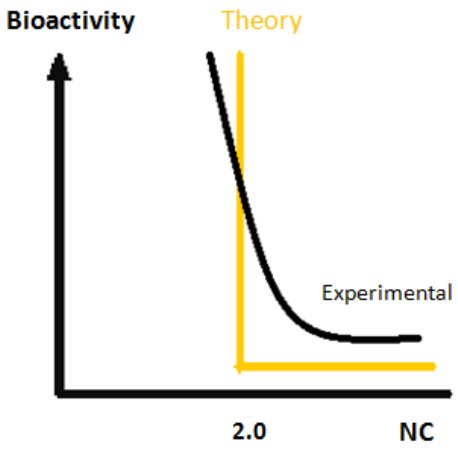

Figure 2.3.1 The relationship between Bioactivity and Network connectivity adapted from Hill [51].

What causes the dramatic change of the bioactivity around NC of 2.0? This could be associated with the change of the glass structure. A NC around 2.0 corresponds to a structure comprised mainly of Q^2 linear silicate chains which is easily degradable by dissolving in buffer solution without breaking Si-O-Si bonds [42]. Thus, a Q^2 glass structure has a favourable bioactivity. As the NC goes above 2.0, the glass structure gradually changes to a cross-linked three-dimensional network. Compared to a highly disrupted linear chain, a three-dimensional glass network is more resistant to dissolution, and therefore, results in fewer available ions in solution such as Ca^{2+}, PO_4^{3-} which are essential, for the apatite formation on the glass surface and, hence, a much slower apatite formation, which is known as low bioactivity. Thus, the low network connectivity (around 2) and highly disrupted silicate structures are favourable to obtain high bioactivity [22].

The sharp cut off profile in the figure infers that bioactivity only occurs when NC is equal to 2 or less, where the glass is represented as a Q^2 linear chain. However, in practice, instead of the sharp cut off at 2, a curved relationship between bioactivity and NC is found. Glasses with a NC between 1.9 and 2.0 demonstrate favourable bioactivity, while the bioactivity decreases dramatically with increased NC (above 2).

When network connectivity is higher than about 2.4, glasses show very low bioactivity or no bioactivity [51]. This practical curved relationship might be caused by the presence of Q^2 ring structures in the glass. For example, a combeite-type structure (Na_2O-2CaO-3SiO_2) which is a six-membered Q^2 ring structure might exist in 45S5 based glasses with a network connectivity of 2.14. The Q^2 ring has a lower molar mass compared to a linear silicate chain, which may result in a more rapid degradation and a higher bioactivity.

2.3.3 The Mechanism of Glass Degradation

The most widely accepted glass degradation mechanism for bioactive glass was proposed by Larry Hench [52]. It is divided into 5 steps, as shown in the following schematic diagram:

1. $Si\text{-}O^-Na^+ + H^+ + OH^- \rightarrow Si\text{-}OH + Na^+ + OH^-$
2. $Si\text{-}O\text{-}Si + H_2O \rightarrow Si\text{-}OH + OH\text{-}Si$
3. $2(Si\text{-}OH) \rightarrow Si\text{-}O\text{-}Si$ (forming rich SiO_2 layer) at the same time, phosphate released from glass into solution
4. $Ca^{2+} + PO_4^{3-}$ (from solution) $\rightarrow$ $CaO\text{-}P_2O_5$ (amorphous rich film)
5. $CaO\text{-}P_2O_5 + OH^- \rightarrow Ca_5(PO_4)_3OH$ (Crystallisation)

Firstly, sodium ion from the glass exchanges with hydrated protons from solution, the residual hydroxyl ions result in an increase in the pH value. Secondly, the Si-O-Si bridge breaks down as a result of alkaline hydrolysis with formation of the Si-OH silanol group, which leads to a breakdown of the glass network. Thirdly, a SiO_2 rich layer (silica-gel) forms as a consequence of silanol condensation, at the same time, phosphate ions release from the glass to the solution. Fourthly, an amorphous calcium phosphate layer precipitates on the silica-gel. Finally, mineralisation occurs when the amorphous calcium phosphate layer gradually transforms into crystalline hydroxyapatite by combining with OH^- [43].

However, this proposed mechanism does not predict the reactivity of bioactive glasses as a function of glass compositions. In addition, in the ion exchange step, the contribution of other network modifiers, such as calcium ions is ignored. A recent work carried out by Bingel *et al.* queries the second step of the mechanism. They found that it might be not necessary to break down Si-O-Si bond by alkaline hydrolysis, since after 3 days immersion no apatite-like phase formed in alkaline buffer solution at pH 9 but a faster apatite formation was detected after 3 hours immersion at pH 5.0 [53].

2.3.4 Evaluation of Bioactivity

Bioactive materials are perfect candidates for bone regeneration, bone substitutions and dental applications, depending on their bioactivity. The ability to design novel biomaterials with controllable and satisfactory bioactivity is of significance. Researchers are interested in the bioactivity of the glasses and use different approaches to study it.

Mneimne and Brauer used Tris buffer solution to investigate the bioactivity of fluoride containing bioactive glasses [9]. Kokubo and Takadama predicted and estimated the in vivo bioactivity of materials in SBF [54]. They suggested that the examination of apatite layer formation on a material in SBF is useful for predicting the bioactivity in vivo. The formation of bone-like apatite on the artificial material surface when implanted in a living body is the indispensable requirement for a material to bond to living bone and tissue. From the experimental results they found that in vivo bioactivity of the material can be reproduced in a simulated body fluid. While Bohner and co-workers argued that even though many research publications test the bioactivity in SBF, there are still not enough scientific data to support this method [55]. Bohner pointed out that although SBF is chemically similar to human blood plasma, they are not the same. There are three big differences between the SBF composition and human blood plasma including the absence of proteins in SBF that are present in blood serum, the addition of Tris to SBF and the fixed CO_2 partial pressure in serum at

0.05 atm. In addition, SBF is saturated with Ca^{2+}, PO_4^{3-} and other ions that could readily deposit in the presence of limited nucleation sites [56].Thus, the accuracy of predicting in vivo bioactivity by testing in SBF needs to be further assessed and improved [55].

It is not easy to perform the bioactivity test using SBF. First of all, SBF contains Mg^{2+}, which is suggested to give a reduction in the apatite formation [57]. Secondly, SBF is a supersaturated solution and it is not stable, when the temperature or pH change, it will be prone to precipitate apatite or $CaCO_3$, which will interfere with the study of the apatite precipitation from the actual tested sample. Therefore, it is vital to keep the conditions constant throughout the study. The bioactivity test in SBF is used systematically in this thesis and the SBF results can be used as a reference for comparison with other materials or glass series which were previously tested and published.

Tris buffer solution was used in the earliest studies on ioglass 45S5 [58]. Cerruti *et al* [56] used Tris buffer solution to analyse the dissolution and reprecipitation processes involving Bioglass® alone. The bioactivity for the glasses with high phosphate content can be investigated in Tris buffer. Tris buffer with a pH value at 7.4 is considered more stable than SBF. The ions available for the apatite precipitation were conferred solely from the degradation of glass or tested sample, and therefore could provide a clearer picture on the apatite forming ability of the tested material with minimum external influence. Moreover, Tris buffer is common and used for kinetic ion release studies, as there are no interfering ions in solution.

In this PhD project, bioactivity was quantified in terms of time to form apatite in both SBF (pH=7.4@37˚C) (corrected SBF published by Kokubo *et al.* [59], in Table 2.3.1) and Tris buffer solution.

Table 2.3.1 Ion concentrations of SBF and human blood plasma

	Ion concentration (mmol/dm^3)							
	Na^+	K^+	Mg^{2+}	Ca^{2+}	Cl^-	HCO_3^{2-}	HPO_4^{2-}	SO_4^{2-}
Human blood plasma	142.0	5.0	1.5	2.5	103.0	27.0	1.0	0.5
Corrected SBF(c-SBF)	142.0	5.0	1.5	2.5	147.8	4.2	1.0	0.5

2.3.5 Role of Glass Design and Glass Components on Bioactivity

Bioactivity is an extremely significant property which needs to be taken into consideration for biomedical and dental applications. Higher bioactivity is favoured and needed. To obtain an enhanced bioactivity, low network connectivity (around 2) and a highly disrupted silicate structure are favourable [22]. Researchers are continually exploring methods from different aspects to enhance the glass bioactivity.

2.3.5.1 Glass design

Bioactive glasses with network connectivity between 1.9 and 2.0 show a favourable bioactivity [60]. These glasses demonstrate a chain-like structure and degrade easily. Thus, network connectivity around 2.0 can be considered as a guideline for designing a glass with high bioactivity.

2.3.5.2 Role of SiO_2

The compositional dependence of the glass bioactivity has been investigated by many research groups. Some researches show that the glass bioactivity decreases with an increase in SiO_2 content. This is explained since as glasses are more cross-linked, the glass degradation retards and release of the modifier ions to the solution reduces, thus silica-gel layer formation is inhibited and fewer sites are provided for apatite deposition [23, 47, 61]. Hench [52] found that the bioactive glass SiO_2-CaO-Na_2O-P_2O_5 series containing 40-52% SiO_2 content can form a bond to hard and soft tissues within 5 to

10 days. However with a higher silica content (55-60%), the bioactive glasses require a longer time to bond to hard tissue, but fail to attach to soft tissue. When the SiO_2 content is more than 60%, the glass lose the ability to bond to living tissues [62]. Thus, the amount of SiO_2 should be taken into account when designing new bioactive glasses.

2.3.5.3 Role of CaO and Na_2O

Hench [52] considered that the presence of network modifier (CaO and Na_2O etc.) is indispensable for apatite formation. However, some researchers suggest that the network modifier (Na_2O) is not essential. Goel, Kapoor *et al*. [25] designed a series of alkali-free bioactive glasses and some of the glasses (TCP-20) formed hydroxyapatite on their surface within 1–12 h of immersion in SBF. In addition, recent studies showed that the degradation of SiO_2-P_2O_5-CaO-Na_2O based glass increased the pH value of the buffer to 7.9 [9]. The increased pH is caused by ion exchange between H^+ and cations of the network modifiers. To some extent, the high pH (7.9) is a potential risk for the oral mucosa and living tissues if this type glasses were added into toothpaste or used as implant materials. Thus, the novel alkali-free glasses that do not generate high alkaline pHs were designed in this PhD project.

2.3.5.4 Role of P_2O_5

The role of phosphate in the glass structure has been studied in the literature. However, it is still under dispute. Historically, it was believed that phosphorus enters the silicate glass network and forms Si-O-P bonds [63, 64]. However, some researches showed that phosphorus exists as an orthophosphate species, rather than entering the silicate glass network by forming Si-O-P bonds [10, 65, 66]. According to Elgayar [66], the ^{31}P NMR spectra for all the investigated glasses based on SiO_2-P_2O_5-CaO-Na_2O system have a single resonance with the chemical shift in the range 2.9-9.5 ppm, which is the evidence of a mixture of Ca-Na orthophosphate.

O'Donnell and Hill designed two series silicate glasses with varying phosphate content (0-9.25 mol%) to study the role of phosphorus by using both ^{31}P and ^{29}Si MAS-NMR [65]. In series I, phosphate replaced SiO_2 and kept the Na_2O:CaO ratio constant, since phosphate was assumed as network former. In series II, phosphate was considered to form an orthophosphate phase instead of entering the silicate network as a network former. Sufficient CaO and Na_2O were added to charge balancing the orthophosphate. With an increase in phosphorus content, the network connectivity of the glasses in series I increased, while the ones in series II did not show any change. The ^{31}P MAS-NMR spectra of series I and series II showed broad resonances around 9 ppm and 10.5 ppm respectively, corresponding to the orthophosphate in an amorphous environment and indicating that there is no preferential association to one of the cations with the orthophosphate [65]. This agrees with the finding by Brauer *et al*. [4] but differs from the conclusions drawn by Lusvardi *et al.* who suggested an ultimate preference of the phosphate units for calcium cations [21].

Edén [49] summarised that 'that as long as the phosphorus remains predominantly as orthophosphate and the network connectivity is less than 2.6, bioactivity can be enhanced monotonically for increasing phosphorus content of the bioactive glass'. According to Tilocca and Cormack [67], for the glasses with P_2O_5 lower than 10 mol%, a higher amount of P_2O_5 results in a higher bioactivity, while a further increase in P_2O_5 content (> 10 mol%) affects the glass bioactivity in a negative way [25].

O'Donnell *et al.* studied the effect of phosphate content on the bioactivity of soda-lime-phosphosilicate glasses, two series of glasses discussed earlier were investigated in SBF [50]. From the FTIR spectra and XRD patterns, the high phosphate containing glasses (> 3.0 mol%) in both series exhibited crystalline apatite by 16 hours immersion in SBF, compared with 2 days for the equivalent low phosphate containing glasses (< 3.0 mol%). This therefore suggests that the enhanced bioactivity can be achieved by increasing phosphate content, whilst the phosphate content has more significant

impact than network connectivity on bioactivity [50, 65]. Moreover, O'Donnell *et al.* compared the bioactivity of glass ICSW9 (Mol%: 38.14 SiO_2, 29.62 Na_2O, 25.91 CaO, 6.33 P_2O_5) against 45S5 bioglass (2.6 mol% P_2O_5) from their FTIR spectra, clear apatite peaks were found after 1 day immersion in SBF for glass ICSW9, while the equivalent peaks for 45S5 were much weaker [50]. Furthermore, it was shown by Mneimne *et al.* that an increase in phosphate content in the fluoride containing bioactive glass favours apatite formation rather than fluorite [9]. Thereby, the high phosphate content leads to a superior bioactivity.

However, the formation of HCA in SBF (20 days) from the phosphate free, CaO-SiO_2 glasses and wollastonite ($CaSiO_3$) ceramics suggests that phosphate is not an essential component for achieving bioactivity [68, 69].

In order to have a better understanding of the role of phosphorus in glass structure and on glass properties, calcium halide containing glasses with high phosphate and no phosphate were synthesised and characterised in this work.

2.3.5.5 Role of CaF_2

Biological Role of CaF_2

Fluoride is a natural ion which is found in many food products and drinking water. It is a significant micronutrient that exists in the mineralised tissues such as bone and teeth [70]. To a great extent, fluoride can benefit dental health by “strengthening” the tooth enamel, suppressing enamel and dentine demineralisation, enhancing enamel remineralisation and inhibiting the bacterial enzymes, it therefore makes tooth enamel more resistant to tooth decay [4]. Additionally, fluoride is introduced into the mineral component of bone during bone formation [71]. Grynpas and Rey [72] found that fluoride affects bone crystals, increasing the stability of the apatite lattice and reducing the solubility of the apatite crystals. This can be explained by forming a fluoride substituted apatite which has a smaller crystal volume compared with HAP and

increasing the crystallinity [73]. Fluoride has also been used for the treatment of osteoporosis. However, excess fluoride results in an anomalous enamel formation by retarding tissue maturation, dental fluorosis and an abnormal bone mineralization [74, 75]. Due to the dual effect of the fluoride, a balance in between maximizing the benefits and minimizing the risks of excess fluoride is very important.

Structural Role of CaF_2

Fluoride containing ionomer glasses have been used in dentistry and for biomedical applications and many studies about the structure of CaF_2 containing glasses have been performed, the structural role of fluorine is still not clearly defined [76, 77]. Whether F^- principally forms Si-F bonds or is coordinated with calcium ions, rather than acting to depolymerize the silicate network is still under debate. Stebbins *et al*. [77] considered that Si-F-Ca(n) bonds exist in molten slag of 39.2 mol% CaO - 58.9 mol% SiO_2 - 2 mol% CaF_2 quenched glasses. Dumas [78] has presented strong infrared and Raman spectroscopy evidence for the presence of Si-F interactions and $[SiO_3F]$ tetrahedral in fluorine doped silicate glass. In the high CaF_2 (> 20%) containing 45S5 based glasses, a negligible amount of Si-F bonds (< 2%) is noticed. However, the addition of a small amount of fluoride (≤ 15 mol%) does not seem to lead to the formation of the Si-F interactions and silicon is coordinated to oxygen atoms [21]. The MD simulation results produced by Lusvardi *et al.* [21] for bioactive glasses suggest that fluorine is almost exclusively bonded to network modifier ions (Ca and Na) and increases the polymerization of silicate tetrahedra by removing network modifier from the siliceous matrix. Brauer *et al*. [4] found that no Si-F interactions or non-bridging fluorine bonds formed to a significant extent in fluoride containing bioactive glasses. Instead, fluorine is present predominately as mixed calcium sodium fluoride species. In a Q^2 silicate glass, it is unlikely to observe Si-F bonds, since there is a large concentration of non-bridging oxygens and silicon has a lower affinity for the F^- ion compared to the O^{2-} ion, thus suggesting that fluorine is only coordinated with Ca^{2+}

and Na^+ [79] . This is in agreement with the findings by Pedone [5], who found that F is entirely coordinated by the modifier ions Na^+ and Ca^{2+}, and no Si-F bonds are present in the real glass structure. ^{19}F MAS-NMR shows that with an increase in CaF_2, the sodium concentration reduces, indicating that fluorine preferentially complexes calcium rather than sodium [4]. However, there are some researchers believe that fluoride has no preference to Ca^{2+} or Na^+ and it is normally present as a mixed species [5, 80, 81].

The presence of fluorine has a significant effect on reducing the glass transition temperature [82]. This effect was thought to be consistent with fluorine replacing bridging oxygens between silicons by non-bridging fluorines and disrupting the glass network. Brauer *et al*. [4] also found that T_g decreased with increasing CaF_2 content. However, it is mostly believed to be caused by forming a "CaF^+" species (Figure 2.3.2), which is analogous to the Na^+ ion. The formation of CaF^+ species reduces the electrostatic force between non-bridging oxygens appreciably and then leads to a less compact network and lower T_g. In contrast, in the CaF_2 free glasses, calcium ions are present as ionic bridges between non-bridging oxygens and bind them together by electrostatic forces. In addition, fluoride can also reduce the melting temperatures by forming CaF^+ species.

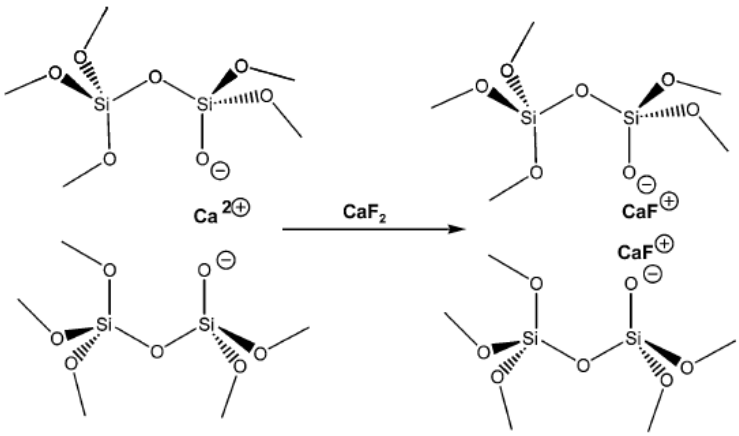

Figure 2.3.2 Illustration of the hypothetical effect of CaF_2 addition on silicate network adapted from Brauer *et.al.* [4]

The fluoride containing bioactive glasses investigated recently [4, 5] favour the formation of fluorapatite (FAP), which is more resistant to the acid attack compared to hydroxycarbonate apatite (HCA) [9, 80]. While excessive CaF_2 leads to calcium fluoride formation instead of FAP. Moreover, a sodium-free glass with a composition of 34.6 SiO_2 - 5.74 P_2O_5 - 50.38 CaO - 0 Na_2O - 9.28 CaF_2 (in mol%) shows an enhanced bioactivity and forms FAP in Tris buffer solution within 6 hours of immersion [9]. When compared to sodium containing glasses, the glass with no sodium shows more pronounced and better resolved apatite peaks in the XRD pattern. This discovery implies that sodium-free CaF_2 containing glasses might be more attractive for biomedical applications.

Moreover, it is shown that when CaF_2 is substituted for network modifiers (CaO or Na_2O), network modifiers are removed from siliceous matrix, in order to form CaF^+ species. As a consequence the available network modifier for forming non-bridging oxygens reduce and form a more cross-linked network, which leads to a reduced reactivity and bioactivity of the glass [4, 21]. In contrast, adding CaF_2 and keeping the ratio of network former to network modifier constant, result in network connectivity staying constant [20]. The incorporation of CaF_2 benefits glass bioactivity by forming fluorapatite, which has a lower solubility product.

2.3.6 Fluoride Containing Bioactive Glasses

Recent research showed that the incorporation of fluoride into silicate glasses is beneficial in reducing glass transition temperatures, probably glass hardness and forming FAP rapidly after immersion in physiological solution [4, 20]. These glasses are also attractive for bone substitutions and the remineralising toothpastes to treat dentine hypersensitivity [4]. However, it is important to control the fluoride content, as the excess fluoride leads to a formation of CaF_2 which is insoluble and might reduce the glass bioactivity [20, 83].

2.3.7 Potential Chloride Containing Bioactive Glasses

Chloride containing silicate glasses have rarely been investigated and only few papers on phosphate free, chloride containing (< 2 mol%) aluminosilicate glasses were published [84-86]. There are no commercial applications of oxychloride glasses to date, since virtually no chlorine is retained in the glass after the synthesis [87]. However, chlorine and fluorine are both halogen elements; it is assumed that chlorine takes a similar role in the glass structure and confers similar properties on the glasses, including reducing melting temperature, T_g and glass hardness and crystallising to ClAP. The chloride ion is larger than fluoride ion (1.67 Å vs 1.19 Å), the presence of chloride might be able to expand the glass network and result in a more open glass structure, thereby giving rapid glass degradation and a higher bioactivity. Moreover, $CaCl_2$ is soluble unlike the fluorite. However, there is no chloride containing bioactive available at the moment.

In order to achieve the benefits of chloride containing bioactive glasses, the problem of chloride volatilisation should be overcome. Research showed that chloride is lost in chloride containing glasses with NC of three or higher [85]. Nevertheless, volatilisation may be possibly be overcome in a Q^2 silicate structure [87].

2.4 Potential Applications of Fluoride and Chloride Containing Bioactive Glasses

2.4.1 Remineralising Toothpaste

Dentine hypersensitivity (DH) is characterised by a short, sharp pain responses to various stimuli, typically thermal, tactile, chemical or osmotic, that can not be ascribed to any other dental disease [88]. It arises from the exposure of the dentinal tubules of the root [9]. Bioactive glass has been incorporated as a remineralising ingredient in dentifrice formulations for treating DH. It forms hydroxycarbonated apatite on the tooth surface and subsequently occludes the exposed dentinal tubules which contribute to

an alleviation of the sensitivity [89]. Fluoride containing bioactive glasses are more attractive for this application [90]. Since FAP is more stable toward acid attack than the HAP and will provide a more durable option for treating DH.

The chloride bioactive glasses could also be of interest for remineralising toothpastes, since chlorine is similar to fluorine in its structural role and its effects on glass properties. Additionally the large chloride is expected to expand glass volume and promotes glass degradation and apatite-like phase formation. The mixed fluoride and chloride containing bioactive glasses may even be more competitive as they might combine the advantages from both fluoride and chloride.

The design criteria of a bioactive glass for toothpaste applications are summarised as below [91]:

- Rapid apatite formation (< 6 hours) in the mouth.
- Formation of FAP rather than hydroxycarbonated apatite.
- Particle size distribution that includes small (< 3 μm) particles for entering dentinal tubules and larger particles for more sustained release.
- Controlled fluoride release.
- pH rise < 8.0.
- No harder than enamel at 3.5 GPa.
- Fluoride content: less than 1500 ppm in Europe; less than 1100 ppm in the US.

2.4.2 Bone Grafts

There is an increasing interest in using bioactive glasses as synthetic bone graft substitutes due to the fact that bioactive glasses degrade over time and bond to bone, release soluble silica and calcium ions that are thought to simulate osteoprogenitor cells [1, 92]. The incorporation of fluoride into bioactive glasses has shown promise in promoting an acid durable fluorapatite formation at low pH (< 6) condition, representative of those present during the inflammation phase of normal bone healing,

consequently the fluoride containing bioactive glasses are suitable for bone grafts [93]. Moreover, fluoride is also known to promote osteoblast differentiation [94]. As mentioned above, the presence of large chloride ion might result in a more degradable glass and forming HAP, which is more soluble than FAP on immersion. Since ClAP convers to HAP with the presence of water [95], the immersion of chloride containing bioactive glasses will form HAP rather than ClAP, more details will be discussion in the following sections. Thus, the chloride containing bioactive glasses are more attractive for resorbable bone grafts.

2.4.3 Air Abrasion

Air abrasion is a minimally invasive approach for cutting dental cavities, which uses the kinetic energy of a high velocity stream of abrasive particles, typically alumina [6, 96]. Bioglass® 45S5 has been investigated as an abrasive particle in air abrasion [97] and also is used clinically for teeth polishing [98]. However, as mentioned previously, Bioglass® 45S5 is harder than the enamel. Therefore a glass with desirable hardness, which is harder than the decayed tooth tissue but softer than enamel (3.5 GPa), is attractive for use in air abrasion to remove carious lesions without damaging the subsurface of the tooth structure. The presence of fluoride and chloride are expected to reduce the glass transition temperature, which has a strong correlation to the glass hardness, the lower the T_g, the lower the hardness [6, 27]. The designed calcium halide containing glasses are potential candidates for air abrasion application. Understanding the relationship between calcium halide content and T_g will have a significant part to play in tailoring the glass properties for air abrasion applications.

2.4.4 Nuclear Waste Immobilisation

Recently, the immobilization of spent nuclear fuel waste containing actinide and chloride ions, has received more attention [99]. Amorphous borosilicate glasses have been selected as one option for the nuclear waste storage [100]. However, chloride ions have very low solubility in borosilicate glasses and there are issues with chloride

volatilisation. It has been suggested that chlorapatite glass-ceramic could be used to retain Cl-bearing waste containing fission products, although with lower waste loadings [101]. However to date no chlorapatite glass-ceramics have been developed.

2.5 Apatite

Apatites are a group of phosphate minerals, which form the mineral component of bones and teeth. Apatites include hydroxyapatite, fluorapatite and chlorapatite. The formula of these apatites are written as $Ca_{10}(PO_4)_6X_2$ (X=OH, F, Cl) [102]. To some extent, they are able to work as a “bridge” to bond implant materials to living tissues [25]. The materials which can form apatite when they are immersed in physiological solutions are defined as biomaterials that have bioactivity [55]. Apatites are increasingly used as bioactive materials for bone remodelling and replacement or for the coating of bone prostheses [102]. In addition, doped apatites are used as phosphors in fluorescent light tubes [102]. The versatility of apatites can be achieved by substituting a variety of ions.

2.5.1 Hydroxyapatite ($Ca_{10}(PO_4)_6(OH)_2$)

Hydroxyapatite has been paid much attention, as it is similar to the inorganic phase of bones and teeth [103]. Due to its excellent biocompatibility, osteoconductivity and good bioactivity, HAP has been used as a biomaterial [104]. However, the poor mechanical property is a big drawback [105].

The structure of HAP is a monoclinic structure with space group $P2_1/b$ with lattice parameters *a* = 9.4214(8), *b* = 2a, *c* = 6.8814(7) Å (1 Å = 0.1 nm), γ = 120 ° [8, 106] (Table 2.4). The results of Neutron diffraction and X-ray diffraction show that hydroxyl oxygen and hydrogen atoms are located at 0, 0, 0.201 and 0, 0, 0.062 respectively, rather than OH ion straddles the mirror plane at z=1/4 [102]. This indicates that there is a short range ordering of OH^- ions into columns, which run vertically down their structure in a head to tail fashion, that is, O-H O-H O-H. Apart from being a monoclinic form, HAP is also believed to be a hexagonal structure [106].

There are two types of Ca^{2+} ion site, Ca(I) and Ca(II) in the hydroxyapatite structure. Ca(I) ions are nine-fold coordinated by oxygen atoms, while Ca(II) ions are bonded to

six oxygen atoms and a OH^- ion. Fluorapatite and chlorapatite have same types of Ca^{2+} ions. The OH^- ion is in three-fold coordinated by Ca^{2+} ions. Three Ca (II) ions form a triangle, OH^- sites above the centre of the triangle of Ca(II) ion (Figure 2.5.1) .

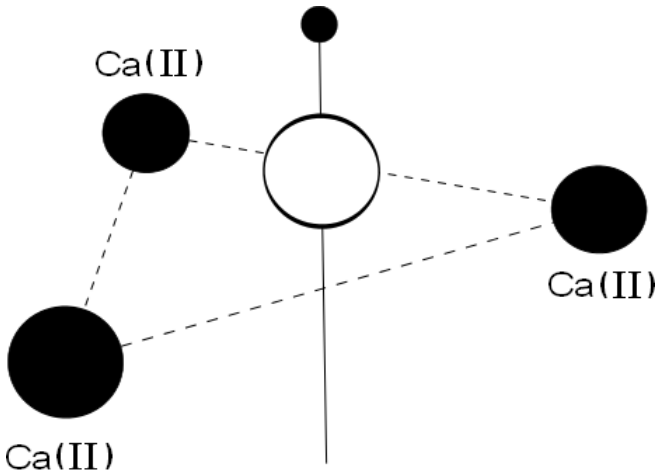

Figure 2.5.1 Arrangement of the ions around OH^- ion in hydroxyapatite

2.5.2 Fluorapatite ($Ca_{10}(PO_4)_6F_2$)

Investigations show that the incidence of dental caries is reduced when water supplies are fluoridated and some bone mineral disorders have been treated using NaF [102]. These can be explained by the fluoapatite formation in early caries lesions. Fluorapatite is chemically more stable in an acidic environment compared with carbonated hydroxyapatite [20]. Fluoride is beneficial in increasing bone density and the prevention of bone fracture. Therefore, fluorapatite is of particular interest in dental applications to prevent dental decay and for treating osteoporosis. In addition, fluorapatite is used as phosphors in fluorescent light tubes, when doped with antimony and manganese [102, 107].

Fluorapatite presents as a hexagonal prism with space group of $P6_3/m$ and the lattice parameters *a* = 9.37523, *b* = 9.37523 and *c* =6.88033 Å [108]. In the FAP structure, the F^- ion locates at 0, 0, 1/4 rather than sitting at 0,0,1/2 [102]. The F^- ion is at the centre and surrounded by three Ca(II), all four ions occurring at a mirror plane (Figure 2.5.2).

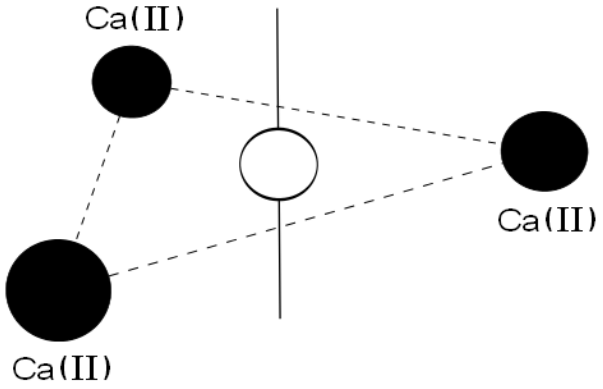

Figure 2.5.2 Arrangement of the ions around F^- ion in fluorapatite

2.5.3 Chlorapatite ($Ca_{10}(PO_4)_6Cl_2$)

Chlorapatite is a chloride substituted apatite, which has a similar functionality to fluorapatite. Mixed fluor/chlorocalcium/strontium apatites ($Ca/Sr_{10}(PO_4)_6(F/Cl)_2$) have been extensively used as commercial lamp phosphors in fluorescent tubes. The recent research shows that chlorapatite ceramics can be the candidate waste forms for incorporation of chloride-bearing waste containing fission products when lower waste loadings are accepted [101].

The structure of chlorapatite is monoclinic, space group of $P2_1/6$ with lattice parameter *a* = 9.628 (5), *b* = 2a, *c* =6.764 (5) Å, γ=120° [102, 109]. There are two Ca sites exist in ClAP, the four 4f Ca (I) sites are 9-fold coordinated by oxygen ions while the six 6h Ca(II) are seven-fold coordinated by six oxygen atoms and a Cl^- ion. The Cl^- ions are occurring in the vertical channel and above the centre of the mirror plane, forming by the triangle of Ca(II) (Figure 2.5.3) [101]. The position of Cl^- ion is 0.0016, 0.2493, 0.4439. There is a distance of 6.7 Å between two Cl^- ion column, these horizontal orders are continued by tilts of the PO_4^{3+} tetrahedral and 0.05 Å shifts of Ca (I) [102].

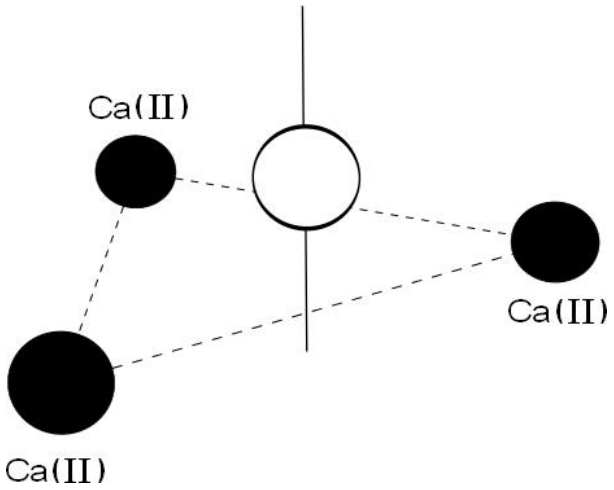

Figure 2.5.3 Arrangement of the ions around Cl^- ion in chlorapatite

Table 2.5.1 Structures of apatites and cell parameters

Formula	Stucture	Space group	a (Å)	b (Å)	c (Å)
$Ca_{10}(PO_4)_6(OH)_2$	Monoclinic	$P2_1/b$	9.4214	18.8428	6.8814
$Ca_{10}(PO_4)_6F_2$	Hexagonal	$P6_3/m$	9.3752	9.3752	6.8803
$Ca_{10}(PO_4)_6Cl_2$	Monoclinic	$P2_1/b$	9.6285	19.257	6.764

2.5.4 Comparison among Apatites

The chloride ion has an ionic radius of 1.67 Å against 1.26 Å and 1.19 Å for the hydroxyl and fluoride ions, respectively. The fluoride ion is the smallest one, it is able to enter the apatite lattice much more easy and occupy the space in the triangle of Ca(II) ions, which results in a reduction in the volume of the unit cell and a more compact structure [73]. Therefore, FAP has a higher chemically stability than HAP and ClAP.

Elliott [102] found that both of fluorapatie and chloraptite are thermally much more stable than hydroxyapatite. FAP has a melting temperature of 1644°C. Coarse FAP particles can be converted to HAP in heat steam at 1360°C for 48h [102]. Comparatively speaking, ClAP is less stable and is readily converted to HAP when heated in steam above 800°C. In addition, ClAP can also convert to HAP with the presence of water [95].

The X-ray diffraction patterns of HAP, FAP and ClAP are given in Figure 2.5.4. Generally, the characteristic diffraction lines for these apatites are quite close to each other, although both HAP and FAP have three main peaks between 30° to 33° 2Θ but only two for ClAP. The diffraction line with 100% intensity for HAP, FAP and ClAP are at 31.766°, 31.82° and 32.284° 2Θ. Since the apatite lattice is very tolerant of substitutions, vacancies and solid solutions occur readily [110], the diffraction lines shift or change in intensity with the substitution. Therefore it is difficult to distinguish among them using XRD alone. The combination of using XRD, XRF, ^{19}F, ^{31}P and ^{35}Cl MAS-NMR is very useful to identify apatites.

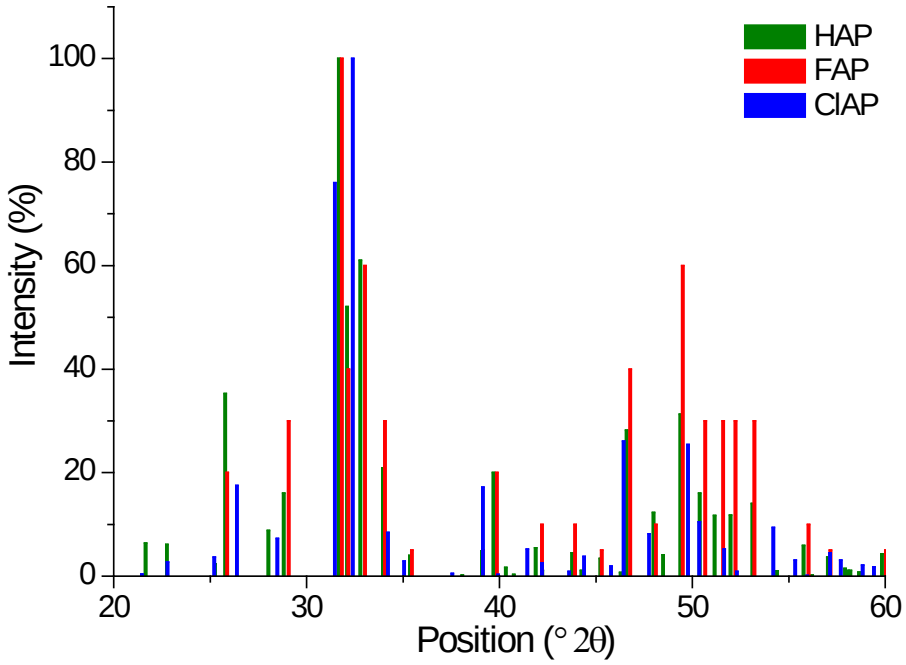

Figure 2.5.4 XRD patterns of hydroxyapatite, fluorapatite and chlorapatite

3 Aim and objectives

3.1 Aims

- To design and synthesise fluoride, chloride and mixed fluoride and chloride containing bioactive glasses.
- To investigate their bioactivity and study their mechanism of degradation and apatite formation.
- To investigate the crystallisation behaviors of the studied halide containing glasses.

3.2 Objectives

- Design and synthesis of the F, Cl, F-Cl containing bioactive glasses and characterisation by DSC, FTIR, XRD and MAS-NMR as follows:
    a. Synthesis and characterisation of the fluoride containing glasses series
    b. Synthesis and characterisation of the chloride containing glasses series
    c. Synthesis and characterisation of the mixed chloride and fluoride containing glasses series
    d. Synthesis and characterisation of the phosphate free glasses series with chloride and fluoride
- Investigation of glass bioactivity in Tris buffer solution and SBF.
- Study the structural role of F and Cl in silicate glasses based on simple models of P free glasses with the F/Cl.
- Study the crystallisation behaviour of the glasses with view to forming apatite glass-ceramics based on FAP /ClAP or mixed F/ClAP.

4 Materials and Methods

4.1 Diagram of Experiments

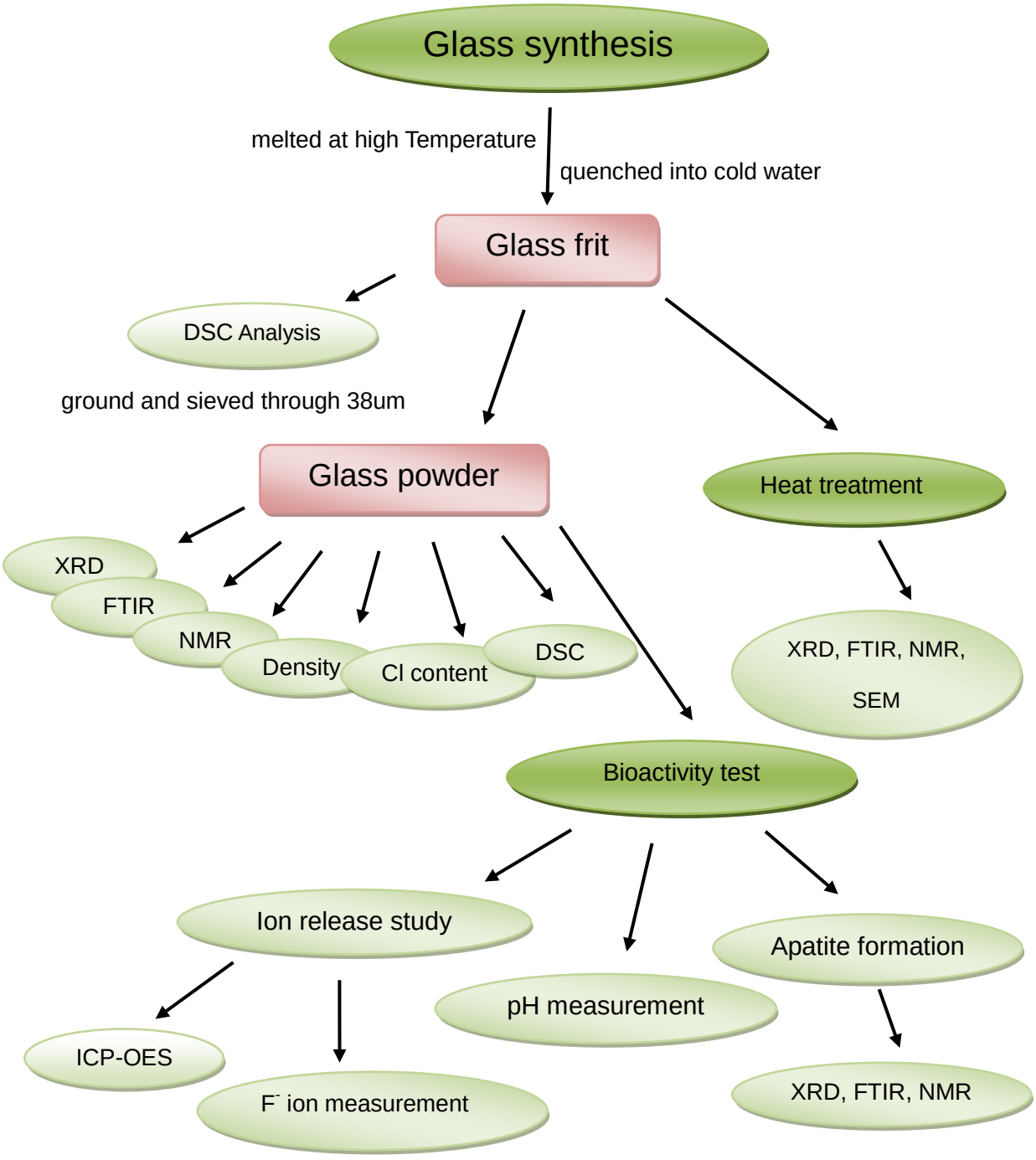

4.2 Glass Synthesis

The sodium-free glasses in the system of SiO_2-CaO-P_2O_5-CaF_2/$CaCl_2$, SiO_2-CaO-CaF_2/$CaCl_2$ were designed and synthesised by a melt-quench route. In this project, rather than substituting CaF_2 and/or $CaCl_2$ for CaO, calcium halides were added to the SiO_2-CaO-P_2O_5 and SiO_2-CaO system, while keeping the ratio of other components and the NC constant. The glass compositions are summarised in Table 4.2.1. The CaF_2 glass series (GPF series) were designed by introducing different amounts of CaF_2 into the GPF 9.3 composition first studied by Mneimne *et al*. [9]. The $CaCl_2$ glass series (GPCl series) were designed by replacing CaF_2 with $CaCl_2{\cdot}2H_2O$ and the mixed $CaCl_2$/CaF_2 series (GPFCl series) by replacing 50% of the CaF_2 by $CaCl_2{\cdot}2H_2O$, since $CaCl_2$ picks up water easily. The P free CaF_2 series (GF series) and the P free $CaCl_2$ series (GCl series) were designed by keeping the ratio of SiO_2: CaO: CaF_2= 50:50:X (X is the CaF_2 content in GF series) and SiO_2: CaO: $CaCl_2{\cdot}2H_2O$= 50:50:Y (Y=X, 30,40,50 and 60), respectively.

A 200 g batch size was made. Glass reagents (analytical grade silica (Prince Minerals Ltd., UK), calcium carbonate, calcium fluoride, calcium chloride dihydrate (all from Sigma-Aldrich) and diphosphorus pentoxide (AnalaR) were weighed, mixed and transferred into a Pt/10Rh crucible, heated up to 1320-1550˚C depending on the glass compositions for 1 hour in an electrical furnace (EHF 17/3 Lenton, Hope Valley, UK), quickly quenched into cold water to inhibit crystallisation. In this work, $CaCO_3$ was used as a reagent instead of CaO, since $CaCO_3$ decomposes to CaO and CO_2 after melting but CaO reactives with CO_2 forming $CaCO_3$. After drying in an electric oven (85°C) overnight, 100 g of the glass frit was ground using a Gy-Ro mill (Glen Creston, London, UK) with two sets of 7 minutes. The obtained glass powder was sieved through a < 45 μm mesh analytical sieve (Endecotts Ltd., London, UK) to get fine powder.

The particle size and distribution of the studied glasses (< 45 μm) were estimated using a Mastersizer/E particle analyser (Malvern Instruments, UK). Small amount of glass powders were added to a circulating water bath. According to the actual powder particle size range, the particle size was measured by spherical volume in the range between 0.1 μm to 100 μm by a 45 mm lens or between 0.5 μm to 180 μm by a 100 mm lens. The particle size distribution was evaluated with the span value defined as:

$$Span = \frac{D[v,0.9] - D[v,0.1]}{D[v,0.5]} \tag{4.2}$$

Where $D[v,0.9]$, $D[v,0.5]$, $D[v,0.1]$ indicate that the volume percentage of the particle with diameter of $D[v,0.9]$, $D[v,0.5]$, $D[v,0.1]$ is 90%, 50% and 10%.

Table 4.2.1 Experimental glass compositions (in Mol%).

Glass	SiO_2	CaO	P_2O_5	CaF_2	$CaCl_2$	T_{firing} (°C)	NC
GPF/GPCl 0.0	38.1	55.5	6.3	-	-	1550	2.08
GPF 3.0	37.0	53.9	6.1	3.0	-	1550	
GPF 4.5	36.4	53.0	6.0	4.5	-	1500	
GPF 6.0	35.9	52.2	6.0	6.0	-	1500	
GPF 9.3	34.6	50.4	5.7	9.3	-	1500	
GPF 13.6	32.9	48.0	5.5	13.6	-	1500	
GPF 17.8	31.4	45.7	5.2	17.8	-	1500	
GPF 25.5	28.4	41.4	4.7	25.5	-	1500	
GPFCl 2.6	37.1	54.1	6.1	1.5	1.1	1550	2.08
GPFCl 4.0	36.6	53.4	6.0	2.3	1.7	1520	
GPFCl 5.3	36.2	52.6	5.9	3.0	2.3	1500	
GPFCl 8.3	35.0	51.0	5.8	4.7	3.6	1500	
GPFCl 12.1	33.5	48.8	5.6	6.9	5.2	1500	
GPFCl 16.0	32.1	46.7	5.3	9.1	6.9	1500	
GPFCl 23.1	29.3	42.7	4.9	13.2	9.9	1500	
GPCl 2.3	37.3	54.3	6.2	-	2.3	1500	2.08
GPCl 3.5	36.8	53.6	6.1	-	3.5	1500	
GPCl 4.6	36.4	53.0	6.0	-	4.6	1500	
GPCl 7.2	35.4	51.6	5.9	-	7.2	1480	
GPCl 10.6	34.1	49.6	5.7	-	10.6	1480	
GPCl 14.0	32.8	47.7	5.4	-	14.0	1480	

GPCl 20.6	30.3	44.1	5.0	-	20.6	1450	
GF 2.9	48.5	48.5	-	2.9	-	1550	2.0
GF 4.3	47.9	47.9	-	4.3	-	1540	
GF 5.7	47.2	47.2	-	5.7	-	1540	
GF 8.5	45.8	45.8	-	8.5	-	1500	
GF 12.0	44.0	44.0	-	12.0	-	1505	
GF 15.1	42.4	42.4	-	15.1	-	1495	
GF 20.3	39.8	39.8	-	20.3	-	1480	
GCl 0.0	50.0	50.0	-	-	0.0	1550	2.0
GCl 2.2	48.9	48.9	-	-	2.2	1550	
GCl 3.3	48.4	48.4	-	-	3.3	1530	
GCl 4.3	47.8	47.8	-	-	4.3	1480	
GCl 6.6	46.7	46.7	-	-	6.6	1480	
GCl 9.3	45.3	45.3	-	-	9.3	1490	
GCl 11.9	44.1	44.1	-	-	11.9	1480	
GCl 16.1	41.9	41.9	-	-	16.1	1470	
GCl 27.4	36.3	36.3	-	-	27.4	1445	
GCl 33.5	33.3	33.3	-	-	33.5	1420	
GCl 43.0	28.5	28.5	-	-	43.0	1395	
GCl 53.1	23.5	23.5	-	-	53.1	1320	

4.3 Glass Characterisation

4.3.1 X-ray Diffraction (XRD)

XRD is a powerful analytical technique for studying the long-range order, determining the different crystalline phases and the crystal structure. In addition, XRD can be used to identify whether glass is amorphous or partially crystalline. The amorphous glass gives a smooth and broad halo, while a crystalline phase shows distinct diffraction lines instead [9].

In this PhD project, an X'Pert Pro X-ray diffractometer (PANalytical, Eindhoven, The Netherlands) was employed to characterise the glasses, the heat treated glass-ceramics and the precipitates collected after immersion in buffer solutions. A small amount of sample was placed in the sample holder. A Bragg-Brentano flat plate

geometry was used along with Cu Kα radiation (λ_1=1.54059 Å and λ_2=1.54442 Å). The patterns of sample were collected from 5 to 70˚ 2θ with an interval of 0.0334˚ and a step time of 200.03 sec. Calibration was carried out using NIST standard reference material 660a (lanthanum hexaboride). XRD data were analyzed using X'Pert HighScore Plus (v2.0, PANalytical, Almelo, The Netherlands) in conjunction with the ICDD database. During the experimental manipulation, the samples were exposed to the atmosphere. The chloride containing glasses made in this project were particularly moisture sensitive and therefore any exposure of the samples to the atmosphere during the measurements including the XRD runs sometimes might result in some reaction with the atmospheric moisture as will be discussed later.

4.3.2 Fourier Transform Infrared Spectroscopy (FTIR)

Chemical bonds in the materials were evaluated by Fourier Transform Infrared Spectroscopy (Spectrum GX, Perkin-Elmer, Cambridge, UK) via interpreting the infrared absorption spectrum. Prior to sample scanning, the lens was cleaned with ethanol, followed by performing a background spectrum scan. After collecting the background, a sufficient amount of powder was transferred to cover the lens. A scan number of 20 was used. The background signal was automatically subtracted by software from the samples spectra. The data were recorded from 500 to 1600 cm^{-1} (wavenumbers).

4.3.3 Magic Angle Spinning-Nuclear Magnetic Resonance (MAS-NMR)

Magic Angle Spinning - Nuclear Magnetic Resonance (MAS-NMR) is a powerful technique for characterising solids and gives information on co-ordination states, next nearest neighbours, bond lengths and bond angles [111]. Figure 4.3.1 illustrates the schematic of MAS-NMR technique. The solid sample is placed in a rotor, rotating with high frequency (5-30 kHz) at a magic angle (ɵ=54.7°, $3\cos^2$ɵ-1=0) with respect to the diraction of main magnetic field (B_0), in order to average the anisotropic interactions, narrow down the broad line and increase the resolution of the spectrum. The

information about chemical shift (atomic environment), the number of peaks (the number of chemically distinct species) and peak integral (the amount of chemically equivalent nuclei giving rise to the peak) can be obtained from the spectrum.

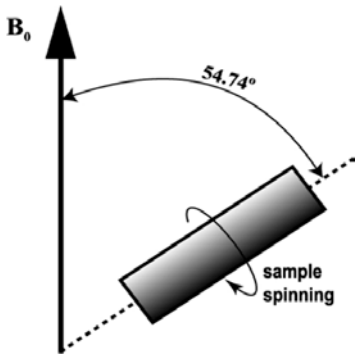

Figure 4.3.1 Schematic representation of the MAS-NMR technique adapted from Alia *et.al.* [112].

Both of ^{19}F and ^{31}P nuclei are 100% abundant with a nuclear spin of 1/2. The ^{19}F nucleus has a large degree of chemical shift anisotropy, which is very sensitive to the cations next to it. The chemical shift of ^{31}P is sensitive to the cationic substitutions. Therefore they are the well-known and excellent technique for providing on the local structure of fluorine and the phosphorus environments in the bioactive glasses [4, 5, 113]. ^{29}Si MAS-NMR is a very powerful technique which is widely used to determine the Q^n structure [4]. However the low nature abundance (4%) of ^{29}Si nucleus increases the cost of the experiment as it is time-consuming.

Unlike ^{19}F or ^{31}P MNR, ^{35}Cl NMR is technically challenging, though the nuclide consists 75% of natural Cl [85]. The ^{35}Cl is a quadrupolar nucleus with a spin of 3/2 and a large nuclear quadrupolar moment, which result in a severely broad NMR peak. Therefore only few studies on glass structure were carried out using ^{35}Cl MAS-NMR [84-86].

In this thesis, ^{19}F MAS-NMR will be used to study the fluorine environment in the glasses and distinguish FAP formation from HAP and ClAP. In addition, ^{29}Si and ^{31}P NMR will also be employed to characterize the glass structure. The ^{31}P, ^{19}F and ^{29}Si

MAS-NMR experiments were performed using a 600 MHz (14.1T) Bruker NMR spectrometer (AV 600 NMR, UK).

For ^{31}P MAS-NMR experiment, glass powder with a particle size less than 45µm and the solid collected after immersion or heat treatment were packed into a 4 mm zirconia rotor and placed in a magnetic field of 242.9 MHz frequency with spinning condition of 8 KHz. Some ^{31}P MAS-NMR measurements were also carried out using the Bruker probe with a 2.5mm rotor at spinning speeds of 18 and 21 kHz. A recycle delay of 60 s was used and the number of scans was set to 16. The chemical shift was referenced using the primary reference, 85% H_3PO_4.

The ^{19}F MAS-NMR measurements were conducted at the resonance frequency of 564.7 MHz using the “fluoride-free” double resonance Bruker probe with a low fluoride background and tuneable to the ^{19}F NMR frequency using the 2.5 mm rotor spinning at 18 kHz and 21 kHz. Either 32 or 64 scans were acquired with 8 preliminary dummy scans and 30 seconds recycling delay. The chemical shift was referenced using the signal from the 1 M NaF solution scaled to -120 ppm relative to the CF_3Cl primary standard.

A resonance frequency of 119.2 MHz was used for ^{29}Si MAS-NMR. Glass powder was packed in a 4 mm zirconia rotor and spun at 5 kHz with a 120s recycle time. The data were collected after 432 scans. The chemical shift of the ^{29}Si NMR spectra was referenced to 0 ppm frequency of the corresponding signal in tetramethylsilane $Si(CH_3)_4$) solution.

NMR data were plotted using TopSpin® and Xwinplot® softwares (Bruker TopSpin 2.1 software, Germany). The full width half maximum (FWHM) of the ^{31}P MAS-NMR spectra were estimated by using Bruker TopSpin® software. Chemical speciation of ^{29}Si, ^{31}P, ^{19}F nuclei and glass structure were evaluated by the chemical shift and the shape of the peaks.

4.3.4 Differential Scanning Calorimetry (DSC)

Differential scanning calorimetry (DSC) is a thermal analytical technique which can be used to observe fusion and crystallisation events, and measure the difference in the heat flow rate between a sample and reference when they are undergone a maintained heat treatment cycle.

Both glass frits (1-2 mm) and fine powders (< 45µm) were used to determine the glass transition temperature, crystallisation (T_c) peak temperature, melting temperature (T_m) and assess the tendency toward surface or bulk nucleation by using a Stanton Redcroft DSC 1500 (Rheometric Scientific, Epsom, UK). A 50 mg sample was packed in a Pt-Rh crucible and heated under Nitrogen (60ml/min^{-1}) from 25 ˚C to 1100˚C at a rate of 20˚C/min against an alumina reference. The glass transition temperature (T_g) was obtained from the DSC traces with an accuracy of ± 5 ˚C.

4.3.5 Compositional Analysis

The chloride contents in the initial chloride containing glasses were quantified using a chloride ion selective electrode (ELIT Cl^- 2844, NICO 2000 UK). Glass powder (75mg) with particle size smaller than 45 um was dissolved in the 50 ml solution (48 ml deionized water, 1 ml 69% HNO_3 and 1 ml 5M $NaNO_3$ (ISA solution)). The samples were prepared in triplicate. The 1000 ppm Cl^- stock solution was prepared by dissolving 1.649 g NaCl (Sigma-Aldrich, Gillingham, UK) into 1 L distilled water. The obtained Cl^- stock was diluted to different concentrations to calibrate the electrode.

4.3.6 Density Measurement

The density of each glass was determined by Helium Pycnometry (AccuPyc 1330-1000, Micromeritics, GmbH, Aachen, Germany). Two grams of glass powder (<45 µm) was used and measured with the pressure at 1.6 bar. The density values reported are the mean of ten measurements performed during the experiment.

The experimental molar volume of the glasses is calculated by using the relation [114]:

$$V_m = \frac{M}{D} \tag{4.3}$$

Where *M* is the relative molecular mass of glass and *D* is the experimental density.

4.4 Bioactivity Test

Glass bioactivity in terms of glass degradation and apatite-like phase formation was investigated in both Tris buffer solution and SBF. The preparation of Tris buffer solution was according to that described by Mneimne *et al*., while SBF was prepared following the method described by Kokubo and Takadama [59] for the corrected SBF (c-SBF, in Table 2.3.1). A 75 mg glass powder (< 45 μm) was dispersed in 50 ml Tris and SBF respectively then transferred to a shaking incubator (KS 4000i Control, IKA, Staufen, Germany) set at 37±1 ˚C with an agitation rate of 60 rpm for different durations (1, 3, 6, 9, 24, 72 and 168 hours). The samples were prepared in duplicate. At the end of the immersion period, samples were removed from the shaker, and pH values were measured by a pH meter with 35811-71 pH electrode (Oakton®, Malaysia). Solutions were subsequently filtered through a filter paper which has a pore size between 5 μm and 13 μm. The filter papers with the precipitates were dried in the oven at 37˚C overnight; the collected precipitates were used to investigate apatite formation by FTIR, X-ray diffraction and MAS-NMR. The filtered solution was kept in the fridge at 4˚C for subsequent ICP analysis.

4.4.1 Inductively Coupled Plasma – Optical Emission Spectroscopy

ICP-OES is a sensitive technique used to measure ion (Ca^{2+}, Si^{4+}, P^{5+}, Na^{+}) concentrations up to a very low concentration (as low as 0.1ppm). The advantages of ICP are high sensitivity, and many different elements can be measured at the same time, good precision and reproducibility.

In this work, the concentrations of Ca, Si and P were quantified using an inductively coupled plasma-optical emission spectroscopy (ICP-OES; Varian Vista-PRO, UK). Solutions were acidified using 69% nitric acid and diluted by a factor of 1:10 or 1:20 for measurements of calcium and silicon content and no dilution was used for measurements of phosphate ion content. According to the calculation of ion release level prediction, standard solutions were prepared by diluting the multi-element stock solution with deionized water. Prior to the sample measurement, a calibration for each element was performed with the standards.

4.4.2 Fluoride Probe Measurement

It is known that the voltage of the probe measured in solution is directly proportional to the logarithms of the concentration of F^{-}. Fluoride concentration in solution was therefore measured using a fluoride ion selective electrode (Orion 9609BN, 710A meter, South Burlington, VT, USA). A sequence of standard solutions with different F^- concentrations (2, 10, 16, 20, 40 and 100 ppm) was prepared by diluting NaF stock solution (1000 ppm) with de-ionised water. A six-point calibration was applied to establish the relationship between the probe voltage and the F^- concentration. Measurements started from high concentrations to low ones.

4.5 Heat Treatment

Glass frit (1-2 mm) and fine powder (< 45 μm) (1 g), which was compacted into a disc under 40 bar pressure for 30s, were placed on a platinum foil and heated up at a rate of 20°C/min from 400ºC to the heat treatment temperature (T_{HT}) in a porcelain furnace (CeramPress, NEY Dental International, USA) without holding. According to the width of the crystallization peak from the DSC traces, T_{HT} was T_c or approximately 10°C above T_c. After heat treatment, samples were immediately withdrawn from the furnace and air quenched. The resulting sintered glass-ceramics were then ground into powder and characterized using XRD, FTIR and MAS-NMR to identify the crystalline phases.

4.6 Scanning Electron Microscopy

In order to investigate the morphology of the crystalline phases, the heat treated glass-ceramics were embedded into epoxy resin (Epofix, Struers, Copenhagen, Denmark) to set, polished with a series of silicon carbide grinding paper (P120, P320, P600, P800, P1000, P2400 and P4000) and finished with 0.3 micron diamond paste (Met Prep Ltd. UK). The well-polished or powder form specimens were gold coated using an automatic sputter coater (Agar Scientific Ltd, Stansted, 108 A, England) at 40mA for 100 seconds and viewed under a scanning electron microscope (FEI Inspect F, Oxford Instruments, UK) using back-scatter and secondary electron imaging modes. In addition, some of the grinding glass-ceramics were spread on the sample holders, gold coated and imaged by using SEM.

5 Sodium-Free CaF_2 Containing Bioactive Glasses

Foreword

Due to the noticeable bioactivity, the first bioactive glass (Bioglass® 45S5) has been in clinical use since 1985 and is widely used under the trademark of NovaBone®, PerioGlas® and NovaMin®. This commercially available glass (Bioglass® 45S5) contains significant amounts of sodium oxide (24.4 mol%), which is beneficial in reducing the glass melting temperature, thus facilitating synthesis at low temperatures. In addition, according to Hench's original mechanism of bioactivity, sodium is a critical component for glass degradation and apatite formation [52].

However, high sodium oxide content is problematic. It makes the bioactive glass phase hygroscopic, and thereby affects stability, degradation and mechanical performance of its composites. This reduces the applicability of conventional high sodium oxide content bioactive glasses as a filler in composites. In addition, according to the mechanism of glass degradation [43], sodium ions exchange with protons followed by the glass dissolution causing an increase in pH value, which is in favour of apatite formation but not beneficial for homeostasis.

As presented in recent research articles, it is possible to form sodium-free fluoride containing bioactive glasses, which crystallise to FAP during quenching or degrade and form FAP upon immersion in buffer solutions [9, 20]. In this project we extended the sodium-free bioactive glass composition studied earlier [9] and developed a series of sodium-free glasses with varied fluoride content.

The presence of fluoride in sodium-free bioactive glasses brings additional benefits to the bioactive material. Fluoridated apatite formed on immersion is less soluble in an

acidic condition than hydroxyapatite, the latter is the main component of enamel and dentine [115-117]. Fluoride is the well-known agent in preventing caries by inhibiting enamel and dentine demineralisation, enhancing remineralisation and inhibiting bacterial enzyme activity [116]. Therefore, fluoride containing bioactive glass is promising for remineralising toothpastes to treat tooth hypersensitivity.

The assessment of bioactivity for bioactive glasses is traditionally carried out on immersion of glass in a buffer solution simulating physiological conditions. Formation of the apatite-like phase on the surface of the solid as a consequence of the reaction with solutions is then evaluated. The earliest immersion time when an apatite-like phase can be determined is used as a measure of bioactivity.

Glass bioactivity in terms of glass degradation and apatite-like phase formation can be modified by introducing specific elements, i.e. fluoride and phosphate, into the glass composition or changing the concentration of components.

The rate and capacity of apatite-like phase formation is dependent on the type of buffer solutions. SBF and Tris buffer solution are the most commonly used buffer solutions. SBF, which was first introduced by Kokubo *et al.*, has an ion concentration close to that of human blood plasma, but it is calcium and phosphate saturated [59]. Thus, potentially any surface exposed to SBF could favour apatite formation regardless whether it is bioactive or not.

Tris buffer has a neutral pH and is used at an identical physiological temperature, but has no additional ions. The Ca^{2+} and PO_4^{3-} ions release and apatite formation after immersion in Tris can be attributed entirely to the glass compositions. However, when glass compositions contain only low phosphate content, no apatite or very slow apatite formation is likely to occur in Tris buffer [50]. Thereby, only the bioactivity test for the phosphate-rich glasses can be evaluated in Tris.

In this chapter we present the results on sodium-free, high phosphate and fluoride containing bioactive silicate glasses and the bioactivity results in both SBF and Tris buffer solution.

5.1 Results of the As-Quenched Glasses

The structure of all the as-quenched glasses (Chapters 5-7) was characterised by XRD, FTIR, ^{31}P and ^{19}F MAS-NMR. Glass density presented in Chapters 5-7 and 9 was determined using Helium Pycnometry. Both glass frits and fine powder were evaluated using DSC for glass thermal properties (Chapters 5-7 and 9). The as-quenched glass frits were optically transparent with the exception of those with a CaF_2 content higher than 9 mol%.

5.1.1 XRD Results of the As-Quenched Glasses

Figure 5.1.1 shows the XRD patterns of the as-quenched sodium-free glasses with varying amounts of CaF_2 (0.0 to 25.5 mol%). The typical amorphous halos at 30° 2θ were found in glasses with low CaF_2 content (≤ 6.0 mol%); however, a minor peak at 31.9° 2θ is seen for the 4.5 and 6.0 mol% CaF_2 containing glasses. Clear diffraction peaks at 25.9°, 31.8°, 32.2° and 33° 2θ are noticed for the higher CaF_2 containing glasses (≥ 9.3 mol%). These peaks match the characteristic diffraction peaks of apatite (FAP: 00-034-0011). A further increase in the CaF_2 content up to 17.8 mol% results in the crystallisation of cuspidine ($Ca_4Si_2O_7F_2$, 00-011-0075) with major diffraction lines at 26.5° and 29.1°. Meanwhile, additional lines at 28.3° and 47° 2θ corresponding to fluorite (CaF_2, 00-004-0864) are also found in the glass with 17.8 or 25.5 mol% CaF_2.

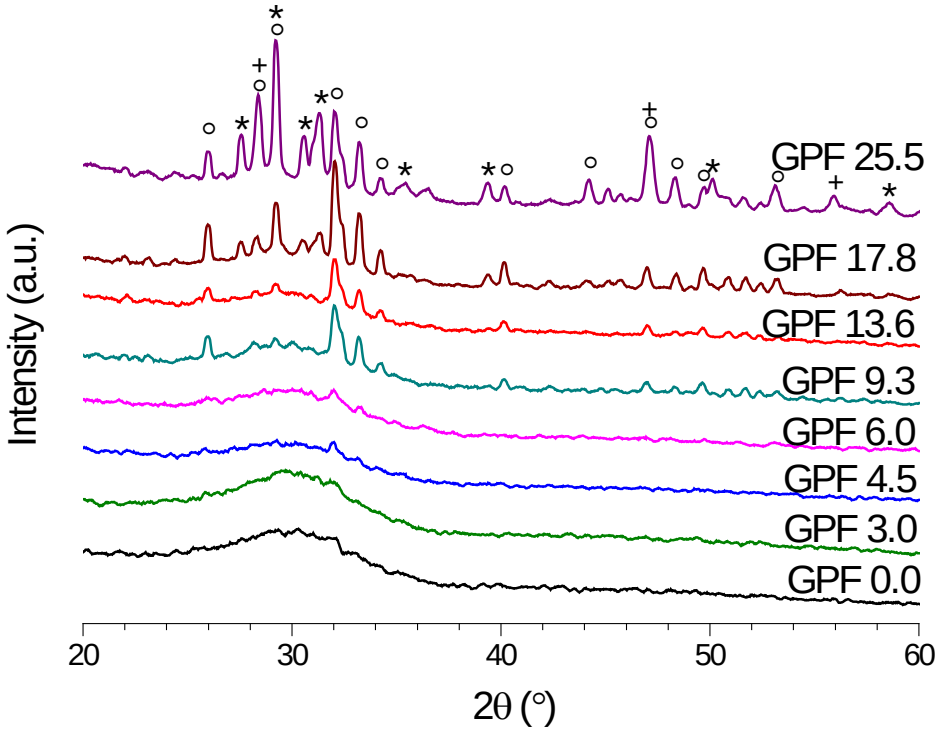

Figure 5.1.1 The XRD patterns of as-quenched CaF_2 containing glasses. (°: $Ca_{10}(PO_4)_6F_2$; *: $Ca_4Si_2O_7F_2$; +: CaF_2).

5.1.2 FTIR Results of the As-Quenched Glasses

The FTIR spectra of the as-quenched CaF_2 containing glasses are given in Figure 5.1.2. The non-bridging oxygen band at 920 cm^{-1} and the Si-O-Si stretching band at 1030 cm^{-1} are found for the whole glass series. For the low fluoride (≤ 6.0 mol%) containing glasses, a small band around 600 cm^{-1} corresponding to amorphous calcium phosphate is noticed, while the typical apatite split bands at 560 and 613 cm^{-1} are seen in high CaF_2 (≥ 9.3 mol%) containing glasses [9]. The sharp band features in the region 800-1050 cm^{-1} in the spectrum of 25.5 mol% CaF_2 containing glass are also detected suggesting the presence of a silicate crystalline phase.

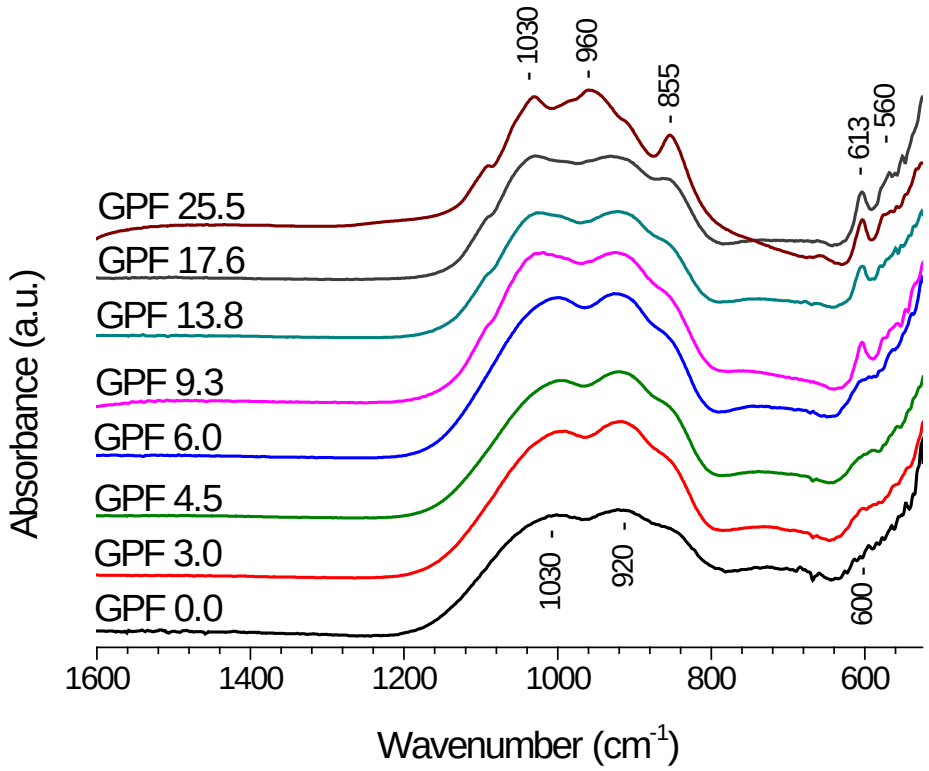

Figure 5.1.2 The FTIR spectra of as-quenched CaF_2 containing glasses.

5.1.3 ^{31}P and ^{19}F NMR Results of the As-Quenched Glasses

The atomic environment of phosphate and fluoride in the synthesised glasses were investigated by ^{31}P and ^{19}F MAS-NMR. The ^{31}P MAS-NMR spectra of CaF_2 containing bioactive glasses are shown in Figure 5.1.3. The broad peak with a centre at 3 ppm is visible in the spectra of glasses with CaF_2 contents lower than 9.3 mol%, indicating an amorphous calcium orthophosphate environment. An increase of CaF_2 content (≥ 9.3 mol%) resulted in a reduction of the line-width of the peak without altering the peak position. This suggests that glasses with CaF_2 content at and above 9.3 mol% tend to partially crystallise to apatite.

Figure 5.1.4 shows the ^{19}F MAS-NMR spectra of the glasses. It is clear that three different fluorine environments are present. The low CaF_2 containing glasses have broad peaks centred at about -96 ppm, suggesting an amorphous F-Ca(n) fluoride environment, while a tiny and sharp peak at -103 ppm appearing on the shoulder of a

broad glass signal in the high CaF_2 containing glasses (≥ 9.3 mol% CaF_2) is attributed to the fluorapatite (F-Ca(3)) environment. Furthermore, a distinctly sharp peak with the chemical shift of -108 ppm is visible in the spectrum of 25.5 mol% CaF_2 containing glass, indicating the crystallisation of CaF_2 (F-Ca(4)). The ^{19}F MAS-NMR confirms fluorapatite crystallisation in the glasses with CaF_2 content at and above 9.3 mol% and the crystallisation of CaF_2 in the highest CaF_2 containing glass (25.5 mol% CaF_2). These are in accordance with the results of XRD, FTIR and ^{31}P MAS-NMR.

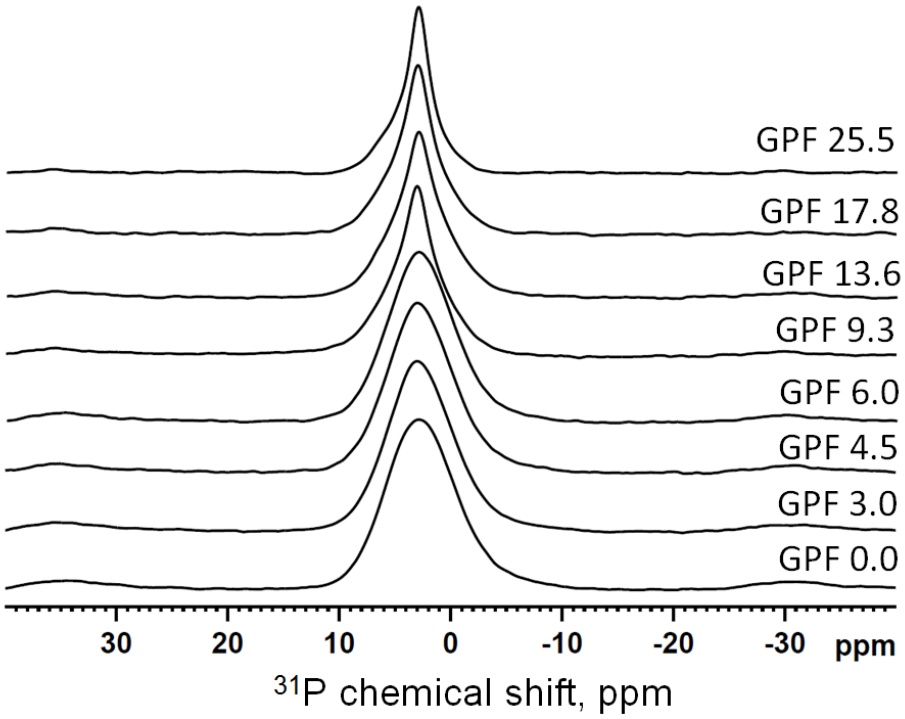

Figure 5.1.3 The ^{31}P MAS-NMR spectra of as-quenched CaF_2 containing glasses.

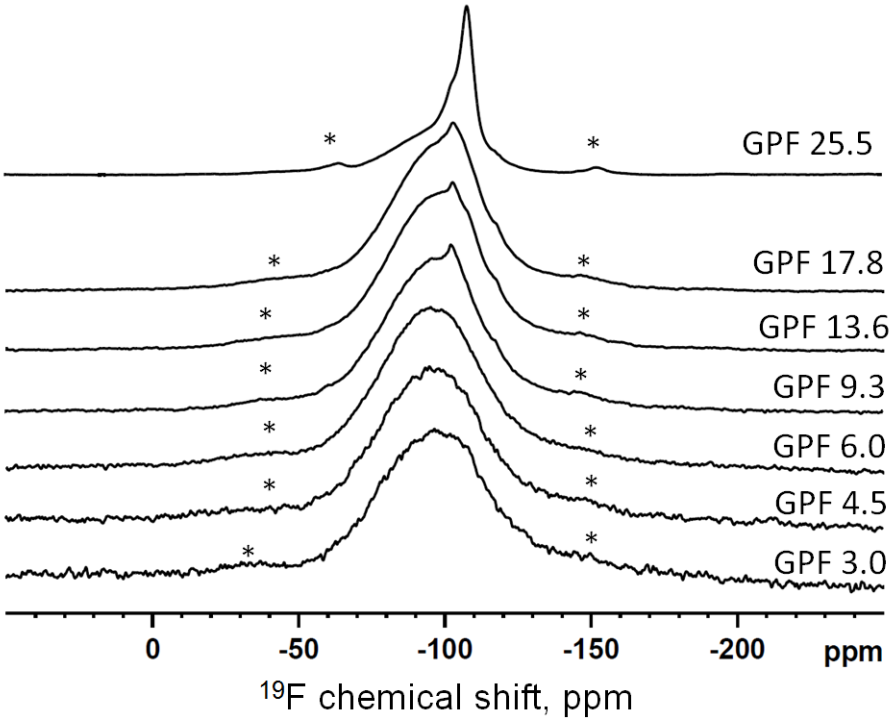

Figure 5.1.4 The ^{19}F MAS-NMR spectra of as-quenched CaF_2 containing glasses, the symmetrical signals labelled by asterisk present spinning side bands.

5.1.4 Glass Density and Molar Volume

The density and molar volume of CaF_2 containing bioactive glasses are plotted as a function of CaF_2 content (Figure 5.1.5). It is clear that the density values increase with an increase in CaF_2 content. At the same time, the glass molar volume increases from 21.47 to 22.26 cm^3/mol with an increase of CaF_2 content from 0 to 25.5 mol%.

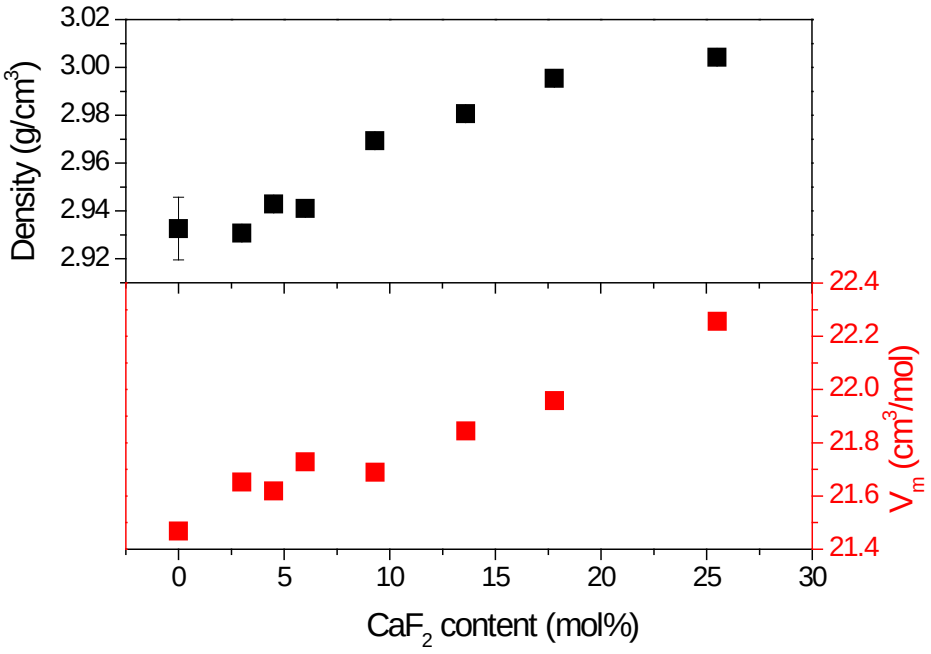

Figure 5.1.5 Glass density and molar volume plotted as a function of CaF_2 content. Note where error bars are not shown they are smaller than the data points.

5.1.5 DSC results of the Na free CaF_2 Containing Bioactive Glasses

Figure 5.1.6 shows the DSC traces for glass frits of the sodium-free CaF_2 containing glasses. The glass transition temperature (T_g), crystallisation peak temperature (T_c) and melting temperature (T_m) were defined from the DSC traces with an accuracy of ±5 °C. The obtained T_g, T_c and T_m are summarised and listed in Table 5.1.1. Some of the glasses have more than one exotherm, corresponding to the crystallisation peak temperature of the first (T_{c1}), second (T_{c2}) and third (T_{c3}) etc.. The number of crystallisation events is not necessarily equal to the number of crystallisation phases. Since a crystalline phase might crystallise in more than one step or two crystalline phases might crystallise at the same temperature and produce a single exotherm in a DSC trace. In addition, there is a clear endotherm peak around 1115 °C in the DSC trace for most of the glasses corresponding to the melting effect.

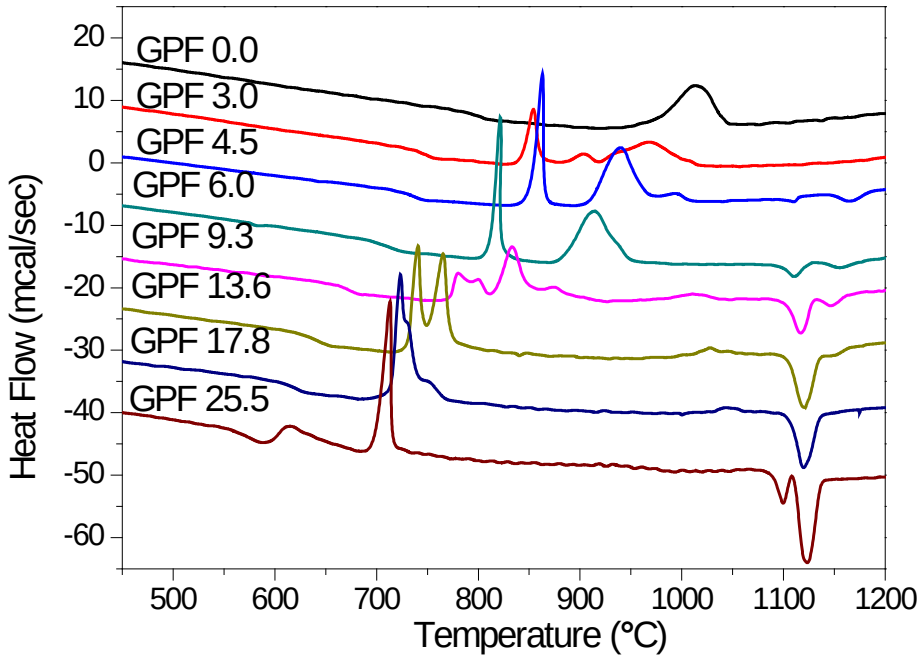

Figure 5.1.6 DSC traces for the glass frits of CaF_2 containing glasses.

Table 5.1.1 Characteristic temperatures for fluoride containing glasses. For each glass composition, the first row is the characteristic temperature of glass frit and the second row is the characteristic temperature of fine powder.

Glass Code	T_g	T_{o1}	T_{c1}	T_{c2}	T_{c3}	T_m
GPF 0.0	786	969	1013	-	-	
	790	901	925	-	-	-
GPF 3.0	736	837	868	901	968	
	735	848	867	888	979	-
GPF 4.5	720	844	863	940	994	
	722	819	860	-	-	-
GPF 6.0	695	806	821	912	-	1110
	693	790	817	844	942	-
GPF 9.3	662	771	780	835	1008	1116
	655	751	780	806	878	1120/1140
GPF 13.6	626	725	740	766	-	1120
	618	699	732	758	977	1112
GPF 17.8	606	712	724	-	-	1120
	601	687	720	-	-	1120
GPF 25.5	560	596	708	-	-	1100/1124
	558	695	713	-	-	1124

The T_g values of both glass frit and fine powder are plotted as a function of CaF_2 content in Figure 5.1.7. A dramatic reduction in T_g can be seen with an increment of CaF_2 content. A linear relationship (Y= -13.331X+780.59,R^2=0.9871) between T_g and CaF_2 content is seen in the glasses with CaF_2 content no more than 9.3 mol%, while a break in the T_g behaviour is found when CaF_2 content was more than 9.3 mol% as a consequence of crystallisation of fluoride containing phases. As suggested from the XRD results of the as-quenched glasses, the glasses crystallise to fluorapatite, cuspidine and fluoride sequentially with an increase in CaF_2 content above 6.0 mol%, thereby, effectively removing fluoride from the glass phase and consequently the reduction in T_g becomes smaller with increasing CaF_2 content. In addition, glasses with different particle sizes have almost identical T_g values, suggesting that T_g is a substantial property of the glass and independent of particle sizes.

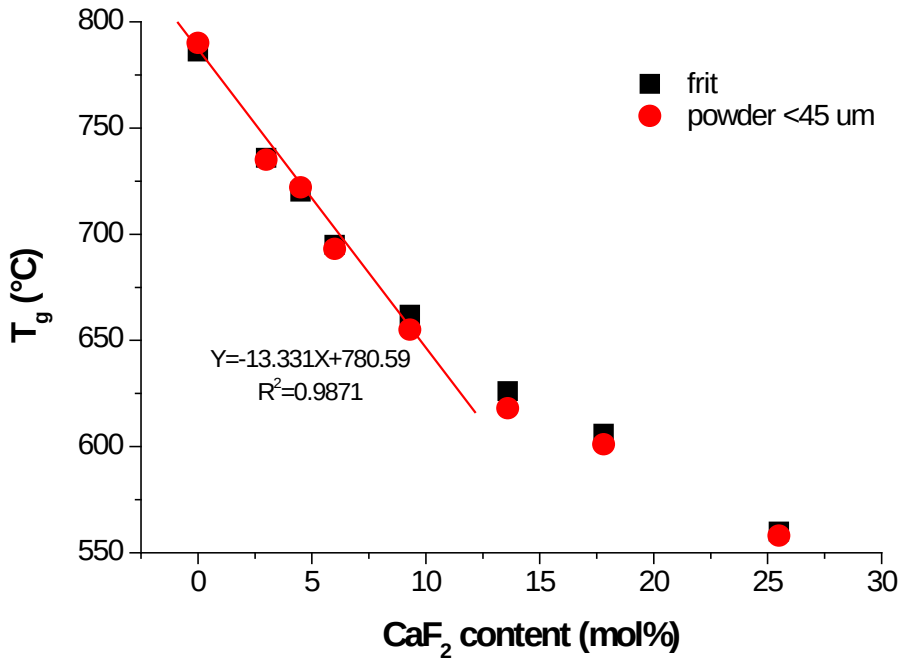

Figure 5.1.7 Glass transition temperature profiled as a function of CaF_2 content. A linear relationship (Y=-13.331X+780.59, R^2=0.9871) between T_g and CaF_2 content was shown in the glasses with CaF_2 content ≤ 9.3 mol%.

Figure 5.1.8 plots T_{c1} for both glass frit and fine powder against CaF_2 content. T_{c1} values decrease significantly with an increase in CaF_2 content. As shown in Figure

5.1.8, apart from the 0.0 mol% CaF_2 containing glass, which exhibits a remarkable temperature difference between the T_{c1} for frit and powder, the rest of CaF_2 containing glasses show almost identical T_{c1} values for different particle sizes.

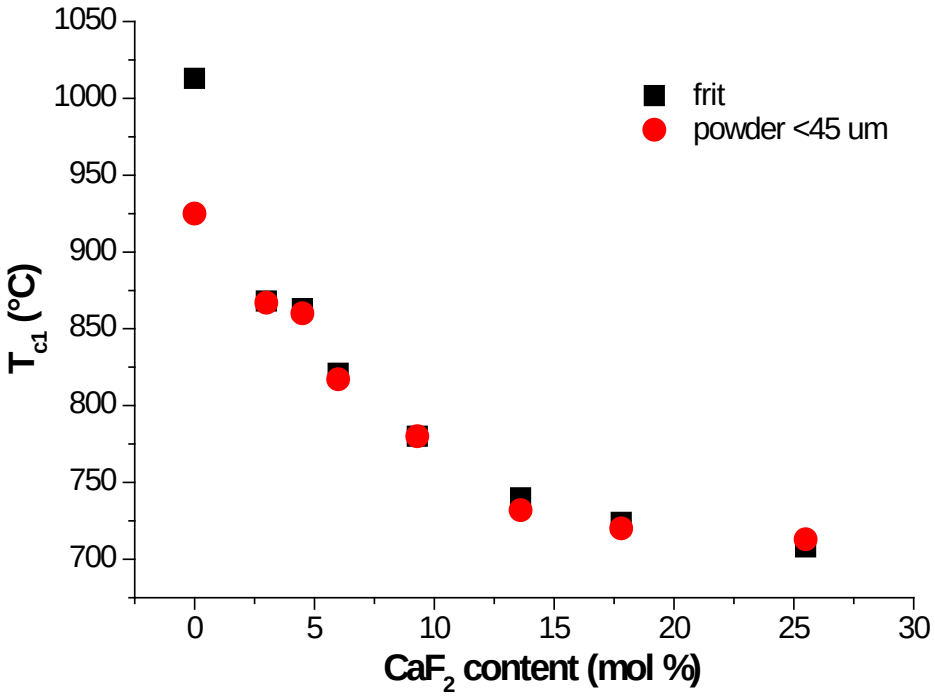

Figure 5.1.8 First crystallization peak temperature (T_{c1}) for frit and fine powder plotted against CaF_2 content.

5.2 Dissolution Study

5.2.1 pH Measurement Results

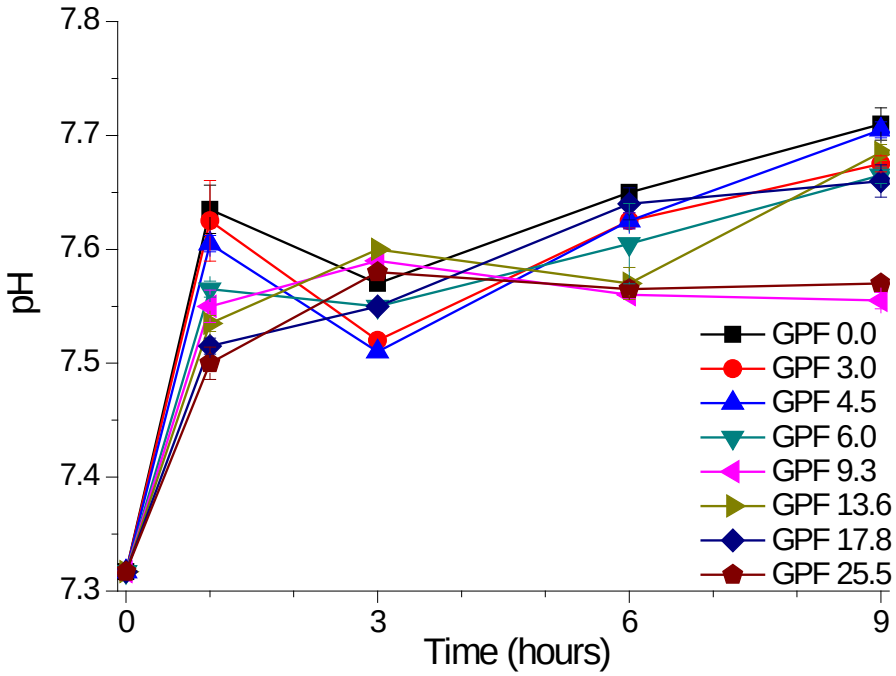

Figure 5.2.1 pH measured at the end of the immersion time in Tris buffer. The numbers are nominal molar percentage of CaF_2 in the compositions. Note where error bars are not shown they are smaller than the data point.

Figure 5.2.1 demonstrates pH changes after immersion the glass powder in Tris buffer for different immersion time. The general trend is similar for all the glass compositions. The data points are joined with solid lines, which help to illustrate the general trend of the data. Solid lines are applied for the same purpose throughout the thesis except for where linear trends are discussed. As shown in Figure 5.2.1, for the lower CaF_2 containing glasses (< 9.3 mol%), pH initially increases after 1 hour followed by a nearly stable pH between 1 and 6 hours with a further increase by 9 hours. For the glasses with CaF_2 content higher than 6.0 mol%, the pH typically increases in first 3 hours, decreases slightly from 3 to 6 hours and no significant change is found there afterwards. The pH became more alkaline after immersion as a consequence of ion exchange between protons and Ca^{2+} ions from glasses. Nevertheless, due to the

buffer capacity and the quantity of ions, which are available for ion exchange, pH does not increase all the time. Moreover, as major amount of calcium is released and the apatite-like phase starts forming, pH values do not increase any longer and may even decrease.

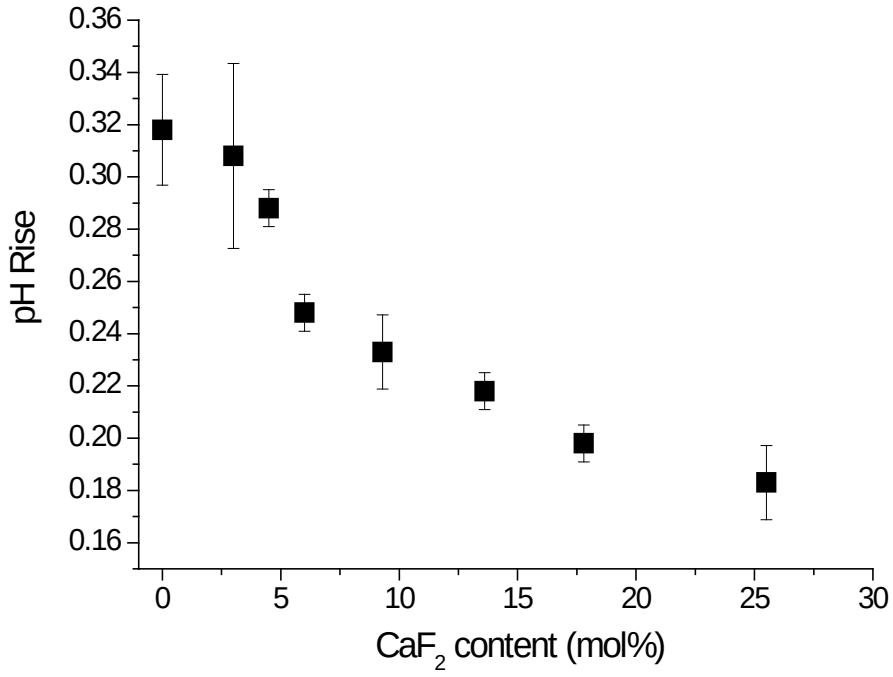

Figure 5.2.2 The pH rise in the solution after immersion of the glass powder in Tris (pH= 7.3) for 1h plotted against CaF_2 content.

It is interesting to note that the fluoride-free glass seems to show a more pronounced rise in pH after 1 hour immersion compared to the CaF_2 containing ones and a less significant pH rise is found in a higher CaF_2 containing glass (Figure 5.2.2). These are consistent with the effects of fluoride incorporated into a bioactive glass to reduce an increase in pH on initial dissolution, which was previously seen and discussed [20, 118].

5.2.2 Ion Release Results

The assessment of glass degradation was performed by measuring the concentration of the ions released into the buffer solutions using Inductively Coupled Plasma Optical Emission Spectroscopy and F^- ion selective electrode.

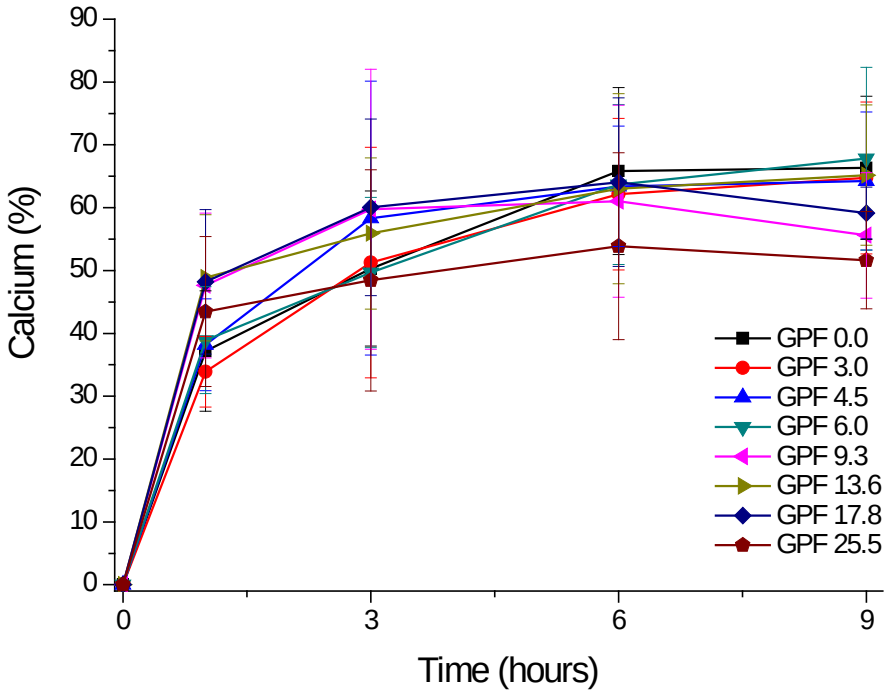

Figure 5.2.3 The concentration of elemental calcium in Tris presented as percentage of the total calcium content in the original CaF_2 containing glasses as a function of time.

The concentrations of Ca^{2+} ion measured after up to 9 hours immersion in Tris buffer presented as a percentage of total amounts of calcium in the nominal glass compositions are shown in Figure 5.2.3. The general trend is similar for all the glass compositions. The calcium concentrations increased to 33-48% after 1 hour; reached 50-60% after 3 hours; was over 60% at 6 hours and remained nearly the same after 9 hours. Thus the percentage of Ca cations released increased significantly from 1hour to 6 hours indicating continuing glass degradation.

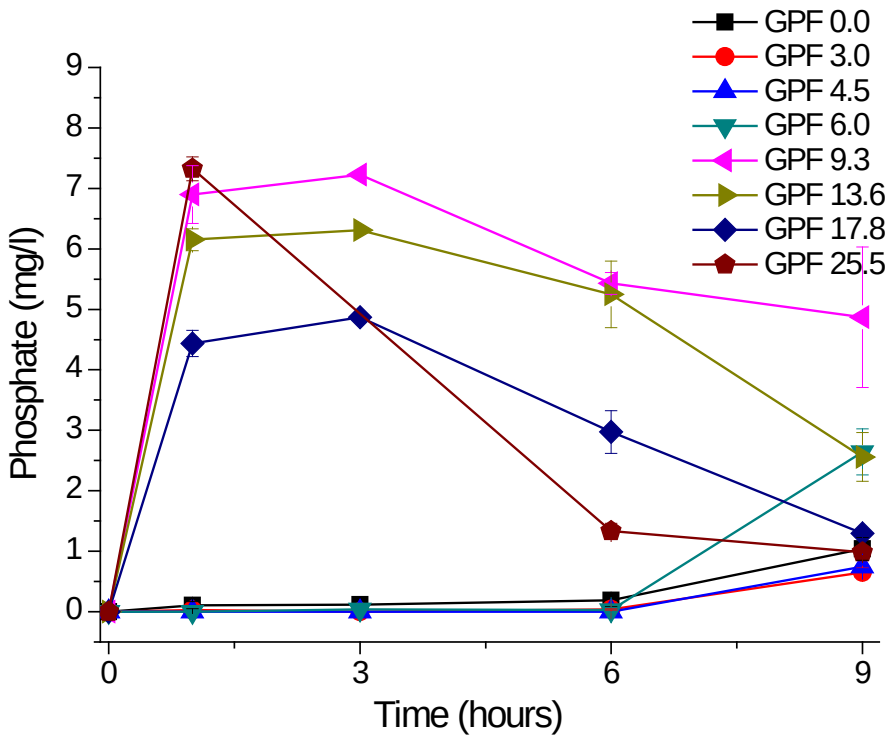

Figure 5.2.4 The concentration of phosphate measured after up to 9 hours immersion in Tris for CaF_2 containing glasses.

Figure 5.2.4 presents the concentration of phosphate for CaF_2 containing glasses in Tris up to 9 hours immersion. It is clear that two different trends are found according to whether glasses were amorphous or partially crystallised. In the case of amorphous glasses (≤ 6.0 mol% CaF_2), very low concentrations (less than 3 mg/l) of phosphate in solution were detected. In the case of partially crystallised glasses, relatively higher concentrations (up to 7.5 mg/l) after 1 hour, followed by a decrease afterwards were obtained. This reduction is consistent with the consumption of phosphate for apatite-like phase formation.

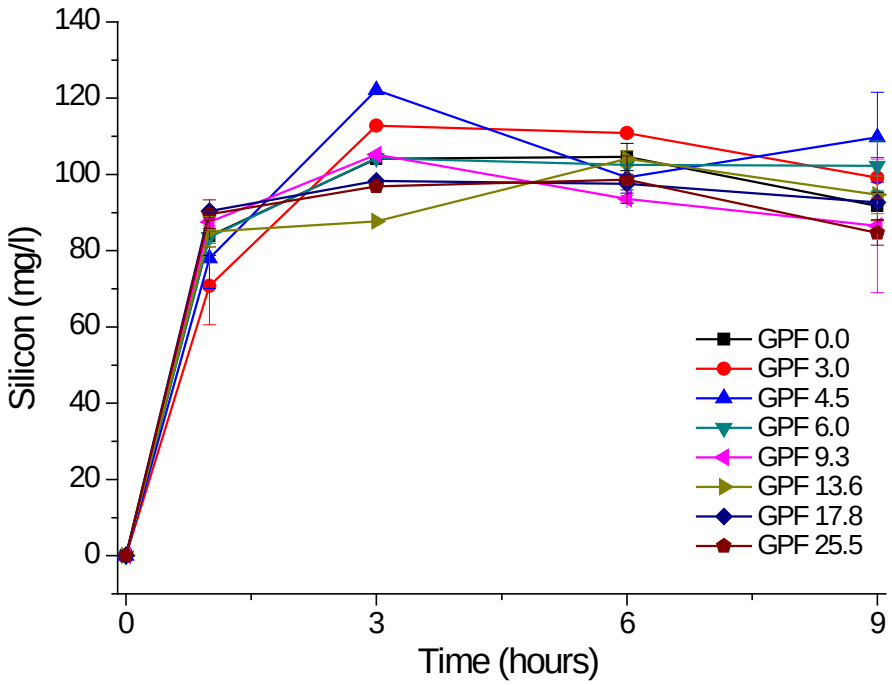

Figure 5.2.5 The concentration of silicon measured in Tris buffer in mg/l plotted as a function of immersion time.

Concentrations of silicon in Tris buffer after the immersion of glass powder within 9 hours for CaF_2 containing glasses have similar trends to the release of calcium (Figure 5.2.5). The silicon concentration measured remained nearly constant after the concentration reaches around 90 mg/l in first 3 hours, with a rapid silicon release particularly within 1 hour.

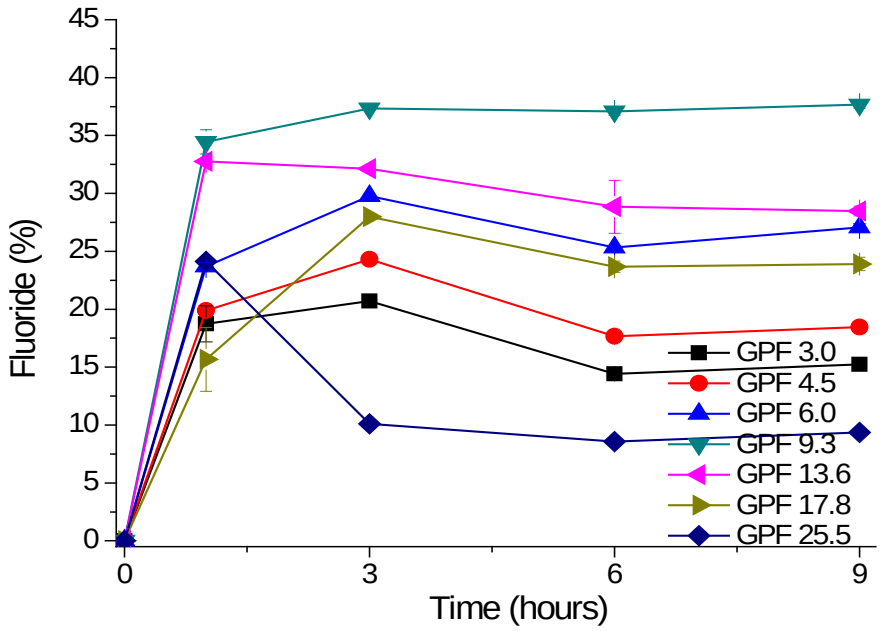

Figure 5.2.6 The concentration of fluoride measured after immersion glass powder in Tris buffer plotted as a percentage of total amounts of fluoride in the glass composition against the immersion time. Note where error bars are not shown they are smaller than the data point.

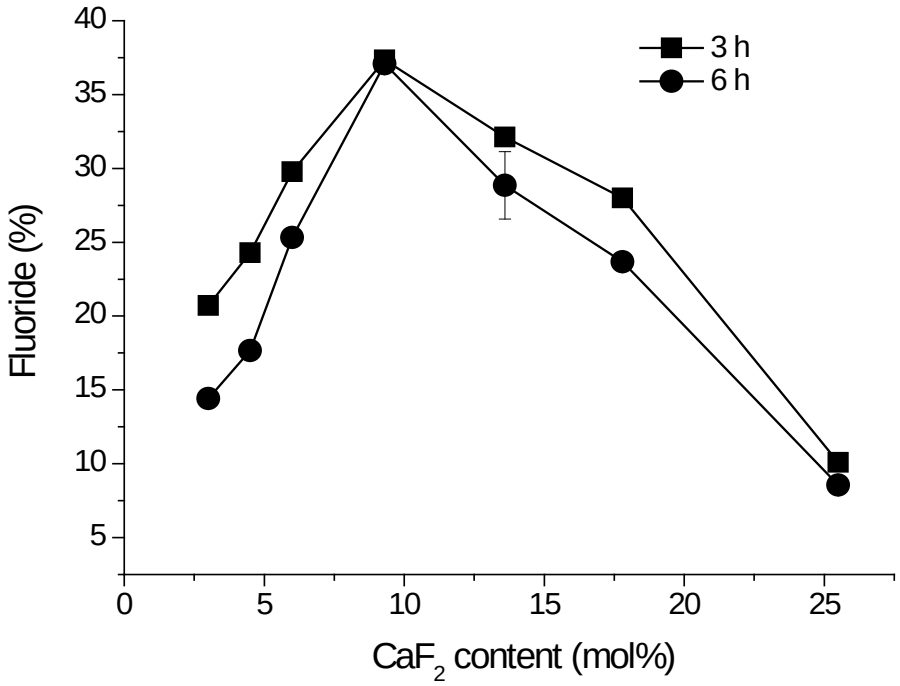

Figure 5.2.7 The percentage of fluoride concentration measured at 3 and 6 h in Tris for CaF_2 containing glasses. Note where error bars are not shown they are smaller than the data point.

The fluoride ion concentrations measured after immersion time in Tris presented as a percentage of total amount of fluoride in the nominal glass composition against different immersion times are shown in Figure 5.2.6. The trends of fluoride concentration in solution for different glass compositions are quite similar. The level of fluoride release increases in the first three hours of immersion then decreases at 6 hours and is almost identical after 9 hours. However, the release of fluoride is not identical for all the glass compositions, in the case of amorphous glasses (3.0, 4.5 and 6.0 mol%), the more fluoride is present in the nominal glass composition, the higher percentage of fluoride in the solution is seen. In contrast, for those partially crystallised glasses (> 6.0 mol% CaF_2), the lower percentage of fluoride in the solution is found in higher fluoride containing glasses.

In Figure 5.2.7, the fluoride concentration measured after 3 and 6 hours of immersion in Tris plotted as a percentage of total amounts of fluoride in the glass composition against CaF_2 content. Apart from the different trends of fluoride ion concentration between amorphous glasses and that of partially crystallised one discussed above, we can also see a small reduction of fluoride concentrations from 3 hours immersion to 6 hours, indicating the possibility of a fluoride consumption by forming a fluoride containing phase, which is fluorapatite or/ and fluorite. The highest percentage of fluoride in solution (over 35% of the nominal fluoride content in the glass) is observed for the glass with 9.3 mol% CaF_2. However, the lowest percentage of fluoride (about 10%) is seen for the glass with the highest fluoride content (25.5 mol%), most of the fluoride in this original composition is present in the crystalline phases as shown from its ^{19}F MAS-NMR spectrum in Figure 5.1.4 and after immersion the soluble fluoride was also consumed to form more CaF_2 as we can see an increasing intensity of CaF_2 after immersion from XRD patterns (in Appendix, Figure 11.2.1). It is seen that the percentage of fluoride released increases with an increase in fluoride content in the glass as long as fluoride remains in the amorphous glass. Once a fluoride containing phase starts crystallising from the glass, the fluoride concentrations decrease. This

suggests that the amorphous fluoride containing glass phase is the primary source of the fluoride release, rather than the crystalline phase.

5.3 Apatite-like Phase Formation in Tris Buffer and SBF Buffer Solution

The apatite-like phase formation on immersion in Tris buffer and SBF buffer solution was evaluated using XRD, FTIR and ^{31}P and ^{19}F MAS-NMR.

5.3.1 X-ray Diffraction Results

XRD results of three glass compositions (GPF 0.0, GPF 4.5, GPF 17.8) after immersion in Tris and SBF were are selected and presented in Figure 5.3.1- Figure 5.3.6. The as-quenched glasses with 0.0 and 4.5 mol% CaF_2 were amorphous, whereas the glass with 17.8 mol% CaF_2 was largely crystallised. An apatite-like phase is expected to be formed after immersing the CaF_2 containing bioactive glasses in buffer solutions.

Clear characteristic peaks of apatite are observed at 25.9° and 31.8° 2θ after 3 h immersion in Tris and 9 h in SBF (Figure 5.3.1-Figure 5.3.4), indicating apatite-like phase formation within 3 h immersion in Tris and 9 h in SBF. The diffraction lines intensify with an increase in immersion time to 9 h in Tris and 1 day in SBF. However, the intensities increase more rapidly in Tris compared to SBF. A further increase in immersion time after 9 h in Tris and 3 days in SBF does not show any significant changes in the XRD patterns. Similar results were obtained for other compositions with 3.0 and 6.0 mol% CaF_2.

The 17.8 mol% CaF_2 containing glass, which crystallised to mainly fluorapatite also exhibits bioactivity. Compared to the as-quenched glass, the intensity of the apatite diffraction lines grows after immersion. Unlike the amorphous glasses (≤ 6.0 mol% CaF_2), there is no distinct difference in the intensity of the apatite diffraction lines

acquired in Tris or SBF for the same immersion time period. Similar results were obtained for other compositions with 9.3, 13.6 and 25.5 mol% CaF_2.

Owing to the presence of crystalline FAP in the as-quenched glasses with high CaF_2 content, it is clearly seen that the apatite diffraction lines are significantly broader for the glass with low CaF_2 content (Figure 5.3.1 - Figure 5.3.4) than the ones for the glass compositions with high CaF_2 content (Figure 5.3.5 and Figure 5.3.6). It is possible that FAP crystals in the initial glasses may serve as nuclei for the apatite-like phase formation during immersion. Thus, in this case the newly formed apatite-like crystals deposited on the surface of the pre-existing apatite phases.

In addition, the XRD patterns also suggest that the crystalline phase of cuspidine in the as-quenched glass-ceramics (17.8 and 25.5 mol% CaF_2) dissolve in the buffer solutions, though slower in SBF compared to the Tris solution, as we can see the intensity of the diffraction lines for cuspidine disappear after 1 day immersion in Tris and 7 days in SBF, whereas, the diffraction lines for CaF_2 are still visible on the XRD patterns of glasses after 7 day immersion in both of Tris and SBF.

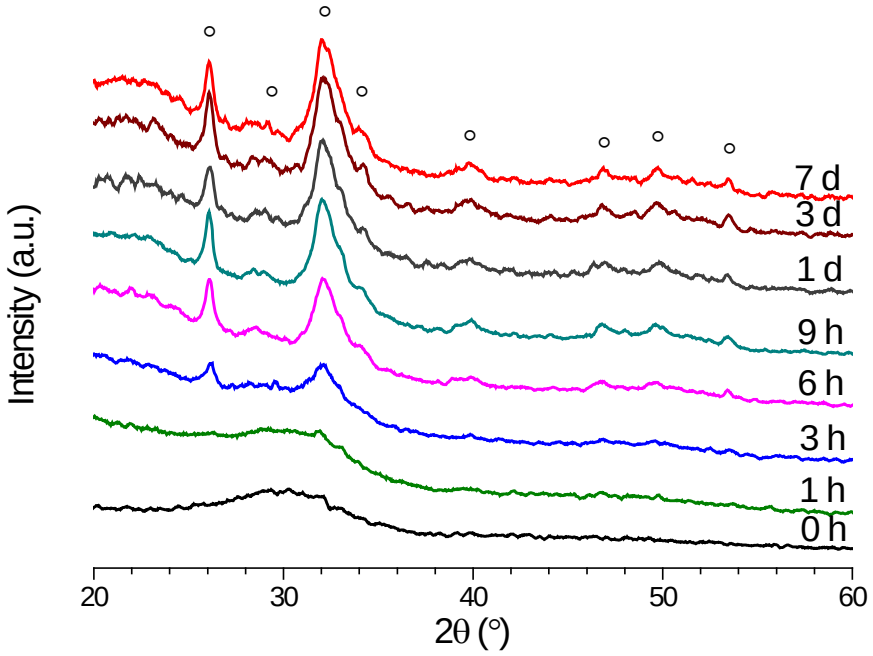

Figure 5.3.1 The XRD patterns of the glass precipitates with 0.0 mol% CaF_2 collected after immersion in Tris up to 1 week (°: $Ca_{10}(PO_4)_6(OH)_2$).

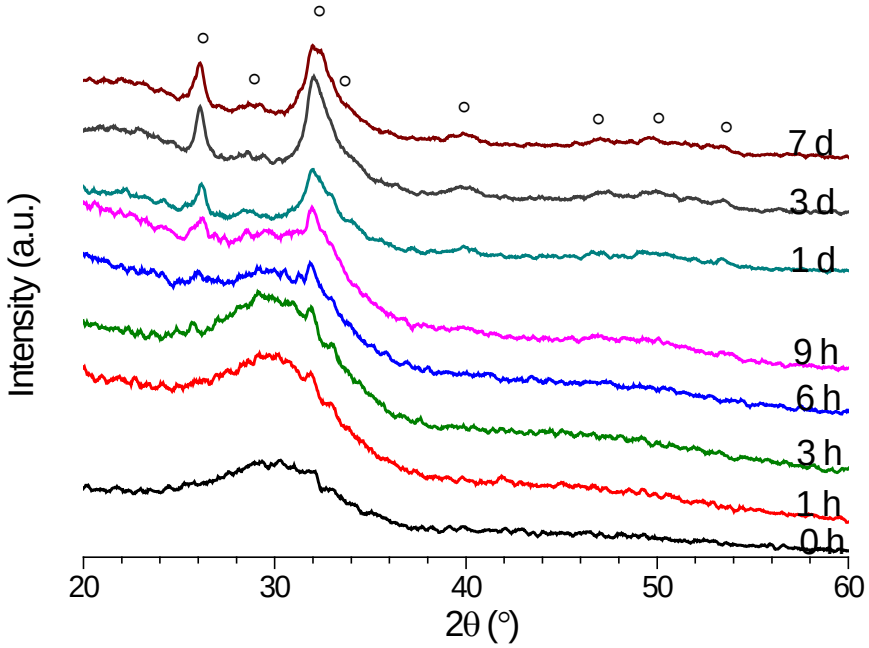

Figure 5.3.2 The XRD patterns of the glass precipitates with 0.0 mol% CaF_2 collected after immersion in SBF up to 1 week (°: $Ca_{10}(PO_4)_6(OH)_2$).

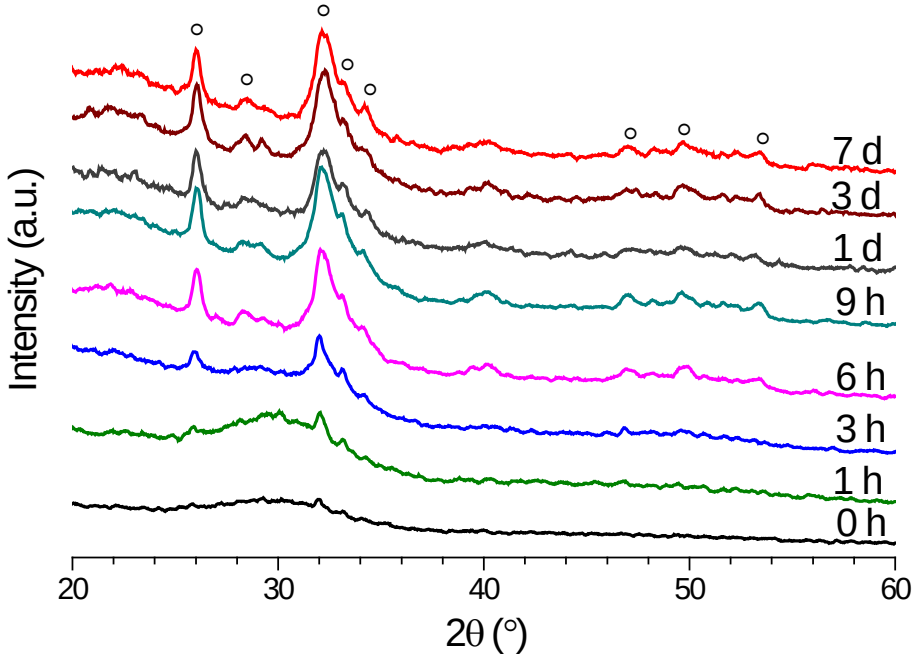

Figure 5.3.3 The XRD patterns of the glass precipitates with 4.5 mol% CaF_2 collected after immersion in Tris up to 1 week (°: $Ca_{10}(PO_4)_6F_2$).

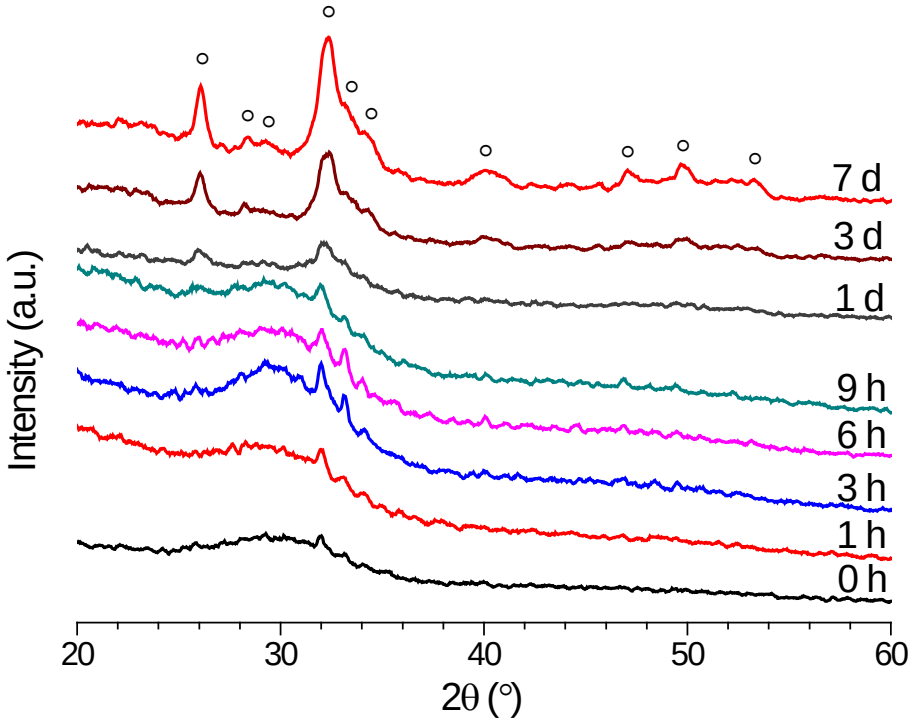

Figure 5.3.4 The XRD patterns of the glass precipitates with 4.5 mol% CaF_2 collected after immersion in SBF up to 1 week (°: $Ca_{10}(PO_4)_6F_2$).

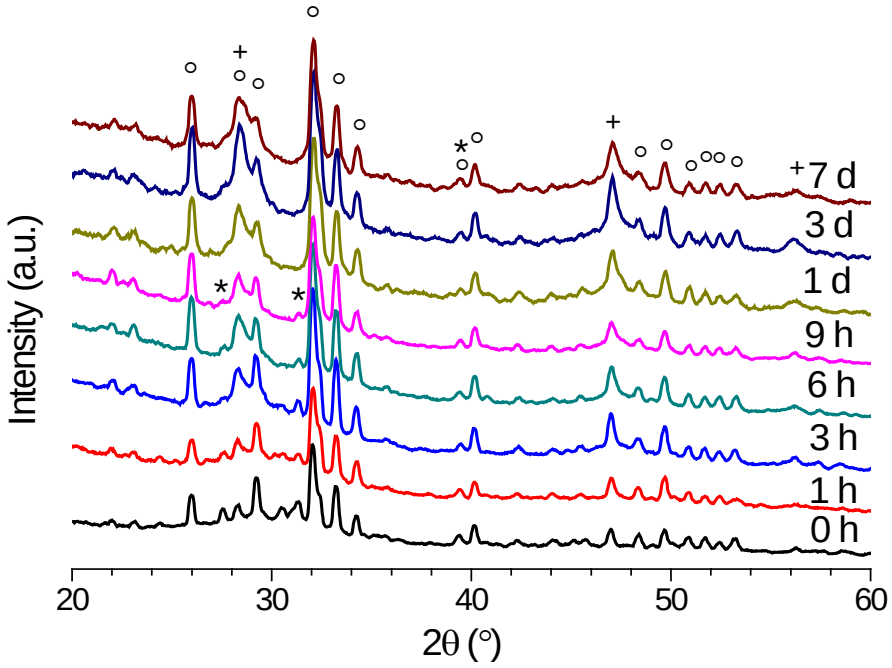

Figure 5.3.5 The XRD patterns of the glass precipitates with 17.8 mol% CaF_2 collected after immersion in Tris up to 1 week (°: $Ca_{10}(PO_4)_6F_2$; *: $Ca_4Si_2O_7F_2$; +: CaF_2).

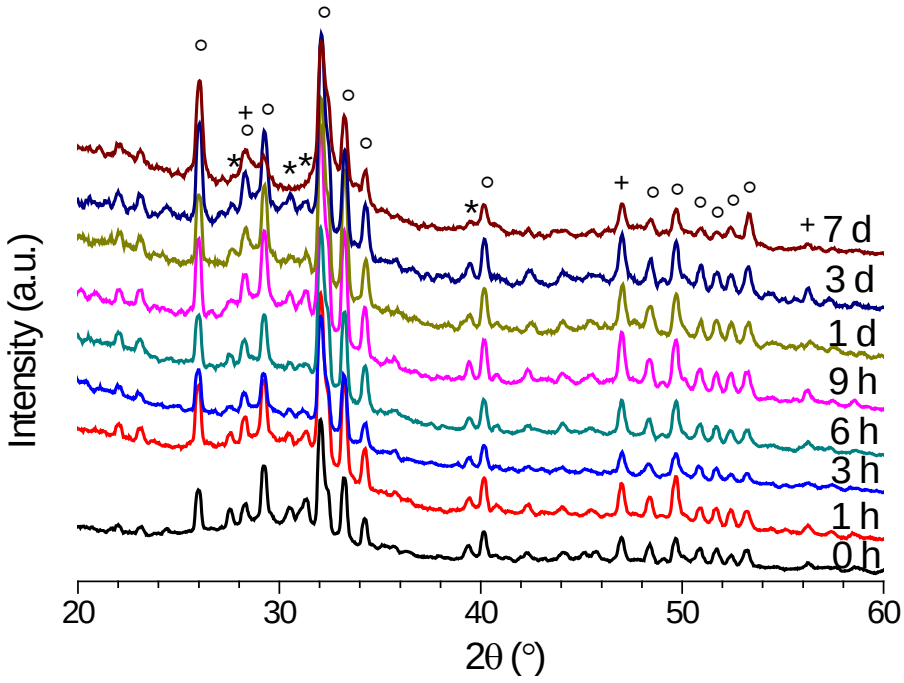

Figure 5.3.6 The XRD patterns of the glass precipitates with 17.8 mol% CaF_2 collected after immersion in SBF up to 1 week (°: $Ca_{10}(PO_4)_6F_2$; *: $Ca_4Si_2O_7F_2$; +: CaF_2).

5.3.2 Fourier Transform Infrared Spectroscopy Results.

Glass degradation and apatite-like phase formation upon immersion of glasses in buffer solution were monitored by using FTIR. Figure 5.3.7- Figure 5.3.12 demonstrate the FTIR results for the same three compositions that were chosen for the XRD results. The spectrum at the bottom of each figure belongs to the as-quenched glass and was discussed above. Glass degradation and apatite formation occurred rapidly when the glasses were immersed in buffer solutions, which resulted in dramatic changes in the FTIR spectra. The intensity of non-bridging oxygen $Si\text{-}O^-$ band at 920 cm^{-1} reduces after 1 h immersion in both of Tris and SBF and disappears at longer immersion times, indicating rapid glass degradation. After immersion, the spectra show sharpening of the band at 1035 cm^{-1}, which is assigned to both of Si-O-Si and crystalline orthophosphate. The formation of crystalline orthophosphate also leads to a development of the shoulder at about 1100 cm^{-1} [9, 20]. In addition, instead of a broad peak at 565 cm^{-1} the typical apatite split bands develops at 613 cm^{-1} and 560 cm^{-1} after 3 h immersion in Tris and 9 h in SBF. The presence of crystalline apatite is also suggested based on another band at about 960 cm^{-1} in the spectra, which corresponds to the P-O stretch in the orthophosphate tetrahedron. Owing to the substitution of carbonate in the apatite-like phase, carbonate bands at 1450 cm^{-1}, 1420 cm^{-1} and 870 cm^{-1} are found [119]. The band at 790 cm^{-1} appearing in the spectra after immersion is assigned to Si-O-Si between the two adjacent silicate tetrahedra [20, 120]. This forms as a result of condensation reactions during glass degradation and essentially presents as a silica-gel. The typical apatite bands at 1035, 613 and 560 cm^{-1} sharpen and intensify with an increase in immersion period, however, no significant difference can be seen in the spectra after 9 h immersion in Tris and 1 day in SBF. Similar results are obtained for GPF 3.0 and GPF 6.0.

The changes in FTIR spectra before and after immersion for glass GPF 17.8 (Figure 5.3.11 and Figure 5.3.12) are similar to the one observed for GPF 0.0 or GPF 4.5. The spectrum of the untreated glass reveals the presence of crystalline apatite in addition

to the Si-O vibration bands. Upon immersion, the decrease of intensity for non-bridging oxygen $Si\text{-}O^-$ band at 920 cm^{-1} and the sharpening of crystalline apatite bands were noticed due to glass degradation and further apatite-like phase formation. These changes are identical for other high CaF_2 containing glasses (9.3, 13.6 and 25.5 mol%) after immersion in buffer solution. However, the sharpening of the bands for glasses GPF 9.3 and GPF 13.6 occur at earlier time points after immersion in Tris than SBF, while no significant difference was seen for GPF 17.8 and GPF 25.5 in Tris and SBF.

FTIR spectroscopy characterises both amorphous and crystalline species presenting in solids, unlike XRD, which generally reveals changes in the crystalline domains of a solid only. The wavenumber of FTIR band wavenumber values with the assignments for glass and apatite is summarised in Table 5.3.1. The presented FTIR results indicate that glass dissolution may occur faster in Tris buffer than in SBF for amorphous and partially crystallised bioactive silicate glasses.

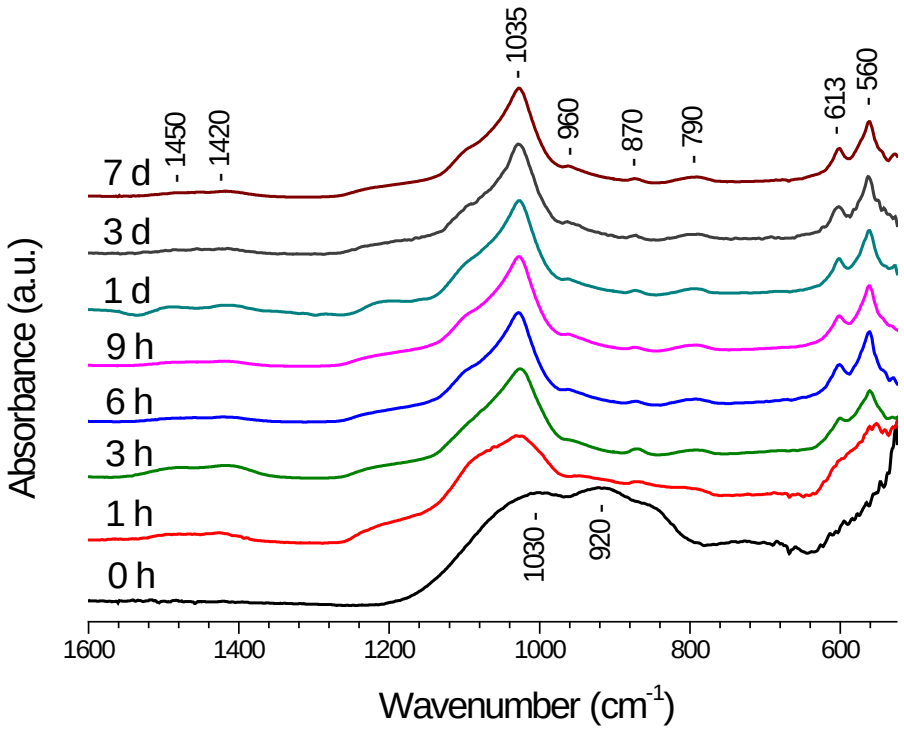

Figure 5.3.7 The FTIR spectra of the glass precipitates with 0.0 mol% CaF_2 collected after immersion in Tris up to 1 week

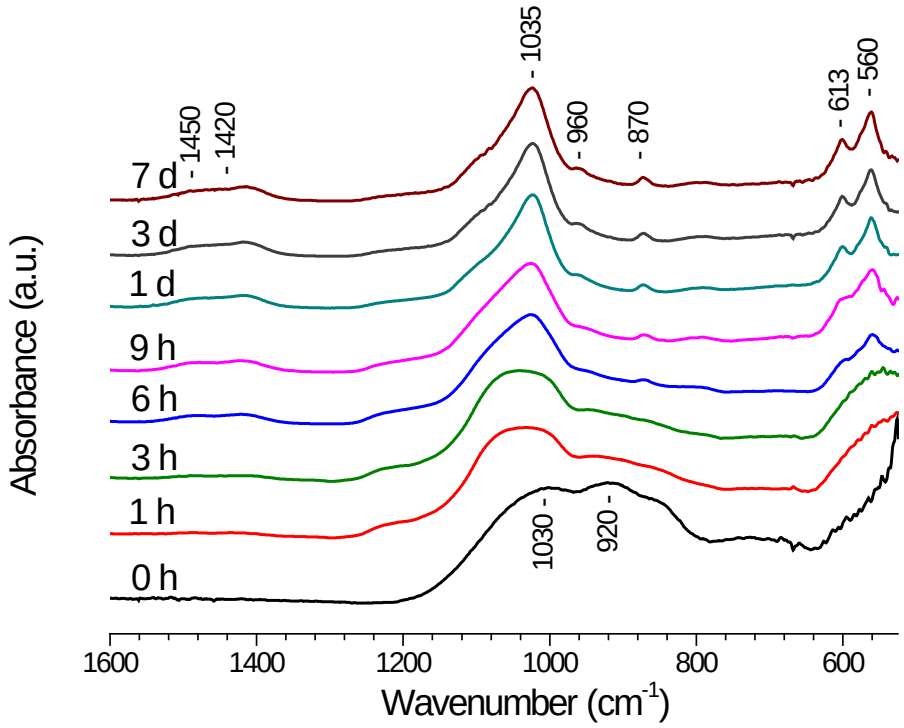

Figure 5.3.8 The FTIR spectra of the glass precipitates with 0.0 mol% CaF_2 collected after immersion in SBF up to 1 week

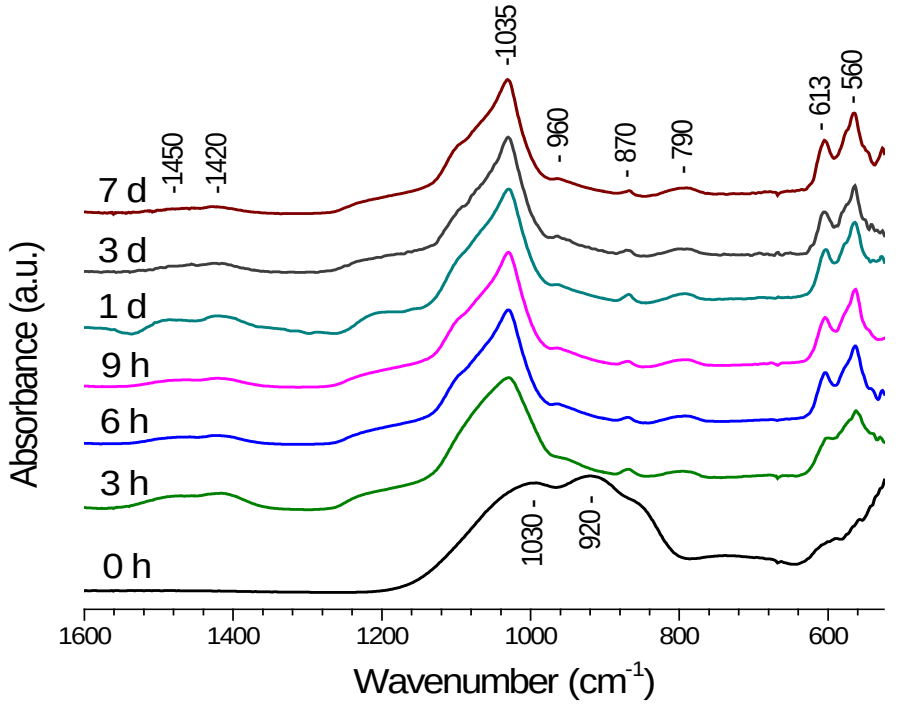

Figure 5.3.9 The FTIR spectra of the glass precipitates with 4.5 mol% CaF_2 collected after immersion in Tris up to 1 week

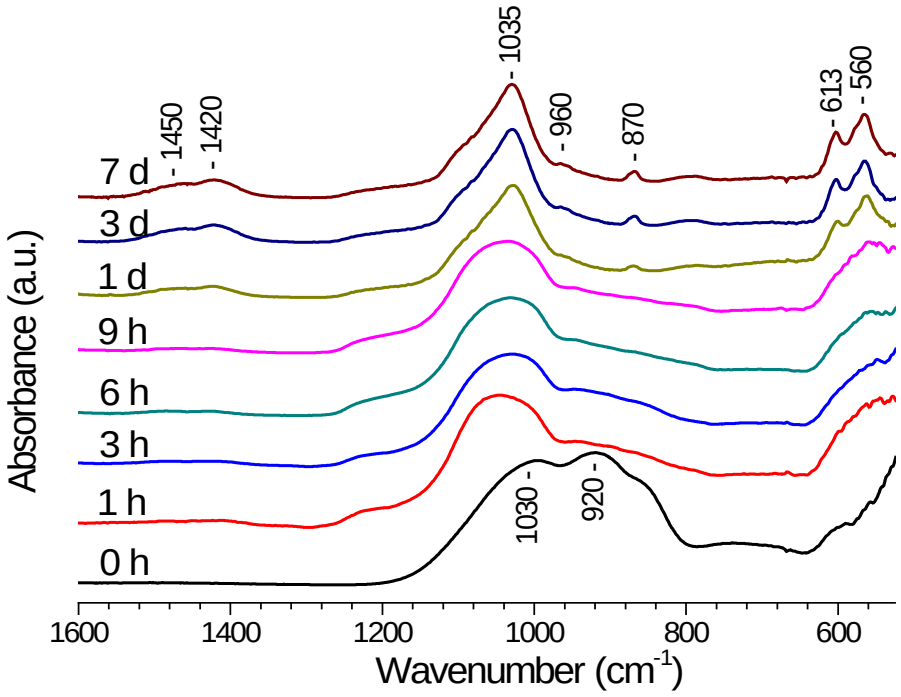

Figure 5.3.10 The FTIR spectra of the glass precipitates with 4.5 mol% CaF_2 collected after immersion in SBF up to 1 week

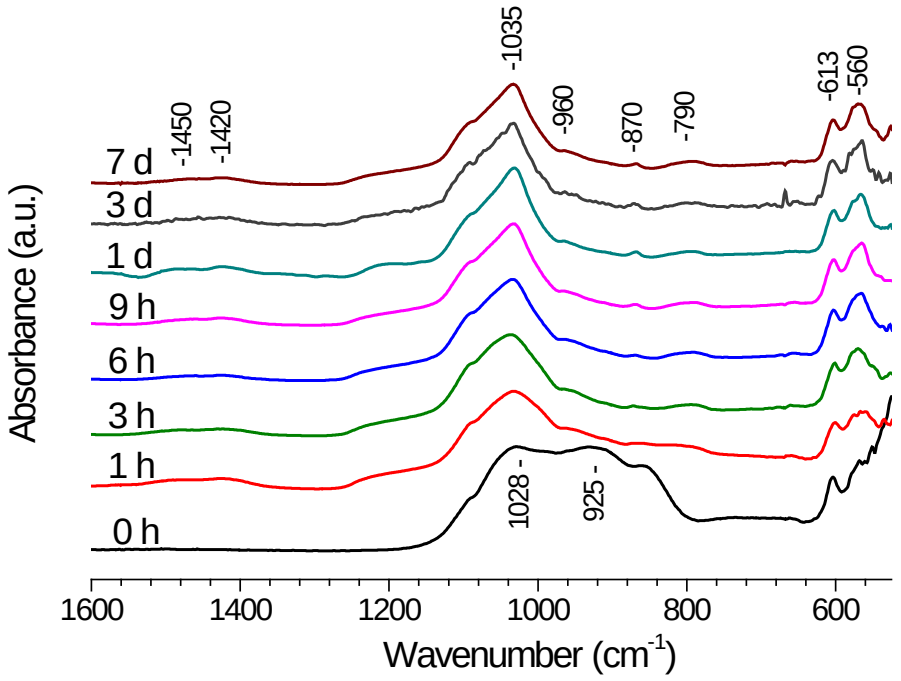

Figure 5.3.11 The FTIR spectra of the glass precipitates with 17.8 mol% CaF_2 collected after immersion in Tris up to 1 week

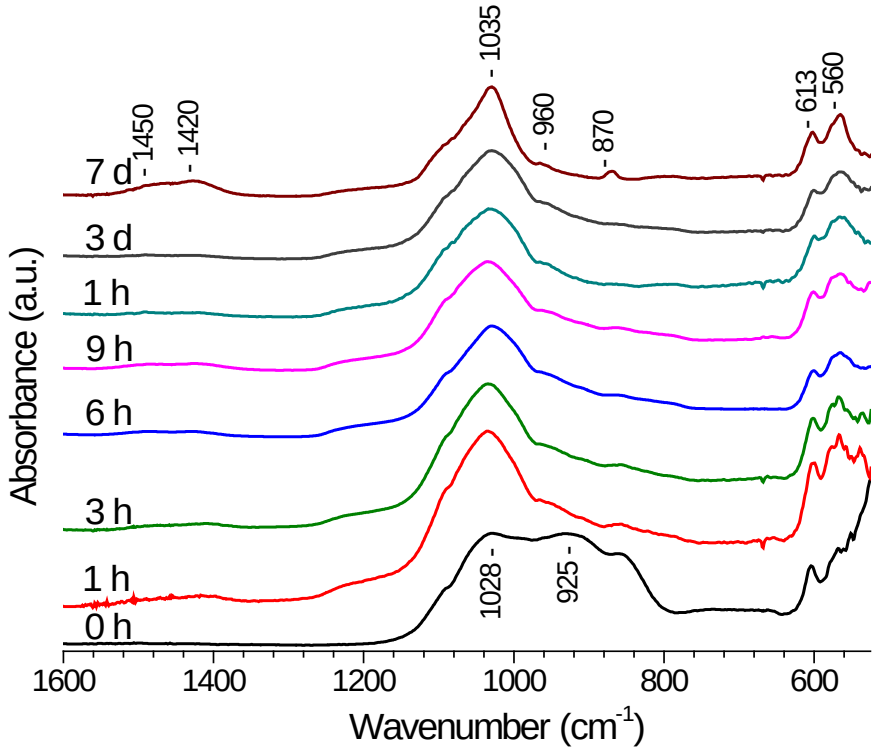

Figure 5.3.12 The FTIR spectra of the glass precipitates with 17.8 mol% CaF_2 collected after immersion in SBF up to 1 week

Table 5.3.1 The FTIR band wavenumber values with the assignments for glasses

	Wavenumber / cm^{-1}	Band
Amorphous glass	1028/ 1030	Si-O-Si
	920	Si-O(NBO)
	565	P-O
Apatite	613 and 560	P-O
	960/ 1035 and 1100	P-O(s)
	870 and 1420,1450	β type C-O

5.3.3 NMR Results of CaF_2 Series Glasses

^{31}P and ^{19}F MAS-NMR were employed to investigate the atomic environments of phosphate and fluoride in the collected precipitates and confirm the formation of an apatite-like phase on immersion.

The ^{31}P MAS-NMR spectra of glass GPF 4.5 before and after immersion in Tris and SBF are presented in Figure 5.3.13 and Figure 5.3.14. The spectra all show a single

peak with a centre at 3.0 ppm, assigned to calcium orthophosphate. Prior to immersion, the peak is relatively broad, suggesting an amorphous orthophosphate environment. After 3 hours immersion in Tris, the line-width of the spectra reduces and further decreases with immersion time, but no changes in the chemical shifts are observed. This implies that amorphous orthophosphate converts to apatite (crystalline orthophosphate) on immersion and apatite-like phase forms within 3 hours of immersion in Tris. Only a small decrease in the line-width of spectra is found after immersion in SBF. The spectra for the rest of the glasses in this series show similar evolution.

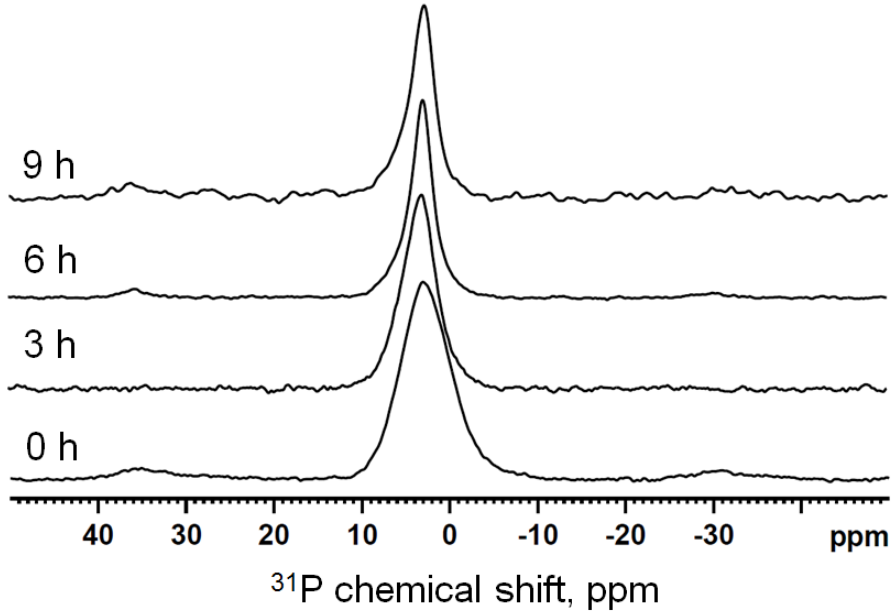

Figure 5.3.13 The ^{31}P MAS-NMR spectra of the glass precipitates with 4.5 mol% CaF_2 collected after immersion in Tris. The bottom spectrum is for the untreated glass powder. The numbers are immersion times.

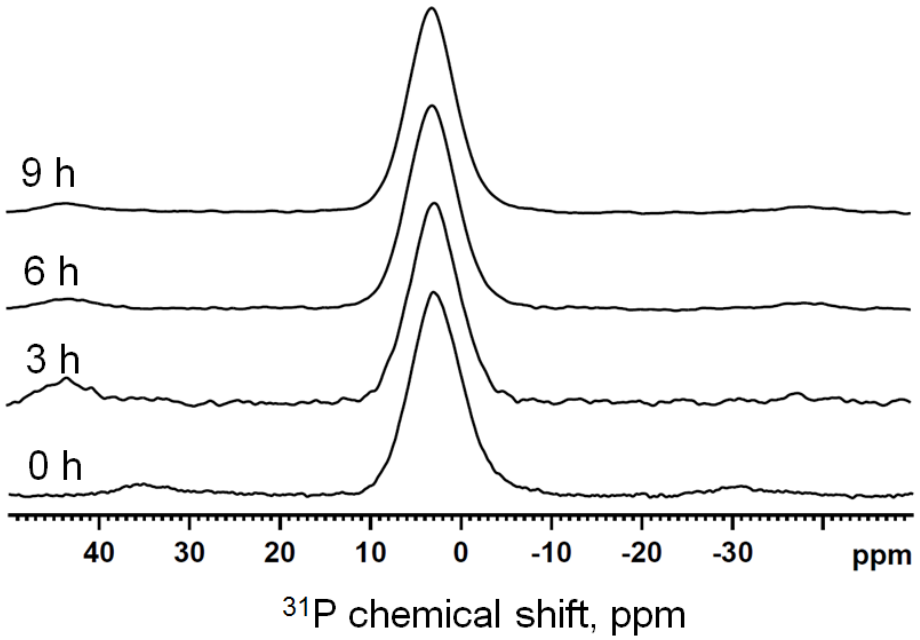

Figure 5.3.14 The ^{31}P MAS-NMR spectra of the glass precipitates with 4.5 mol% CaF_2 collected after immersion in SBF. The bottom spectrum is for the untreated glass powder. The numbers are immersion times

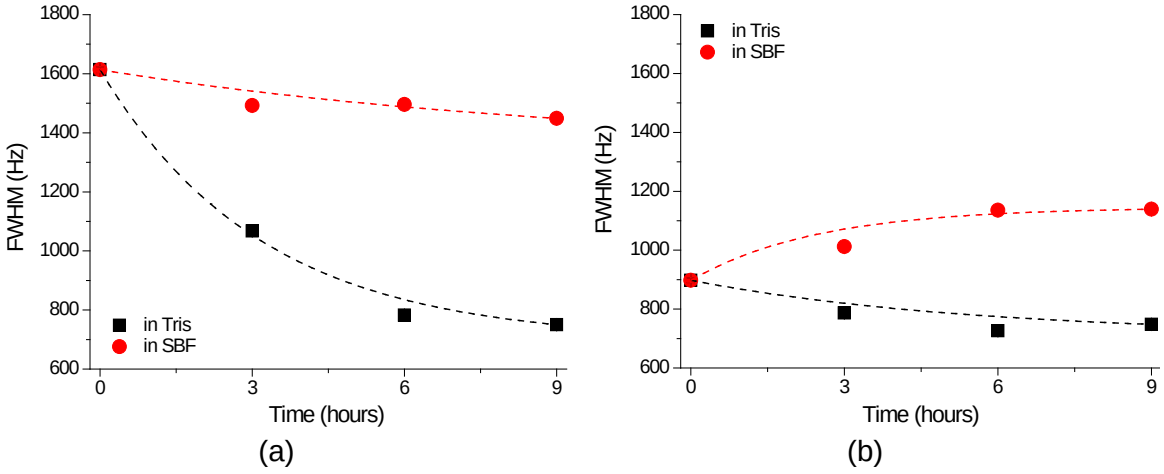

Figure 5.3.15 FWHM for ^{31}P MAS-NMR spectra plotted against immersion time, (a) for GPF 4.5; (b) for GPF 13.6. The estimated errors (10 Hz) are smaller than the data points.

The full width half maximum (FWHM) of ^{31}P MAS-NMR spectra for 4.5 (amorphous) and 13.6 (crystallised) mol% CaF_2 containing glasses on immersion in Tris and SBF were estimated by using Bruker Top-Spin software and plotted as a function of immersion time (Figure 5.3.15 (a) and (b)). The statistically significant difference of the

results between different groups was carried by Student's t-test. P value less than 0.05 was considered to be significant. The obtained P values were summarized in Table 11.2.2 (in Appendix). In general, the changes of FWHM before and after immersion for both glasses in SBF are smaller compared to the changes of the line-width in Tris. In addition, the line-width of the signal for the initially amorphous glass is wider than the partially crystallised one; therefore, the changes of line-width for amorphous glasses were more distinct than the partially crystallised glasses. As described previously, the FWHM of GPF 4.5 in Tris decreases with an increase of immersion time up to 9 hours, while the reduction of FWHM for GPF 13.6 mainly occurs within 6 hours immersion in Tris. An increase of FWHM is seen after up to 6 hours immersion in SBF. After 6 hours immersion the FWHM for GPF 13.6 remains nearly constant in both Tris and SBF. The increase of FWHM for the crystallised glass in SBF might be contributed to by forming a more disordered fluorapatite by the possibility of the presence of CO_3^{2-} in the apatite lattice after immersion compared with the fluorapatite crystallised during quenching.

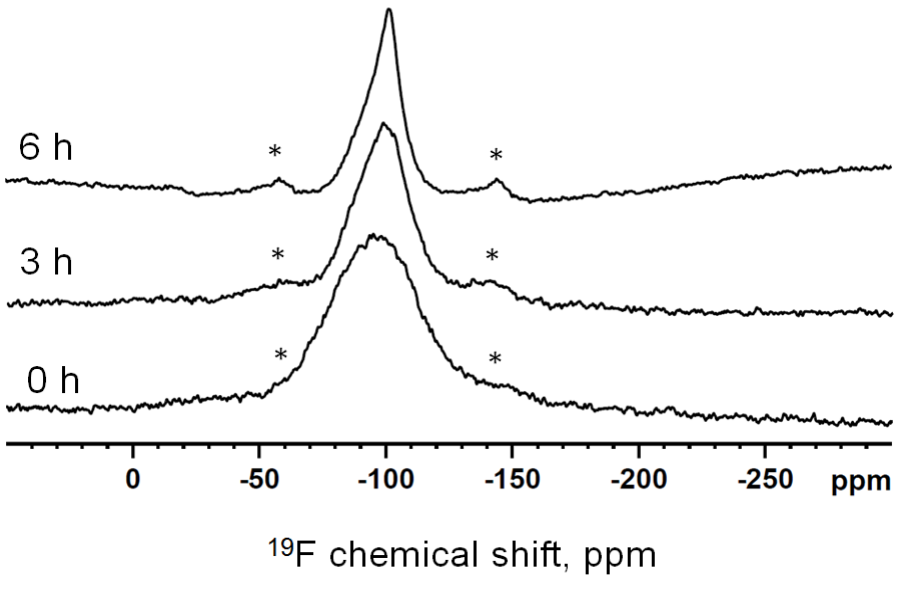

Figure 5.3.16 The ^{19}F MAS-NMR spectra of the glass precipitate with 4.5 mol% CaF_2 collected after immersion in Tris, the signals symmetrically situated on both sides of the main signal and labelled by asterisk present side bands.

Figure 5.3.16 presents the ^{19}F MAS-NMR spectra of glass GPF 4.5 immersed in Tris up to 6 hours compared to the as-quenched glass. The symmetrical signals labelled by asterisks are side bands. The broad peak at -96 ppm in the spectrum of the as-quenched glass was shown and discussed above. After 3 hours immersion, the line-width of ^{19}F NMR peak decreases, in agreement with the ^{31}P MAS-NMR results and the peak shifts towards -103 ppm. A sharp feature at about -103 ppm which is found by 6 hours immersion is attributed to the F-Ca(3) fluorapatite environment [4].

Further Discussion

The incorporation of fluoride leads to a significant reduction of the glass transition temperature and crystallisation temperature. These effects can both be associated with fluoride complexing calcium [4]. In the fluoride-free glass (GPF 0.0), divalent calcium ions bind together silicate anions by electrostatic forces and the calcium ions can effectively ionically bridge two non-bridging oxygens (NBOs), therefore it is less disruptive to the glass work compared to two sodium ions [10, 79]. Thus, the sodium-free glass has relatively high T_g and T_c. When CaF_2 is introduced, hypothetical 'CaF^+' species, which acts like a Na^+ cation forms and thus the electrostatic forces between NBOs reduces considerably, resulting in a decrease in T_g and T_c [4, 121]. The effect of CaF_2 on T_g is less pronounced at high fluoride contents as shown by the break in T_g dependence in Figure 5.1.7. This could be ascribed to the crystallisation of fluoride containing phases, which are FAP, $Ca_4Si_2O_7F_2$ and CaF_2 during quenching.

The XRD patterns, FTIR spectra and NMR spectra of the as-quenched glasses consistently indicate an increasing crystallisation tendency of the glasses with increasing CaF_2 content, where fluorapatite, cuspidine and fluorite crystallised successively.

The single peak with chemical shift around 3 ppm in the ^{31}P MAS-NMR spectra suggests that in the studied sodium-free fluoride containing bioactive glasses phosphorus is present as an orthophosphate charge balanced with Ca^{2+} [20, 122]. ^{19}F

MAS-NMR spectra confirm the presence of amorphous F-Ca(n) species in low CaF_2 containing glasses, spontaneous crystallisation of FAP (F-Ca(3)) in the high CaF_2 (≥ 9.3 mol%) containing glasses and a clear crystallisation of CaF_2 with a F-Ca(4) environment for the glass with 25.5 mol% CaF_2 on quenching.

The presence of CaF_2 in the glasses has an opposite effect on the density compared to its effect on T_g and T_c. As shown in the Figure 5.1.5, the introduction of CaF_2 leads to an increase in glass density. Since CaF_2 was added into the glass composition rather than being substituted for CaO, the resultant glasses have constant network connectivity. In addition, the ^{19}F MAS-NMR spectra suggest that fluorine forms F-Ca(n) species in the glasses instead of forming Si-F bonds. Therefore, the density of glass is likely to consist of a combination of the densities of both silicate glass and CaF_2-like phase, as presented in the paper by Brauer *et al*. [123]. In all designed glasses, the proportion of each component in the silicate glass matrix is the same as GPF 0.0 and thus the density of silicate glass part is same. However, the density of CaF_2-like species is greater than the glass matrix (3.13 cf 2.94 g/cm^3). With an increase in CaF_2 content, the proportion of silicate part decreases and therefore results in a reduction of glass density.

The presence of significant amount of sodium oxide in the first discovered bioactive glass, 45S5 composition, 46.1SiO_2-2.6P_2O_5-26.9CaO-24.4Na_2O (mol%), suggests that sodium cations to play an essential role in mechanism of bioactivity. However, the results of FTIR, XRD and ^{31}P MAS-NMR experiments performed on the collected precipitates after the immersion of sodium-free glass powders in buffer solutions, along with the pronounced pH rise and early release of calcium, fluoride and silicon into Tris and SBF upon immersion, all consistently show that excellent bioactivity can be achieved in the glass compositions without the presence of sodium. In the case of the initially amorphous glasses containing relatively low fluoride (≤ 6.0 mol%), rapid glass degradation was clearly observed after 1 hour immersion and fast apatite-like phase

formation was found within 3 hours immersion in Tris and 9 hours in SBF. In the case of high fluoride (≥ 9.3 mol%) containing glasses, which are partially crystallised to an apatite-like phase during quenching, rapid glass degradation was also found after 1 hour immersion and an increased quantity of apatite occurred after 3 hours immersion in both of Tris and SBF. The rates of apatite formation are much higher than it is possible to achieve for the 45S5 glass composition, the latter contains large amount of sodium oxide and less than half amount of P_2O_5 than the glasses studied here and requires at least 24 hours of immersion under similar conditions for an apatite-like phase to form [50]. This result also illustrates that enhanced bioactivity can be achieved by having a higher phosphate content in the glass composition, as suggested by the earlier finding of Mneimne *et al.* [9] and by Eden [49].

The enhanced bioactivity of sodium-free glasses demonstrated here questions the initial steps of the accepted Hench mechanism of bioactivity. The mechanism of glass bioactivity involves two processes, the glass degradation and apatite formation. The role of sodium cations appeared to be essential in the classical mechanism, especially for the glass degradation part. The first step in the widely accepted Hench mechanism of bioactivity assumes an ion exchange between sodium cations from the glass and protons from solution, which then enables the next step, the alkaline hydrolysis of the Si-O-Si linkages with the formation of the silanol Si-OH groups at the interface between glass and solution.

In contrast, the results obtained here validate the view that these glasses are so sufficiently disrupted that it is not necessary for the Si-O-Si hydrolysis to occur [43]. The low level of polymerization or low network connectivity for this type of glasses controls the rate of glass degradation, rather than an ion exchange of the highly mobile alkali cations following by hydrolysis of Si-O-Si linkages. Thus, sodium is not necessarily an essential component of a bioactive glass.

For the dissolution studies in Tris buffer, due to the absence of ionic species in Tris buffer, the phosphate required for apatite formation originates entirely from the glass. Therefore, a high content of phosphate present as orthophosphate in the glass is beneficial for early apatite formation. The rapid glass degradation can be mirrored by the ionic concentration in the buffer solution. Interestingly, the phosphorus concentration measured after the immersion of glass powder into Tris buffer was low although an apatite-like phase formation was noticed at early immersion time. This indicates that phosphate might release at even earlier time points (< 1 hour) or in these sodium-free glasses the phosphate does not necessarily dissolve into the solution, prior to the precipitation of an apatite-like phase. The apatite formation could be achieved as consequence of phosphate re-arrangement in the glass without phosphate dissolution.

Experimental results suggest that apatite formation readily occurred within 3 hours of immersion in Tris buffer and 9 hours in SBF for all the studied glasses regardless of whether the glass was amorphous or partially crystalline. Moreover, the FTIR and ^{31}P MAS-NMR spectra, as well as XRD patterns were practically identical after 6 and 9 hours of immersion in Tris for the same sodium-free compositions, which suggests that reaction has been completed by 6 hours in Tris. This is also consistent with nearly constant concentration of silicon, calcium and fluoride ions measured in solution between 6 and 9 hours.

It is well known that a crystalline solid has a lower dissolution rate than the equivalent amorphous phase [124]. Therefore the crystalline ceramics are expected to exhibit a lower bioactivity than an amorphous glass. However, the studied glasses with CaF_2 content over 6.0 mol% that have partially crystallised to mainly FAP exhibit excellent bioactivity comparable to the amorphous glasses (≤ 6.0 mol% CaF_2). This is attributed to the fact that the existing FAP crystals reduce the activation energy required for forming apatite nuclei and serve as a seeding phase for further apatite crystal growth.

FAP is attractive in medical and dental applications, owing to its higher stability in acidic environment compared to hydroxyapatite. ^{19}F MAS-NMR was used to obtain evidence for the formation of fluorapatite upon immersion of these fluoride containing bioactive glasses. By comparison with the 3 hours apatite formation from the XRD, FTIR and ^{31}P NMR results, ^{19}F NMR results show clear fluorapatite formation after 6 hours for the amorphous glasses (GPF 3.0, GPF 4.5 and GPF 6.0), which is consistent with the decrease in fluoride concentration in solution between 3 and 6 hours (Figure 5.2.7), suggesting the consumption of fluoride for fluorapatite formation before 6 hours. These results suggest that an apatite-like phase formed after 3 hours does not necessarily contain a significant amount of fluoride in the apatite. It is probably exist as a hydroxyapatite in a big scale. A mixed hydroxy-fluorapatite is likely to exist between 3 and 6 hours immersion.

By comparison, the glass degradation and apatite formation rate are lower in SBF than Tris. This can be attributed to a higher ionic strength and lower ionic diffusion of the SBF solution, which suppresses the dissolution of ionic species and thus delays the glass dissolution [125]. However, it is more likely the presence of Mg^{2+} in SBF inhibits the apatite-like phase formation [22, 57]. Therefore, the direct comparison of the results in Tris buffer with the results in SBF buffer is not strictly comparable [126].

Summary

The sodium-free, high phosphate bioactive silicate glasses with different CaF_2 content have been synthesised. The crystallisation tendency of the glasses increases with increasing CaF_2 content. Glasses with CaF_2 contents less than 9.3 mol% are amorphous while the glasses with fluoride content above 6.0 mol% are partially crystallised. The presence of fluoride effectively reduces the glass transition temperature and crystallisation temperature, while increasing glass density. The amorphous glasses degrade rapidly and form an apatite-like phase within 3 hours (clear fluorapatite formation at 6 hours) in Tris and 9 hours in SBF. The partially

crystalline glasses show amorphous phase degradation and an increase in fraction of apatite-like phase by 3-6 hours in Tris and SBF. Therefore, sodium is not an essential component for enhanced bioactivity of glasses.

6 Sodium-Free $CaCl_2$ Containing Bioactive Glasses

Foreword

In addition to the benefits of fluoride for biomineralisation and formation of FAP discussed in the previous chapter, adding fluoride into a silicate glass typically reduces the glass melting temperature, glass transition temperature and potentially reduces the glass hardness [6, 27].

However, high fluoride content in bioactive glasses resulted in the uncontrolled crystallisation of calcium fluoride, rather than FAP on quenching. A fluoride content in the toothpaste for children is strictly controlled as high fluoride concentration might cause dental fluorosis [127]. The regulatory authorities set a restriction on the fluoride content of toothpastes for adults at 1500 ppm in Europe and 1200 ppm in the US. Therefore, an alternative component to fluoride in bioactive glass that behaves in a way similar to fluoride with regards to glass structure, bioactivity and other properties, e.g., reducing T_g and potentially reducing the hardness and abrasivity of the glass, is highly desirable.

Chlorine belongs to the same halogen group as fluorine. It is likely to behave like fluorine within glass structure and might have similar effects on the glass properties. The chloride ion is substantially larger than the fluoride ion (1.67 Å vs 1.19 Å) and on incorporation into a glass, the large chloride ion might expand the glass volume resulting in a more open and less compact glass structure. This could contribute to forming softer and less abrasive chloride containing bioactive glasses that might also dissolve faster and form apatite more rapidly. Moreover, chloride containing glasses are expected to be less likely to crystallise compared to the equivalent fluoride glasses.

A more open glass structure is less likely to transform into a crystalline lattice around the bigger chloride compared to the more compact structure around the smaller fluoride ion.

It is important to note that chloride is naturally present in the human body with relatively high concentrations and is biologically acceptable [128, 129]. Approximately 81.7 g chloride is present in a normal adult human body and the normal serum chloride concentrations range from 96 to 106 mEq/l, i.e. 3.408-3.763 g/l. Although, it has been reported that sodium chloride at concentrations above 2.5 g/l produces hypertension, this effect is thought to be related to the excess sodium concentration rather than chloride [129]. The toxicity of chloride salts is believed to depend on the cation present; that of chloride itself is unknown. In addition, chlorides (strontium chloride and potassium chloride) have widely been incorporated into toothpaste for treating dentine hypersensitivity. There is no restriction on the chloride content in toothpastes unlike with fluoride [130].

However, the incorporation of chloride into silicate glasses is fraught with the issues of chloride volatilisation during synthesis, resulting in most of the chlorine being lost [87]. Although the same problem might exist with incorporating fluoride, it is not as severe. As shown in the paper by Brauer *et al.*, fluoride can be retained readily in silicate glasses, though 5-23 % fluoride can be lost as HF during melting [118]. Losses of chloride during melting of silicate glasses are known to be much higher and can reach up to 95% [87]. Chloride is known as a refining agent in silicate glass industry, due to its rigorous volatilisation, it reduces the amount of bubbles as it evaporates from the silicate melt and thus improves technical quality of a glass. As a consequence the incorporation of chloride in silicate glasses has rarely been investigated compared to fluoride. The limited number of oxychloride glasses that have been studied in the literature have chloride contents typically less than 2 mol% [85].

In this chapter, we investigate chloride as an alternative for fluoride in sodium-free Q^2 silicate bioactive glasses based on the SiO_2-P_2O_5-CaO-$CaCl_2$ system. Kiprianov *et al.* [87] proposed that chlorine is likely to volatise as NaCl when the glass contains sodium oxide. Hence, the absence of sodium should effectively minimise chlorine volatilization during melting. The bioactivity of these glasses was determined in Tris and SBF buffer solution.

6.1 Results of the As-Quenched Glasses

All the as-quenched sodium-free chloride containing (0-16.7 mol% $CaCl_2$) glasses gave optically transparent glass frits.

6.1.1 Compositional Analysis

The percentages of the retained chloride in the initial glasses after volatilization are plotted against the as-designed chloride content (Figure 6.1.1). A large fraction (73-87%) of chloride was retained in the glasses. This suggests that up to 16.7 mol% $CaCl_2$ has been successfully incorporated into these phosphosilicate glasses.

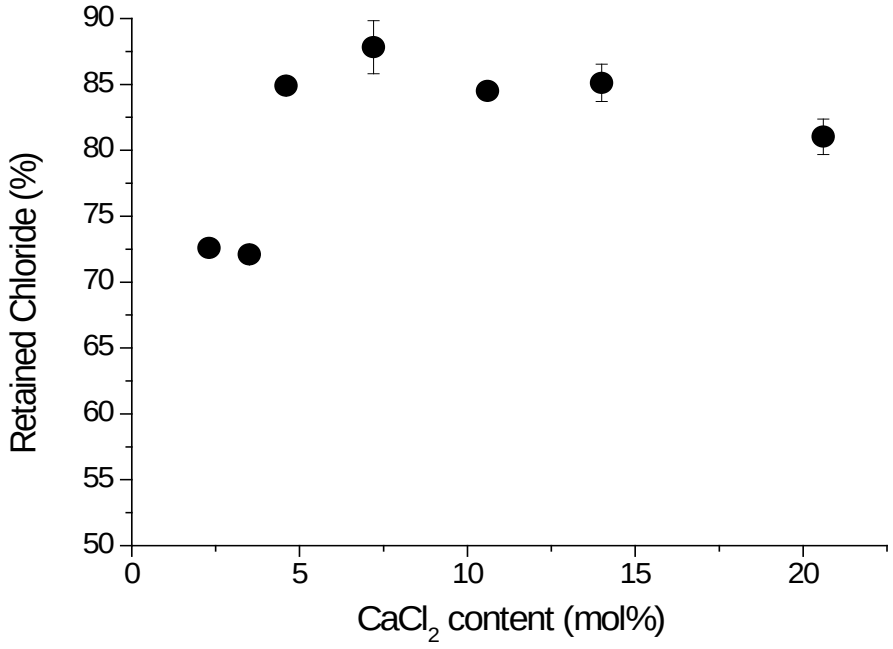

Figure 6.1.1 The percentage of the retained chloride in the initial glasses plotted against the as-designed chloride content.

Table 6.1.1 Glass compositions in mol%. For each glass, the first row is the nominal composition as-designed and the second row is composition re-calculated based on the chloride component analysis.

Glass code	SiO_2	CaO	P_2O_5	$CaCl_2$
GPCl 0.0	38.1	55.5	6.3	0.0
	38.1	55.5	6.3	0.0
GPCl 2.3	37.3	54.3	6.2	2.3
	37.5	54.6	6.2	1.7
GPCl 3.5	36.8	53.6	6.1	3.5
	37.2	54.1	6.2	2.5
GPCl 4.6	36.4	53.0	6.0	4.6
	36.7	53.4	6.1	3.9
GPCl 7.2	35.4	51.6	5.9	7.2
	35.7	52.0	5.9	6.3
GPCl 10.6	34.1	49.6	5.7	10.6
	34.7	50.5	5.8	9.0
GPCl 14.0	32.8	47.7	5.4	14.0
	33.6	48.9	5.6	11.9
GPCl 20.6	30.3	44.1	5.0	20.6
	31.8	46.3	5.3	16.7

6.1.2 XRD Results of the As-Quenched Glasses

The XRD patterns of the as-quenched $CaCl_2$ containing glasses are shown in Figure 6.1.2. The typical amorphous halos at 30° 2θ were found in all the glasses. However, there are some evidences of diffraction lines corresponding to apatite, which is likely to be hydroxy-chlorapatite. This detected apatite is likely to arise through reaction of the fine glass powder with moisture at the surface during the data collection.

6.1.3 FTIR Results of the As-Quenched Glasses

The FTIR spectra of the as-quenched $CaCl_2$ containing glasses are given in Figure 6.1.3. The non-bridging oxygen band (920 cm^{-1}), the Si-O-Si stretching band (1030 cm^{-1}) and the amorphous calcium phosphate band (600 cm^{-1}) appeared in the spectra. There is no clear evidence of crystalline apatite in the as-quenched glasses from the spectra.

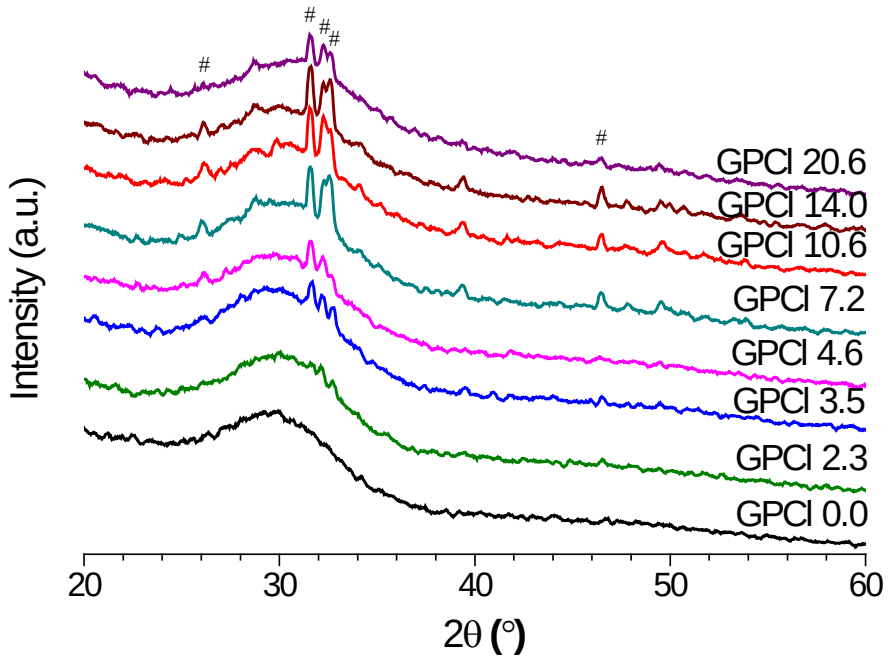

Figure 6.1.2 The XRD patterns of as-quenched $CaCl_2$ containing glasses ($^{\#}$:$Ca_{10}(PO_4)_6(OH/Cl)_2$).

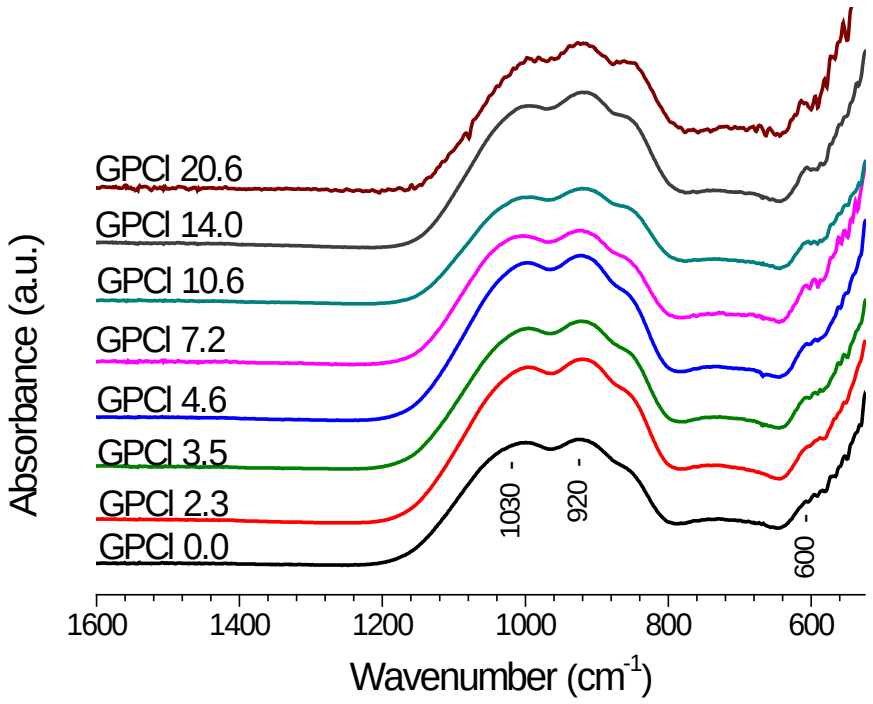

Figure 6.1.3 The FTIR spectra of as-quenched $CaCl_2$ containing glasses.

6.1.4 ^{31}P NMR Results of the As-Quenched Glasses

The ^{31}P MAS-NMR spectra of $CaCl_2$ containing bioactive glasses (Figure 6.1.4) show a single broad peak with a centre around 2-3 ppm, indicating that most of the phosphorus is present as orthophosphate charge balanced by Ca^{2+} cations [20]. In the series, the chemical shift moves from 3 ppm to 2 ppm with increasing $CaCl_2$ content. This slight shift of the peak position is probably the consequence of the shielding effect by the presence of chlorine, which has a high electron density. Furthermore, there is no clear evidence of crystalline apatite in the as-quenched glasses.

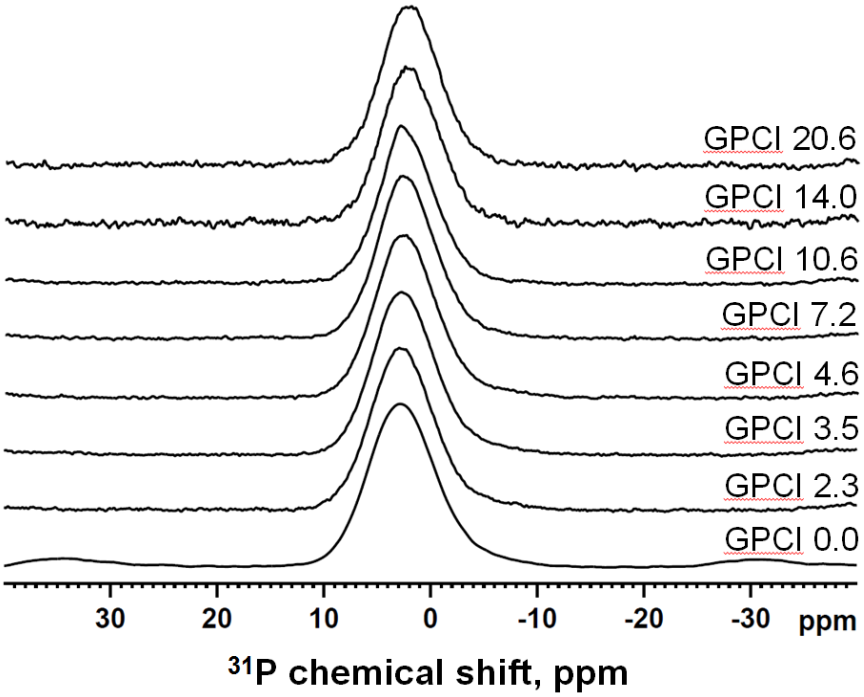

Figure 6.1.4 The ^{31}P MAS-NMR spectra of as-quenched $CaCl_2$ containing glasses.

6.1.5 ^{29}Si NMR Results of the As-Quenched Glasses

The ^{29}Si MAS-NMR spectra of the 2.3 and 20.6 mol% $CaCl_2$ containing glasses are shown in Figure 6.1.5. Although the signal-to-noise of the spectra is relatively low it is possible to distinguish an asymmetric broad peak with the centre at around -80 ppm. This peak position corresponds to the Q^2 silicate glass structure.

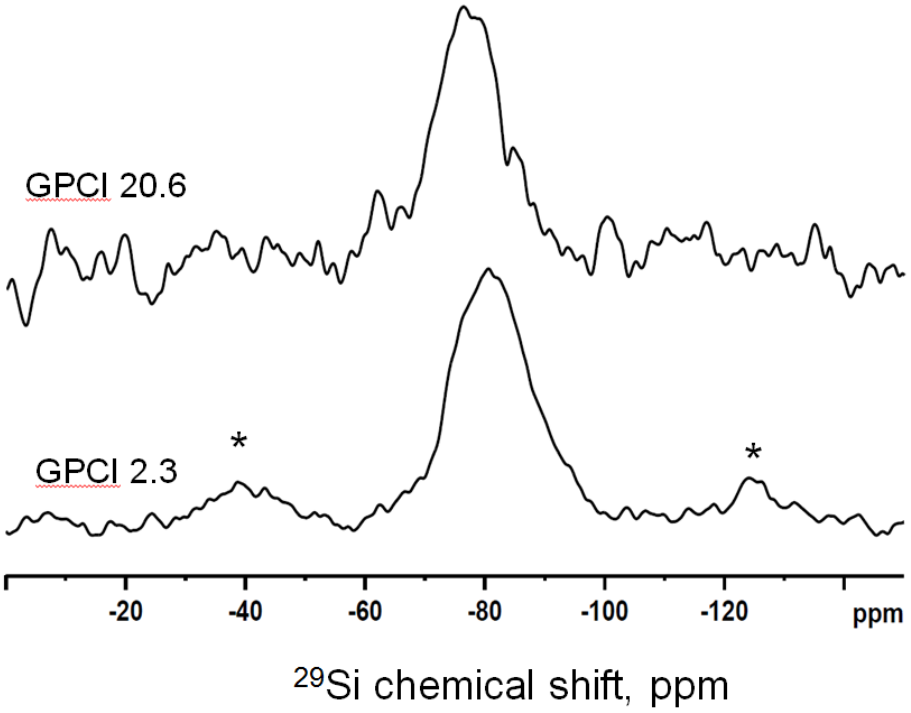

Figure 6.1.5 ^{29}Si MAS-NMR spectra of the as-quenched GPCI 2.3 and GPCI 20.6. The symmetrical signals labelled by asterisk represent spinning side bands.

6.1.6 Glass Density

The density and molar volume of $CaCl_2$ containing bioactive glasses are plotted as a function of the $CaCl_2$ content (Figure 6.1.6). It is clear that the density values decrease linearly (Y= - 0.0069X+2.9391, R^2=0.9792) with an increase in $CaCl_2$ content, while the molar volume increases linearly (Y=0.223X+21.423, R^2=0.999) with increasing $CaCl_2$ content. This indicates that the incorporation of chloride leads to an expansion of glass volume, to some extent, diluting the glass network.

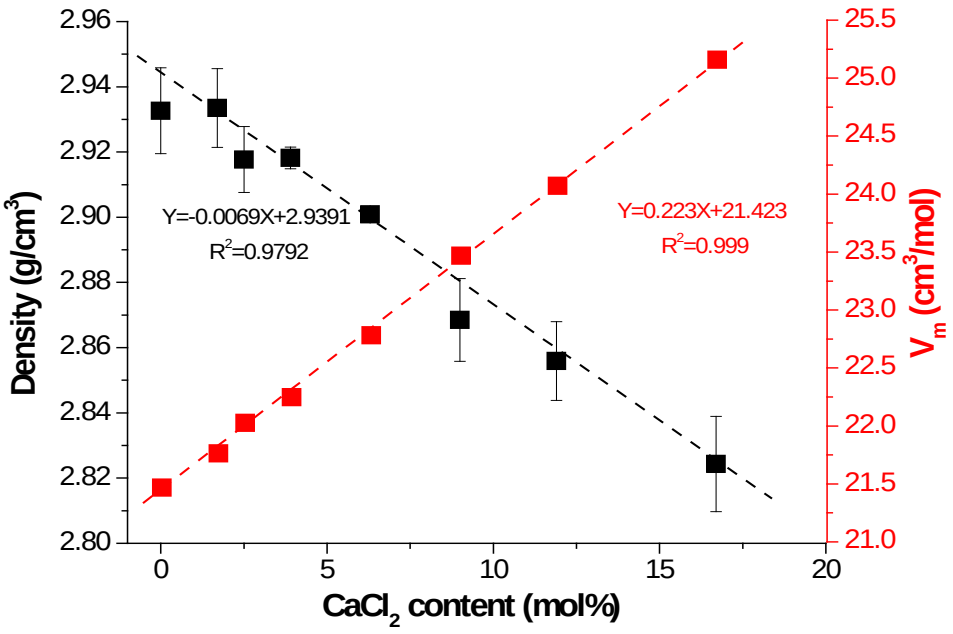

Figure 6.1.6 Glass density and molar volume profiled as a function of $CaCl_2$ content.

6.1.7 DSC Results of the Na free $CaCl_2$ Containing Bioactive Glasses

In Figure 6.1.7, the DSC traces for glass frits of sodium-free $CaCl_2$ containing glasses are similar to the equivalent CaF_2 containing glasses, the latter have been demonstrated and discussed in Chapter 5. In general, the first crystallisation peaks of chloride containing glasses are very sharp, while the second crystallisation peaks are relatively broad. The small endotherm peaks occur at about 1050°C when the chloride content is at and above 6.3 mol% that should correspond to a melting event. The recorded T_g, T_{o1}, T_c and T_m from DSC traces are summarised and presented in Table 6.1.2.

The glass transition temperature (T_g) of frit is plotted as a function of $CaCl_2$ content in Figure 6.1.8. T_g values reduce with increasing $CaCl_2$ content. A linear relationship (Y=-12.505X+786.27, R^2=0.989) between T_g and $CaCl_2$ content is seen in the glasses with $CaCl_2$ content up to 11.9 mol%, while the T_g of GPCl 20.6 is clearly off the trend. This suggests that $CaCl_2$ percentage losses during glass melting in glasses with $CaCl_2$ content no more than 11.9 mol% are small and nearly identical.

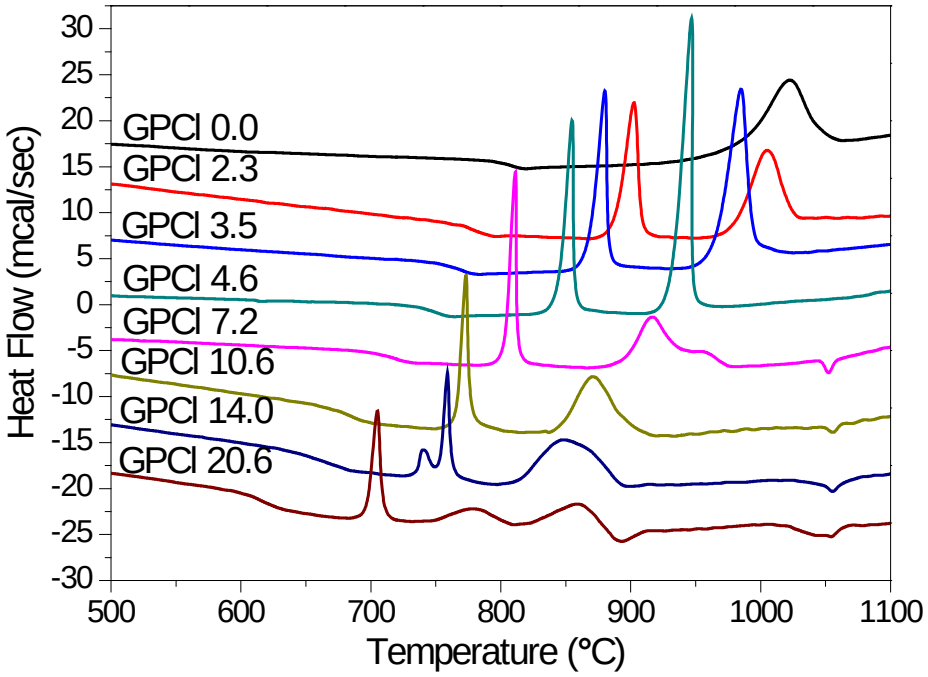

Figure 6.1.7 DSC traces for the glass frits of $CaCl_2$ containing glasses.

Table 6.1.2 Characteristic temperatures for chloride containing glasses. For each glass composition, the first row is the characteristic temperatures of glass frit and the second row is the characteristic temperatures of fine powder.

Glass Code	T_g	T_{o1}	T_{c1}	T_{c2}	T_{c3}	T_m
GPCl 0.0	786	969	1013	-	-	
	790	901	925	-	-	-
GPCl 2.3	765	882	903	1105	-	
	765	886	891	952	987	-
GPCl 3.5	753	862	880	985	-	-
	748	843	861	989	-	-
GPCl 4.6	737	841	855	947	-	
	726	826	846	903	-	-
GPCl 7.2	699	800	811	917	955	1052
	701	792	803	855	-	-
GPCl 10.6	671	763	775	874	-	1056
	670	762.5	775	825	-	1061
GPCl 14.0	645	731	740	760	850	1055
	639	731	741	793	-	890/1050
GPCl 20.6	601	695	706	780	860	892/1055
	600	688	704	805	857/880	900/1045

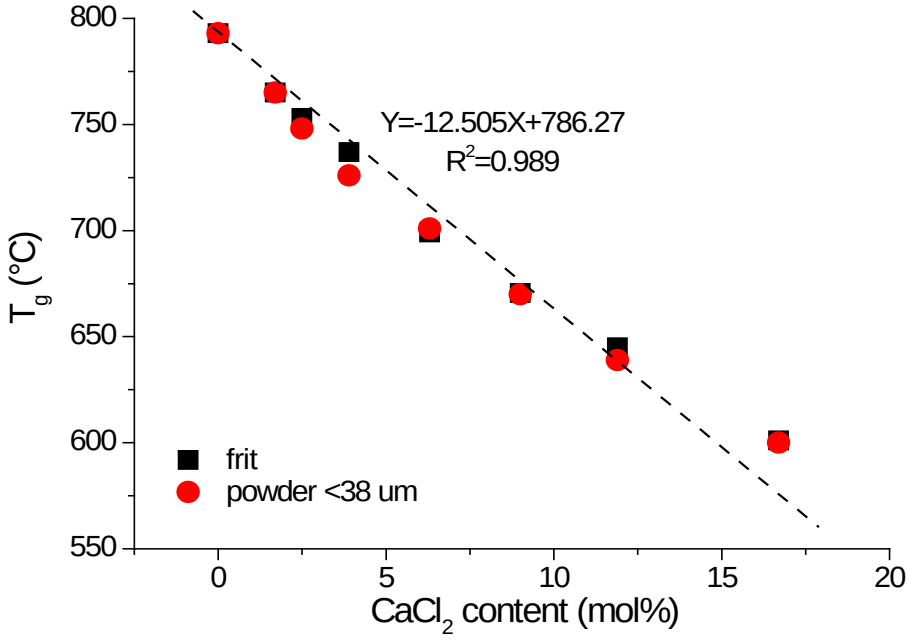

Figure 6.1.8 Glass transition temperature profiled as a function of $CaCl_2$ content.

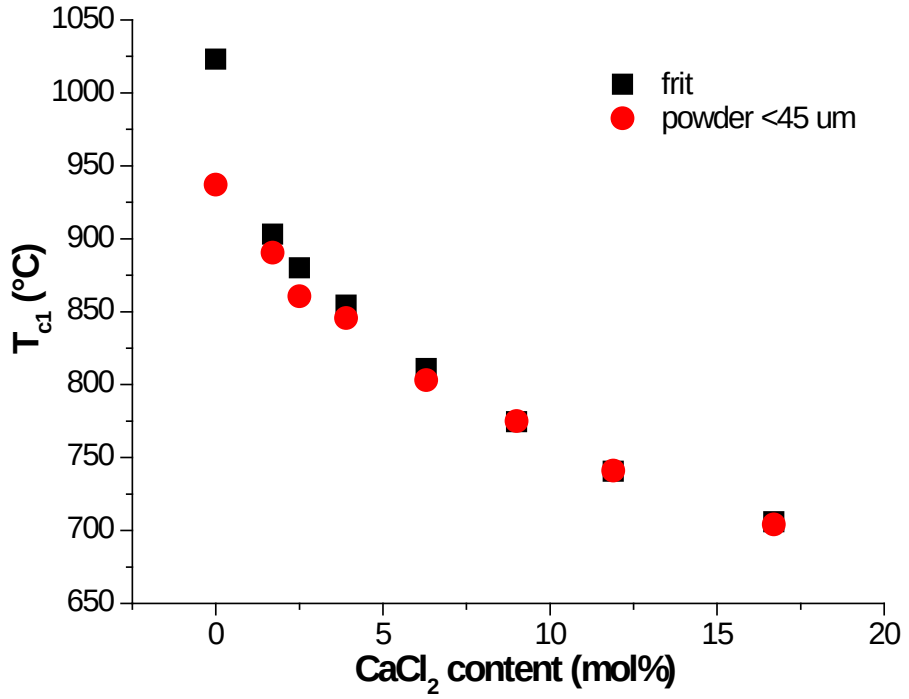

Figure 6.1.9 First peak crystallization temperature (T_{c1}) for frit and fine particles plotted against $CaCl_2$ content.

T_{c1} for both of glass frit and fine powder are plotted against the $CaCl_2$ content in Figure 6.1.9. It is clear that T_{c1} values decrease dramatically with an increase in $CaCl_2$

content. With the introduction of 9 mol% $CaCl_2$, T_{c1} for different particle size are identical.

6.2 Dissolution Study

6.2.1 pH Measurements Results

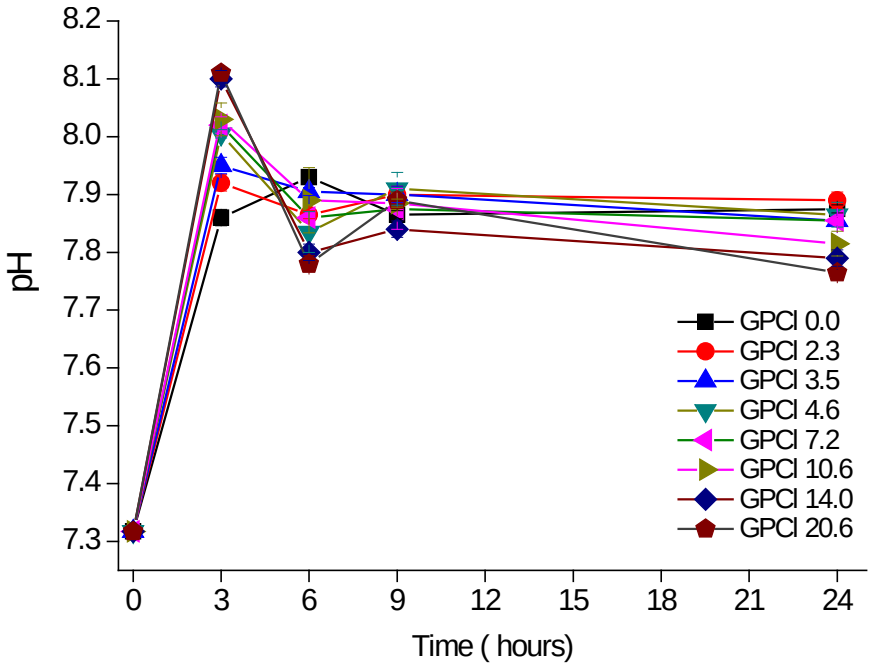

Figure 6.2.1 pH values measured at the end of the immersion time in Tris buffer.

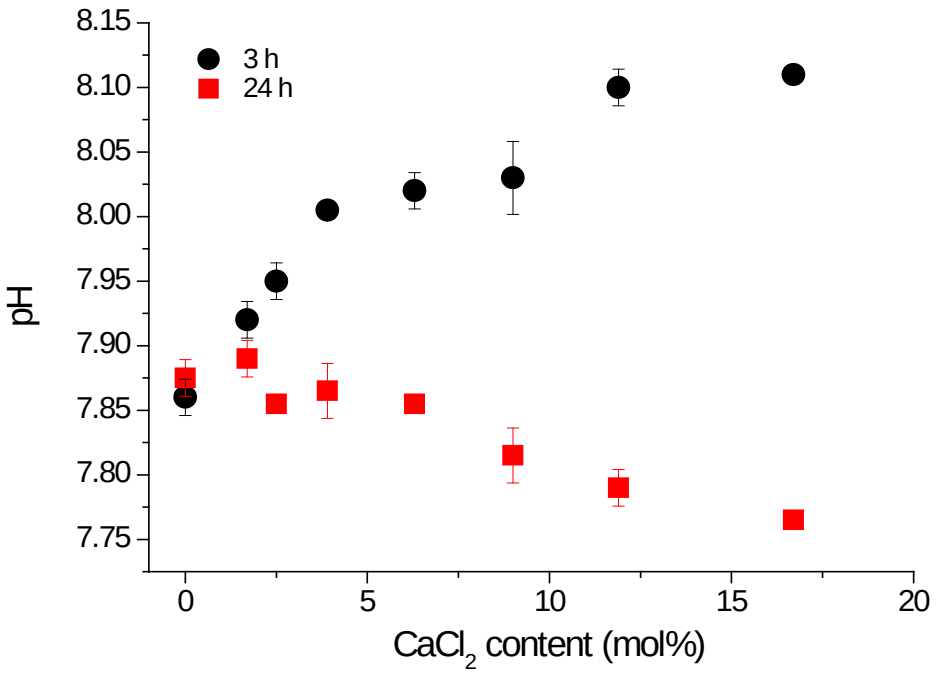

Figure 6.2.2 The measured pH values of the solution after immersion of the glass powder in Tris for 3h and 24h plotted against $CaCl_2$ content.

The pH values measured after immersion the glass powder in Tris buffer are plotted against immersion time (Figure 6.2.1). The general trend is similar for all the glass compositions. The pH values increase in the first 3 hours and decrease afterwards. There is no significant change after 6 hours. The increase in pH is ascribed to the ion exchange between Ca^{2+} in the glasses with protons in solution. The consumption of OH^- for apatite-like phase formation leads to a reduction of pH.

Figure 6.2.2 shows the pH values measured after 3 and 24 hours immersion in Tris buffer for each glass. Two trends of pH values after 3 and 24 hours immersion are distinct. After 3 hours immersion, an increase in pH is seen with increasing $CaCl_2$ content, while a reduction in pH is visible after 24 hours immersion. Overall, a reduction of pH from 3 hours to 24 hours is found and the change is more pronounced for the glasses with higher $CaCl_2$ content.

6.2.2 Ion Release Results

The glass degradation was mainly estimated by measuring the level of ions released into the buffer solutions using Inductively Coupled Plasma - Optical Emission Spectroscopy (ICP-OES).

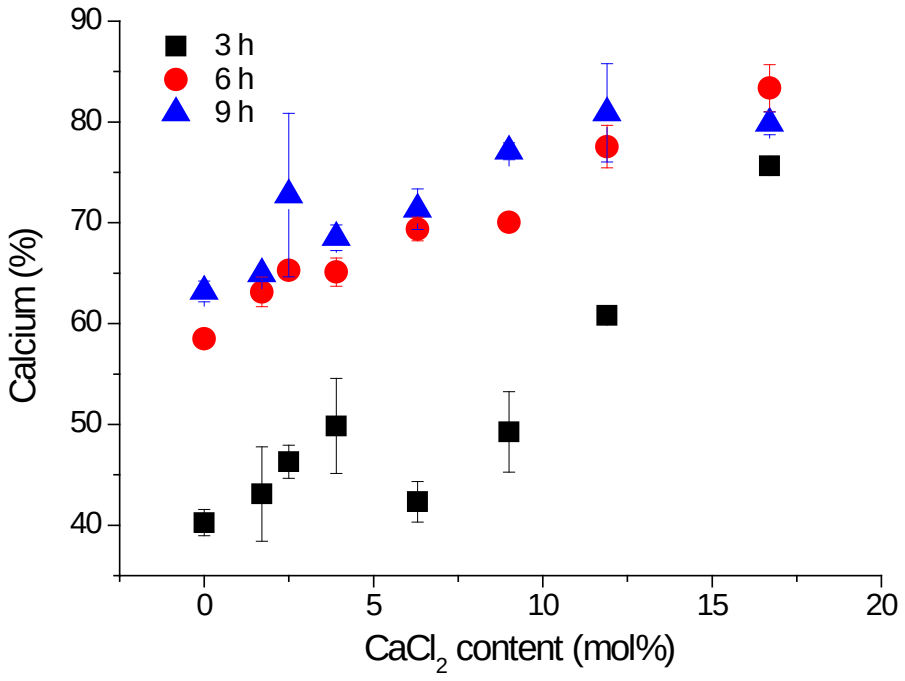

Figure 6.2.3 The concentration of elemental calcium in Tris presented as percentage of the total calcium content in the glass composition plotted against the $CaCl_2$ content.

The concentrations of calcium measured after up to 9 hours immersion in Tris were plotted as a percentage of total amount of calcium in the nominal glass compositions against the $CaCl_2$ content (Figure 6.2.3). The percentage of Ca^{2+} found in solution increases dramatically with an increase in $CaCl_2$ content after each respective immersion time period. For the individual glasses, the percentage of Ca^{2+} also increases with immersion time from 3 to 6 hours. Only slight increase in the percentage of Ca^{2+} concentration is seen from 6 to 9 hours. These consistently suggest that glass degradation and apatite formation mainly occurred before 9 hours immersion. As we can see, up to 83% of Ca^{2+} is detected in the solution after 6 hours immersion in Tris for the glass with 16.7 mol% $CaCl_2$. This increasing percentage of Ca

release with an increase in $CaCl_2$ content is ascribed to the expansion of glass volume by the presence of the large chloride ion.

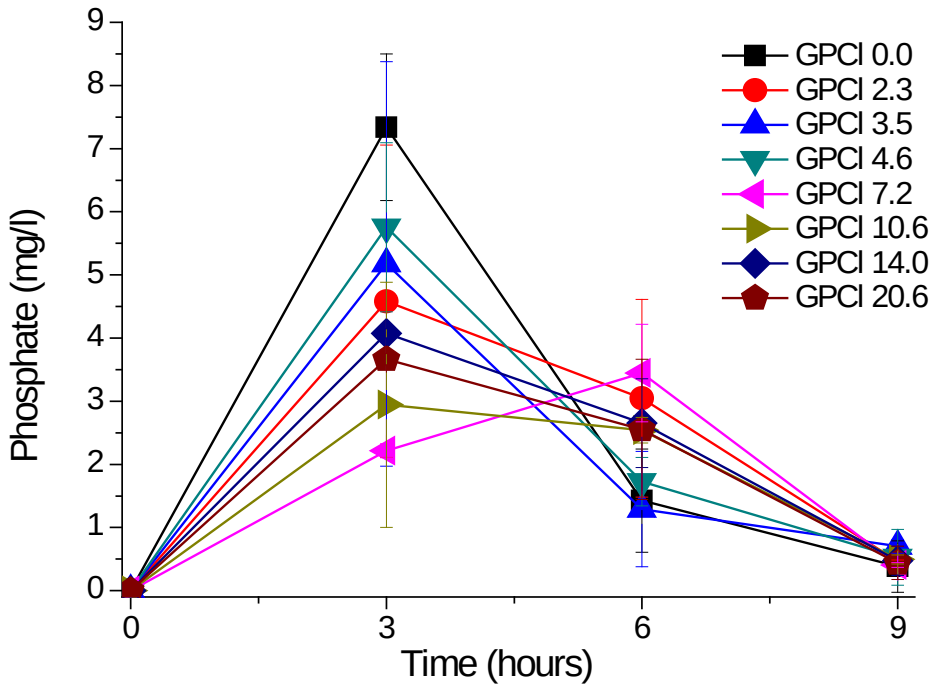

Figure 6.2.4 The concentration of phosphate measured after up to 9 hours immersion in Tris for $CaCl_2$ containing glasses.

In general, the trends of the evolution for phosphate concentration measured in solution with increasing immersion time are similar for all the glasses and shown in Figure 6.2.4. A relatively low phosphate concentration (< 9 mg/l) is observed for all the glasses. In addition, the concentration of phosphate for each glass mainly increases in the first 3 hours and decreases afterwards. These indicate that large amounts of phosphate were likely consumed or converted to a crystalline phosphate in the first 3 hours and a further consumption of phosphate for apatite-like phase formation was carried on with immersion time.

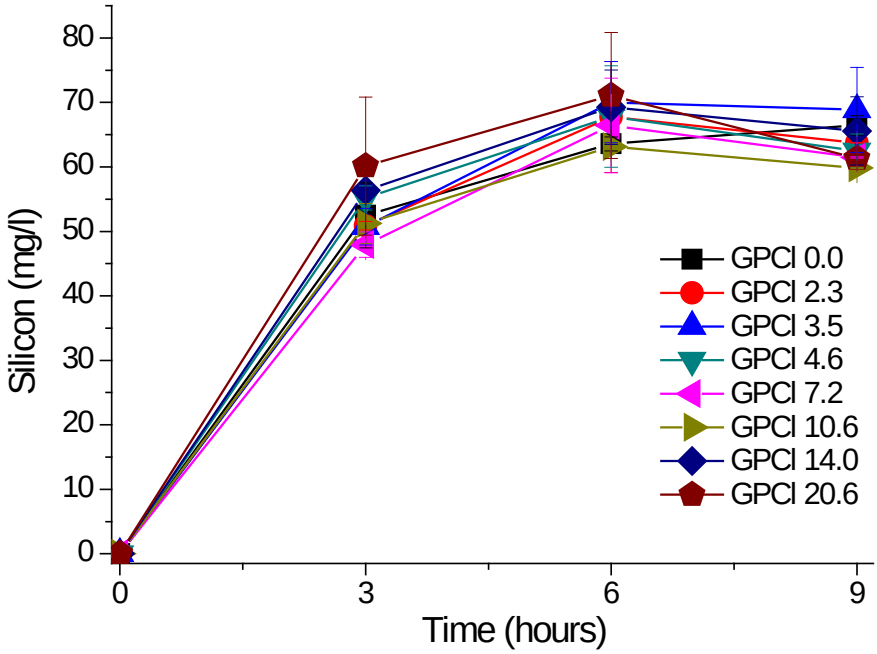

Figure 6.2.5 The concentration of silicon measured in Tris buffer in mg/l plotted as a function of immersion time. The numbers are nominal molar percentage of $CaCl_2$ in the compositions.

The silicon concentration (mg/l) measured in Tris buffer after up to 9 hours immersion plotted as a function of immerision time is shown in Figure 6.2.5. It is seen that the concentration of Si increases up to 60-70 mg/l in the first 6 hours immersion, with no distinct change after further immersion. There is no substantial difference in the measured silicon concentration among different glass compositions.

6.3 Apatite-like Phase Formation in Tris Buffer and SBF Buffer Solution

The apatite-like phase formation on immersion in Tris buffer and SBF buffer solution for the $CaCl_2$ containing bioactive glasses was evaluated by using XRD, FTIR and ^{31}P MAS-NMR.

6.3.1 X-ray Diffraction Results

Similar evolution of the XRD patterns before and after immersion in Tris and SBF for each glass is seen. The XRD patterns of the bioactive glass with 3.9 mol% $CaCl_2$ content (GPCl 4.6) on immersion up to 24 hours in Tris and SBF are selected as an example and presented in Figure 6.3.1 and Figure 6.3.2. As mentioned previously, the as-quenched glass shows a broad amorphous halo centred at 30° 2θ. After 3 hours immersion in Tris and SBF, the amorphous halo broadened out and the diffraction lines corresponding to the typical apatite diffraction lines developed at 25.9° and 32° 2θ. The developed peaks intensified with immersion time up to 9 hours in Tris and 1 day in SBF. Interestingly, after 6 hours immersion in Tris and 1 day in SBF, the intensity of three main diffraction lines between 30-33° 2θ changed and the middle diffraction line at (32.2° 2θ) became predominant. After 24 hours in Tris, the peak at 25.9° 2θ slightly narrowed down, suggesting the growth of apatite crystals.

Moreover, the XRD patterns of the collected precipitates after 3 hours immersion in Tris are summarised in Figure 6.3.3. It is clear seen that the XRD patterns for all the samples have diffraction lines at 25.9°, 31.5° 32.2° and 32.6° 2θ, which are identical to the major diffraction lines of apatite. The intensities of the diffraction lines increased with an increase in $CaCl_2$ content, particularly, in the glasses with $CaCl_2$ content lower than 9.0 mol%. However, the diffraction peaks are relatively broad, rather than sharp, suggesting the formed apatite crystals are quite small.

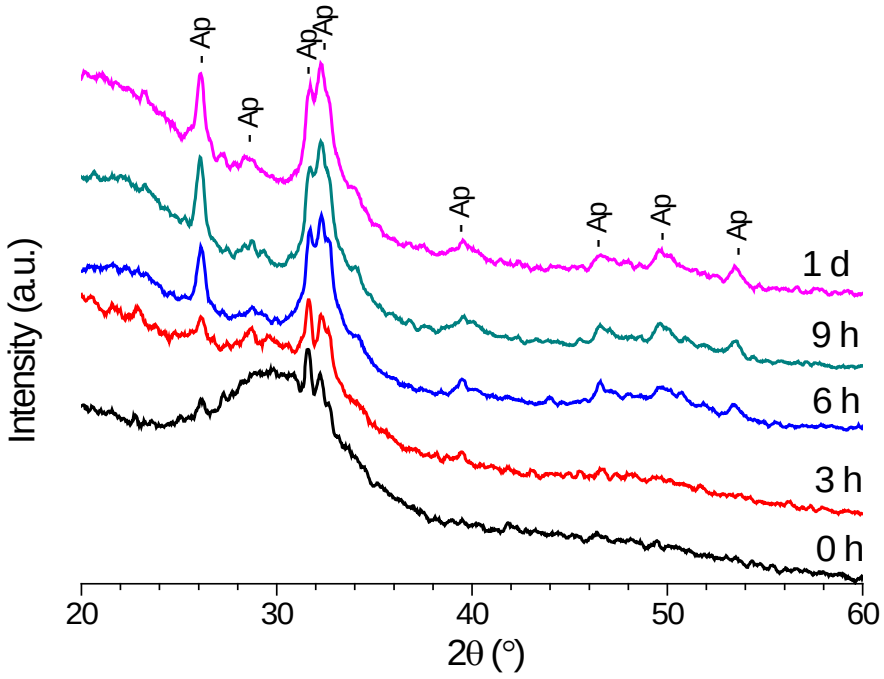

Figure 6.3.1 The XRD patterns of the glass precipitates with 3.9 mol% $CaCl_2$ collected after immersion in Tris up to 1 day. The numbers are immersion time (Ap: apatite).

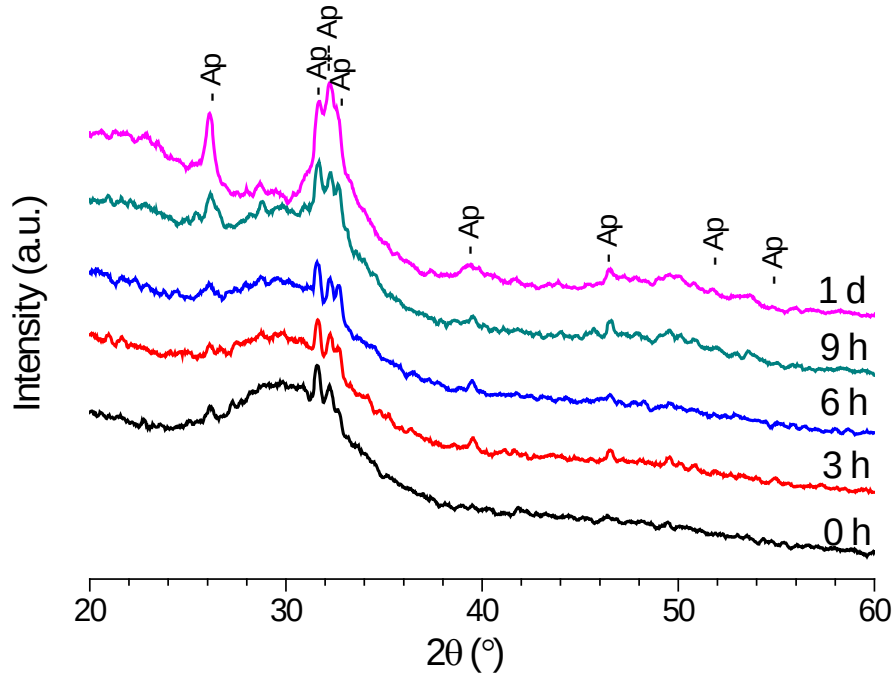

Figure 6.3.2 The XRD patterns of the glass precipitates with 3.9 mol% $CaCl_2$ collected after immersion in SBF up to 1 day. The numbers are immersion time (Ap: apatite).

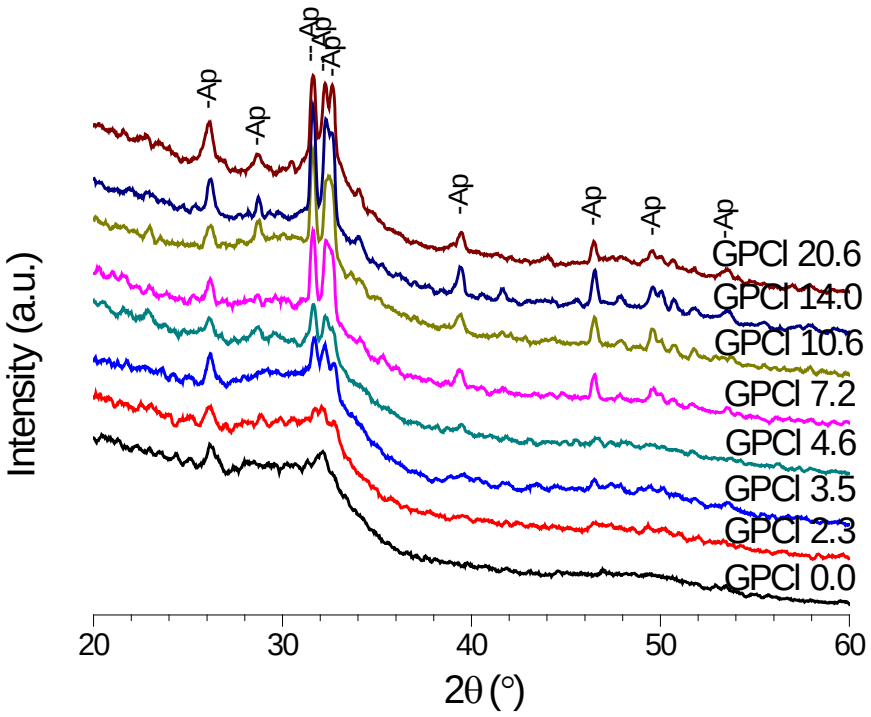

Figure 6.3.3 The XRD patterns of the glass precipitates collected after 3 hours immersion in Tris.

6.3.2 Fourier Transform Infrared Spectroscopy Results.

Glass degradation and apatite-like phase formation upon immersion of glasses in buffer solution were monitored by using FTIR. Figure 6.3.4 and Figure 6.3.5 demonstrate the FTIR spectra for the 3.9 mol% $CaCl_2$ containing glass before and after immersion in Tris and SBF up to 24 hours. The spectrum of the as-quenched glass shown at the bottom was discussed above. After 3 hours immersion in Tris, the considerable changes of the spectra are observed, including the elimination of non-bridging oxygen bands at 920 and 850 cm^{-1}, the sharpening of crystalline calcium orthophosphate band at 1030 cm^{-1}, the appearance of typical apatite split peaks at 560 and 613 cm^{-1} and the development of carbonate bands at 1420, 1450 and 870 cm^{-1}. Similar evolution of FTIR spectra for the collected precipitates of other $CaCl_2$ containing glasses after 3 hours immersion were found and demonstrated in Figure 6.3.6. On a further increase in immersion up to 9 hours in Tris, the typical apatite bands at 1030, 613 and 560 cm^{-1} sharpened and intensified, however, no significant

difference can be seen in the spectra after that. The FTIR spectra also changed after immersion in SBF. The non-bridging oxygen bands at 920 and 850 cm^{-1} were largely lost after 3 hours. The apatite split peaks started to appear after 9 hours immersion and sharpened with immersion time. Clear apatite bands at 1030, 613 and 560 cm^{-1} were seen after 1 day immersion.

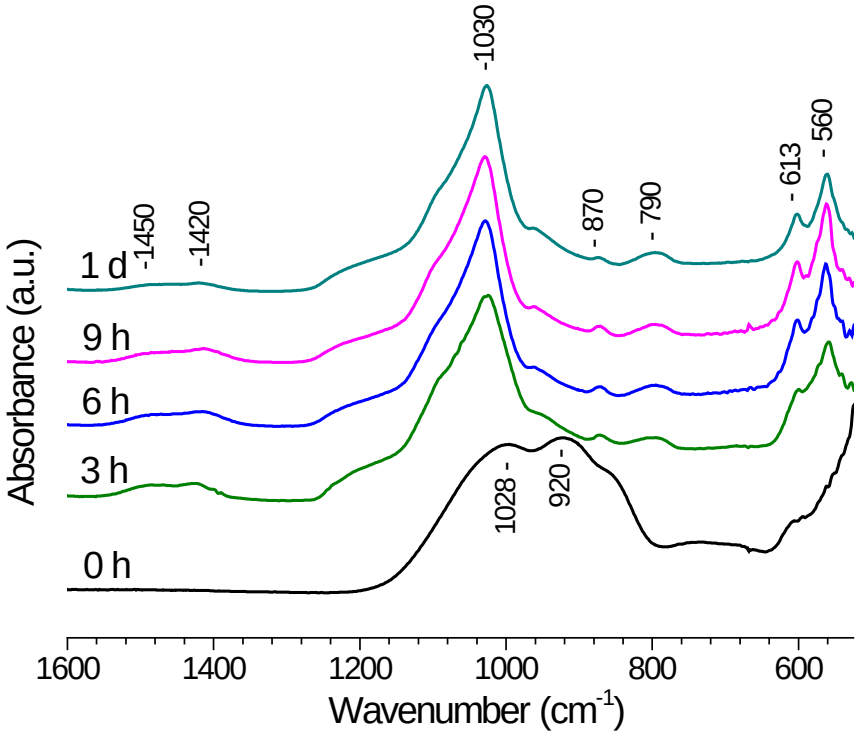

Figure 6.3.4 The FTIR spectra of the glass precipitates with 3.9 mol% $CaCl_2$ collected after immersion in Tris up to 1 day.

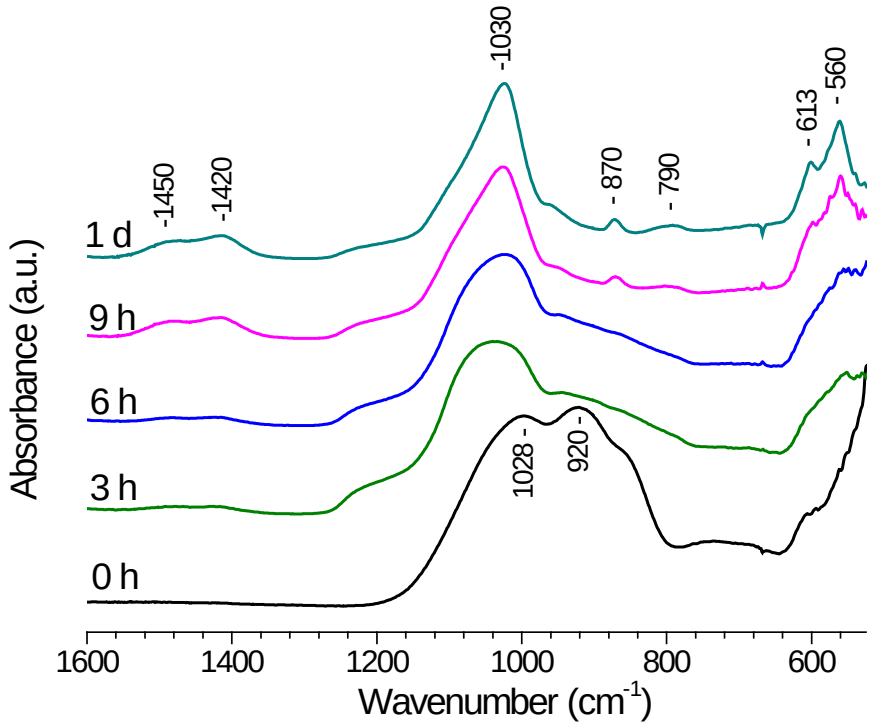

Figure 6.3.5 The FTIR spectra of the glass precipitates with 3.9 mol% $CaCl_2$ collected after immersion in SBF up to 1 day

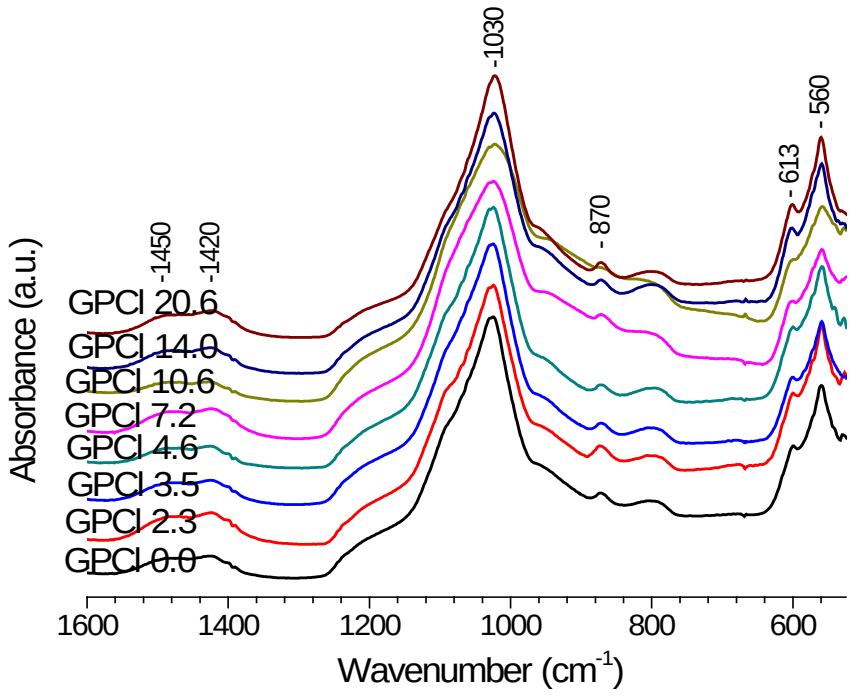

Figure 6.3.6 The FTIR spectra of the glass precipitates collected after 3 hours immersion in Tris.

6.3.3 NMR Results of $CaCl_2$ Series Glasses

The apatite-like phase formation on immersion was investigated by using ^{31}P MAS-NMR. The FWHM values were estimated from Bruker Top-Spin software. The estimated errors are about 10 Hz.

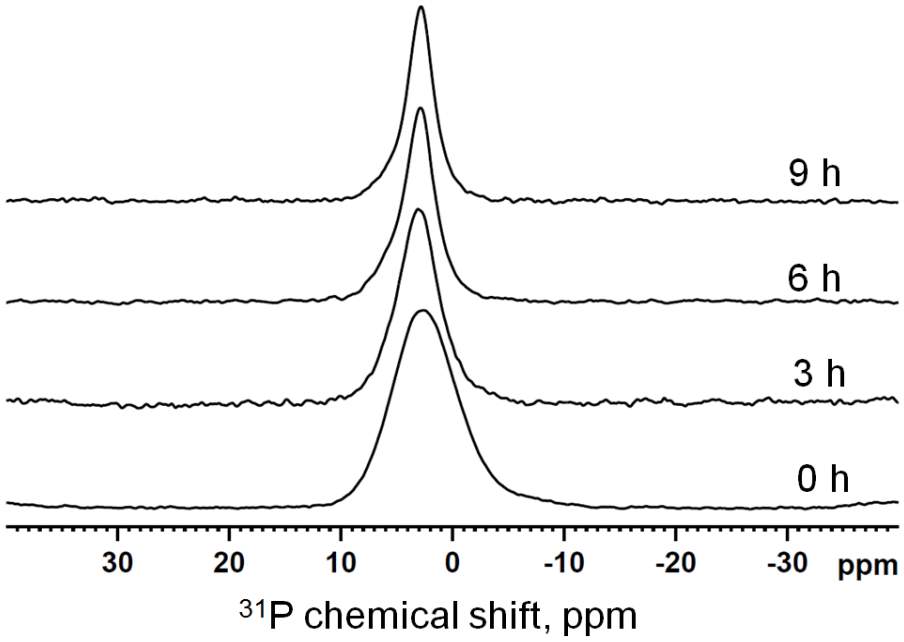

Figure 6.3.7 The ^{31}P MAS-NMR spectra of the glass precipitates with 3.9 mol% $CaCl_2$ collected after immersion in Tris. The bottom spectrum is for the untreated glass powder. The numbers are immersion times.

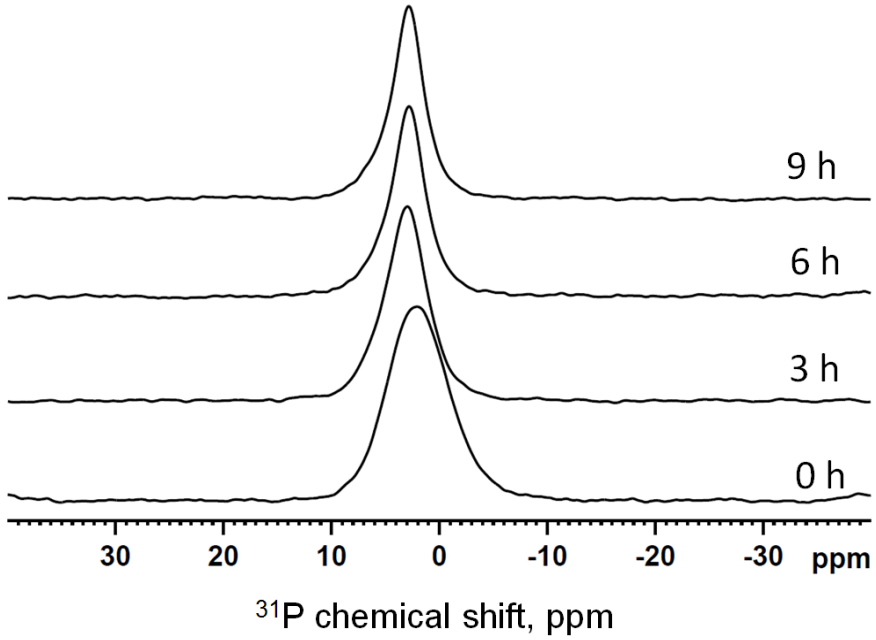

Figure 6.3.8 The ^{31}P MAS-NMR spectra of the glass precipitates with 16.7 mol% $CaCl_2$ collected after immersion in Tris. The bottom spectrum is for the untreated glass powder. The numbers are immersion times.

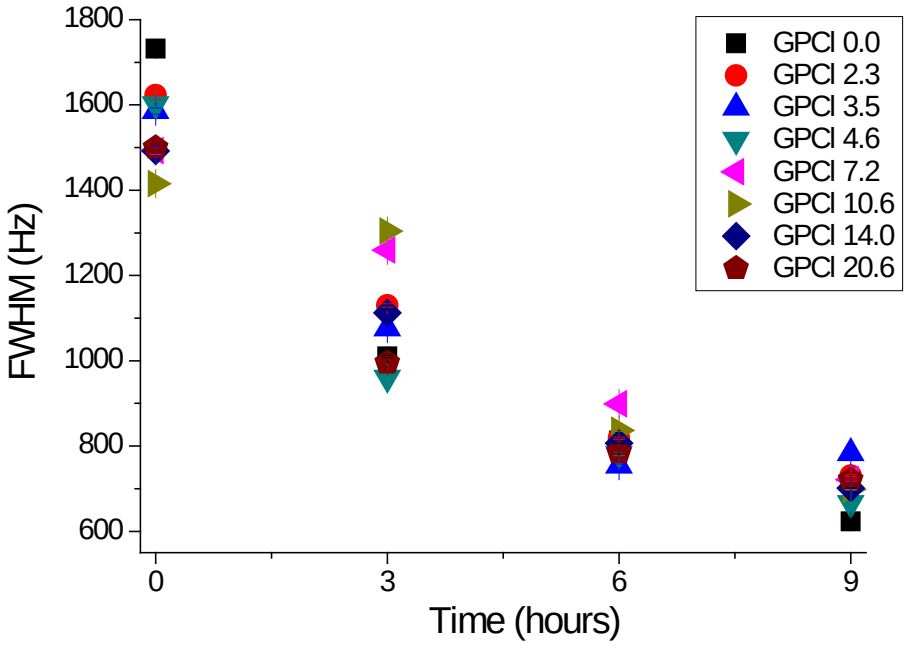

Figure 6.3.9 FWHM for ^{31}P MAS-NMR spectra plotted as a function of immersion times in Tris buffer. The estimated errors (10 Hz) are smaller than the data point.

The ^{31}P MAS-NMR spectra of glass GPCl 4.6 and GPCl 20.6 before and after immersion in Tris are presented in Figure 6.3.7 and Figure 6.3.8. The spectra for the as-quenched glasses were shown above in Figure 6.1.4. For both glass compositions, after 3 hours immersion the peaks narrow down. There is no clear change in chemical shift before and after immersion for glass GPCl 4.6, whilst the chemical shift for GPCl 20.6 moved “downfield” to 3 ppm after immersion, suggesting rapid apatite-like phase (likely to be HAP) formation within 3 hours immersion. A further reduction of the line-width of the peak was seen from 3 to 9 hours for both glasses. The similar evolutions were found in the other $CaCl_2$ containing glass compositions.

The full width half maximum (FWHM) of ^{31}P MAS-NMR spectra for $CaCl_2$ containing bioactive glasses before and after immersion in Tris are plotted as a function of immersion times in Figure 6.3.9. A clear reduction of FWHM with an increase in immersion period is seen for all the chloride containing glasses. In the case of before immersion, the amorphous calcium orthophosphate results in a broad amorphous peak and a relatively large FWHM, since there are local variations in the local environment around the phosphorus. In the case of after immersion, the calcium orthophosphate peak gradually becomes sharper as the result of the formation of a crystalline calcium orthophosphate (apatite) and the amorphous calcium phosphate species in the glass dissolving. Thus, a progressive reduction in FWHM of ^{31}P peak is noticed with an increase in immersion time.

Further Discussion

The FTIR spectra and ^{31}P NMR spectra of the as-quenched glasses consistently suggest that the resultant chloride containing bioactive glasses are amorphous, while the XRD patterns demonstrate a small fraction of diffraction lines corresponding to mixed hydroxy-chlorapatite in the glasses with $CaCl_2$ content more than 1.7 mol%. The hydroxyl groups in the formed apatite might come from surface reaction with moisture during data collection since there is unlikely to be significant quantities of hydroxyl groups in the original glasses. The XRD experiments were carried out by placing the glass powder inside a sample holder (32 mm) and exposing sample to the air during the experiment, which requires a couple hours of contacting with atmosphere. The moisture in the atmosphere might aid the apatite (hydroxy-chlorapatite) formation on the glass surface. Compared with XRD experiments, powder samples were packed in the rotor with a small cross sectional area (2.5 or 4 mm) and spun in a closed chamber during the MAS-NMR spectra collection, whilst, the FTIR measurements took less than 5 min to perform. Both of these studies minimise the contact between glass powder and atmospheric water. Therefore, no apatite was detected from the NMR and FTIR spectra.

Owing to known chloride volatilisation during melting, resulting in most of the chloride being lost, and the incorporation of chlorine in silicate glasses is described in the literature as problematic and challenging. However, the results of chloride quantification in this study indicate that 70 - 90% of the chlorine is retained in the as-quenched glasses after melting at 1500-1550^{o}C. Thus, the majority of chloride is retained in the silicate glass during melting. Generally, the glasses with lower $CaCl_2$ content show higher amount of $CaCl_2$ loss. This can be attributed to a higher melting temperature of 1550^{o}C for synthesis of the lower $CaCl_2$ containing glasses (1.7 and 2.5 mol%).

It is important to note here that most chlorides with the notable exception of $CaCl_2$ have low boiling points (1413°C for NaCl, 1412°C for $MgCl_2$, 1420°C for KCl, 1250 °C for $SrCl_2$ and 756 °C for $ZnCl_2$) and this has generally resulted in either no or very little chloride remaining in the silicate glass. Consequently chloride containing glasses have rarely been studied and those that have been looked at typically have very low $CaCl_2$ concentrations (< 2 mol%) [85, 86].

The chloride volatilisation is probable by two routes; direct volatilisation as $CaCl_2$ and loss as HCl by reaction with water vapour in the furnace atmosphere. If chloride volatilises as HCl, the CaO content in the actual glass composition would increase and the SiO_2 and P_2O_5 contents would decrease. Therefore, the glass network connectivity (NC) would decrease with an increase in $CaCl_2$ content and the glasses would tend to crystallise. However, if chloride volatilises as $CaCl_2$, the CaO, P_2O_5 and SiO_2 would increase in proportion and the glass NC would remain constant.

The ^{29}Si MAS-NMR spectra (Figure 6.1.5) suggest that the obtained glasses are mainly Q^2 structure rather than a mixture of Q^1 and Q^2. Moreover, the FTIR and ^{31}P MAS-NMR suggests that all the glasses are largely amorphous and there is no clear crystallisation tendency with an increase in $CaCl_2$ content. Thereby, the chloride loss is likely to occur as $CaCl_2$ rather than HCl. According to the fixed NC and actual $CaCl_2$ content, the actual glass compositions have been calculated and summarised in Table 6.1.1. As can be seen, up to 16.7 mol% $CaCl_2$ was retained in the glasses.

The DSC and glass density results reveal that the incorporation of $CaCl_2$ results in a very remarkable reduction in the glass transition temperature and glass density. It is proposed that in this $CaCl_2$ containing glass system, that a Cl-Ca(n) species is formed in an identical fashion to the F-Ca(n) species in the CaF_2 containing glasses [20, 111]. The formation of Cl-Ca(n) species has been found in very low $CaCl_2$ (< 2 mol%) containing glasses by Sandland *et al.* [131].

Possible formation of hypothetical "$CaCl^+$" species, which has same field strength as Na^+ but lower than Ca^{2+}, weakens the electrostatic force between two NBOs in the glass structure. Therefore, the more $CaCl_2$ is introduced into the glass composition, the weaker electrostatic forces between the two NBOs form and the lower is the glass transition temperature.

As shown in Figure 6.1.6, the glass density decreases with an increase in $CaCl_2$ content. This is due to the fact that the chloride ion is large. Incorporation of chloride therefore increases the glass molar volume and results in a more open and less compact glass structure. Hence, to some extent the presence of chloride dilutes the glass network and expands the glass volume, which leads to a decrease in density and packing density of the glass. Moreover, the formation of large "$CaCl^+$" species in the glasses results in a weakening of the silicate glass network. The effects observed in this study are comparable with the effect on the replacement of Na_2O for CaO (replaced one Ca^{2+} ion by two Na^+ ions) and K_2O for Na_2O (K^+ is larger than Na^+, ion radius: 1.52 Vs 1.16 Å) in the glass.

The chloride ion is substantially large in size, the presence of chloride not only leads to a reduction of glass density but also a fast glass degradation rate. The ion exchange process between Ca^{2+} from glass matrix and protons from the Tris buffer in the present study is aided by incorporation of chloride ions, which have the capacity to expand the glass network. This more open and expanded glass structure allows ions to diffuse much more easily into and out of the glass and therefore facilitates ion exchange, particularly for short immersion times. As a consequence there is a more rapid release of Ca^{2+} ions and a more rapid rise in pH in the glasses with higher $CaCl_2$ content during the first few hours of immersion compared to the glasses with the lower $CaCl_2$ content. However after a longer immersion period (24 hours), there is a less pronounced rise in pH of the glasses with more $CaCl_2$ content. This can be attributed

to a decrease of non-bridging oxygen concentration as a result of dilution by the $CaCl_2$, which provides Ca^{2+} to exchange with H^+ with an increase in $CaCl_2$ content.

Rapid glass degradation and release of Ca^{2+} and PO_4^{3-} ions facilitate apatite-like phase formation. Apatite-like phase formation of these $CaCl_2$ containing bioactive glasses was evaluated in Tris Buffer and SBF. As discussed above, chloride promotes glass degradation as a result of expanding glass network and the rapid glass degradation provides ions, such as Ca^{2+}, PO_4^{3-} and OH^- for apatite-like phase formation.

From the ion release data, the highest amount of phosphate was present in solution is around 7.85% after 3 hours immersion, this indicates a probable consumption of phosphate for apatite-like phase formation at an even earlier immersion time than 3 hours. The studied glasses are phosphate deficient, as the ratio of Ca:P ratio in glasses is 4.4:1, while the Ca:P ratio in apatite is only 1.67:1. Therefore, the amount of apatite-like phase formation depends mainly on the phosphate content and high phosphate contents are favourable for apatite-like phase formation.

All the XRD, FTIR and NMR results consistently suggested rapid apatite-like phase formation within 3 hours immersion in Tris and 9 hours in SBF, which is comparable to the equivalent CaF_2 containing bioactive glasses in Chapter 5. For those studied chloride containing bioactive glasses, we would expect mainly HAP to form on dissolution, contrasting with FAP for the fluoride containing bioactive glasses. This is due to the fact that the size of hydroxyl ion (1.26 Å) is smaller than chloride ion (1.67 Å) but slightly larger than fluoride in (0.119 nm). In the apatite crystal lattice, the fluoride ion is situated at the centre of Ca(II) triangle, while the hydroxyl ion is too large to fit in the space at the centre of Ca(II) triangle and is displaced above the plane of the triangle. The substantially larger chloride ion displaces even further above the plane of the Ca(II) triangle compared with the hydroxyl ion. Therefore, chlorapatite is less stable than hydroxyapatite, which is less stable than fluorapatite, and is unlikely to form in an

identical fashion to fluorapatite after immersion of the bioactive glass. Furthermore chlorapatite is known to convert to hydroxyapatite with time in the presence of water [95]. These highly bioactive chloride containing glasses with their rapid dissolution rate are attractive for use in toothpastes and resorbable materials, especially bone grafts and scaffolds.

As shown in the XRD patterns, the diffraction lines developed after 3 hours immersion in Tris matched to the typical diffraction lines of hydroxyapatite, however, the intensities of the three main peaks between 31° to 33° 2θ are not completely identical with those for hydroxyapatite. This suggests a disordered crystal structure and the possibility of the presence of CO_3^{2-} or Cl^- in the apatite lattice.

Owing to the presence of Mg^{2+} in SBF, the apatite-like phase formation for the studied $CaCl_2$ containing bioactive glasses is slower in SBF compared with being immersed in Tris. The details have been discussed in Chapter 5. Fagerlund *et al*. found that bioactive glasses 45S5 (2.6 mol%), S53P4 (1.6 mol%), 13-93 and 1-98 (0.86 mol%) formed Ca-P layer more readily and faster in SBF than in Tris [132]. It seems contradictive to what was found in this project. However, those glasses in fact have much lower phosphate content (0.86 - 2.6 mol%) compared with the ones (5.0 - 6.3 mol%) studied here. Unlike simulated body fluid, which is rich in Ca^{2+} and PO_4^{3-}, Tris buffer contains no Ca^{2+} or PO_4^{3-}. In the case of the bioactivity study in Tris, the Ca and P detected in solution and any apatite detected entirely originated from the glass composition. For those low phosphate containing glasses, the lack of phosphate leads to no or much slower apatite formation in Tris while the PO_4^{3-} from SBF effectively aids the formation of apatite. Therefore, the choice of immersion solution for the estimation of glass bioactivity is highly important.

Summary

The sodium-free, high phosphate $CaCl_2$ containing (0 – 16.7 mol%) bioactive silicate glasses have been successfully synthesised by a melt-quench route and studied for

the first time. The compositional analysis demonstrates that a significant retention of chloride is achieved in the Q^2 type silicate glass. The bioactivity study has revealed that the chloride containing bioactive glasses are highly degradable and form an apatite-like phase within 3 hours immersion in Tris buffer. Glass degradation rate increased with $CaCl_2$ content. A reduction of density and an increase of glass molar volume on increasing $CaCl_2$ suggests that chloride expands the glass volume and dilutes glass network, therefore, promoting ion exchange and glass degradation. The DSC results demonstrated a distinct reduction in the glass transition temperature (T_g) correlating linearly with an increase in chloride content up to 11.9 mol%. The decrease of T_g indicates a potential decrease in the glass hardness. These novel chloride containing bioactive glasses have outstanding potential for applications in remineralising toothpastes and resorbable bone substitutions.

7 Sodium-Free Mixed CaF_2 - $CaCl_2$ Containing Bioactive Glasses

Foreword

The presence of fluoride in sodium-free bioactive glass resulted in formation of fluoride substituted apatite on immersion, as shown in Chapter 5. However, the crystallisation tendency of the as-quenched glasses increased dramatically with an increase in CaF_2 content and the excess CaF_2 led to an uncontrolled crystallisation of fluorite during quenching or upon immersion in buffer solutions.

As shown in Chapter 6, the crystallisation tendency of the chloride containing glasses was much lower than the fluoride ones. All the studied chloride containing glasses with $CaCl_2$ content up to 16.7 mol% were largely amorphous. Moreover, chloride caused a reduced glass transition temperature, an increased glass molar volume and a faster glass degradation rate. However, a hydroxyapatite-like phase was the only phase formed on immersion.

In this chapter we investigate the possibility of incorporating both fluoride and chloride into silicate bioactive glasses and to take advantage of the benefits associated with the presence of both. Thus mixed fluoride/chloride series can serve as a prototype for a potential commercial product where an excessive amount of fluoride in the bioactive glass is replaced by chloride. A glass, which is able to form fluorapatite and also has lower abrasivity is particularly attractive for remineralising and desensitising toothpastes. In this chapter the results on a mixed fluoride/chloride system are presented. Glass bioactivity in terms of glass degradation and apatite formation was estimated in Tris buffer as for the other systems.

7.1 Results of the As-Quenched Glasses

Except for the optically transparent glass with the lowest amount of fluoride and chloride (2.6 mol% CaX_2 X=F+Cl) the as-quenched glass frits (>2.6 mol% CaX_2 (X=F+Cl)) were optically slightly opaque.

7.1.1 Compositional Analysis

The percentages of the retained chloride in the initial glasses after volatilization are plotted against the as-designed CaX_2 (X=F+Cl) content in Figure 7.1.1. A large fraction (77-90%) of chloride is retained in the glasses, whilst the highest amount of $CaCl_2$ losses is found in the lowest $CaCl_2$ containing glasses. Similar proportions of chloride (73-88%) have been retained in the chloride containing glasses as seen in Chapter 6. As discussed in detail in Chapter 6, chloride is likely to evaporate as $CaCl_2$ rather than HCl. Therefore, based on this assumption and taking into account the results of chloride quantitative analysis the actual glass compositions recalculated are given in Table 7.1.1.

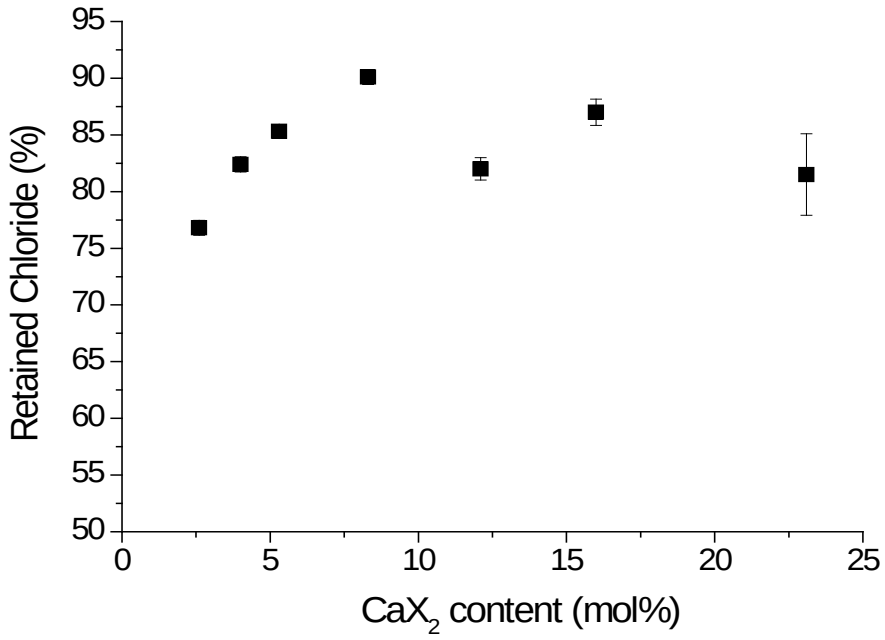

Figure 7.1.1. The percentage of the retained chloride in the initial glasses plotted against the as-designed CaX_2 (X=F+Cl) content. Note where error bars are not shown they are smaller than the data point.

Table 7.1.1 For each glass, the first row is the nominal composition as-designed and the second row is composition re-calculated based on the chloride component analysis and assumed chlorine losses as $CaCl_2$.

Glass code	SiO_2	CaO	P_2O_5	CaF_2	$CaCl_2$	Total CaX_2
GPFCl 0.0	38.1	55.5	6.3	0.0	0.0	0.0
	38.1	55.6	6.3	0.0	0.0	0.0
GPFCl 2.6	37.1	54.1	6.1	1.5	1.1	2.6
	37.2	54.2	6.1	1.5	0.9	2.4
GPFCl 4.0	36.6	53.4	6.0	2.3	1.7	4.0
	36.8	53.5	6.1	2.3	1.4	3.7
GPFCl 5.3	36.2	52.6	5.9	3.0	2.3	5.3
	36.3	52.8	6.0	3.0	1.9	4.9
GPFCl 8.3	35	51.0	5.8	4.7	3.6	8.3
	35.1	51.2	5.8	4.7	3.2	7.9
GPFCl 12.1	33.5	48.8	5.6	6.9	5.2	12.1
	33.8	49.3	5.6	7.0	4.3	11.3
GPFCl 16.0	32.1	46.7	5.3	9.1	6.9	16.0
	32.4	47.1	5.4	9.2	6.0	15.2
GPFCl 23.1	29.3	42.7	4.9	13.2	9.9	23.1
	29.9	43.6	5.0	13.4	8.1	21.5

7.1.2 XRD Results of the As-Quenched Glasses

Figure 7.1.2 shows the XRD patterns of the as-quenched mixed CaF_2 and $CaCl_2$ containing bioactive glasses. The amorphous glass halo at 30° 2θ is found in all the CaX_2 (X=F+Cl) containing glasses. The typical apatite diffraction lines at 25.9°, 31.8°, 32.2° and 33° 2θ (FAP: 00-034-0011) are noticed in the glasses with CaX_2 content higher than 2.6 mol%. The intensities of the apatite diffraction lines are relatively low in glass GPFCl 8.3. The additional minor diffraction lines at 28.3° and 47° 2θ possibly corresponding to fluorite (CaF_2, 00-004-0864) are found in the GPFCl 16.0 and GPFCl 23.1. Unlike in the GPF glass series, the crystallisation of cuspidine has not been seen in the mixed glass series.

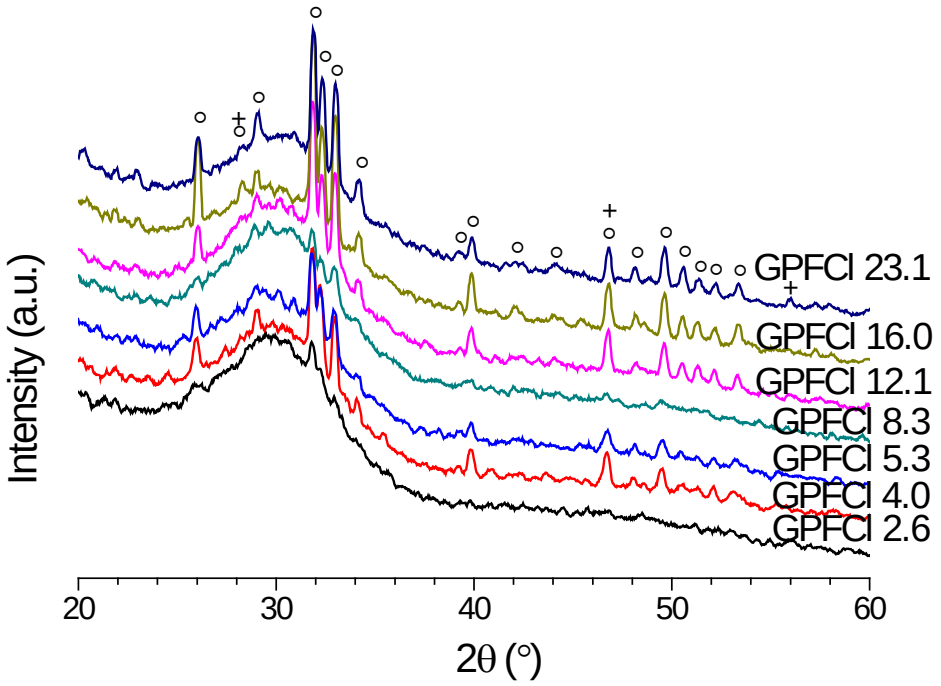

Figure 7.1.2 The XRD patterns of as-quenched CaX_2 (X=F+Cl) containing glasses (°: $Ca_{10}(PO_4)_6F_2$; +: CaF_2).

7.1.3 FTIR Results of the As-Quenched Glasses

The FTIR spectra of the as-quenched CaX_2 containing glasses are shown in Figure 7.1.3. The non-bridging oxygen band at 920 cm^{-1} and the Si-O-Si stretching band at 1030 cm^{-1} are found in the whole glass series. The characteristic apatite split bands at 560 and 613 cm^{-1} are seen in the spectra of most CaX_2 containing glasses apart from glass GPFCl 2.6, the latter has a small band corresponding to amorphous calcium phosphate around 600 cm^{-1} [133].

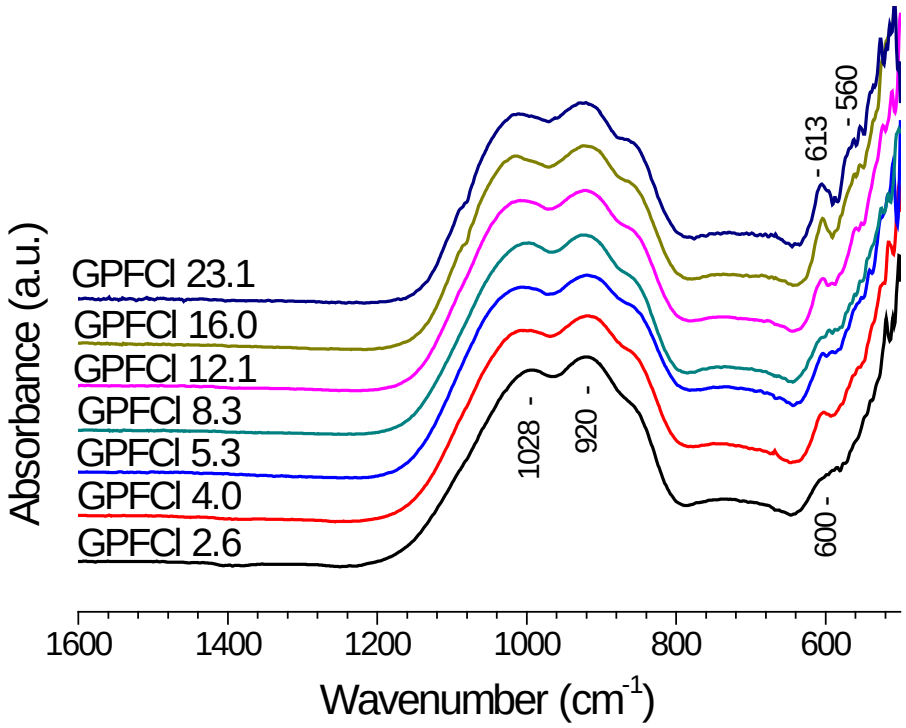

Figure 7.1.3 The FTIR spectra of as-quenched CaX_2 (X=F+Cl) containing glasses.

7.1.4 ^{31}P and ^{19}F NMR Results of the As-Quenched Glasses

The ^{31}P MAS-NMR spectra of the as-quenched mixed CaF_2 and $CaCl_2$ containing bioactive glasses are shown in Figure 7.1.4. The single peak located at about 3-3.3 ppm is visible in the spectra of all the glasses, suggesting that phosphate is present as calcium orthophosphate [4]. In general, for those glasses with CaX_2 content higher than 2.4 mol%, the orthophosphate peak is slightly sharper and narrower with an

increase in CaX_2 content down the series and clearly shows the presence of more than one signal strongly overlapping with each other. This can potentially indicate the minor presence of the crystalline phase and that the glasses with CaX_2 content higher than 2.4 mol% tend to partially crystallise to apatite. Moreover, the peak position shifts downfield to a slightly higher ppm value when the glasses have CaX_2 content equal and higher than 11.3 mol%. In other words, a higher deshielding of the phosphorus nuclei occurs in the glass with higher mixed CaF_2 and $CaCl_2$ local environment. A similar deshielding effect was illustrated in the ^{31}P MAS-NMR spectra for mixed fluoro-chloroapatite ($Ca_5(PO_4)_3F_{1-x}Cl_x$, when X<0.5) by O'Donnell [134]. This suggests that presence of mixed fluoride and chloride might have similar effects on the phosphate environment in the glass phase as the ones in the mixed apatite phase.

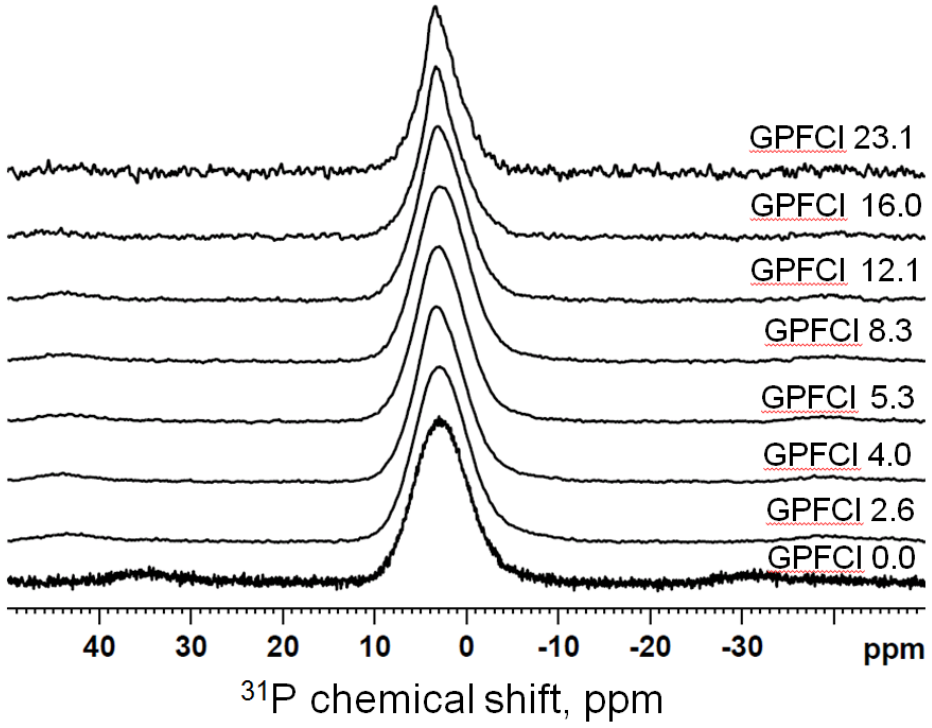

Figure 7.1.4 The ^{31}P MAS-NMR spectra of as-quenched CaX_2 (x=F+Cl) containing glasses.

Figure 7.1.5 shows the ^{19}F MAS-NMR spectra of the as-quenched mixed CaF_2 and $CaCl_2$ containing glasses. The single broad peak with a chemical shift about -96 ppm is seen in all the glass spectra. In addition, a small shoulder at -103 ppm corresponding to FAP appears in the spectra for the glasses with CaX_2 contents higher

than 2.4 mol%. The broad peak contains signals from the amorphous F-Ca(n) environment in the glass, the F-Ca(3) site in the apatite structure in addition to the overlapping spinning side bands from both signals. Note that a clear increase in the line-width occurs in the spectra of GPFCl 16.0 and GPFCl 23.1. It can be attributed to the presence of an additional crystalline F-Ca(4) site at -108 ppm as a result of CaF_2 crystallisation and its spinning side bands in the spectra.

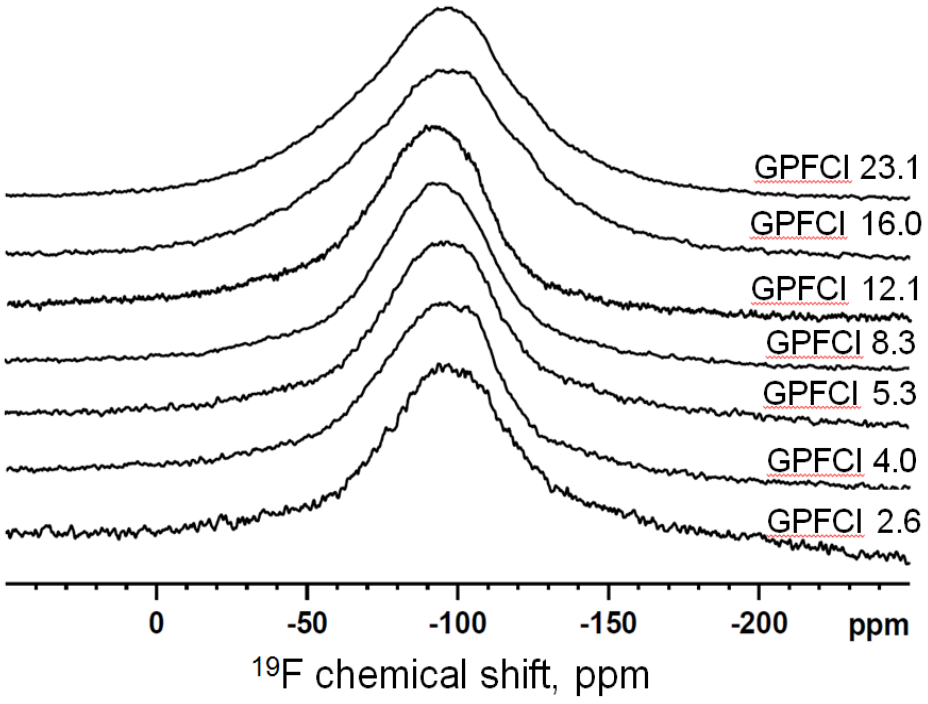

Figure 7.1.5 The ^{19}F MAS-NMR spectra of the as-quenched mixed CaF_2 and $CaCl_2$ containing glasses.

7.1.5 Glass Density

The density and molar volume of CaX_2 containing bioactive glasses are plotted as a function of the CaX_2 content in Figure 7.1.6. The density values fluctuate between 2.90 to 2.93 g/cm^3, whereas the glass molar volume increases linearly and significantly with increasing calcium halide content. The black dotted line is just for eye guiding. Owing to the fact that the chloride ion is much larger than fluoride ion and therefore the expansion of glass volume is thought to be mainly contributed by the presence of chloride.

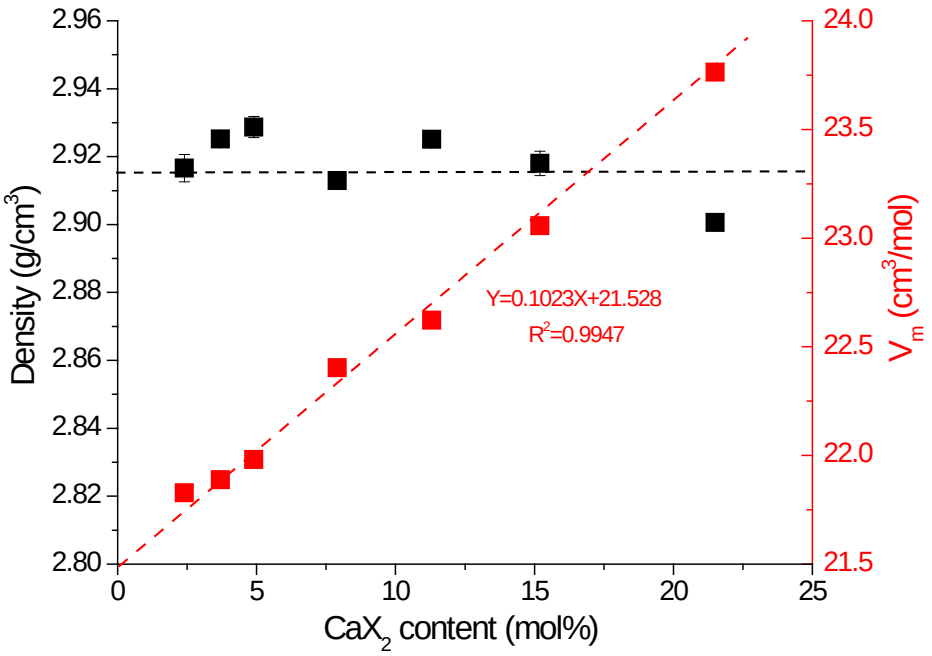

Figure 7.1.6 Glass density and molar volume plotted as a function of CaX_2 (X=F+Cl) content.

7.1.6 DSC Results of the Na free Mixed CaF_2 and $CaCl_2$ Containing Bioactive Glasses

Figure 7.1.7 presents the DSC traces for glass frits of sodium-free mixed CaF_2 and $CaCl_2$ containing glasses. All the glasses have at least two exotherms, but no endotherm peak is found in any glass composition. The obtained T_g and T_c from the DSC traces with an accuracy of ±5 °C are summarised and listed in Table 7.1.2.

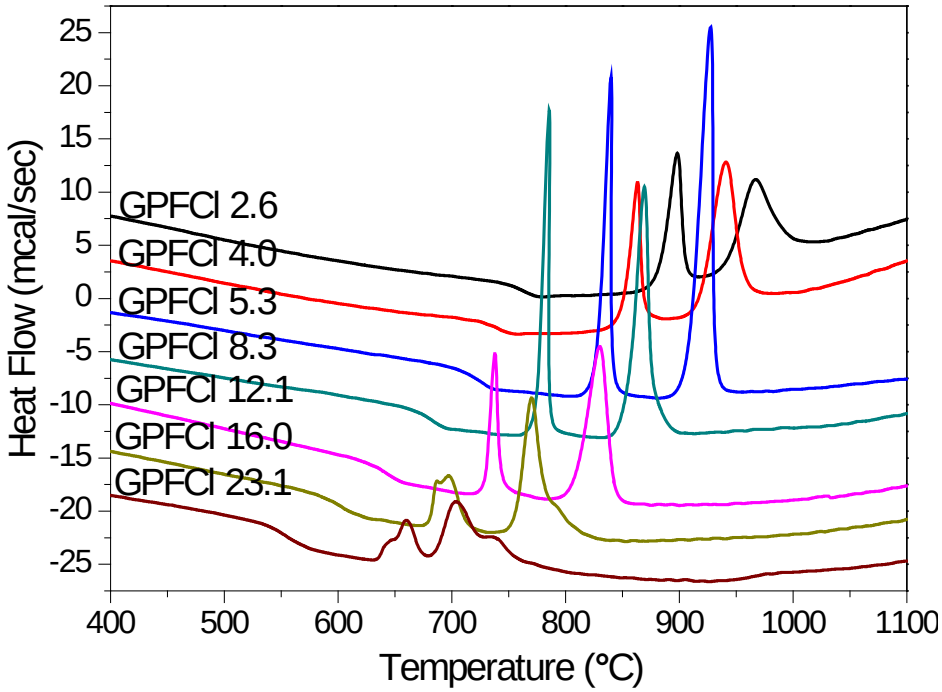

Figure 7.1.7 DSC traces for the glass frits of mixed CaF_2 and $CaCl_2$ containing glasses. The numbers are molar percentage of CaX_2 (X=F+Cl) in the compositions.

Table 7.1.2 Characteristic temperatures for mixed fluoride and chloride containing glasses. For each glass composition, the first row is the characteristic temperature of glass frit and the second row is the characteristic temperature of fine powder.

Glass Code	T_g	T_{o1}	T_{c1}	T_{c2}	T_{c3}	T_m
GPFCl 0.0	786	969	1013	-	-	
	790	901	925	-	-	-
GPFCl 2.6	749	875	902	967	-	-
	733	840	906	-	-	-
GPFCl 4.0	727	846	865	942	-	-
	723	825	856	876	-	-
GPFCl 5.3	707	821	840	930	-	-
	705	807	830	867	-	-
GPFCl 8.3	665	771	785	871	-	-
	664	750	777	811	-	-
GPFCl 12.1	626	725	737	825	-	-
	625	713	733	786	-	-
GPFCl 16.0	578	680	689	700	771	-
	581	675	695	758	-	-
GPFCl 23.1	534	638	658	704	795	-
	534	578	655	710	-	-

The glass transition temperature (T_g) of frit is plotted as a function of the mixed CaF_2 and $CaCl_2$ content in Figure 7.1.8. It is clear that, an increase of CaX_2 content results in a reduction in T_g. A linear relationship (Y= -13.609X+779.34, R^2=0.9949) between T_g and CaX_2 content is seen in the CaX_2 containing glasses with the exception of GPFCl 23.1, which contains crystalline CaF_2 in addition to FAP.

The visible linear relationship between T_g and CaX_2 content could be the result of either no halide loss or similar proportion of halide loss for the compositions lying on the straight line. However, the XRD, FTIR and ^{31}P NMR results of the as-quenched glasses consistently indicate that glass GPFCl 2.6 is largely amorphous and the glasses with CaX_2 higher than 2.4 mol% are partially crystallised, whilst the results of chloride content in the as-quenched glasses show a similar proportion (10-23 %) of chloride loss during melting. Therefore a conclusion can be drawn that a relatively small and similar proportion of fluoride containing phases (FAP and CaF_2) are formed during quenching in those glasses (GPFCl 4.0, GPFCl 5.3, GPFCl 8.3, GPFCl 12.1 and GPFCl 16.0).

Figure 7.1.9 shows that T_{c1} values for both glass frit (1-2 mm) and fine powder decrease significantly with an increase in CaX_2 content.

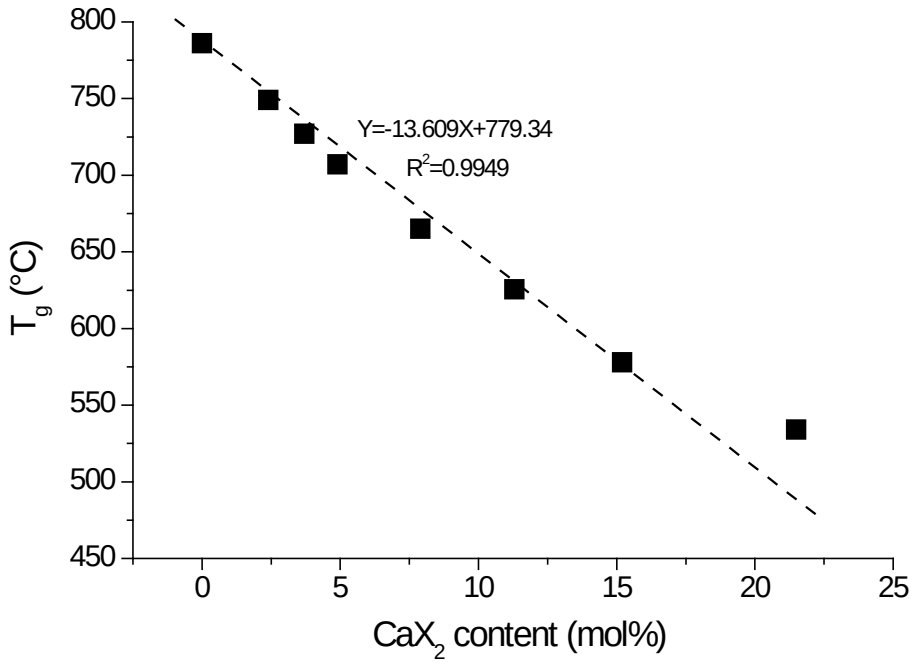

Figure 7.1.8 Glass transition temperature of the frit profiled as a function of CaX_2 (X=F+Cl) content. A linear relationship (Y=-13.609+779.34, R^2=0.9949) between T_g and CaX_2 content was shown in the glasses with CaX_2 content ⩽ 16.0 mol%.

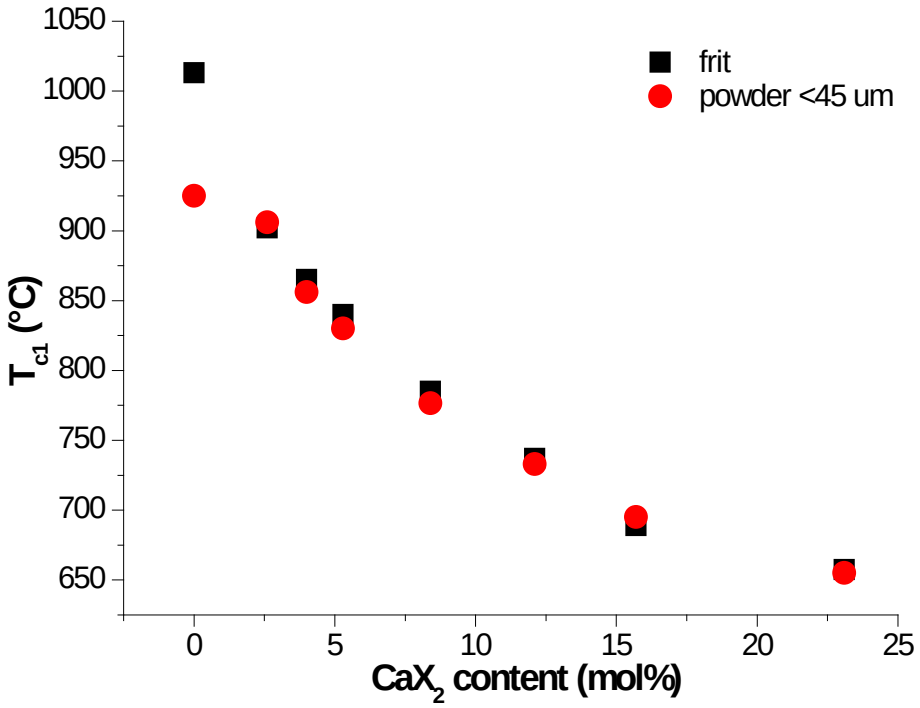

Figure 7.1.9 First Crystallization Peak temperature (T_{c1}) for frit and fine particles plotted against mixed CaF_2 and $CaCl_2$ content.

7.2 Dissolution Study

7.2.1 pH Measurement Results

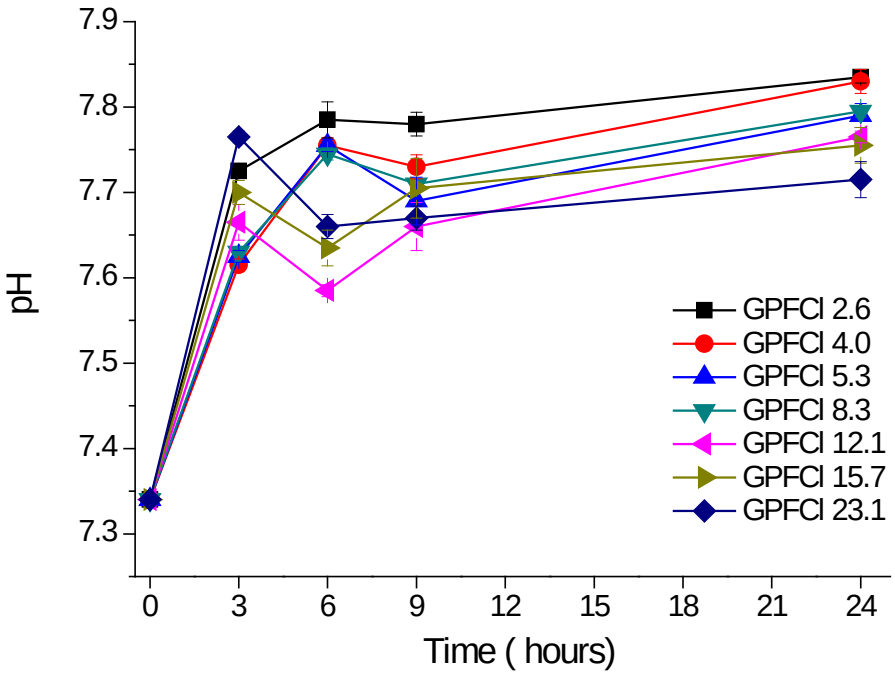

Figure 7.2.1 pH values measured at the end of the immersion time in Tris buffer. The numbers are molar percentage of CaX_2 (X=F+Cl) in the compositions. Note where error bars are not shown they are smaller than the data point.

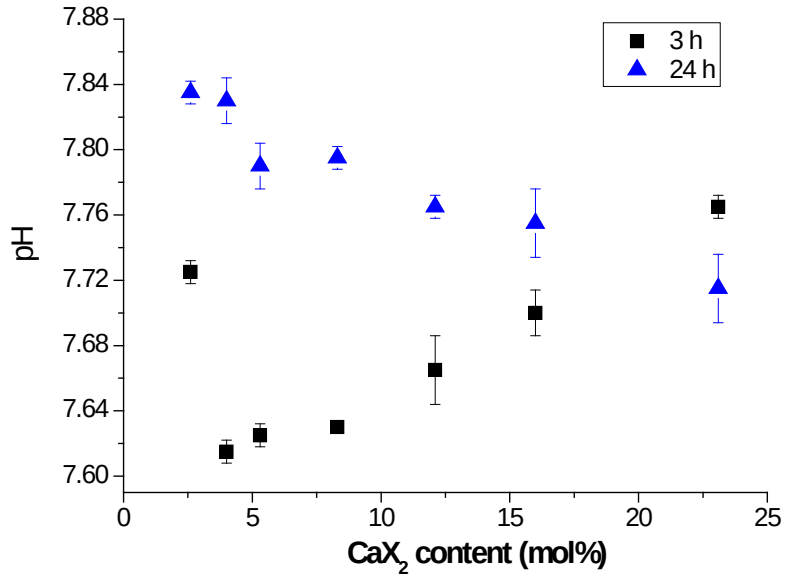

Figure 7.2.2 pH values measured at the end of 3 and 24 hours immersion in Tris buffer plotted against CaX_2 (X=F+Cl) content.

Figure 7.2.1 demonstrates pH changes after immersing the glass powder in Tris buffer for different CaX_2 contents. The general trend is similar for all the glass compositions, though some differences in compositions behaviour can be noticed. For the glasses with CaX_2 content less than 11.3 mol%, pH increases in first 6 hours, decreases slightly from 6 to 9 hours and increases again afterwards. For the glasses with CaX_2 content higher than 7.9 mol%, pH initially increases after 3 hour following a reduction of pH between 3 and 9 hours with a further increase by 24 hours.

Interestingly, Figure 7.2.2 shows two different trends for pH as a function of the CaX_2 content after 3 and 24 hours immersion. The pH of the solution increases with an increase in CaX_2 content after 3 hours but decreases after 24 hours with the exception of GPFCl 2.6. The relatively high pH of GPFCl 2.6 after 3 hours is likely contributed by the faster glass degradation rate of the fully amorphous glass compared with the partially crystallised ones. As shown in Figure 7.1.6, the presence of mixed fluoride and chloride expands glass volume resulting in a more disrupted glass structure, therefore, facilitating the ion exchange between protons from solution and the Ca^{2+}

ions ionically connected to non-bridging oxygens from glass and, thus, aiding glass degradation. The latter causes an increase in Ca concentration found in solution, which will be shown in the next few paragraphs and the pH rise for glasses with higher CaX_2 content after 3 hours of immersion.

7.2.2 Ion Release Results

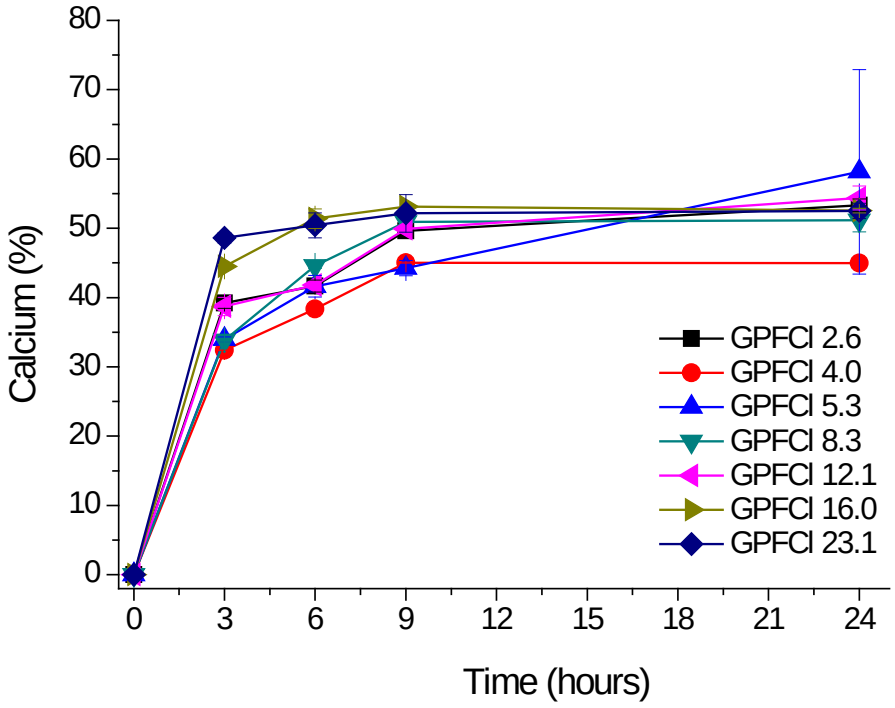

Figure 7.2.3 The concentration of elemental calcium in Tris presented as percentage of the total calcium content in the original mixed CaF_2 and $CaCl_2$ containing glasses as a function of time.

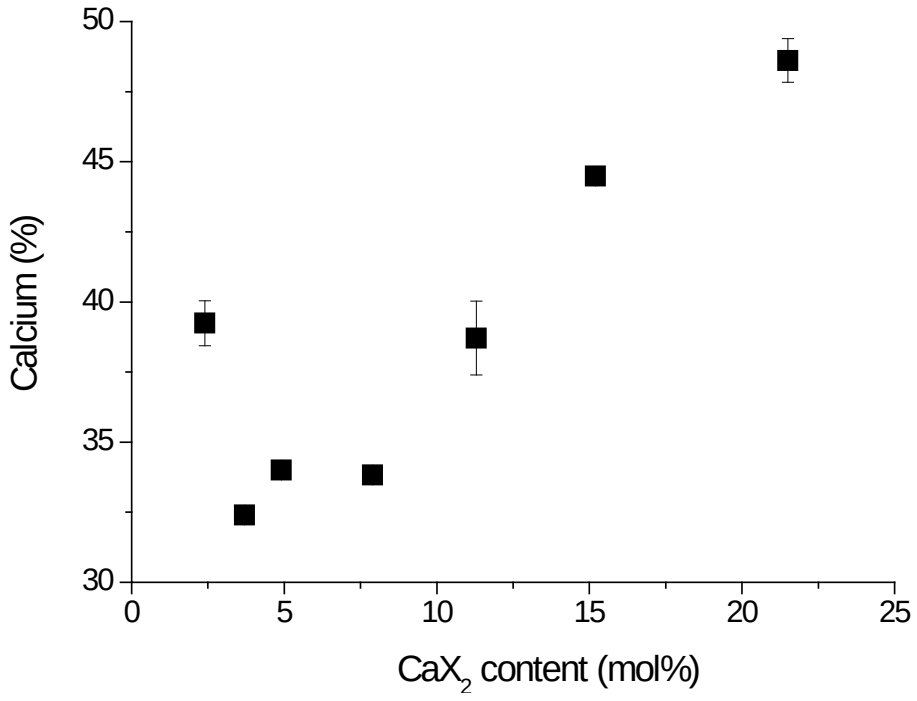

Figure 7.2.4 The Ca concentration measured after 3 hours immersion in Tris buffer plotted as the percentage of the total calcium content in the glass composition against the CaX_2 content.

Figure 7.2.3 shows the concentrations of calcium measured after up to 24 hours immersion in Tris buffer presented as a percentage of total amounts of calcium in the glass compositions. The general trend is similar for all the glass compositions. The percentage of calcium detected in the solution increases in the first 9 hours (particularly in the initial 3 hours) with a nearly stable pH afterwards. This suggests that glass almost completely degrades before 9 hours, whereas apatite formation was very clear between 3 and 9 hours as will be shown further.

The percentage of calcium retained in the solution after 3 hours immersion is plotted as a function of the as-quenched mixed CaF_2 and $CaCl_2$ content in Figure 7.2.4. Apart from GPFCl 2.6, the glasses with higher CaX_2 content have higher percentage calcium release as a consequence of a more expanded glass volume caused by the presence of higher $CaCl_2$ contents. The trend shown is in agreement with the trend for the pH measured after 3 hours immersion in Figure 7.2.2.

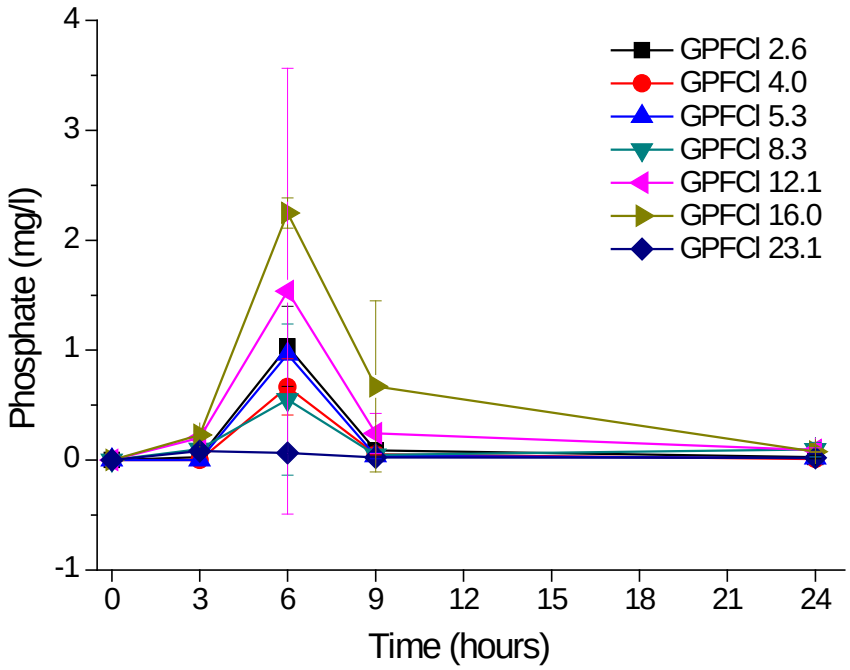

Figure 7.2.5 The concentration of phosphate measured after up to 24 hours immersion in Tris. The numbers are molar percentage of CaX_2 in the compositions.

The similar trends of the phosphate concentration measured up to 24 hours immersion in Tris buffer for mixed CaF_2 and $CaCl_2$ containing glasses are presented in Figure 7.2.4. The phosphate concentration increased in the first 6 hours and decreased afterwards. Low phosphate concentrations (<3 mg/l) are seen for all the glass compositions at different immersion time points.

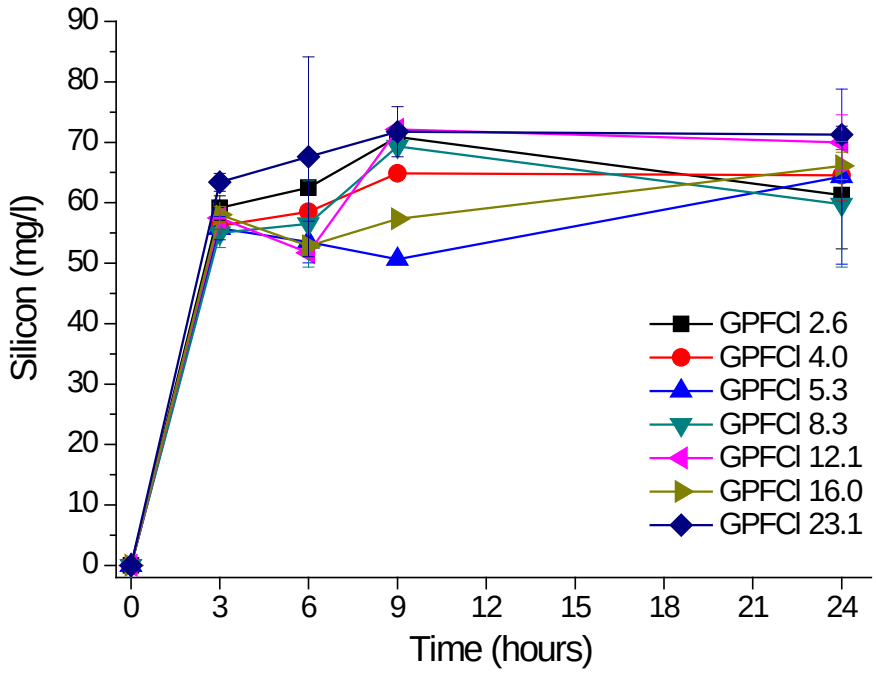

Figure 7.2.6 The concentration of silicon measured in Tris buffer in mg/l plotted as a function of immersion time.

The silicon concentrations in Tris buffer after the immersion of glass powder within 24 hours for mixed CaF_2 and $CaCl_2$ containing glasses have similar trends to the release of calcium (Figure 7.2.6), increasing to 55-65 mg/l in the first 9 hours and keeping nearly constant afterwards.

7.3 Apatite-like Phase Formation in Tris Buffer Solution

Apatite-like phase (mixed hydroxyl-fluorapatite for GPFCl 2.6 and fluorapatite for the rest of glasses) was expected to precipitate after immersing the mixed CaF_2 and $CaCl_2$ containing bioactive glasses in Tris buffer. The formation of apatite-like phase was evaluated using XRD, FTIR and ^{31}P and ^{19}F MAS-NMR.

7.3.1 X-ray Diffraction Results

The XRD patterns of the glasses before and after immersion in Tris are similar for all the mixed CaF_2 and $CaCl_2$ containing glasses. The ones for GPFCl 2.6 are selected and presented as an example in Figure 7.3.1.

After 3 hours immersion in Tris, the amorphous glass halo (30° 2θ) broadens out, whilst the characteristic diffraction lines of apatite at 25.9°, 31.8° and 33° 2θ observed indicate rapid apatite-like phase formation within 3 h immersion. The intensity of those diffraction lines are enhanced within 9 h immersion.

The XRD patterns of the precipitates collected after 3 hours immersion in Tris for all the mixed CaF_2 and $CaCl_2$ glasses are shown in Figure 7.3.2. The amorphous glass halos at 30°2θ largely disappear. The diffraction lines corresponding to apatite occur in all the XRD patterns. However, the intensity of diffraction lines for those partially crystallised glasses is much stronger than the equivalent amorphous glass (GPFCl 2.6). Moreover, additional diffraction lines at 28.3° and 47°2θ associated with CaF_2 appear in the XRD patterns of GPFCl 16.0 and GPFCl 23.1.

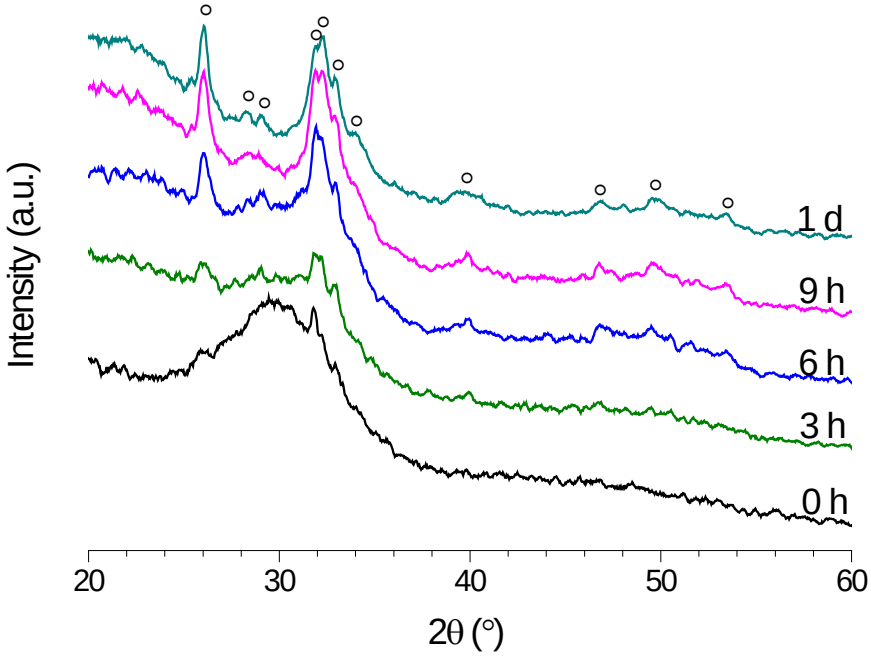

Figure 7.3.1 The XRD patterns of the glass precipitates with 2.4 mol% CaX_2 collected after immersion in Tris up to 1 day (°: $Ca_{10}(PO_4)_6F_2$).

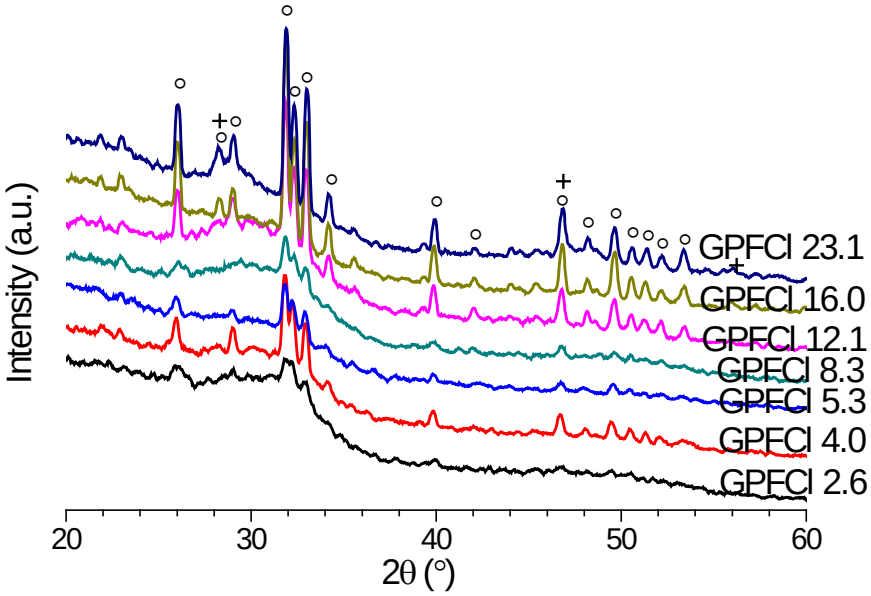

Figure 7.3.2 The XRD patterns of the glass precipitates collected after 3 hours immersion in Tris (°: $Ca_{10}(PO_4)_6F_2$; +: CaF_2).

7.3.2 Fourier Transform Infrared Spectroscopy Results.

In addition to the ion release study by ICP-OES, FTIR was also used to monitor glass degradation and apatite-like phase formation upon immersion. Figure 7.3.3 shows the spectra of the precipitates collected after immersion in Tris up to 1 day for GPFCl 2.6, while Figure 7.3.4 summaries the spectra of precipitates collected after 3 hours of immersion for all the CaX_2 containing glasses. After immersing glass powder in Tris for 3 hours, the FTIR spectra changed significantly. The intensity of non-bridging oxygen $Si\text{-}O^-$ bands at 850 and 920 cm^{-1} reduces. The amorphous calcium orthophosphate bands disappear, while the crystallised orthophosphate (apatite) bands develop at 560, 613 and 1035 cm^{-1}. These typical apatite bands intensify with immersion time up to 9 hours but do not alter significantly with a further increase in immersion time. In addition, carbonate bands at 1450 cm^{-1}, 1420 cm^{-1} and 870 cm^{-1} are visible after 3 hours immersion, suggesting the substitution of carbonate in the apatite lattice. These evolutions are similar to the seen above in the previous Chapters and have been discussed in more details in Chapter 5.

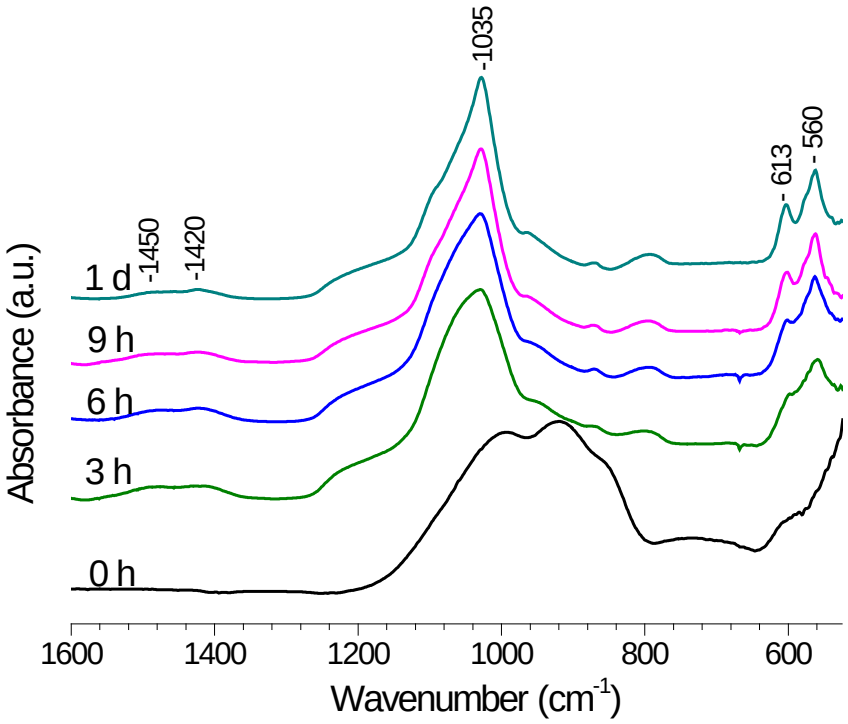

Figure 7.3.3 The FTIR spectra of the glass precipitates with 2.4 mol% CaX_2 collected after immersion in Tris up to 1 day.

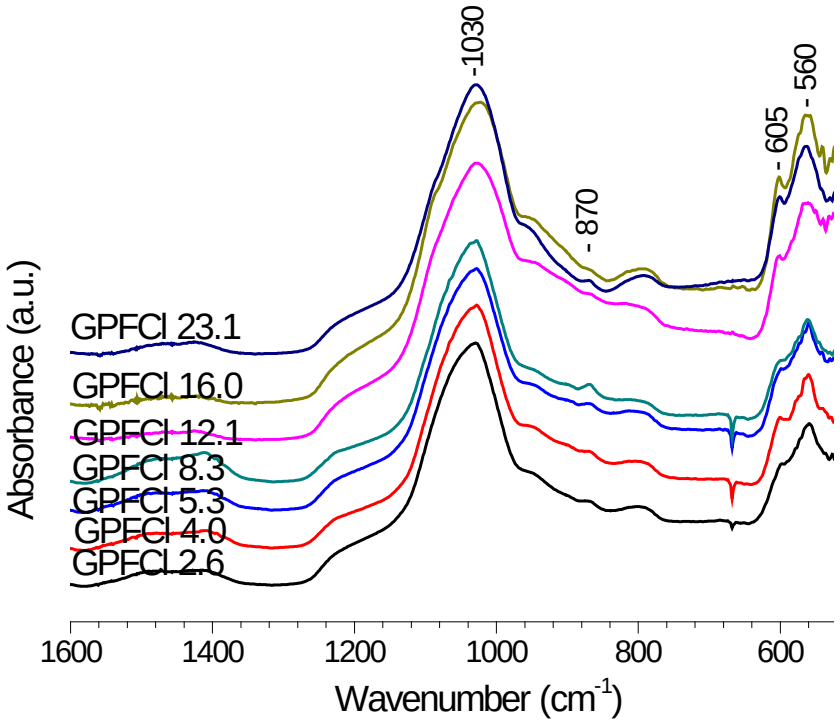

Figure 7.3.4 The FTIR spectra of the glass precipitates collected after 3 hours immersion in Tris for mixed CaF_2 and $CaCl_2$ containing glasses.

7.3.3 NMR Results of Mixed CaF_2 and $CaCl_2$ Series Glasses

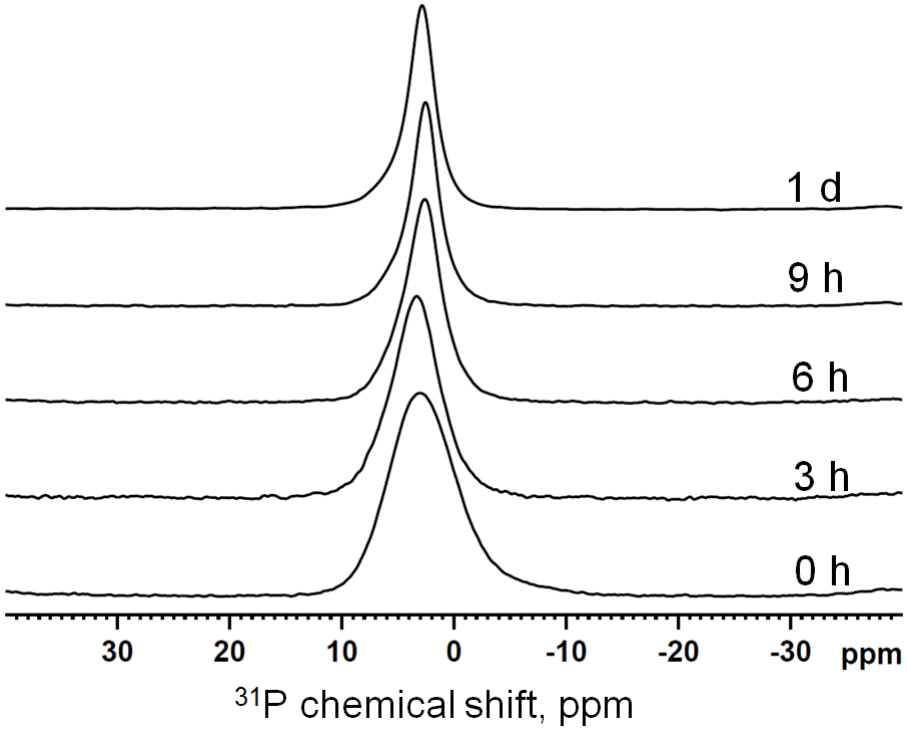

Figure 7.3.5 The ^{31}P MAS-NMR spectra of the glass precipitates with 2.4 mol% CaX_2 (GPFCl 2.6) collected after immersion in Tris. The bottom spectrum is for the untreated glass powder. The numbers are immersion times.

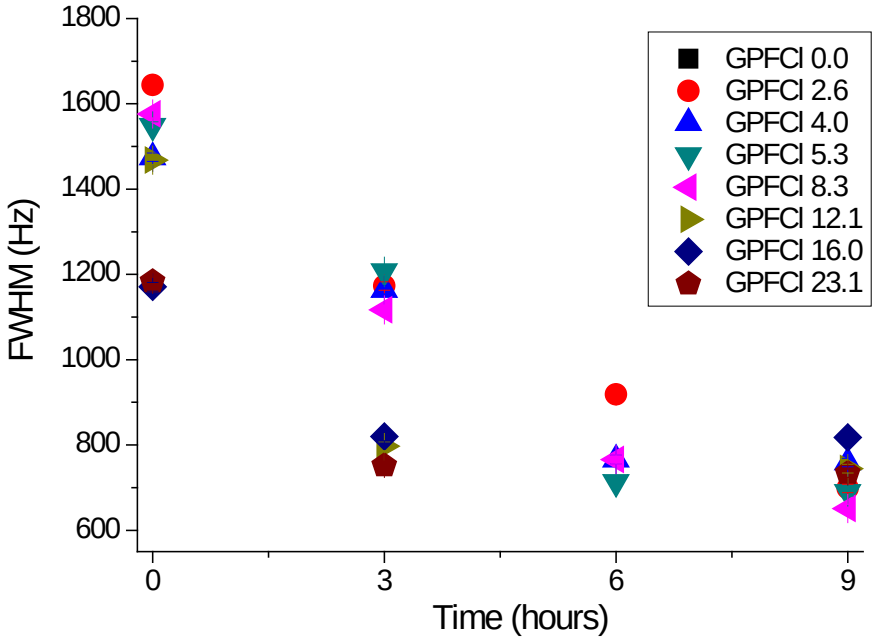

Figure 7.3.6 FWHM for ^{31}P MAS-NMR spectra plotted as a function of immersion times in Tris buffer. The estimated errors (10 Hz) are smaller than the data point.

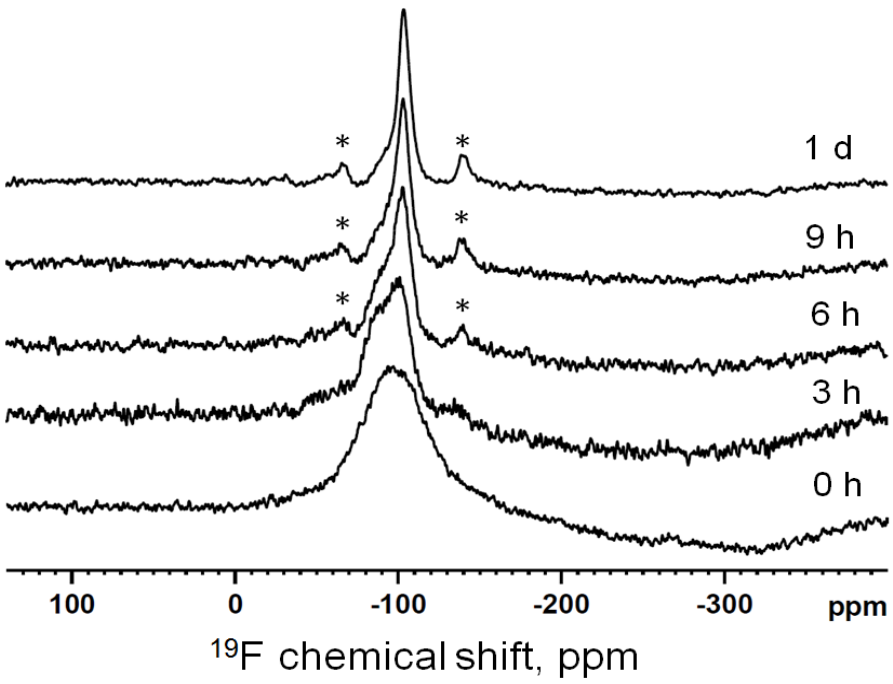

Figure 7.3.7 The ^{19}F MAS-NMR spectra of the glass precipitate with 2.4 mol% CaX_2 collected after immersion in Tris, the signals symmetrically situated on both sides of the main signal and labelled by asterisk present side bands.

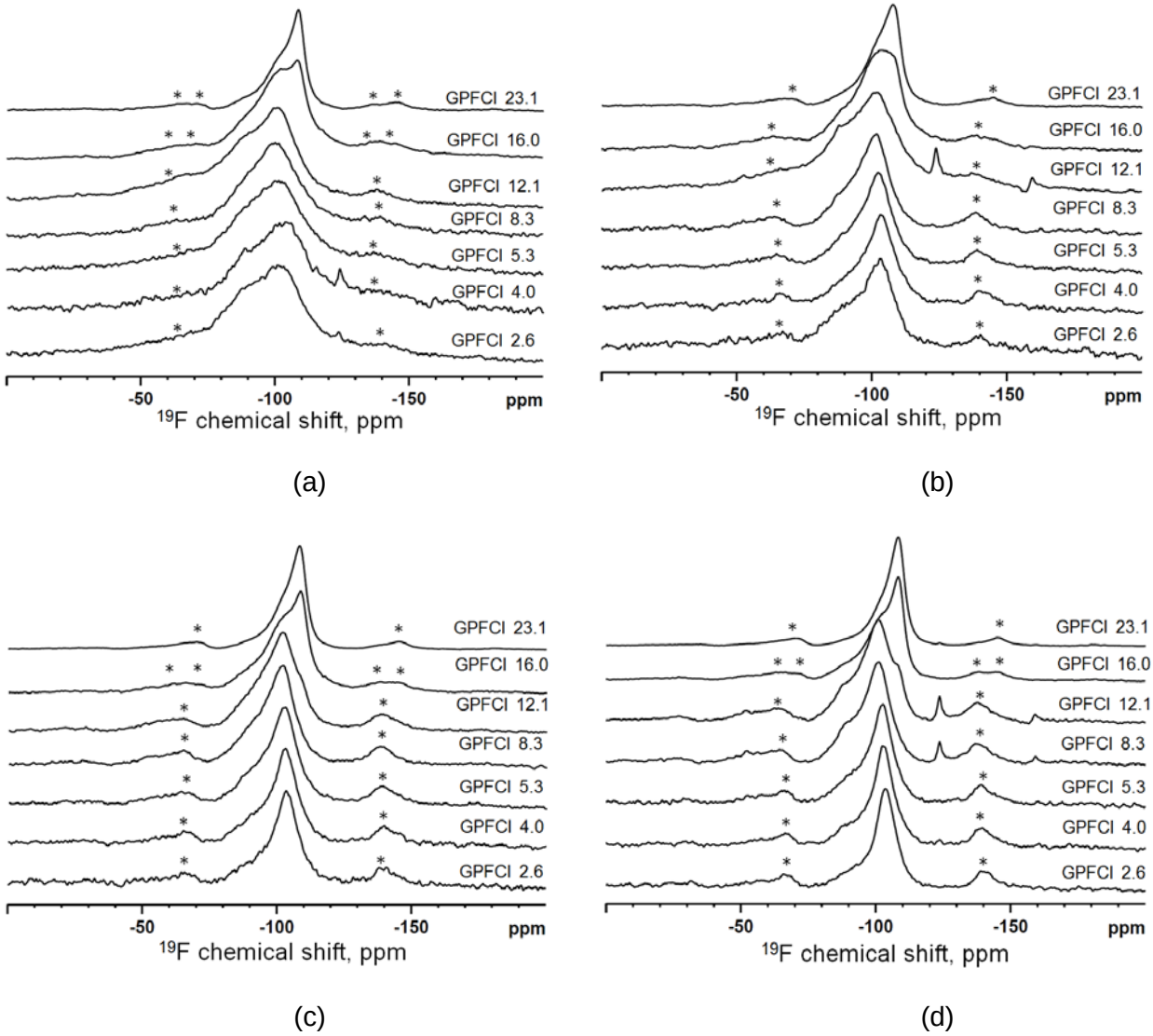

Figure 7.3.8 The ^{19}F MAS-NMR spectra of the glass precipitates collected after immersion in Tris for mixed CaF_2 and $CaCl_2$ containing glasses. (a) after 3 hours; (b) after 6 hours; (c) after 9 hours and (d) after 1 day.

The atomic environment of phosphate in the precipitates collected after immersion was determined by using ^{31}P MAS-NMR. As we can see in Figure 7.3.5, which demonstrates the ^{31}P MAS-NMR spectra of GPFCl 2.6 after immersion in Tris, the single broad peak assigned to amorphous calcium orthophosphate narrows down gradually with increasing immersion time. However, the chemical shift is almost kept constant at 3 ppm. Similar changes are found in the rest glass compositions.

The full width half maximum (FWHM) of ^{31}P signals for mixed CaF_2 and $CaCl_2$ containing bioactive glasses before and after immersion in Tris are plotted as a function of immersion times in Figure 7.3.6. Before immersion, the glasses with CaX_2 content equal to and less than 11.3 mol% have bigger FWHM than glasses GPFCl 16.0 and GPFCl 23.1, indicating that there is more apatite formed with the glasses with 15.2 and 21.5 mol% CaX_2. In addition, it is clear that, the FWHM of the ^{31}P spectra for the glass before immersion is much larger than the ones after immersion. The FWHM values decrease with increasing in immersion time up to 6 hours. A smaller reduction is observed for further immersion from 6 to 9 hours, in particular for the glasses with CaX_2 over 11.3 mol% that with a relatively higher crystallinity. Those changes suggest the transformation of orthophosphate from an amorphous state to a crystalline state on immersion, particularly before 6 hours immersion. Whilst, those high CaX_2 containing glasses (≥ 11.3 mol%) have more pronounced apatite formation on immersion, as a result of the seeding effect arising from the presence of apatite nuclei in the initial glasses.

Figure 7.3.7 presents the ^{19}F MAS-NMR spectra of the precipitates collected after immersion in Tris up to 24 hours compared with the as-quenched glass for glass GPFCl 2.6. The symmetrical signals labeled by asterisks present side bands. After 3 hours immersion, the line-width of ^{19}F NMR peak decreases, suggesting the amorphous F-Ca (n) converts to the crystalline one. This is in good agreement with the ^{31}P MAS-NMR results in Figure 7.3.5. The asymmetric peak with a broad shoulder at low frequency shifts towards -103 ppm (F-Ca(3)) assigned to fluorapatite and indicate the presence of both fluorapatite and residual amorphous glass phase in the collected precipitates. A decrease in intensity of the broad low frequency shoulder and the increasing magnitude of fluorapatite peak at -103 ppm indicate a continuous process of glass dissolution and fluorapatite formation. Similar changes are found in the spectra of those glasses with CaX_2 contents less than 16.0 mol % as presented in Figure 7.3.8 (a)-(d). Note that, the peak at -108 ppm corresponding to crystalline CaF_2

appears in the spectra of GPFCl 12.1, GPFCl 16.0 and GPFCl 23.1 after 9 hours immersion and is more pronounced by 24 hours (Figure 7.3.8 (c)-(d)).

Moreover, for the glasses with CaX_2 content equal or higher than 16.0 mol%, the spectra are slightly different from the lower CaX_2 containing glasses. For instance, after 3 hours immersion in Tris, apart from seeing a reduction in intensity of amorphous F-Ca (n) signal, the split peaks at -103 and -108 ppm corresponding to FAP and CaF_2 are also seen in the spectra of GPFCl 16.0. Whereas the distinct and sharp peak at -108 ppm with a small shoulder at -103 ppm is observed in the spectra of GPFCl 23.1 (Figure 7.3.8 (a)). These differences indicate that the glasses with high CaX_2 content (≥ 16.0 mol%) are not only crystallised to fluorapatite but also CaF_2. The CaF_2 peak becomes more dominant with increasing immersion time (Figure 7.3.8 (b)-(d)). Furthermore, it is also worth mentioning that, in some of the spectra from Figure 7.3.8, a shoulder at - 88 ppm or / and a small peak at -123 ppm are also visible.

Further Discussion

In the present study, 77-90% of the chloride has also been successfully retained in the Q^2 type mixed CaF_2 and $CaCl_2$ containing silicate glasses similar to the GPCl glass series studied in Chapter 6. Therefore a conclusion can be drawn that adding chloride into a Q^2 type silicate glass effectively minimizes the chlorine loss.

The incorporation of mixed CaF_2 and $CaCl_2$ content above 2.4 mol% into glass compositions results in the crystallisation of FAP and an additional CaF_2 phase in glass GPFCl 16.0 and glass GPFCl 23.1. It is unlikely to see ClAP crystallisation in an identical fashion of FAP in those glasses. The fundamental cause is the fact that fluoride ion is much smaller than chloride ion. The formation of FAP requests less lattice energy compares with equivalent ClAP. In addition, the studied glass system is phosphate deficient and the fluoride content in the composition is sufficient to combine all the phosphate for FAP formation.

Experimental results provide an overwhelming evidence to reveal the fact that adding fluoride and chloride into a silicate bioactive glass allows one to obtain the benefits associated with the presence of both fluoride and chloride. The presence of chloride expands glass volume dramatically, resulting in faster glass degradation, in agreement with the pH data (Figure 7.2.2) and Ca ion release data by 3 hours immersion (Figure 7.2.4). Meantime, the presence of fluoride favors a more acid resistant FAP formation on immersion. However the mixed halide glasses crystallised more readily on quenching than the fluoride glasses (GPF series).

It is well-known that the Ca:P:F ratio in fluorapatite is 5:3:1. However, the studied glass GPFCl 2.6 is fluoride deficient as the ratio of Ca:P:F is 17.9 : 4.05 : 1, whilst the rest glasses are phosphate deficient and F rich. Therefore, a mixed hydroxyl-fluorapatite is likely occur for glass GPFCl 2.6 after immersion in Tris buffer, while fluorapatite is expected for the glasses with CaX_2 content higher than 2.4 mol%. Moreover, the

excess fluoride, which is over the stoichiometric F in FAP, could lead to CaF_2 precipitation or fluoride rich phase formation after immersion. These consistently account for the fact that FAP is the dominating phase formed after immersion in Tris for the GPFCl glass series, though CaF_2 and some fluoride containing phases with chemical shifts at -88 and -123 ppm are present in some ^{19}F MAS-NMR spectra.

A previous ^{19}F MAS-NMR study by Yi *et al.* [135] reported that a signal at - 88 ppm corresponds to a second fluorine environment in the apatite structure, which is different from the signal assigned to channel fluoride ions in the FAP structure at -103 ppm [136]. This second fluorine environment is the candidate for the electrostatic charge compensation of carbonate groups forming $(CO_3F)^{3-}$, which is incorporated at the B-site (the site for the phosphate tetrahedron) of the apatite structure. The occurrence of such $(CO_3F)^{3-}$ would require the concentration of 6.0 wt% of CO_3^{2-} and higher F content than the stoichiometric F content in FAP.

The substitution of a carbonate group which is locally charge-compensated by fluoride ion at the tetrahedral phosphate site in the apatite structure accounts for the existing chemical shift of fluorine at - 88 ppm in the present study, in agreement with the observed carbonate stretching bands at 1420 and 1450 cm^{-1} and the carbonate bending band at 870 cm^{-1} from FTIR spectra in Figure 7.3.4.

Moreover, with the exception of ^{19}F NMR signals at -88 ppm, an additional peak at -123 ppm is consistent with the non-specifically adsorbed fluoride (NSAF) signal detected previously [137-139]. This NSAF peak originally proposed by Arends *et al.* [137] and latter verified by White *et al*. and is described as the fluoride that is hydrogen-bonded to the phosphate protons on the apatite surface. It is proposed by White *et al.* that the NSAF species may have significant contributions to anticaries reactivity of fluoride [139]. The quantity of NSAF formation is mainly determined by the size of the apatite crystal and F^- concentration in the solution, due to the fact that fluoride reacts only with a small portion of the crystalline lattice on the surface layers.

Summary

A series of high phosphate, mixed CaF_2 and $CaCl_2$ containing bioactive silicate glasses were synthesised. With the exception of glass GPFCl 2.6, which is largely amorphous, the studied glasses are partially crystallised to fluorapatite during quenching. In addition, CaF_2 is also found in glass GPFCl 16.0 and 23.1. The result of chloride content analysis suggests that about 77-90% of chloride is retained in the glasses after melting. The glass transition temperature and crystallization temperature decrease with an increase in CaX_2 content. In contrast, the glass molar volume increases significantly with increasing CaX_2 content, therefore promotes glass degradation. The rapid fluorapatite formation is detected within 3 hours immersion, which is comparable to GPF and GPCl glass series. It is clear that the mixed CaF_2 and $CaCl_2$ containing bioactive glasses combine the benefits from the presence of both CaF_2 and $CaCl_2$. Based on these results it is possible to design silicate glass compositions with the high phosphate, low fluoride and high chloride content that will be particularly of interest to remineralising toothpastes.

8 A Preliminary Study of Bioactive Glass-Ceramics Based on Apatite

Foreword

Glass-ceramics are polycrystalline materials that consist of amorphous phases and crystalline phases, which can be produced by heating the base glasses at or above their crystallisation temperature [140, 141]. Their properties depend on the amount and composition of the crystalline phase formed and the residual glass composition. It is important to note that glass-ceramics are not the products of a physical mixture of glass and crystals but the formation of crystals in a base glass [142].

The controlled crystallisation of glasses is an effective way to synthesise a wide range of glass-ceramics with unusual microstructures and characteristic physical and chemical properties fulfilling a variety of potential applications. The glass crystallisation process consists of two stages, namely nucleation and crystal growth [143]. In the former stage, a high density of the small and stable nuclei are formed throughout the interior of the base glass. In the latter stage, the subsequent growth of the small nuclei occurs. In the first simple approximation, the crystallisation mechanism type can be indicated by measuring the crystallisation temperature of the same glass powder but with different particle sizes. Compared with frit, fine powder has a larger surface area, which provides more nucleation sites for crystallisation. Therefore fine powder is prone to crystallise at a lower temperature [57] if crystal nucleation occurs on the surface. In contrast, when the crystallisation peak temperature is independent of particle size, then this may indicate bulk crystal nucleation.

Bioactive glass-ceramics are promising materials as bone grafts, bone fillers and implants that have received attentions for their favourable biocompatibility and

osteoconductivity arising from the presence of apatite [144-146]. There are two main bioactive glass-ceramics systems: 1). apatite wollastonite (AW) system developed by Kukobo *et al*. [144, 147] and 2). apatite mullite (AM) system synthesised by Hill and co-workers [145, 148]. The AW glass-ceramics system has a fairly high mechanical strength and even exhibits excellent integration with living tissue. However, because of the strong tendency towards surface nucleation of wollastonite, AW glass-ceramics are difficult to cast to the desired shape directly. It has to be sintered and machined to complex shapes using diamond tooling and consequently it is less commercially attractive. Moreover, the relatively low CaF_2 (< 1 mol%) content used in the AW system results in a restricted content of fluoride substitution in the apatite lattice and formation of a mixed oxy-fluorapatite crystal [145]. In contrast to this, the glass-ceramics that are derived from internal nucleation and crystallisation of bulk glasses are more advantageous, in particular they have ability to be cast into complex shapes.

The apatite mullite (AM) glass-ceramics based on the CaO-Al_2O_3-SiO_2-P_2O_5-CaF_2 system, predominantly bulk nucleates, via prior amorphous phase separation and crystallise to fluorapatite (FAP) and mullite crystals. These bioactive glass-ceramics exhibit high fracture toughness and strength and as a consequence of exhibiting bulk nucleation can be readily cast to shape. AM glass-ceramics also show excellent osseo-intergration similar to the AW system [146, 149]. Nevertheless, the possibility of toxicity caused by the release of aluminium in vivo is perceived as being problematic for AM glass ceramics, although the aluminium is incorporated in the mullite phase that is insoluble and almost completely inert.

Brauer *et al.* [4, 150] studied two glass-ceramic series with different amounts of P_2O_5 in the system of Na_2O-CaO-SiO_2-P_2O_5-CaF_2. Mixed sodium calcium fluoride phosphate, FAP, and combeite ($Na_2Ca_2Si_3O_9$) were detected as the main crystalline phases in the glasses with high P_2O_5 content (> 4.7 mol%) [150], whilst no FAP crystallised from low P_2O_5 (< 1.1 mol%) containing glasses [4]. In addition, Brauer *et al*. also found that a

sodium-free CaF_2 containing glass with high P_2O_5 content crystallised to FAP upon heat treatment [150]. These findings reflect the possibility of apatite crystallisation from aluminium free glasses is strongly influenced by the phosphate content.

Fluorapatite glass-ceramics are attractive in dental and orthopaedic application, as a result of their excellent osteoinductivity and osteoconductivity contributed by the FAP crystals and the well-documented bone-regenerative properties of the bioactive glass phase [1, 146, 151]. FAP is comparatively chemically stable in acidic environment and is not very resorbable, FAP glass-ceramics are used for dental crowns [152, 153]. However, in the case of those medical and dental applications particularly where resorption and replacement by bone is desired, HAP glass-ceramics are of particular interest and more attractive compared with FAP glass-ceramics, as hydroxyapatite is more readily dissolved under acidic conditions than fluorapatite. On the other hand, considering glass-ceramics, it is important to note that hydroxyl groups are volatilised during glass melting and are unlikely to be retained in the glass at a sufficient concentration to form hydroxyapatite. This is the main reason for incorporating fluoride and forming the fluorapatite analogue of hydroxyapatite. The substitution of fluoride for hydroxyl has been used with a wide range of glass-ceramics [111, 154, 155].

Elliott and Young [95] have shown that chlorapatite converts to hydroxyapatite in the presence of water. Esther *et al.* [156, 157] also showed that millimetre-size hydroxyapatite single crystals can be obtained from ClAP crystals via the ionic exchange of Cl^- for OH^- under high temperature hydrothermal conditions. Compared with fluorapatite glass-ceramics, ClAP glass-ceramics would be a more favourable alternative to FAP glass-ceramics for medical and dental applications that requires high resorption rate.

Chlorapatite and fluorapatite exhibit extensive solid solution phase formation [108, 134, 158], although the substitution of chlorine and fluorine in the lattice may not be completely random. Forming a mixed fluor-chlorapatite should enable the solubility of

the apatite to be controlled. The solubility could be further optimized by substitution of strontium for calcium, which is known to occur in hydroxyapatite [159] and fluorapatite glass-ceramics [160].

In this chapter the crystallisation events observed via thermal analysis of oxyhalide bioactive glasses were followed. The investigation of the crystallisation was carried out by using DSC, while the identification of crystallisation phases was performed using XRD, FTIR, MAS-NMR and SEM.

8.1 Crystallisation Exotherm

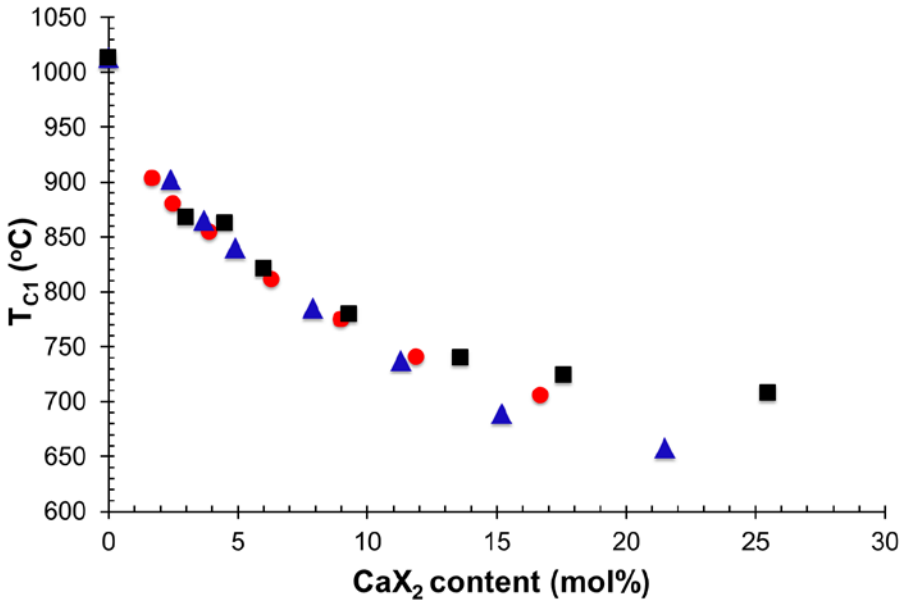

Figure 8.1.1 T_{c1} for glass frit plotted as a function of the actual CaX_2 (X=F/Cl/F+Cl) content. (■ = GPF series, ● = GPCl series, ▲= GPFCl series).

Figure 8.1.1, the first crystallisation temperature of glass frit for GPF glass series, GPCl glass series and GPFCl glass series are plotted against the actual CaX_2 content (the chloride volatilisation as $CaCl_2$ was taken into account). It is clear that T_{C1} decreases with an increase in CaX_2 content mirroring the T_g behaviour (Figure 10.2.1). In addition, the reduction of T_{c1} for the glasses with CaX_2 content less than 10 mol% is more pronounced than the glasses with CaX_2 content higher than 10 mol%, in particular for CaF_2 containing glasses. This is attributed to the crystallisation of fluoride containing phases on a large scale for GPF glass series (> 9.3 mol%) while crystallisation occurs at a relatively small scale for GPFCl series, in good agreement with the glass characterisation results in Chapter 5, 6 and 7.

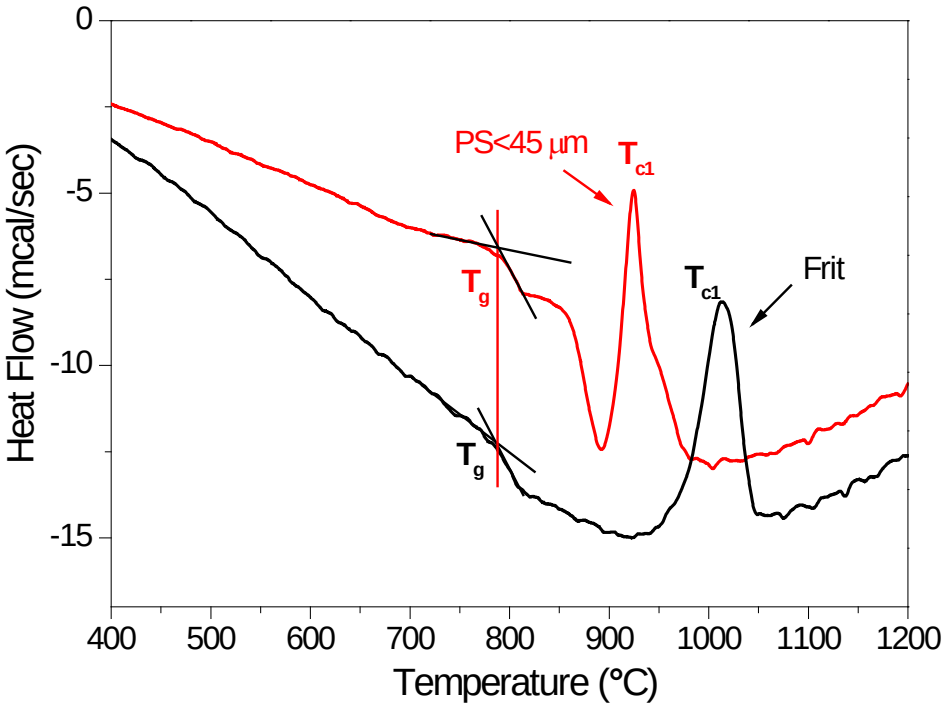

Figure .8.1.2 DSC traces for frit and PS<45 µm powder of GPF 0.0 demonstrating surface nucleation of the first crystallisation phase.

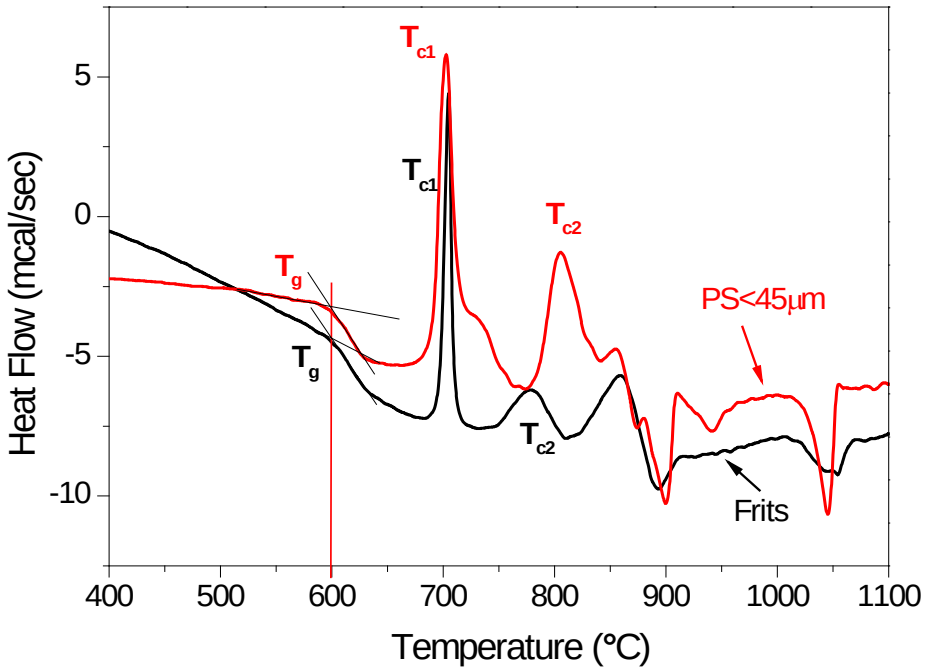

Figure 8.1.3 DSC traces for frit and PS<45 µm powder of GPCl 20.6 (16.7 mol% $CaCl_2$) demonstrating bulk nucleation of the first crystallisation peak.

DSC traces for frit (1-2 mm) and fine powder (< 45 µm) of GPF 0.0 and GPCl 20.6 are shown in Figure .8.1.2 and Figure 8.1.3 respectively. T_{c1} of frit is much higher than the equivalent one for powder in glass GPF 0.0, while T_{c1} of powder and frit are pretty much identical for glass GPCl 20.6. This indicates two different crystallisation mechanisms of the first crystallisation phase for GPF 0.0 and GPCl 20.6.

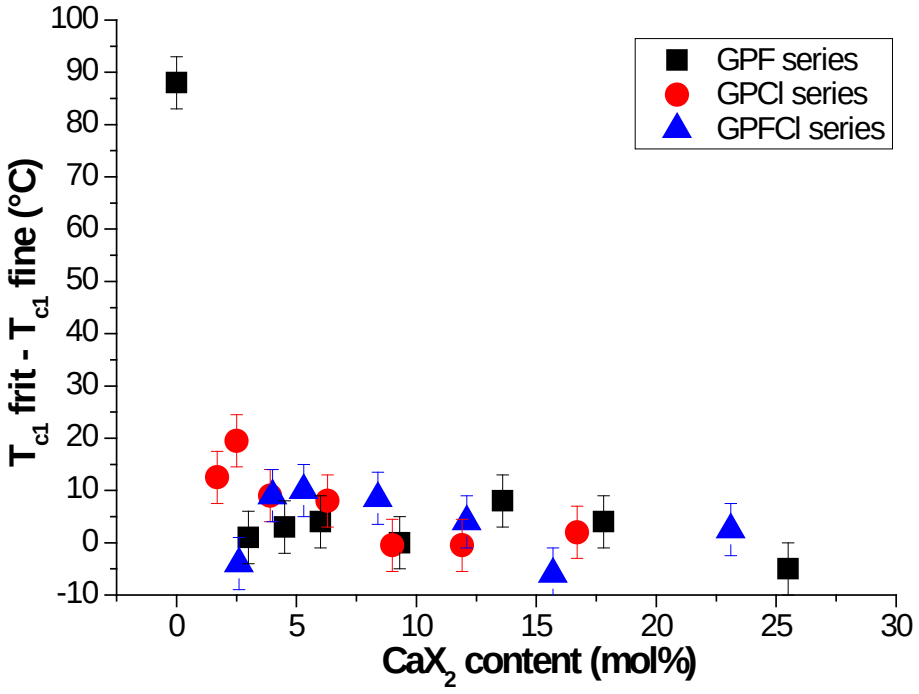

Figure 8.1.4 The difference of first crystallisation temperature between frit and fine powder (T_{c1}frit-T_{c1}fine) plotted against mixed CaF_2 and $CaCl_2$ content.

The difference of first crystallisation temperature between frit and fine powder (T_{c1}frit-T_{c1}fine) for GPF, GPCl and GPFCl glass series are plotted against CaX_2 content in Figure 8.1.4. It is obvious that, for the glass without the presence of CaX_2 (GPF 0.0), the first crystallisation temperature of frit is much higher than the one for fine powder. The incorporation of CaX_2 results in a marked reduction of T_{c1}frit-T_{c1}fine from 88 °C to < 20 °C. This reveals that the T_{c1} for glass GPF 0.0 is particle size dependent, thus, the first crystalline phase is strongly surface-nucleated, while the T_{c1} in the CaX_2 containing glasses tends to be particle size independent and the first crystalline phase

is likely to bulk-nucleate. Thereby a conclusion can be made that the incorporation of calcium halide favours a bulk nucleation.

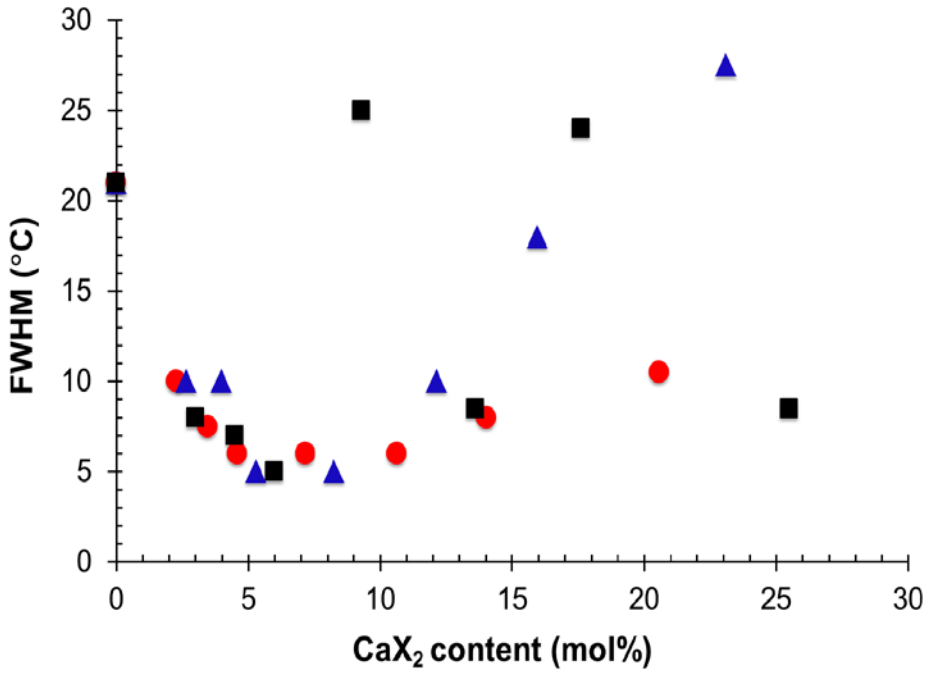

Figure 8.1.5 FWHM for first crystallisation exotherm (T_{c1}) plotted against CaX_2 (X=F/Cl/F+Cl) content. (■ = GPF series, ● = GPCl series, ▲ = GPFCl series) The errors in determining the FWHM are estimated to be<1°C, which is about the size of the data points.

The FWHM of the first crystallisation peak temperature for the three glass series are illustrated in Figure 8.1.5. In general, the FWHM reduces first, then increases with CaX_2 content for all three glass series and exhibits minimum values at about 6-9 mol% CaX_2 content, but there is no clear trend for the FWHM data for the GPF series glasses with CaF_2 content above 6.0 mol%. This reflects the fact that these glasses are largely crystalline and crystallised to FAP, cuspidine and fluorite. As mentioned in Chapter 5, both cuspidine and fluorite have an F-Ca(4) structure with one fluoride ion surrounded by four Ca^{2+}, while fluorapatite has an F-Ca(3) structure with three Ca^{2+} ions surrounding each fluoride. Therefore, cuspidine and fluorite are likely to form at higher fluoride contents relative to fluorapatite. The minimum values of FWHM at 6-9

mol% CaX_2 content for all three glass series suggest that these glasses with the first crystallisation phase crystallised from the bulk are the most suitable for forming apatite glass-ceramics.

8.2 XRD Results of Heat Treated Glasses

XRD patterns of heat treated glasses GPF 0.0, GPF 4.5, GPF 17.8, GPCl 4.6 and GPFCl 23.1 are shown in Figure 8.2.1 - Figure 8.2.5 and the phases identified are summarised in the Table 8.2.1 and Table 8.2.2. The typical apatite (HAP: 01-074-0565) and β-$CaSiO_3$ (04-012-1776) diffraction lines developed at the heat treatment temperature of 1030°C for halide-free composition (GPF 0.0) are found. In the case of the amorphous glass GPF 4.5, upon heat treatment at 860°C, the amorphous glass halo disappears and distinct diffraction lines corresponding to FAP (00-003-0736) and wollastonite ($CaSiO_3$-2M, (00-010-0489)) occur. The same crystalline phases are formed for GPF glass series with CaF_2 less than 9.3 mol%. In the case of the partially crystalline glass GPF 17.8 that already crystallised to FAP, $Ca_4Si_2O_7F_2$ and CaF_2 in the initial glass show an increase in the diffraction line intensities, particularly the ones for $Ca_4Si_2O_7F_2$ and CaF_2 suggesting a further crystallisation after heat treated at 720°C. Similar changes were found in glasses GPF 13.6 and GPF 25.5. The XRD patterns of 4.6 mol% $CaCl_2$ containing glass, which is thought to be almost amorphous show the crystallisation of chlorapatite on heat treatment at 865°C and 962°C, as the diffraction lines match that of ClAP although some hydroxyl substitution in the apatite lattice can not to be entirely ruled out. There is also a trace of wollastonite present. In the case of GPFCl 23.1, the XRD pattern of glass after heat treated to 659°C is similar to the equivalent initial glass but higher in intensity which corresponds to FAP and CaF_2. At 708°C, cuspidine is found as an additional crystalline phase, while the intensity of CaF_2 reduces slightly compared to the one at 659°C. The XRD results of these heat treated sample confirms that the first crystallisation exotherm evaluated above is a

crystallisation of a single phase for GPF 9.3, GPCl 2.3, GPCl 14 and GPCl 20.6 but crystallisation of several phases for the rest glasses.

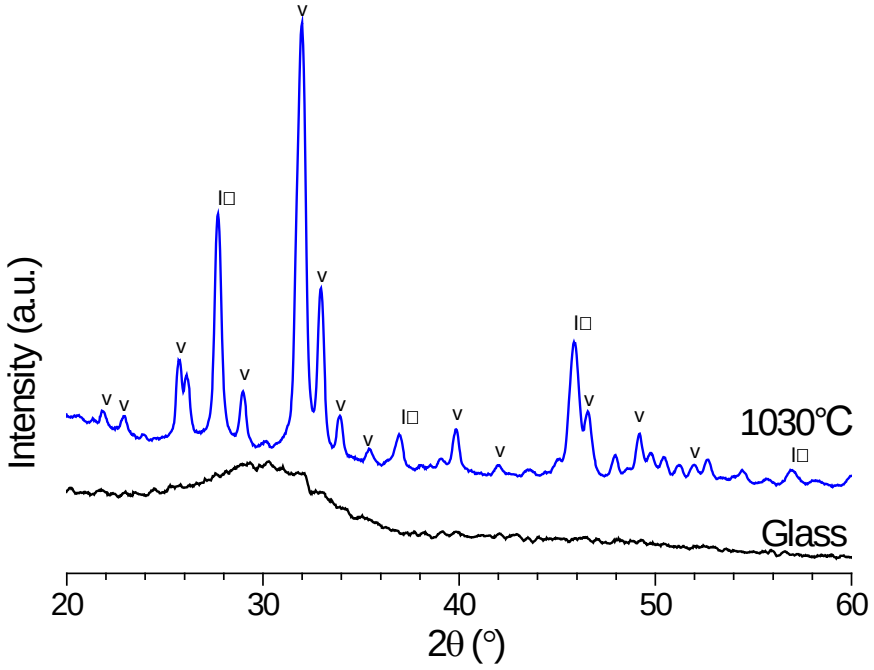

Figure 8.2.1 The XRD patterns of the as-quenched and heat treated GPF 0.0. (ᵛ: $Ca_{10}(PO_4)_6(OH)_2$; l: β-$CaSiO_3$ (Pseudowollastonite)).

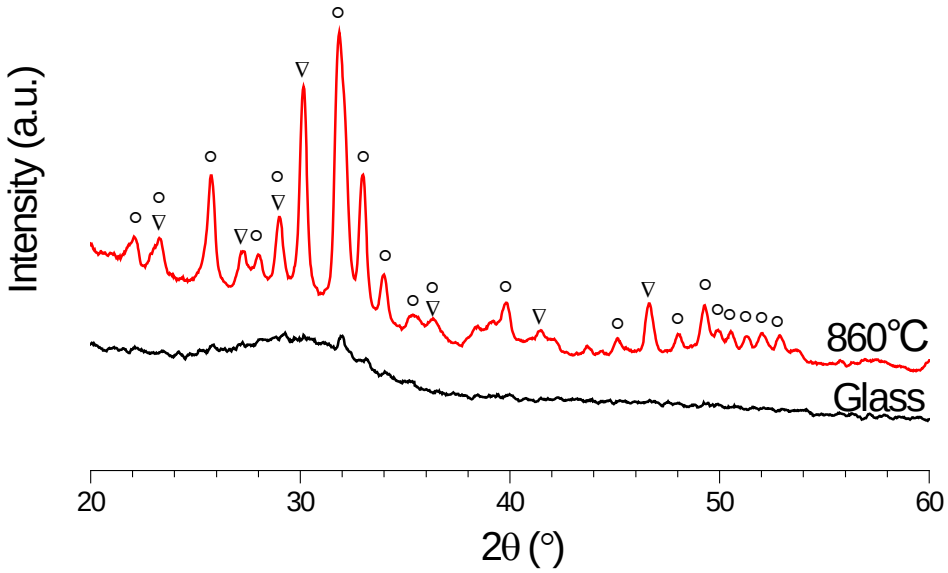

Figure 8.2.2 The XRD patterns of the as-quenched and heat treated GPF 4.5. (°: $Ca_{10}(PO_4)_6F_2$; ∇: $CaSiO_3$).

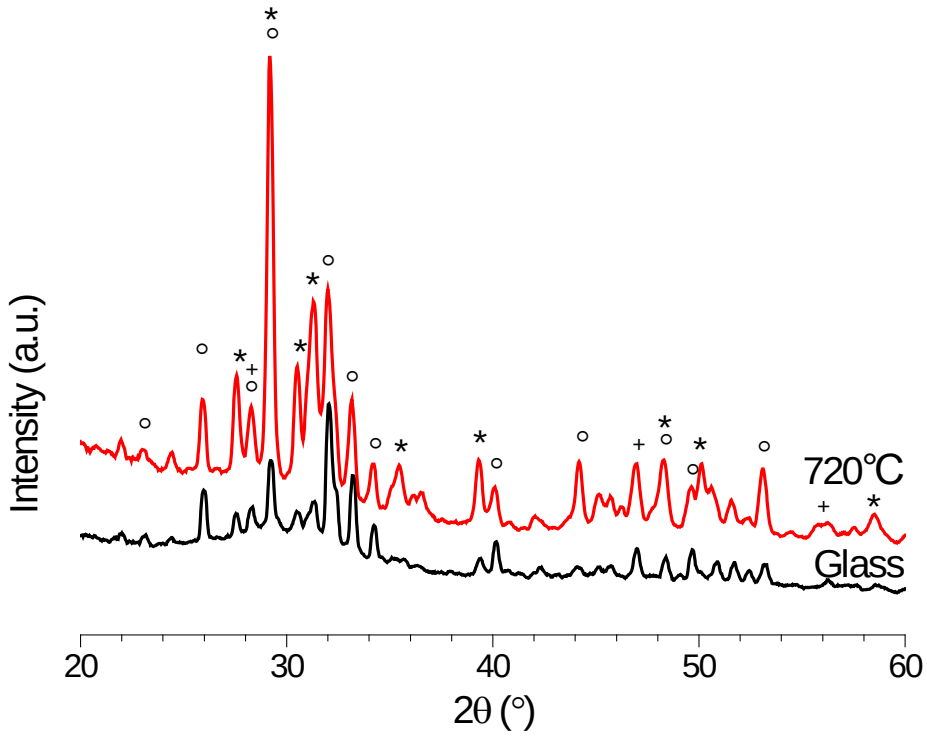

Figure 8.2.3 The XRD patterns of the as-quenched and heat treated GPF 17.8. (°: $Ca_{10}(PO_4)_6F_2$; *: $Ca_4Si_2O_7F_2$; +: CaF_2)

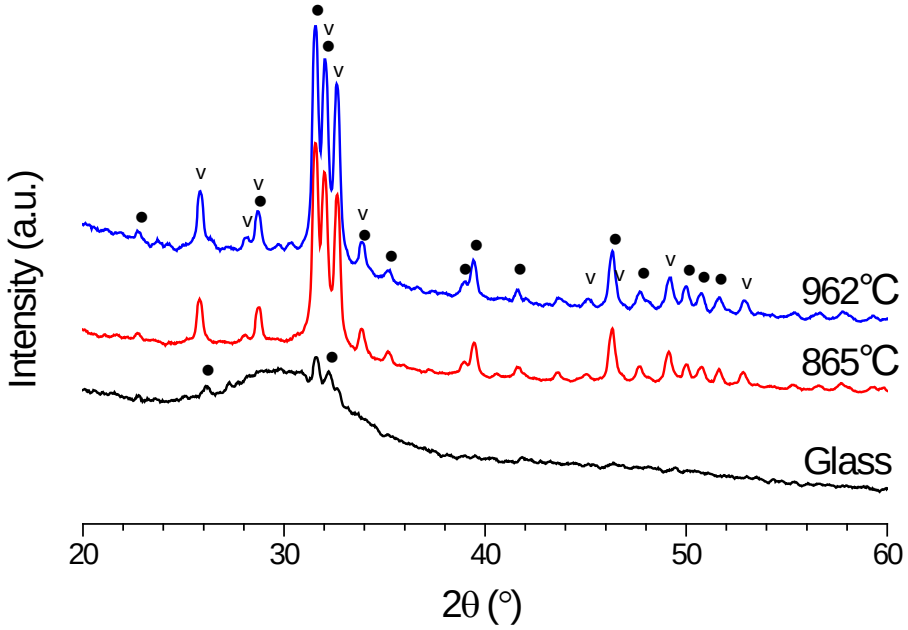

Figure 8.2.4 The XRD patterns of the as-quenched and heat treated GPCl 4.6. (•: $Ca_{10}(PO_4)_6(OH+Cl)_2$; ^{v}: $Ca_{10}(PO_4)_6(OH)_2$)

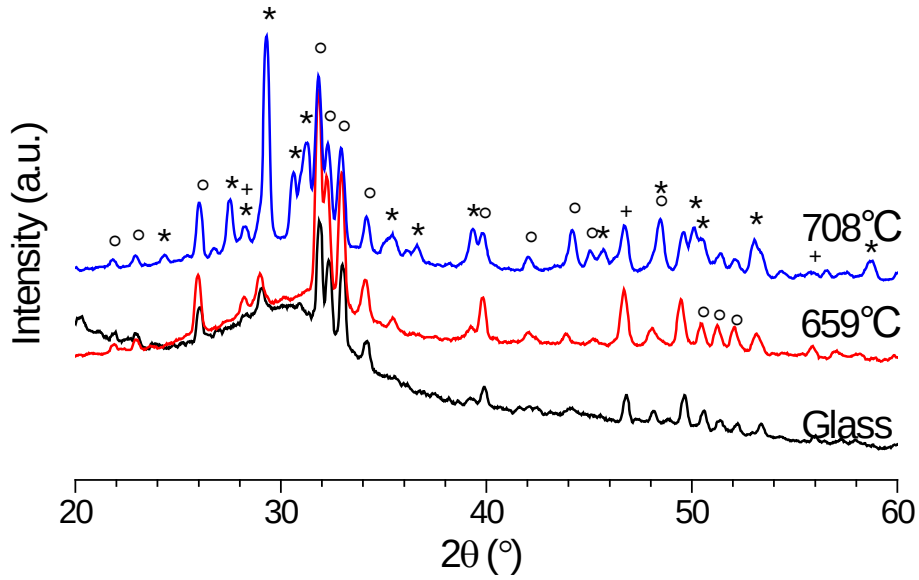

Figure 8.2.5 The XRD patterns of the as-quenched and heat treated GPFCl 23.1. (°: $Ca_{10}(PO_4)_6F_2$; *: $Ca_4Si_2O_7F_2$; $^{+}$: CaF_2)

Table 8.2.1 Summary of phases crystallising on heat treatment for GPF series. β-$CaSiO_3$: pseudowollastonite, $Ca_{10}(PO_4)_6(OH)_2$: hydroxyapatite, $Ca_{10}(PO_4)_6F_2$: fluorapatite, $CaSiO_3$: wollastonite-2M, $CaSiO_3$ (hexagonal): wollastonite-1A, $Ca_4Si_2O_7F_2$: cuspidine, CaF_2: fluorite.

Glasses	T_{HT} (°C)	Crystalline Phases
GPF 0.0	1030	β-$CaSiO_3$ and $Ca_{10}(PO_4)_6(OH)_2$
GPF 3.0	867	$Ca_{10}(PO_4)_6F_2$ and $CaSiO_3$
	888	
	979	
GPF 4.5	860	
GPF 6.0	817	
	844	
	942	$Ca_{10}(PO_4)_6F_2$ and $CaSiO_3$ (hexagonal)
GPF 9.3	780	$Ca_{10}(PO_4)_6F_2$
	806	$Ca_{10}(PO_4)_6F_2$ and $Ca_4Si_2O_7F_2$
	878	
GPF 13.6	732	
	758	
	977	
GPF 17.8	720	$Ca_{10}(PO_4)_6F_2$, $Ca_4Si_2O_7F_2$ and CaF_2
GPF 25.5	713	

Table 8.2.2 Summary of phases crystallising on heat treatment for GPCl series. β-$CaSiO_3$: pseudowollastonite, $Ca_{10}(PO_4)_6(Cl+OH)_2$: chlorapatite with OH^- substitution, $CaSiO_3$: wollastonite-2M

Glasses	T_{HT} (°C)	Crystalline Phases
GPCl 2.3	913	$Ca_{10}(PO_4)_6(Cl+OH)_2$
	1020	$Ca_{10}(PO_4)_6(Cl+OH)_2$ and $CaSiO_3$
GPCl 3.5	890	$Ca_{10}(PO_4)_6(Cl+OH)_2$ and $CaSiO_3$
GPCl 4.6	865	
	962	
GPCl 7.2	821	$Ca_{10}(PO_4)_6(Cl+OH)_2$ and β-$CaSiO_3$
	932	
GPCl 10.6	785	$Ca_{10}(PO_4)_6(Cl+OH)_2$ and trace amount of $CaSiO_3$
	889	$Ca_{10}(PO_4)_6(Cl+OH)_2$ and β-$CaSiO_3$
GPCl 14.0	751	$Ca_{10}(PO_4)_6(Cl+OH)_2$
	775	
GPCl 20.6	716	
	795	$Ca_{10}(PO_4)_6(Cl+OH)_2$ and unidentified phase

8.3 FTIR Spectra of Heat Treated Glasses

Figure 8.3.1- Figure 8.3.3 show the FTIR spectra of heat treated glasses GPF 4.5, GPF 17.8 and GPCl 4.6. For the initially amorphous glasses GPF 4.5 and GPFCl 4.6, upon heat treatment, the broad peak at about 500 - 600 cm^{-1} disappears and distinct split peaks at 560 and 613/605 cm^{-1} occur corresponding to P-O bending in the crystalline orthophosphate. The sharp peak at 1035 cm^{-1} corresponding to P-O stretching also appears. In addition, the spectrum for glass GPF 4.5 heat treated at 860 °C also presents sharp band features in the region of 620-1000 cm^{-1}, suggesting the formation of an ordered Q^2 silicate crystalline phase, that $CaSiO_3$ is one of the examples [161, 162]. This result is consistent with the presence of $CaSiO_3$ in the XRD patterns (Figure 8.2.1). The partially crystallised glass GPF 17.8 (Figure 8.3.2), that demonstrates apatite split peaks and a sharp crystalline orthophosphate peak at 1035 cm^{-1} in the initial glass shows the disappearance of amorphous Si-NBOs at 920 cm^{-1}, increasing amplitude of the peaks at 845, 950 and 1090 cm^{-1} which corresponding to Q^1 silicate in cuspidine and the presence of an additional distinctly sharp peak at 645 cm^{-1} after heat treatment. This additional unidentified peak matches the OH bending in hydroxyapatite [163]. However, it is unlikely to form HAP in the heat treated glass-ceramics, since in this glass composition the F/P ratio is higher than 1:3 and consequently phosphate is preferential to combine with F. It is worth noting that the intensity of the split peaks (P-O bending) do not change significantly on heat treatment for these partially crystalline glasses, while a sharpening of P-O stretching at 1035 cm^{-1} is visible.

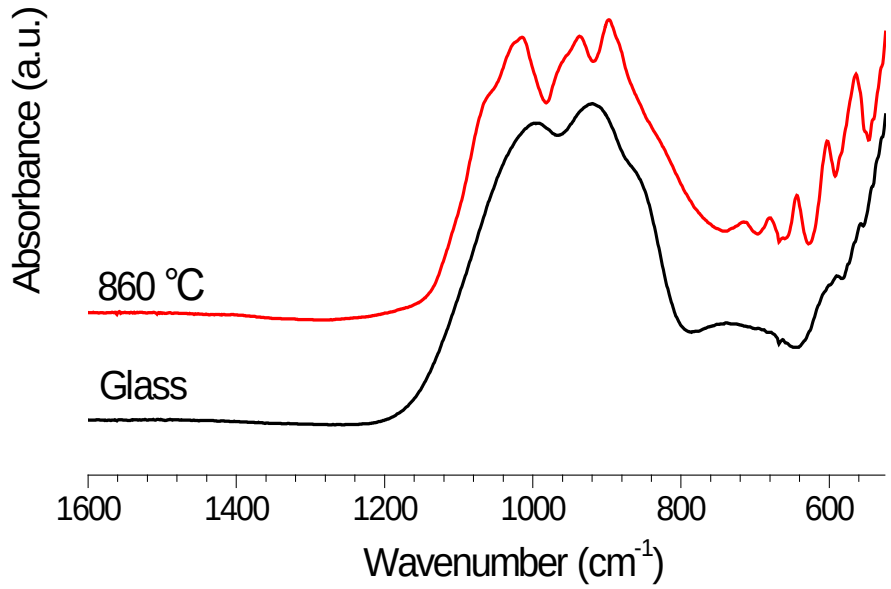

Figure 8.3.1 The FTIR Spectra of the as-quenched and heat treated GPF 4.5.

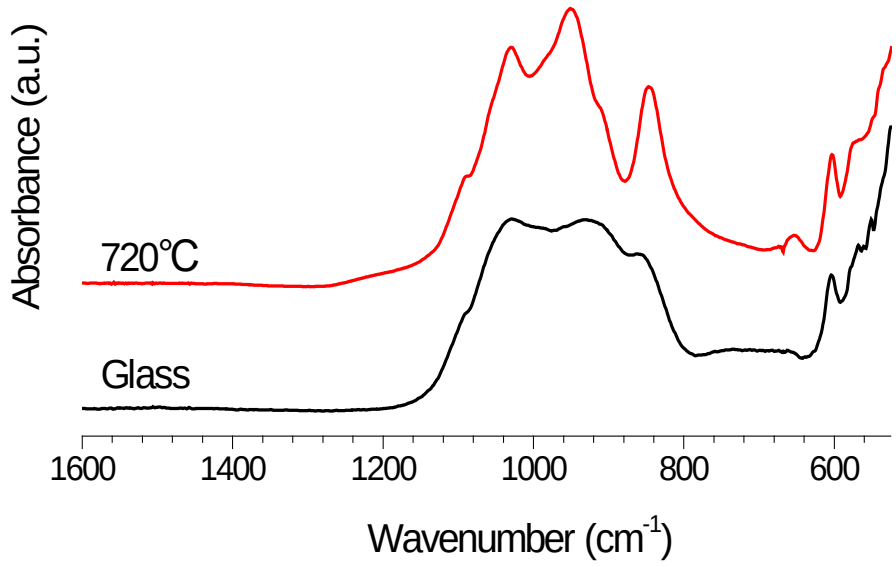

Figure 8.3.2 The FTIR Spectra of the as-quenched and heat treated GPF 17.8.

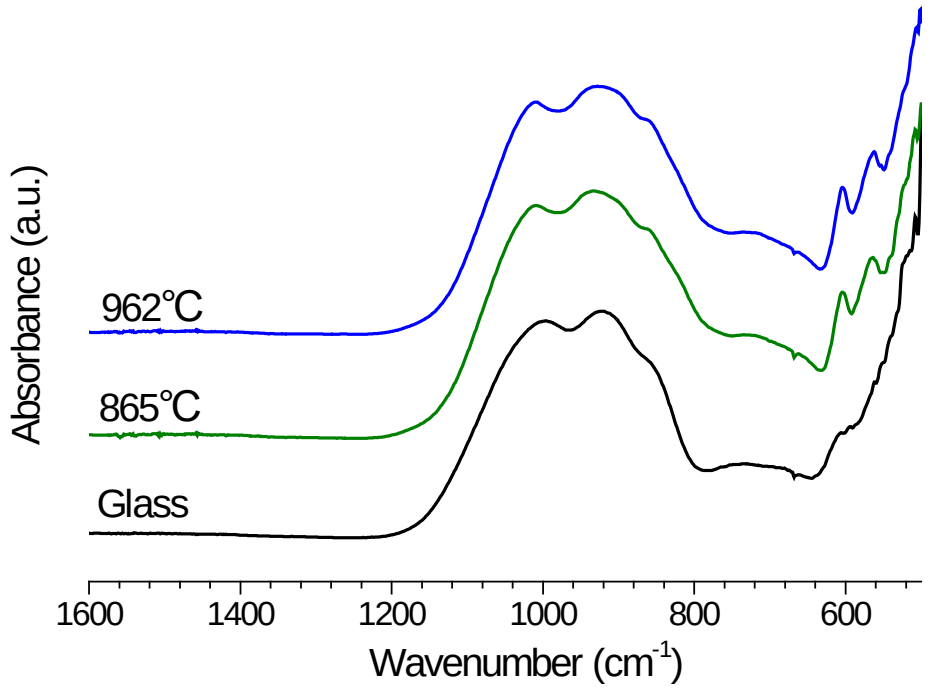

Figure 8.3.3 The FTIR Spectra of the as-quenched and heat treated GPCl 4.6

8.4 MAS-NMR Spectra of Heat Treated Glasses

8.4.1 ^{31}P MAS-NMR Spectra of Heat Treated Glasses

The ^{31}P MAS-NMR spectra for heat treated glasses GPF 4.5, GPF 17.8 and GPCl 4.6 are presented in Figure 8.4.1-Figure 8.4.3. The spectra for all the heat treated samples show a progressive sharpening of the calcium orthophosphate peak at about 3 ppm. This sharpening of the peak is an indicative of apatite crystallisation. In the initial amorphous glasses GPF 4.5 and GPCl 4.6, phosphorus is randomly arranged in the glass and consequently the peaks are relatively broad. After heat treatment, most of the phosphorus in the glass matrix crystallises to apatite, which has a much more ordered structure, resulting in a sharp peak at 2.9 ppm. Moreover, for the largely crystallised glass GPF 17.8, most of the phosphorus has converted to apatite during the quench and only a small amount of amorphous phosphorus that did not have enough time to crystallise can convert to apatite upon heat treatment. Therefore a

relatively small change is seen for GPF 17.8 in Figure 8.4.2. Similar changes are shown in other partially crystalline glasses.

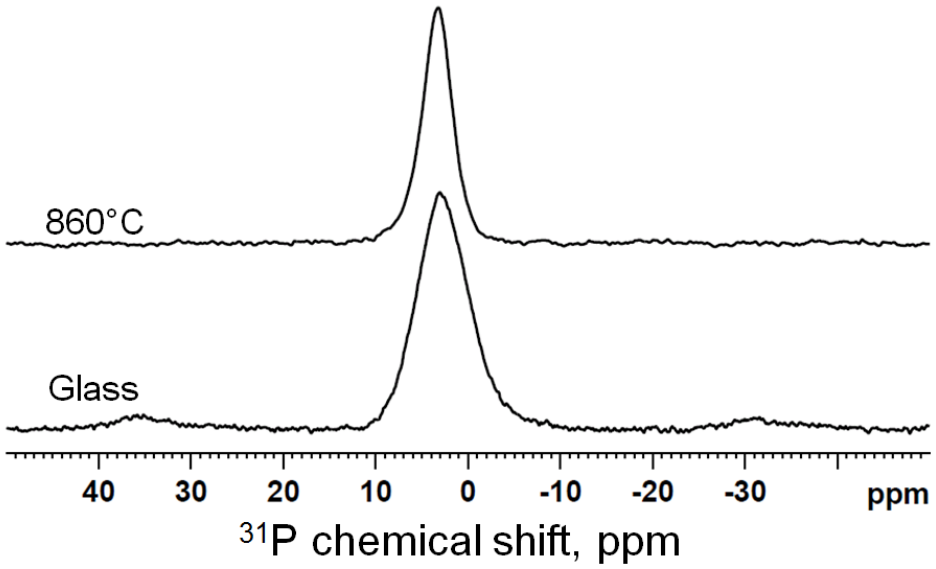

Figure 8.4.1 The ^{31}P NMR-NMR Spectra of the as-quenched and heat treated GPF 4.5.

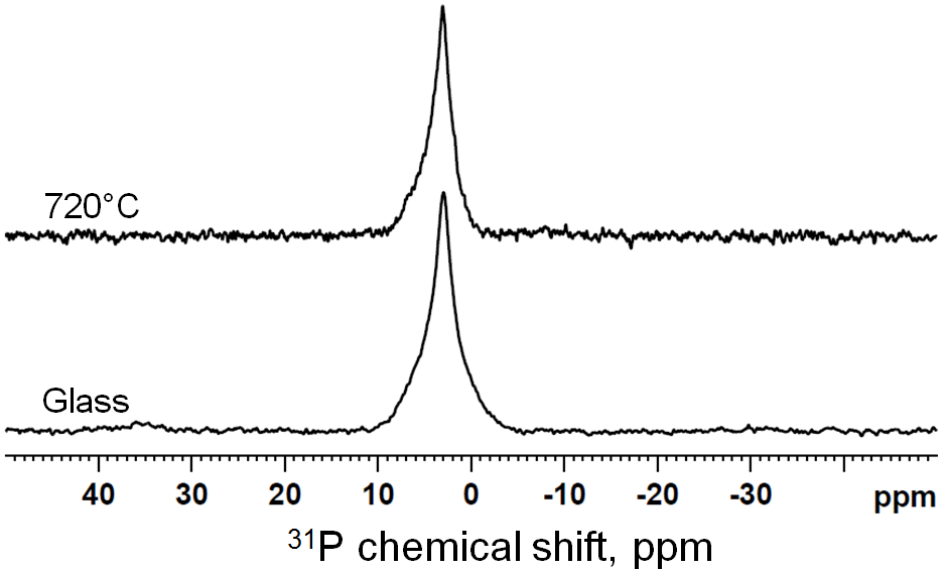

Figure 8.4.2 The ^{31}P NMR-NMR Spectra of the as-quenched and heat treated GPF 17.8.

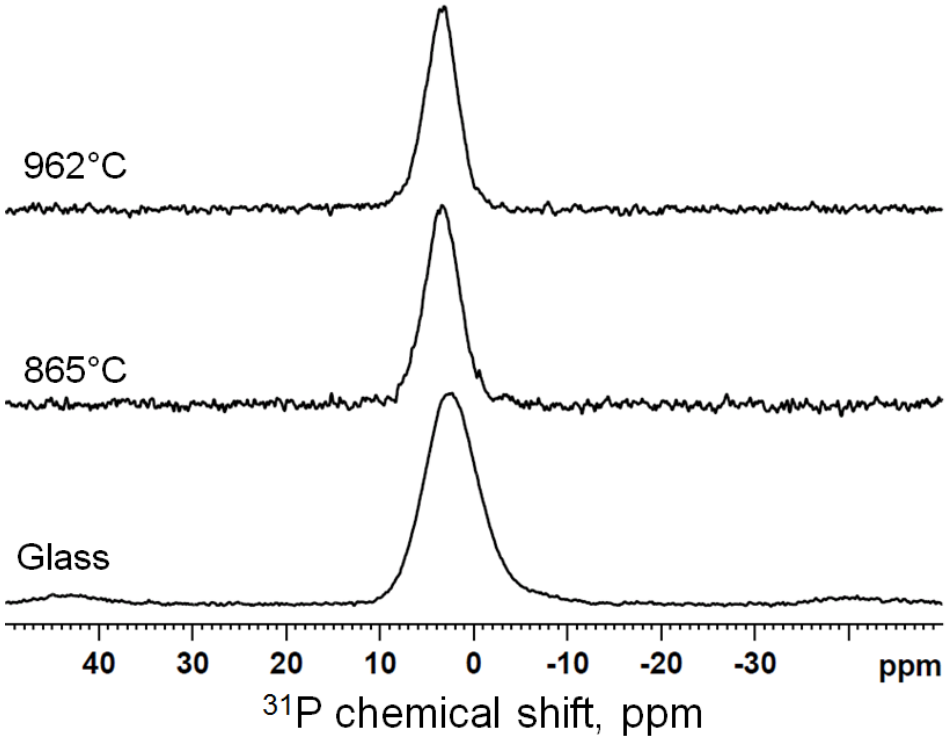

Figure 8.4.3 The ^{31}P NMR-NMR Spectra of the as-quenched and heat treated GPCl 4.6

8.4.2 ^{19}F MAS-NMR Spectra of Heat Treated Glasses

Figure 8.4.4 - Figure 8.4.6 present the ^{19}F MAS-NMR spectra of the heat treated GPF 4.5, GPF 17.8 and GPFCl 23.1. As can be seen, the NMR spectra change significantly upon heat treatment for all the glass compositions. The spectrum for glass GPF 4.5 heat treated at 860 °C has a sharp maximum at -104.5 ppm and an additional broad shoulder at -118 ppm corresponding to nonspecifically adsorbed F^- [138]. In the case of GPF 17.8 on heat treatment at 720 °C, the full-height half width of the spectrum reduces considerably compared to the equivalent as-quenched glass and the maximum sits at -108 ppm corresponding to CaF_2, the F-Ca(4) species. In addition, a shoulder at about -103 to -104 ppm assigns to FAP, F-Ca(3) species and cuspidine, F-Ca(4) is also observed [164], which is in accord with the XRD patterns in Figure 8.2.2 and Figure 8.2.3.

As mentioned in Chapter 7, owing to the overlapping of different fluoride signals (amorphous F-Ca(4), crystalline F-Ca(3), crystalline F-Ca(4) and spinning side bands), a broad peak is observed for the as-quenched glass GPFCl 23.1. Upon heat treatment,

the amorphous fluoride species converts to a crystalline one which results in a reduction in FWHM of the signal, in particular for the sample heat treated at 708 °C. In addition, a distinctly sharp peak at -107.5 ppm with a shoulder at -103.5 ppm is detected (Figure 8.4.6), indicating the crystallisation of CaF_2 and FAP after heat treatment at 708°C.

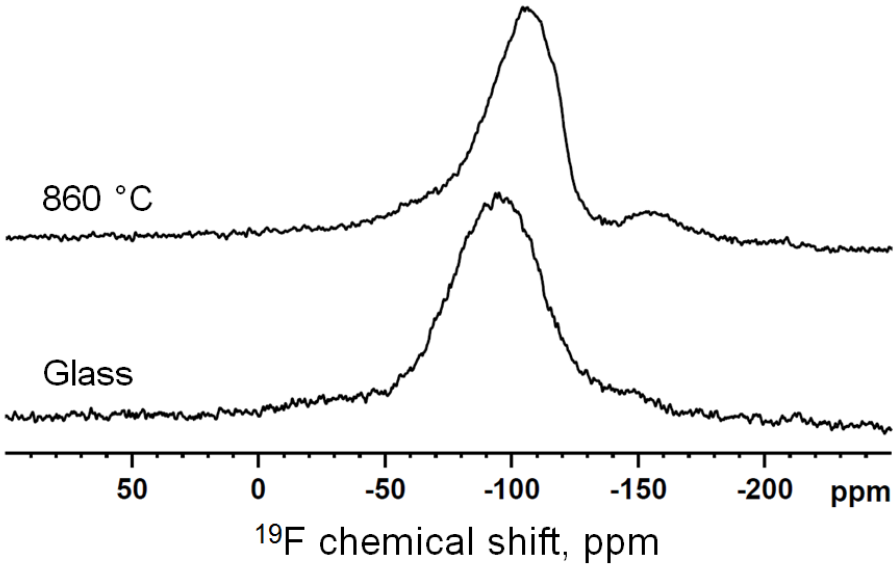

Figure 8.4.4 The ^{19}F NMR-NMR Spectra of the as-quenched and heat treated GPF 4.5.

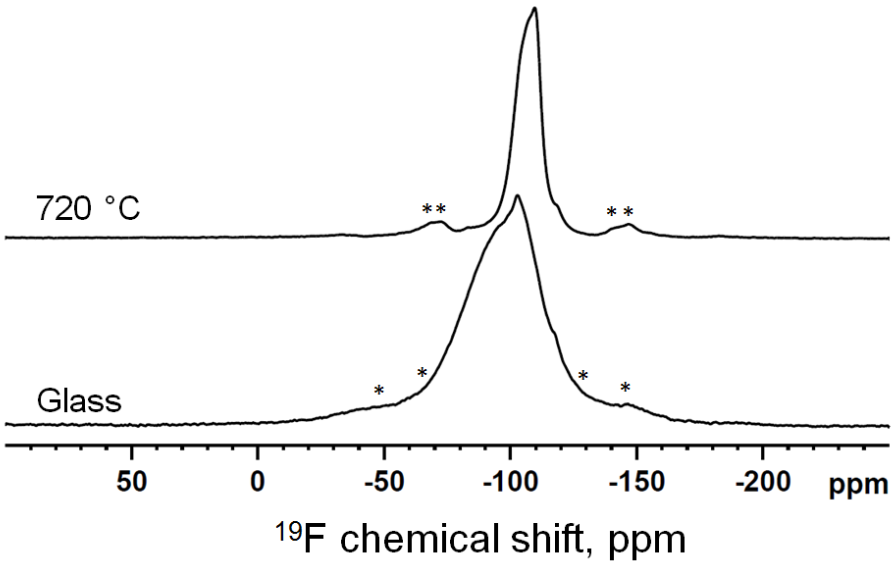

Figure 8.4.5 The ^{19}F NMR-NMR Spectra of the as-quenched and heat treated GPF 17.8.

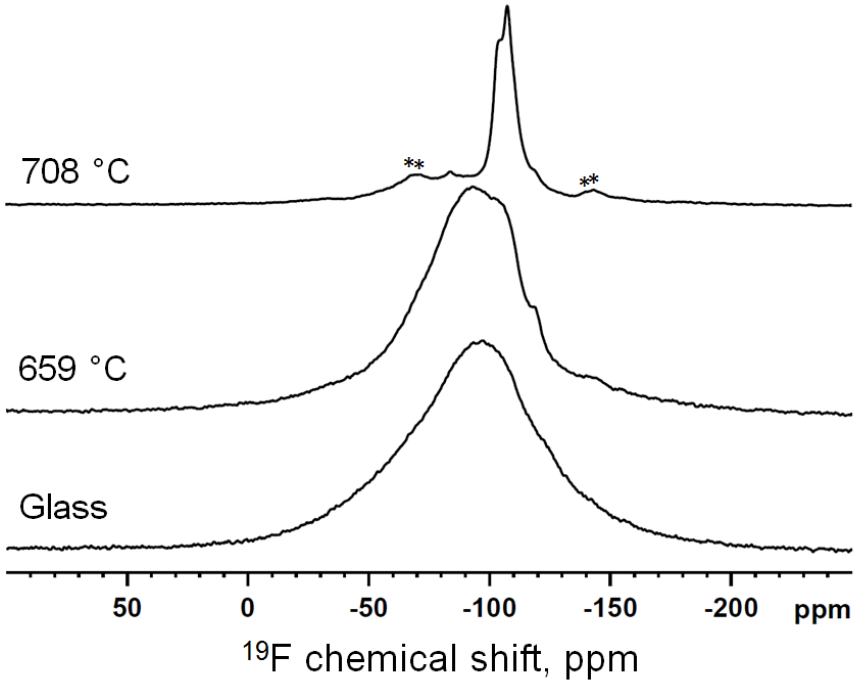

Figure 8.4.6 The ^{19}F NMR-NMR Spectra of the as-quenched and heat treated GPFCl 23.1.

8.5 SEM Results of Apatite Glass-ceramics

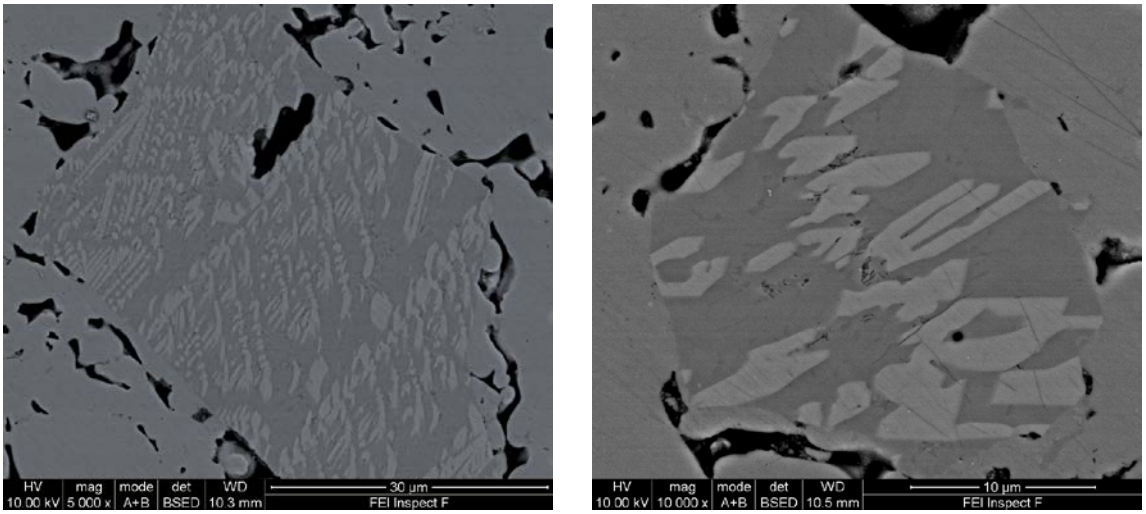

(a) (b)

Figure 8.5.1 SEM of the fractured surface of GPF 4.5 (4.5 mol% CaF_2) glass-ceramics heat-treated at 860 °C.

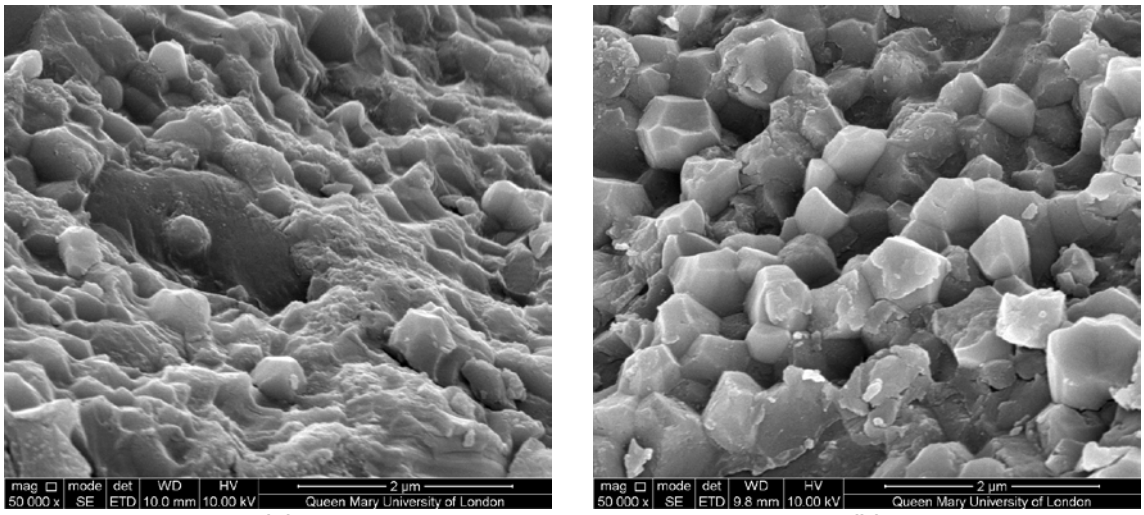

(a) (b)

Figure 8.5.2 SEM of the fractured surface of (a) GPCl 3.5 (2.5 mol% $CaCl_2$) glass-ceramics heat treated at 890 °C and (b) GPCl 4.6 (3.9 mol% $CaCl_2$) glass-ceramics heat-treated at 962 °C.

The surface morphologies of GPF 4.5, GPCl 3.5 and GPCl 4.6 glass-ceramics investigated by SEM are shown in Figure 8.5.1 and Figure 8.5.2. Glass GPF 4.5 crystallised to FAP with an elongated and interlocking crystal structure (dendritic) upon heat treatment at 860 °C with coexisting FAP and wollastonite phase (Figure 8.5.1 (a)). The typical needle-like and hexagonal crystal morphology of fluorapatite is also seen in Figure 8.5.1 (b) [148, 152, 165]. In contrast, the microstructure that consists of short polyhedra of chlorapatite is visible for GPCl 3.5 glass-ceramics heat-treated at 890 °C and GPCl 4.6 glass-ceramics heat-treated at 962 °C, in agreement with the equiaxed prisms of chlorapatite morphology detected by Esther *et.al.* [166]. To some extent, Figure 8.5.2 (a) suggests that on heat treatment the equiaxed chlorapatite crystals grew from the glass surface, whereas they are likely to form a spherical shape first then grow to a uniform equiaxed hexagonal crystal.

Further Discussion

As both glass transition temperature and crystallisation temperature are dependent on the strength of the chemical bonding in the glass, the marked reduction in the both T_g and T_{C1} with increasing in CaX_2 (X=F/Cl/F+Cl) content suggests formation of a less strongly bound network in higher halide containing glasses [150]. This reduction is the consequence of forming "CaX^+" species, which is also the key factor resulting in the decrease in T_g that has been discussed in detail in Chapter 5.

The halogen free glass composition exhibits a marked temperature difference between the T_{c1} values for frit and fine powder, while T_{c1} of frit is higher than the equivalent powder. In addition the FWHM of the first exotherm increases markedly for the frit particles compared to the fine powder indicating pronounced surface nucleation of the first crystallisation phase. XRD shows that this zero halide containing glass crystallises largely to β-CaSiO3 along with apatite. β-$CaSiO_3$ is a Q^2 ring silicate, which is a phase known to strongly surface nucleate. The apatite is thought to be a hydroxyapatite, presented in hexagonal-like morphology (in Appendix, Figure 11.2.2). It is interesting but surprising that an apatite formed in the absence of fluoride, since in AM glass-ceramics system apatite only forms when fluoride is present [148]. Here the detected hydroxyapatite is either thought to form initially as an oxyapatite, which subsequently reacts with water or a consequence of water vapour in the furnace atmosphere diffusing into the glass and enabling apatite formation from the glass surface.

The incorporation of calcium halide (CaF_2 / $CaCl_2$ / CaF_2+$CaCl_2$) reduces the difference between the T_{c1} values for frits and fine powder and leads to a largely bulk-nucleated haloapatite being formed as the first crystallisation phase. As can be seen, the diffraction patterns of the heat treated glasses for the CaF_2 series matched that of FAP, while the ones for $CaCl_2$ series matched to chlorapatite diffraction lines although some hydroxyl substitution in the lattice cannot be entirely ruled out. Note that the diffraction patterns of the heat treated glasses for the mixed CaF_2 and $CaCl_2$ system

with the exception of GPFCl 2.6 are consistent with fluorapatite formation, rather than chlorapatite. This is simply because the fact that F^- ion is smaller than Cl^- ion and the FAP is more stable than ClAP. Once there is sufficient fluoride available for apatite formation, FAP will form preferentially. In the case of GPFCl 2.6, a mixed fluor-chlorapatite is possible to form upon heat treatment, since the F/P ratio in glass composition is 1: 4.07 which is smaller than the equivalent 1:3 in FAP. The relatively excess P could combine with Cl to form chlorapatite.

Upon heat treatment, all the GPF glass series with CaF_2 lower than 9.3 mol% CaF_2 crystallised to FAP along with wollastonite. The heat treatment temperatures are too high to see FAP crystalline phase without wollastonite. The wollastonite phase was expected on the grounds that the residual glass phase following crystallisation of FAP would have a Q structure close to Q^2 and also close to the stoichiometry of wollastonite. In the case of GPCl glass series, ClAP and wollastonite are typical crystallisation phases on heat treatment, while FAP and CaF_2 are the major crystalline phase for GPFCl glass series. It is worth noting that in these glasses the Q structure does not change on crystallisation and remains at about 2 (NC=2.08) irrespective of how much apatite crystallises, as it is the orthophosphate phase which crystallises. This is an attractive feature of these glass-ceramics, since the essentially Q^2 speciation of the residual amorphous glass will confer bioactivity. The formed apatite may provide seed crystals for the formation of more apatite as the Q^2 residual glass phase dissolves in body fluids. These glass-ceramics may combine the beneficial effects of a bioactive glass phase and the apatite crystals.

In the case of glasses (GPF series) with CaF_2 content over 6.0 mol% and GPFCl 23.1, FAP, cuspidine and CaF_2 are found as the crystalline phases following heat treatment. Due to the fact that cuspidine is a Q^1 species, the further increase of cuspidine formation upon heat treatment would probably lead to a more cross-linked glass network of the residual glass, which might reduce the bioactivity of the formed glass-

ceramics. Although the initial glasses with cuspidine and CaF_2 crystals showed a comparable glass degradation rate in Chapter 5 and 7. The comparison of bioactivity of the as-quenched glass and glass-ceramics formed upon heat treatment will be a subject for further research.

Interestingly, the FTIR spectra of the heat treated CaF_2 samples (in Appendix, Figure 11.2.3) indicate that the amount of apatite formed during quenching for the glasses with CaF_2 contents higher than 9.3 mol% is already as high as is possible to crystallise in total from these glasses. The spectra of those initially amorphous glasses (GPF 3.0, GPF 4.5 and GPF 6.0) demonstrate a clear development of the apatite split band at approximately 610 and 560 cm^{-1} on heat treatment and more pronounced in intensity with increasing heat treatment temperature. In contrast, the spectra (in Appendix, Figure 11.2.4) of those partially crystallised glasses that already contain the split bands at 560 and 613 cm^{-1} do not show a significant increase in intensity following heat treatment. This indicates that a further significant FAP formation did not happen. However, the further crystallisation of cuspidine was suggested from both of XRD and FTIR. The sharpening of 1030 cm^{-1} band might be attributed to the loss of some Si-O stretching vibrations which reduces the overlapping of PO_4^{3-} and Si-O stretch at 1030 cm^{-1}.

Moreover, it is important to realize that the studied chloride glasses (GPCl series) are very reactive and appear to react with atmospheric water, as the glass is thought to contain calcium chloride like structural domains. It is possible that these domains inherit the extreme ability of the crystalline $CaCl_2$ to absorb water causing structural transformations due to hydration reactions. This can account for the formation of chlorapatite with OH^- substitution rather than pure chlorapatite upon heat treatment.

Summary

The crystallisation temperature for the three glass series reduces with an increase in CaX_2 content. The halogen free glass predominantly surface nucleates and crystallises to pseudowollastonite and apatite. The glasses with fluoride or chloride crystallised first to a haloapatite (FAP/ClAP/F-ClAP). The obtained chlorapatite glass-ceramics is the first set of ClAP glass-ceramics based on phosphosilicate glasses in the world. Glasses with 2.3 to 9.3 mol% CaX_2 have a reduced tendency to surface nucleate to a haloapatite and are attractive for potential apatite glass-ceramics. The second crystallisation phase of low CaF_2 containing glasses, chloride containing glasses and low CaX_2 glasses is wollastonite. This strongly surface nucleated wollastonite is undesirable and would probably stop the AW glass-ceramics being produced by a direct casting route. However, it would be possible to crystallise these glasses to only apatite to form apatite glass-ceramics with a bioactive residual glass phase. The bioactive glass-ceramics with FAP as the only crystalline phase are potentially attractive for bone regeneration in medical and dental application, while the ClAP glass-ceramics are more promising as fully resorbable bone substitutes. Tailoring the fluoride and chloride ratio enables mixed haloapatites glass-ceramics with specific microstructures and in vivo resorbability to be produced.

9 Preliminary Results of Sodium and Phosphate-Free $CaCl_2$ Glasses

Foreword

Bioactive glasses are silicate glasses that generally contain phosphate and that dissolve in physiological solutions forming hydroxycarbonated apatite on their surface [1, 52].

Hench has expressed the bioactivity of bioactive glass in terms of composition on a phosphate free ternary SiO_2-CaO-Na_2O diagram. The region of bioactivity does not extend to the binary SiO_2-CaO line, which would indicate that a wollastonite stoichiometry glass and especially one with the absence of phosphate would not be expected to be bioactive.

Ebisawa and Ohura *et al.* [167, 168] investigated the bioactivity of wollastonite stoichiometry (SiO_2-CaO) glass in simulated body fluid and found this glass to be bioactive and to form an apatite layer on its surface, although it is widely believed that bioactive glasses must contain sodium in order to be bioactive.

Spilman *et.al* [169] first investigated the incorporation of CaF_2 in the 45S5 glass composition and substituted CaF_2 for CaO or Na_2O in the original composition. However based on the ^{19}F solid state nuclear magnetic resonance studies of silicate glasses by Hill *et al*. [79, 111, 113, 170], the studies of Brauer *et al.* [7, 150] and the computer simulations of Christie *et al.* [171] fluoride ions would be expected to be complexed by Ca forming F-Ca(n) species. The substitution of CaO by CaF_2 would therefore result in a reduction in the non-bridging oxygen content and an increase in the network connectivity of the glass [20]. The resultant glasses with a more cross-

linked network structure are expected to exhibit a reduced solubility and bioactivity [83]. Conversely, adding CaF_2 as carried out by Brauer *et al.* [14-16] does not lead to the change in the silicate speciation or network connectivity. Under these circumstances, adding CaF_2 would be expected to favour glass degradation and apatite-like phase formation. Therefore, in this work, the dissolution behaviour and crystallisation event of a simpler SiO_2-CaO glass system to which CaF_2 and $CaCl_2$ have been added were investigated.

Chlorine is expected to behave in a similar fashion as fluoride by forming Cl-Ca(n) species analogous to F-Ca(n) species. In addition, the large chloride ion is expected to expand glass volume and result in a much less compact glass structure. Moreover, a large chloride ion is likely to have the calcium cations more randomly arranged around it, therefore it is possible that a large amount of $CaCl_2$ could be introduced into the glasses without significant crystallisation occurring.

The simpler ternary glass system (SiO_2-CaO-$CaCl_2$) is expected to simplify the characterisation of glass structure and crystallisation events, and therefore could provide a better understanding of the role of Cl in the glass structure and glass properties. The extensive crystallisation in the SiO_2-CaO-CaF_2 glass series seen in the previous work [172] substantially complicated the characterisation; with the exception of the glass with 2.9 mol% CaF_2, the rest of glasses were largely crystallised to wollastonite, psedowollastonite, cuspidine and CaF_2. However, significant crystallisation was not expected to occur in the chloride containing silicate glasses, therefore, in the following the dissolution behaviour and crystallisation events of this glass series are presented and discussed.

9.1 Results of the As-Quenched Glasses

All of the studied glass frits of GCl series are optically transparent. Note that the glasses GCl 43.0 and GCl 53.1 were extremely reactive, the as-quenched glass frits

largely dissolved before being taken out from the water used for quenching the glass. The glass frits collected from the crucible of GCl 43.0 and GCl 53.1 were used for the further characterisation. .

9.1.1 Compositional Analysis

Figure 9.1.1 demonstrates the percentages of the retained chloride in the initial glasses after volatilization as $CaCl_2$ against the as-designed chloride content. About 63 -75 % of chloride was retained in the P free Q^2 silicate glasses. The actual glass compositions were re-calculated based on the chloride component analysis and presented in Table 9.1.1. Note that, due to the fact that glass GCl 53.1 is very reactive, no fine glass powder (< 45 μm) was obtained for the compositional analysis. Here the actual glass composition for glass GCl 53.1 was calculated according to the linear relationship between T_g and $CaCl_2$ content, which will be presented in section 9.1.4.

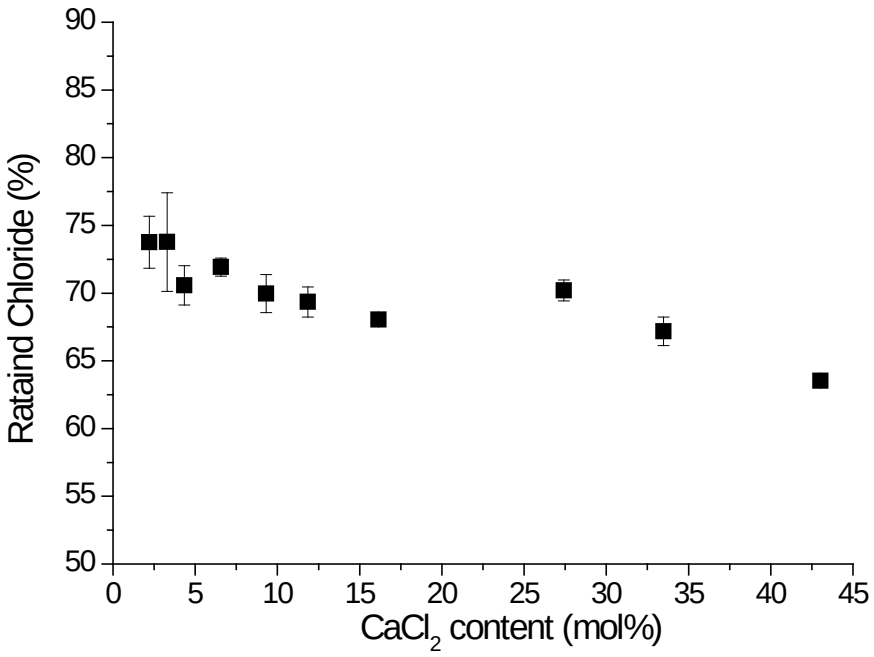

Figure 9.1.1 The percentage of the retained chloride in the initial glasses plotted against the as-designed chloride content.

Table 9.1.1 Glass compositions in mol%. For each glass, the first row is the nominal composition as-designed and the second row is the actual glass composition.

Glass code	SiO_2	CaO	$CaCl_2$
GCl 0.0	50.0	50.0	0.0
	50.0	50.0	0.0
GCl 2.2	48.9	48.9	2.2
	49.2	49.2	1.6
GCl 3.3	48.4	48.4	3.3
	48.8	48.8	2.4
GCl 4.3	47.8	47.8	4.3
	48.5	48.5	3.1
GCl 6.6	46.7	46.7	6.6
	47.6	47.6	4.7
GCl 9.3	45.3	45.3	9.3
	46.7	46.7	6.5
GCl 11.9	44.1	44.1	11.9
	45.9	45.9	8.2
GCl 16.1	41.9	41.9	16.1
	44.8	44.8	10.5
GCl 27.4	36.3	36.3	27.4
	40.4	40.4	19.2
GCl 33.5	33.3	33.3	33.5
	38.8	38.8	22.5
GCl 43.1	28.5	28.5	43.0
	36.3	36.3	27.3
GCl 53.1	23.5	23.5	53.1
	34.2	34.2	31.6

9.1.2 XRD Results of the As-Quenched Glasses

Figure 9.1.2 shows the XRD patterns of the as-quenched Na and P free glasses with varying amount of $CaCl_2$ (0.0 to 27.3 mol%). In the case of $CaCl_2$ free SiO_2-CaO glass composition (GCl 0.0), clear diffraction peaks at 25.99°, 27.56°, 31.7°and 45.91° 2θ are noticed. These peaks match the characteristic diffraction peaks of Pseudowollastonite (β-$CaSiO_3$: 04-012-1776). It is clear that all the studied $CaCl_2$ containing glasses are amorphous, as the XRD patterns only show amorphous halos.

Taking a closer look, the maxima of the amorphous halos move slightly to a higher 2θ value (32° 2θ) when the $CaCl_2$ content is over 10.5 mol%, while the glasses with $CaCl_2$ content lower than 19.2 mol% have the halos at about 30° 2θ.

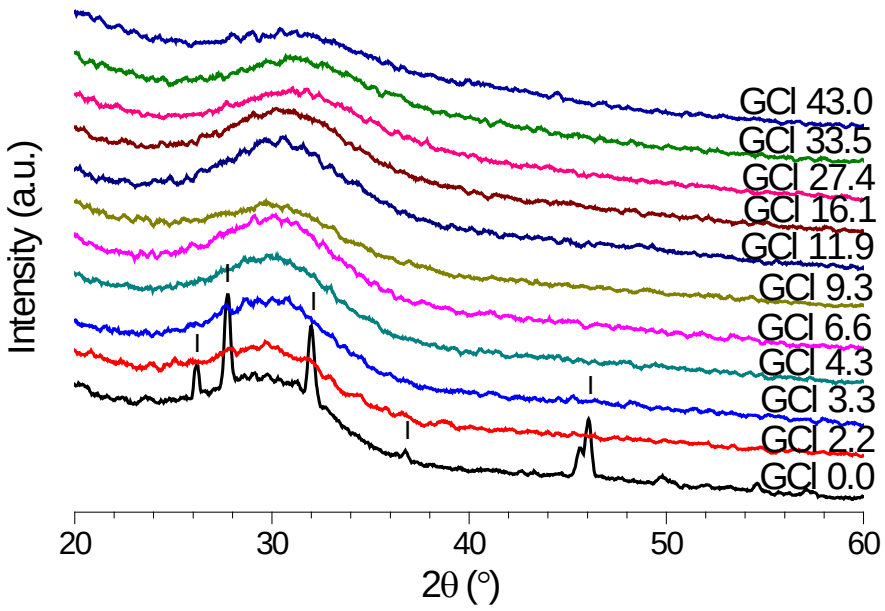

Figure 9.1.2 The XRD patterns of as-quenched P free $CaCl_2$ containing glasses. (I: β-$CaSiO_3$).

9.1.3 FTIR Results of the As-Quenched Glasses

The FTIR spectra of the as-quenched P free $CaCl_2$ containing glasses are given in Figure 9.1.3. With the exception of glasses GCl 0.0, GCl 33.5 and GCl 43.0, the spectra of the rest of the glasses are similar to the ones for GPCl glass series in Chapter 6, which have the non-bridging oxygen ($Si\text{-}O^-$) band at 920 cm^{-1}, a band centred at 860 cm^{-1} assigned to the Si-O stretching band with two non-bridging oxygens per SiO_4 tetrahedron and the Si-O-Si stretching band 1030 cm^{-1} [9, 173, 174]. The spectrum of GCl 0.0 shows in addition to those bands mentioned above the sharp band features at 720, 937 and 985 cm^{-1} corresponding to an ordered Q^2 silicate

crystalline phase [161], which is $CaSiO_3$ as suggested by XRD results (Figure 9.1.2). In the case of GCl 33.5 and GCl 43.0, an additional peak emerges at 683 cm^{-1}.

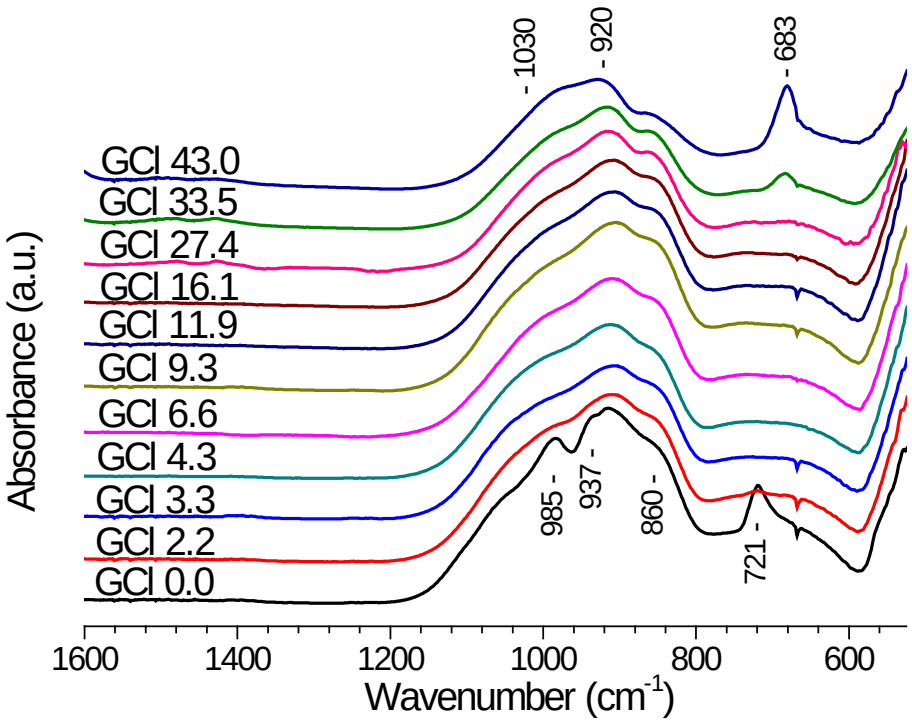

Figure 9.1.3 The FTIR spectra of as-quenched P free $CaCl_2$ containing glasses.

9.1.4 Glass Density and Molar Volume

A reduction of glass density with an increase in $CaCl_2$ content is shown in Figure 9.1.4. There is a break in density behaviour at the $CaCl_2$ content of 19.2 mol%. The glasses with $CaCl_2$ content either less or more than 19.2 show a linear relationship (Y=-0.0139X+2.8886 R^2=0.9883 or Y=-0.0301X+3.2175, R^2=0.9972) between density and $CaCl_2$ content for the both ranges.

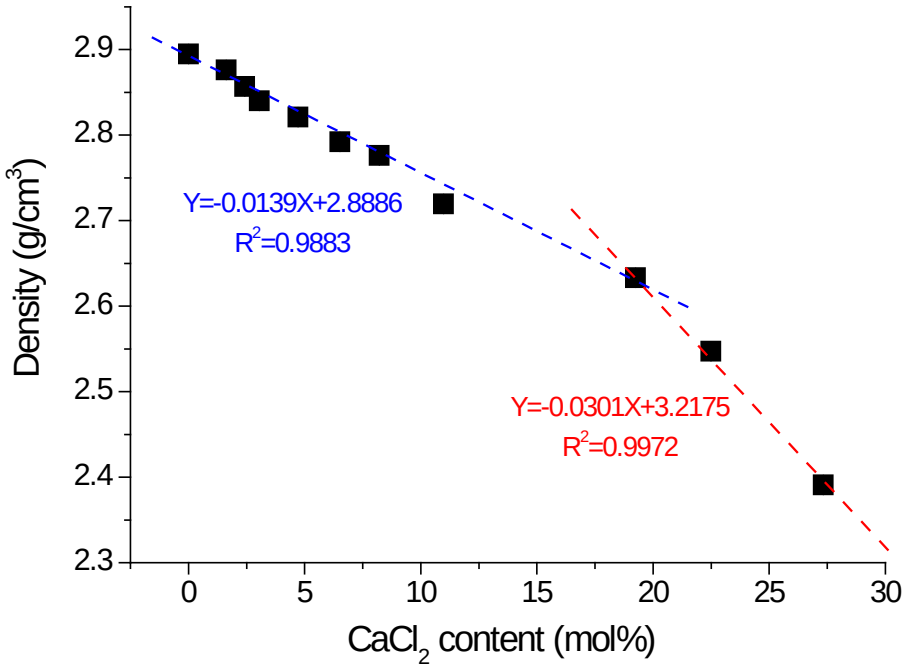

Figure 9.1.4 Glass density plotted as a function of the $CaCl_2$ content. Note where error bars are not seen they are smaller than the data point.

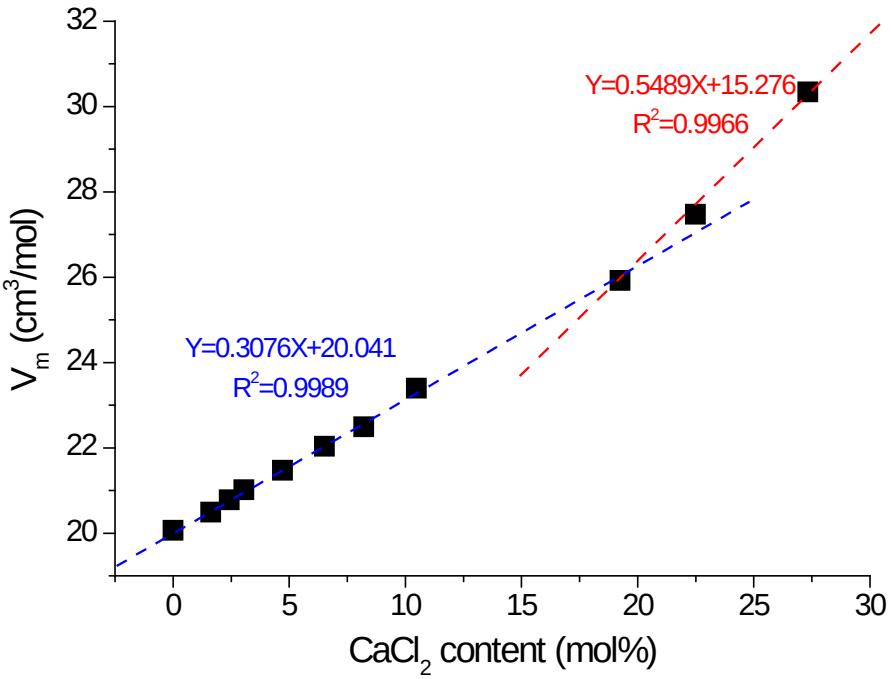

Figure 9.1.5 Glass molar volume plotted as a function of $CaCl_2$ content. Note where error bars are not seen they are smaller than the data point.

In Figure 9.1.5, glass molar volume is plotted as a function of the actual $CaCl_2$ content. In contrast with the change of density with increasing $CaCl_2$ content, the glass molar volume increases markedly from 20 cm^3/mol for GCl 0.0 to 30.34 cm^3/mol for GCl 43.0. This is due to the fact that the large chloride ion expands glass volume, to some extent diluting the glass network. A break in V_m behaviour is observed at the $CaCl_2$ content of 19.2 mol%, the identical transition point was seen in Density behaviour in Figure 9.1.4. Linear correlation ($Y=0.5489X+15.276$, $R^2=0.9966$ or $Y=3076X+20.041$, $R^2=0.9989$) was observed between glass molar volume and $CaCl_2$ content before and after the transition point.

9.1.5 DSC Results of the Na and P Free $CaCl_2$ Containing Bioactive Glasses

Figure 9.1.6 presents the DSC traces for glass frits of P free $CaCl_2$ containing glasses. The obtained T_g, T_c and T_m from DSC traces with an accuracy of ±5 °C are summarised in Table 9.1.2. As shown in the Figure and table, all the glasses have at least one clear exotherm. Generally, T_{c1} moves to lower temperatures with an increase in $CaCl_2$ content and also reduces in amplitude. Whilst, the onset temperature for crystallisation occurs at least 140 °C above the T_g for the glasses with $CaCl_2$ content lower than 27.3 mol%, but less than 100°C for those glasses with $CaCl_2$ content of 27.3 and 31.6 mol%. Furthermore, the clear endotherm peak around 120-150 °C corresponding to loss of water is found in the DSC trace for glasses with $CaCl_2$ contents higher than 19.2 mol%. This could be attributed to the $CaCl_2$-like behaviour of chloride in the glass, which therefore absorbs water in the glass. The absorbed water is driven out on heating, resulting in an endothermic peak. This phenomenon is more pronounced in the high $CaCl_2$ containing glasses. In addition, several other endotherm peaks also appear at about 782 °C, 895°C and 1060°C.

Figure 9.1.7 shows the T_g, T_{c1} and T_{m1} of glass frit and melting point of $CaCl_2$ plotted as a function of $CaCl_2$ content. The circles represent the T_g values and the squares

represent T_{c1} values. Additionally, the red squares belong to the glasses with $CaCl_2$ content less 19.2 mol%, while the blue squares belong to the glass compositions with higher $CaCl_2$ (≥ 19.2 mol%). The dark cyan diamond represents T_{m1} of the glasses, while the magenta triangle represents the melting point of $CaCl_2$ (782 °C). It can be seen that, the T_g values decrease linearly (Y= -13.183X+786, R^2=0.9991) from 783 to 370 °C on adding 31.6 mol% $CaCl_2$, suggesting that it is possible to keep large amount of $CaCl_2$ in the glasses, whilst T_{c1} values also reduce significantly with increasing $CaCl_2$. Taking a closer look, a break in T_{c1} behaviour is seen at 19.2 mol% of $CaCl_2$ content, which is analogous to that of glass density and molar volume. The Linear relationships (Y= -10.775X+955, R^2=0.9753 or Y= -21.806X+1157, R^2=0.9994) between T_{c1} and $CaCl_2$ content were observed in the glasses with $CaCl_2$ content either lower or higher than 19.2 mol%. Additionally, it is interesting to note that the intersection of two linear relationships between T_{c1} and $CaCl_2$ meet at the melting point of $CaCl_2$ at 782 °C. Furthermore, the glasses with $CaCl_2$ content equal to or higher than 19.2 mol% have the T_{m1} values close to 782 °C.

The first crystalline phase of the glasses with $CaCl_2$ contents less than 19.2 mol% is thought to be wollastonite, while the first crystalline phase of the glasses with higher $CaCl_2$ (≥ 19.2 mol%) is thought to be $CaCl_2$. Since these high $CaCl_2$ containing compositions crystallise at lower temperature than 782°C, which is the melting point of $CaCl_2$ and they all have a low melting temperature shown by the magenta triangles close to 782 °C. Thereby, the studied chloride glasses could have crystallised to $CaCl_2$ though they cannot do this, until the crystallisation temperature falls below the melting point of $CaCl_2$. This indicates that in the chloride containing glasses, the chlorine is likely to be present as a Cl-Ca(n) species in an analogous fashion to F-Ca(n) in fluoride containing glasses [4, 79, 150]. The formation of Cl-Ca(n) species is supported by the limited study by Sandland *et al* [84].

Figure 9.1.8 and Figure 9.1.9 show the DSC traces for frit (1-2 mm) and fine powder of GCl 0.0 and GCl 2.2. As mentioned in previous chapters, T_g is an inherent characteristic of glasses and is independent of particle size, which agrees with the identical T_g values for the glass with different particle sizes shown in Figure 9.1.8 and Figure 9.1.9. In contrast with the T_g behaviour, T_{c1} for both glass compositions are particle size dependent, while the T_{c1} for frit is much higher than the equivalent one for fine powder. This indicates that the first crystallisation phase for both GCl 0.0 and GC 2.2 is likely to crystallise from surface. The same crystallisation mechanism is shown for the glasses with $CaCl_2$ content no more than 10.5 mol% in the GCl series. This is consistent with the assumption proposed above that the first crystalline phase of the glasses with $CaCl_2$ less than 19.2 mol% is wollastonite.

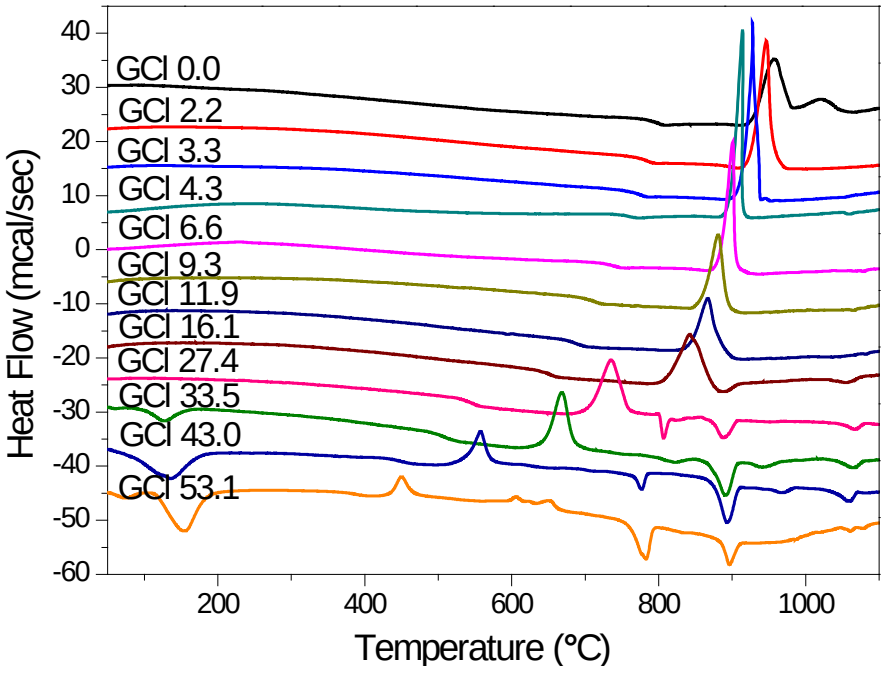

Figure 9.1.6 DSC traces for the glass frits of P free $CaCl_2$ containing glasses. The numbers are nominal molar percentage of $CaCl_2$ in the compositions

Table 9.1.2 Characteristic temperatures (°C) of glass frits for P free $CaCl_2$ containing glasses.

Glass Code	T_g	T_{o1}	T_{c1}	$T_{c2/c3}$	T_{m1}	$T_{m2/m3}$	T_{o1}-T_g
GCl 0.0	782	922	958	1020	-	-	140
GCl 2.2	768	919	948	-	-	-	151
GCl 3.3	757	906	927	-	-	-	149
GCl 4.3	749	892	913	-	-	-	143
GCl 6.6	728	875	901	-	-	-	147
GCl 9.3	697	850	880	-	-	-	153
GCl 11.9	673	837	867	-	-	-	164
GCl 16.1	639	803	842	-	1061	-	164
GCl 27.4	528	700	736	-	806	891	172
GCl 33.5	491	637	669	-	822	890/1062	146
GCl 43.0	429	528	560	-	778	892/1060	99
GCl 53.1	370	432	450	607/605	782	898/1060	62

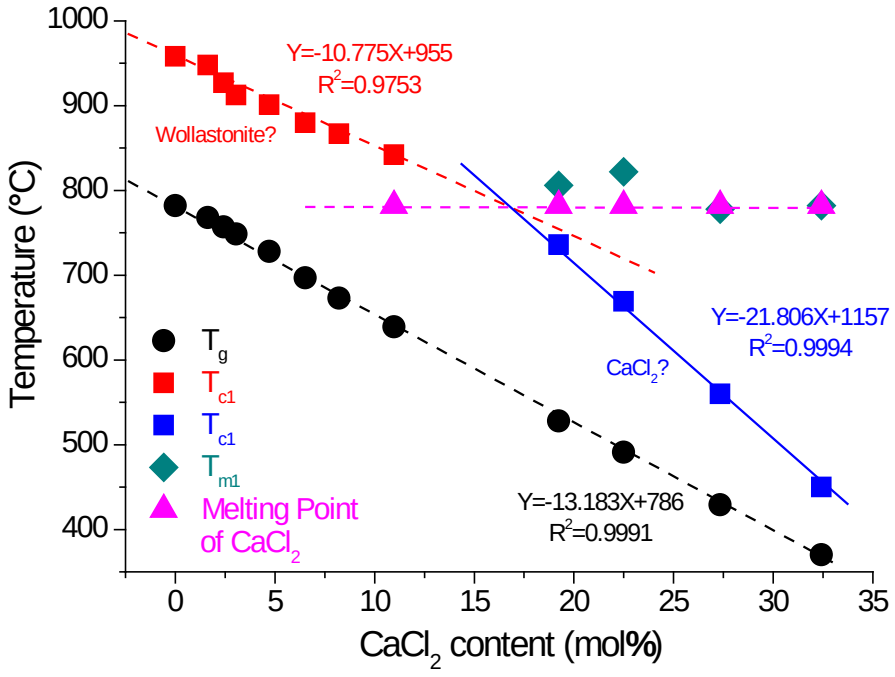

Figure 9.1.7 Glass transition temperature, first crystallisation temperature, first melting temperature and the melting point of $CaCl_2$ profiled as a function of $CaCl_2$ content. Linear relationship (Y=-13.183X+786, R^2=0.9991) between T_g and $CaCl_2$ content are shown in the glasses. Another liner relationships (Y=-10.775X+955, R^2=0.9753 or Y=-21.806X+1157, R^2=0.9994) between T_{C1} and $CaCl_2$ content are shown in the glasses with $CaCl_2$ content either lower or higher than 19.2 mol%.

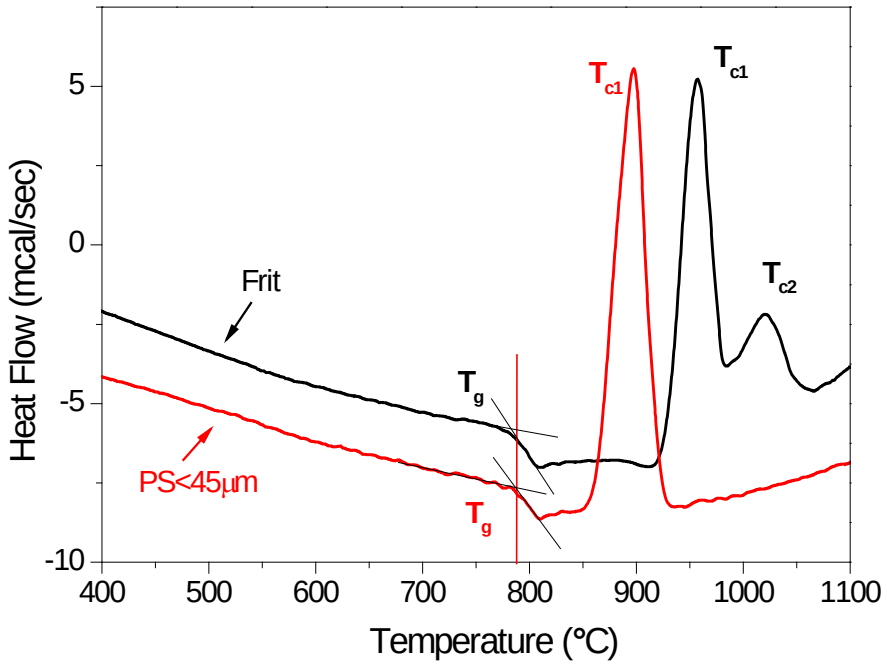

Figure 9.1.8 DSC traces for frit and <45 µm powder of GCl 0.0 demonstrating surface nucleation of the first crystallisation phase.

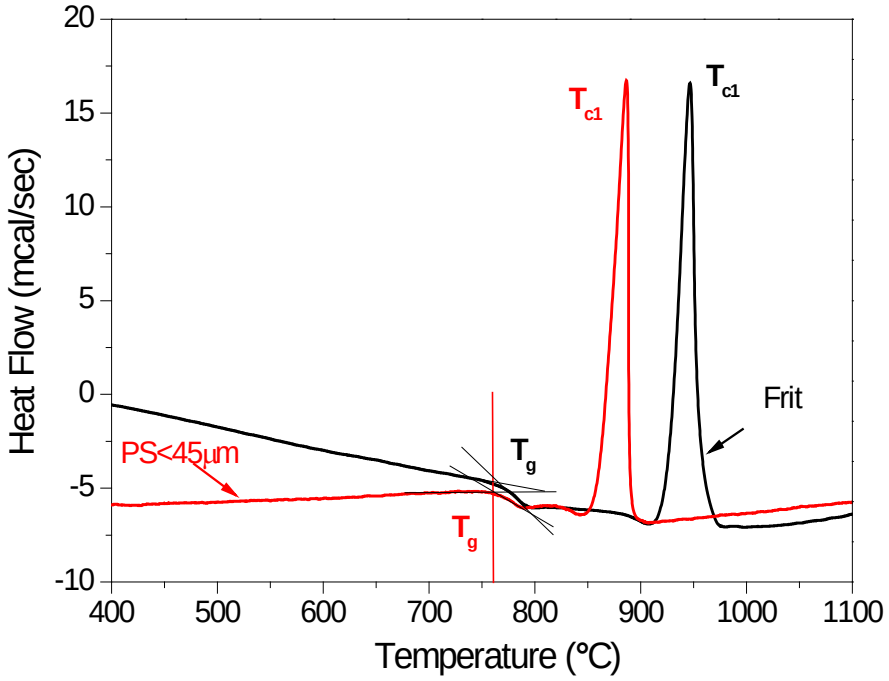

Figure 9.1.9 DSC traces for frit and <45 µm powder of GCl 2.2 demonstrating surface nucleation of the first crystallisation phase.

9.2 Dissolution Study in Tris Buffer Solution

The dissolution study of the P free $CaCl_2$ containing glasses was carried out in Tris buffer solution. The characterisation of the collected precipitates was performed by using XRD and FTIR. Note that only those glasses with $CaCl_2$ content no more than 10.5 mol% underwent the dissolution study and are presented in this chapter. This is because glasses with high $CaCl_2$ content (≥ 19.2 mol%) are extremely hygroscopic which makes studies problematic.

9.2.1 X-ray Diffraction Results

XRD patterns of glass compositions GCl 0.0 and GCl 2.2 before and after 3 days immersion in Tris are selected and presented in Figure 9.2.1 and Figure 9.2.2. The partially crystalline glass GCl 0.0 that crystallised to β-$CaSiO_3$ during quenching showed a reduction in intensities of the β-$CaSiO_3$ diffraction lines after 3 days immersion, suggesting the dissolution of the β-$CaSiO_3$ crystals. It is clear that the amorphous glass phase dissolves much faster than the crystalline phase (β-$CaSiO_3$). In addition, the amorphous glass halo disappears at 30° 2Θ 2Θ while another halo appears at 22° 2Θ, indicating the degradation of glass phase and the formation of an ion-depleted glass [9, 20]. In the case of the initial amorphous glass GCl 2.2, the position of amorphous halo has shifted to 22° 2Θ compared to the untreated glass, this is thought to be attributed to formation of an ion-depleted glass or silica-gel [20]. A similar evolution was observed in the rest of the $CaCl_2$ containing glasses, which are shown in Figure 9.2.3.

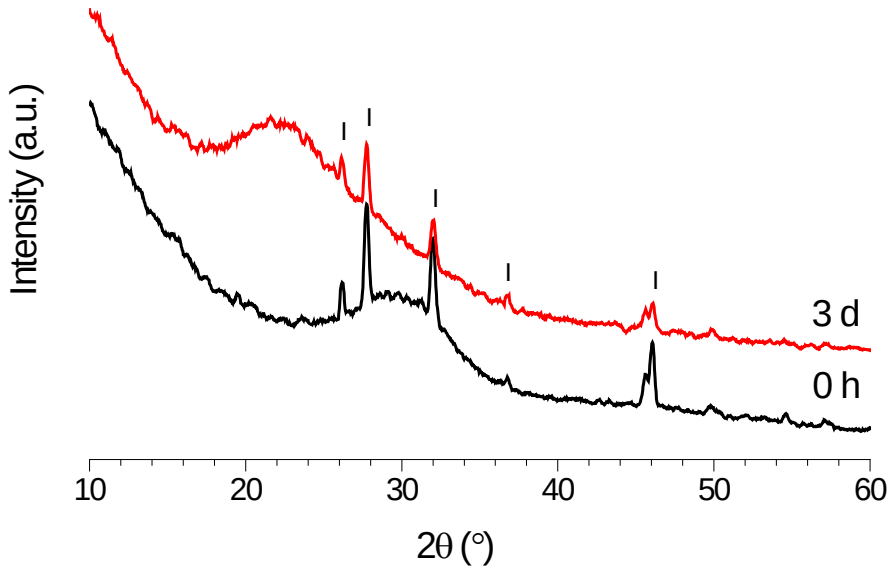

Figure 9.2.1 The XRD patterns of the glass precipitates with 0.0 mol% $CaCl_2$ collected after 3 days immersion in Tris (I: β-$CaSiO_3$).

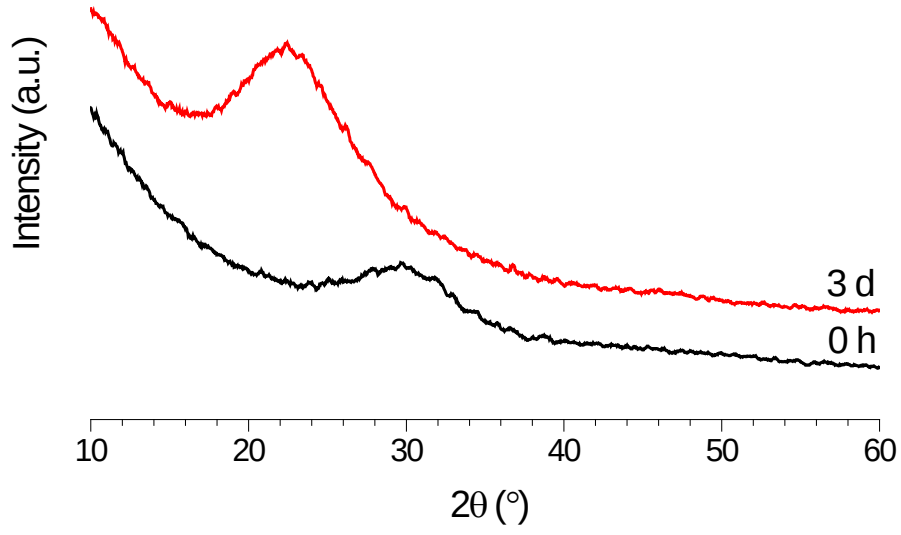

Figure 9.2.2 The XRD patterns of the glass precipitates with 1.6 mol% $CaCl_2$ collected after 3 days immersion in Tris.

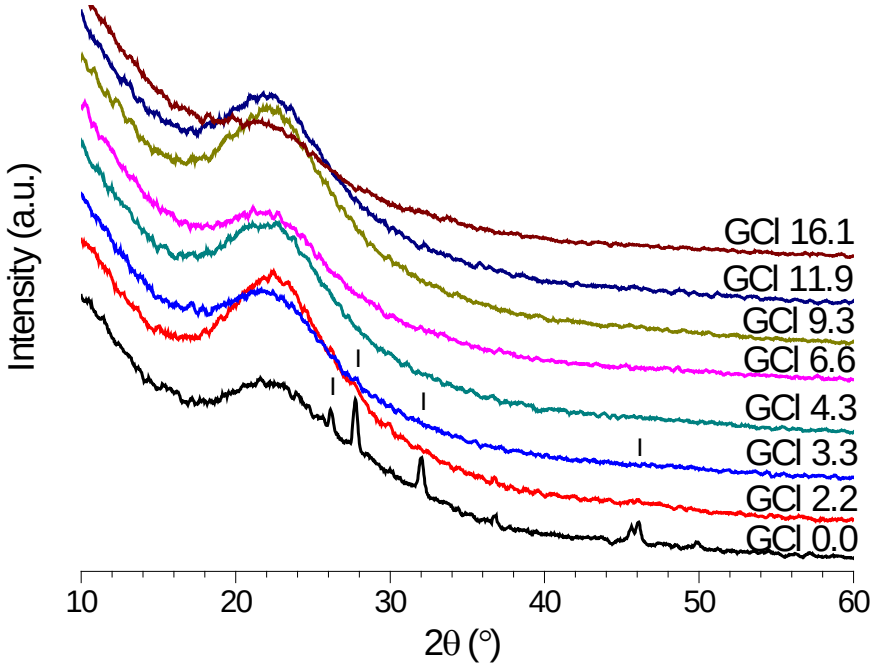

Figure 9.2.3 The XRD patterns of the glass precipitates collected after 3 days immersion in Tris (I: β-$CaSiO_3$).

9.2.2 Fourier Transform Infrared Spectroscopy Results

Figure 9.2.4 and Figure 9.2.5 show the FTIR results of glasses GCl 0.0 and GCl 2.2 that were chosen above for the XRD results after 3 days immersion in Tris buffer. The spectrum at the bottom of each figure belongs to the as-quenched glass that was discussed above. For those two glasses, after three days immersion the non-bridging oxygen bands at 920 and 860 cm^{-1} disappear, while the clear peaks at 792 (the Si-O bending vibrations), 945 and 1042 cm^{-1} (Si-O stretching) and a broad band at 1200-1250 cm^{-1} (Si-O-Si stretching) develop [174-176]. The changes suggest the loss of the non-bridging oxygen bands due to leaching of Ca^{2+} and dissolution of soluble silica at the glass interface and the formation of silica-gel [175]. Similar changes were found in the rest studied $CaCl_2$ containing glasses (Figure 9.2.6). Moreover, for the glass GCl 0.0, a clear decrease in intensity of the peak at 721 cm^{-1} indicates the dissolution of crystalline $CaSiO_3$. This is in good agreement with the XRD results shown above.

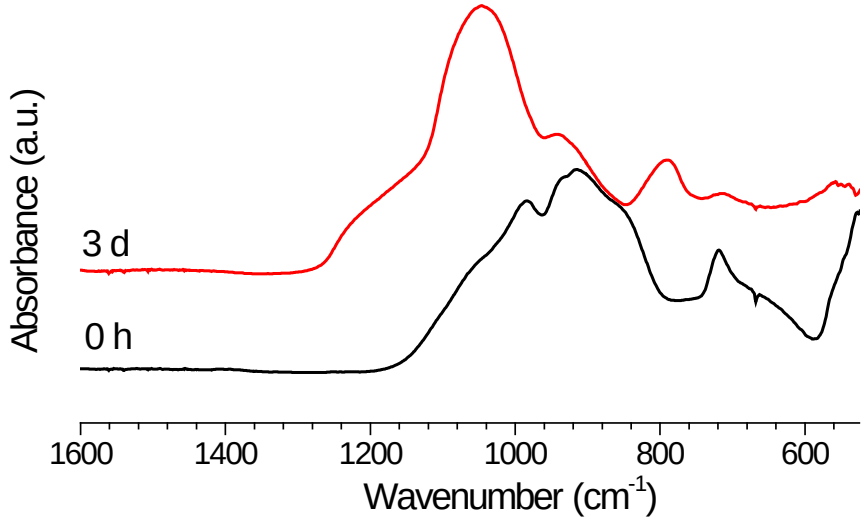

Figure 9.2.4 The FTIR spectra of the glass precipitates with 0.0 mol% $CaCl_2$ collected after 3 days immersion in Tris.

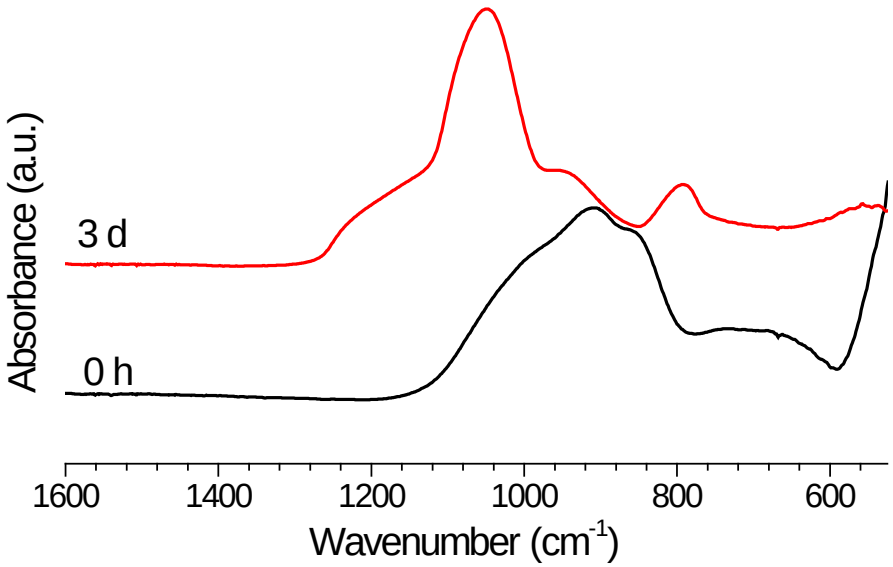

Figure 9.2.5 The FTIR spectra of the glass precipitates with 2.2 mol% $CaCl_2$ collected after 3 days immersion in Tris.

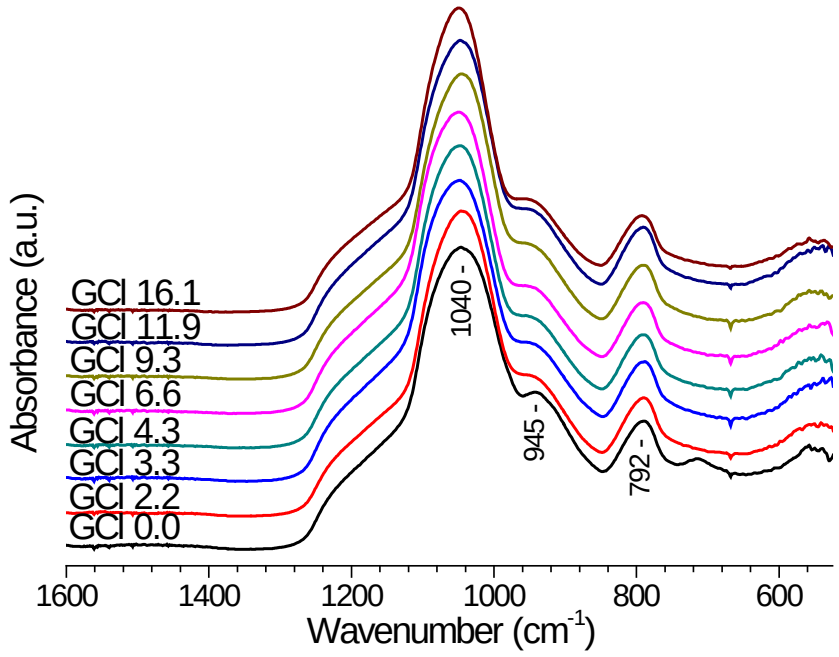

Figure 9.2.6 The FTIR spectra of the glass precipitates collected after 3 days immersion in Tris.

9.3 Crystallisation Phase Identification

9.3.1 X-ray Diffraction Results of Heat Treated Glasses

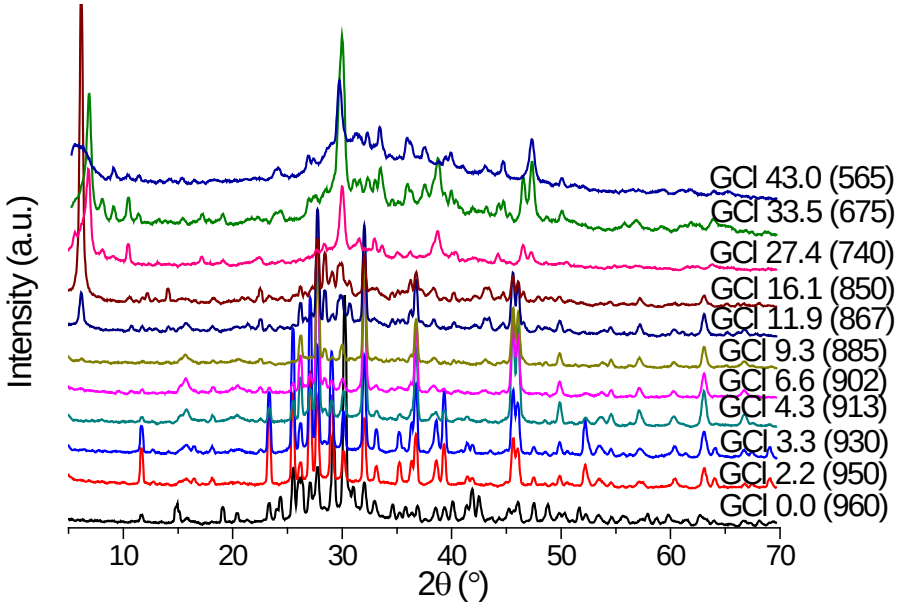

Figure 9.3.1 The XRD patterns of the GCl glass series upon heat treatment. The numbers in the brackets represent the heat treatment temperature.

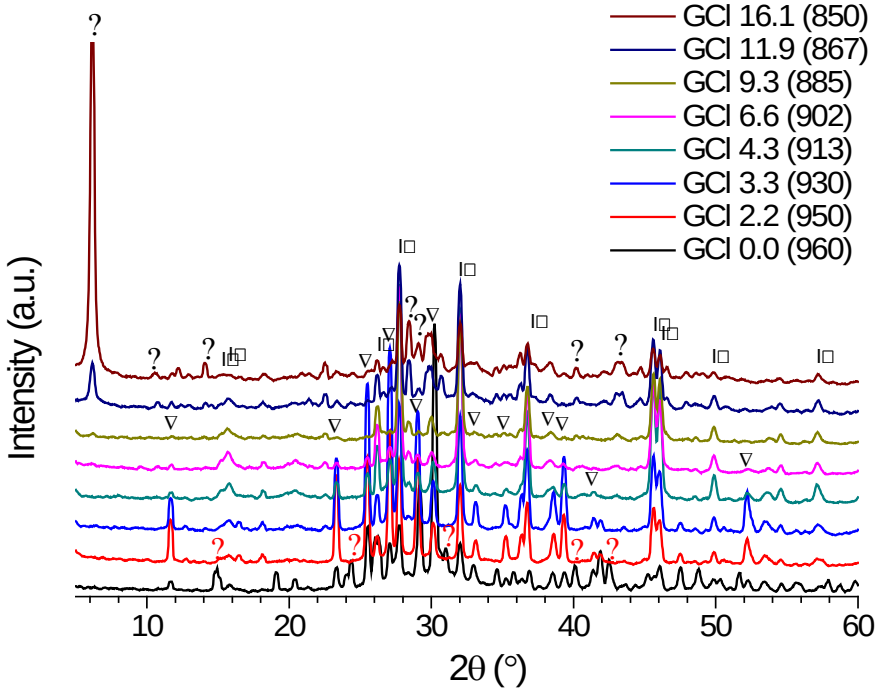

Figure 9.3.2 The XRD patterns of the GCl glass series ($CaCl_2$ content ≤ 16.1 mol%) upon heat treatment. The numbers in the brackets represent the heat treatment temperature. (□: β-$CaSiO_3$; ∇: $CaSiO_3$; ?: UP (unidentified phase) I; ?: UP II)

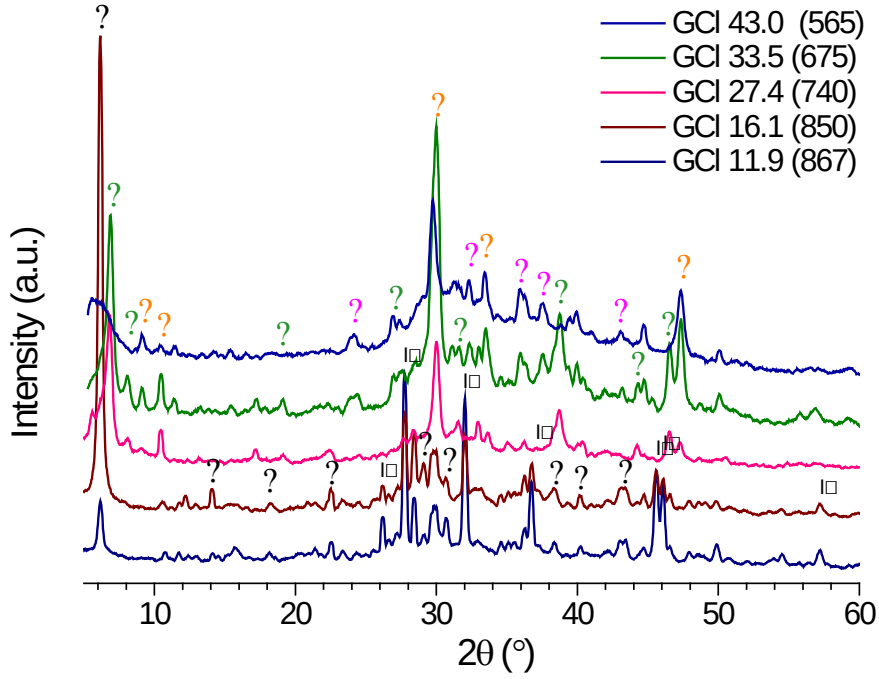

Figure 9.3.3 The XRD patterns of the GCl glass series ($CaCl_2$ content ≥ 11.9 mol%) upon heat treatment. The numbers in the brackets represent the heat treatment temperature. (□: β-$CaSiO_3$; ∇: $CaSiO_3$; ?: UP II; ?: UP III; ?: UP IV; ?: UP V)

Figure 9.3.1 shows the XRD patterns of all the heat treated P free $CaCl_2$ containing glasses. Several crystalline phases contribute to the diffraction lines that strongly overlap. In order to have a better and clearer view, the glasses with $CaCl_2$ contents up to 10.5 mol% are presented in Figure 9.3.2, while the glasses with $CaCl_2$ content equal to or higher than 11.9 mol% are shown in Figure 9.3.3. Figure 9.3.2 shows, the diffraction lines developed upon heat treatment for the studied glasses (≤ 10.5 mol%) largely match those for β-$CaSiO_3$. In addition, for the glasses with $CaCl_2$ content equal to or less than 6.5 mol%, the diffraction lines also match those of $CaSiO_3$ are also seen. The intensity of those diffraction lines reduce when the $CaCl_2$ content is over 3.1 mol%. On close examination of the pattern for GCl 0.0, some unknown peaks that are labelled as red question mark corresponding to an unidentified phase are seen. However, due to the fact that more than one crystalline phase forms upon heating and the lack of reference patterns for chlorosilicate phases, it is extremely difficult to determine the crystalline phases upon heat treatment. In the case of GCl 11.9 and GCl 16.7, apart from the diffraction lines corresponding to the β-$CaSiO_3$ after heat treatment, additional diffraction lines (labelled as black question mark corresponding to unidentified phase two) at 6.06°, 24.44°, 29.55°, 29.79° and 30.56° 2θ are also observed. However, these diffraction lines do not match completely with any known phase in the database although some of them match the ones for $Si_3O_6{\cdot}H_2O$ (00-25-1332).

The XRD patterns of the heat treated glasses GCl 27.4 and GCl 33.5 (in Figure 9.3.3) also have a similar distinct diffraction line at low two theta values (6.75° 2θ) as glasses GCl 11.9 and GCl 16.7. Moreover, several additional lines emerge at 7.99°, 10.3°, 31.41°, 38.54° and 46.36° corresponding to unidentified phase three, which might be $H_2Si_{14}O_{29}{\cdot}5.4H_2O$ (labelled as green question mark). In the case of GCl 43.0, the diffraction lines at 9.03°, 24.1°, 32.22°, 35.83°, 37.33° and 44.55° are visible after heat treatment at 565°C. These peaks are also found in the XRD pattern for glass GCl 33.5 after heat treated at 675 °C and assigned to unidentified phase four (labelled as

magenta question mark), $Ca_{10}Si_6O_{21}C_{l2}$ could be a possibility. Furthermore, diffraction lines at 10.3° 29.91°, 33.29° and 47.16° corresponding to unidentified phase five (labelled as orange question mark) present in the patterns of the heat treated GCl 27.4, GCl 33.5 and GCl 43.0. The unidentified phase five is very likely to be $CaCl_2$. DSC traces of these three glasses all have a relatively sharp endotherm around 782°C. Moreover, one of the acquired XRD patterns of the heat treated GCl 43.0 showed a weak evidence of the diffraction lines corresponding to $CaCl_2 \cdot 4H_2O$. Owing to the extremely reactive nature of these high $CaCl_2$ containing glasses, the collected XRD patterns are very complicated and another technique is required for independent verification of possible phases forming. To further analyse the crystallisation phases, ^{35}Cl and ^{29}Si MAS-NMR would be very useful.

9.3.2 Fourier Transform Infrared Spectroscopy Results of Heat Treated Glasses

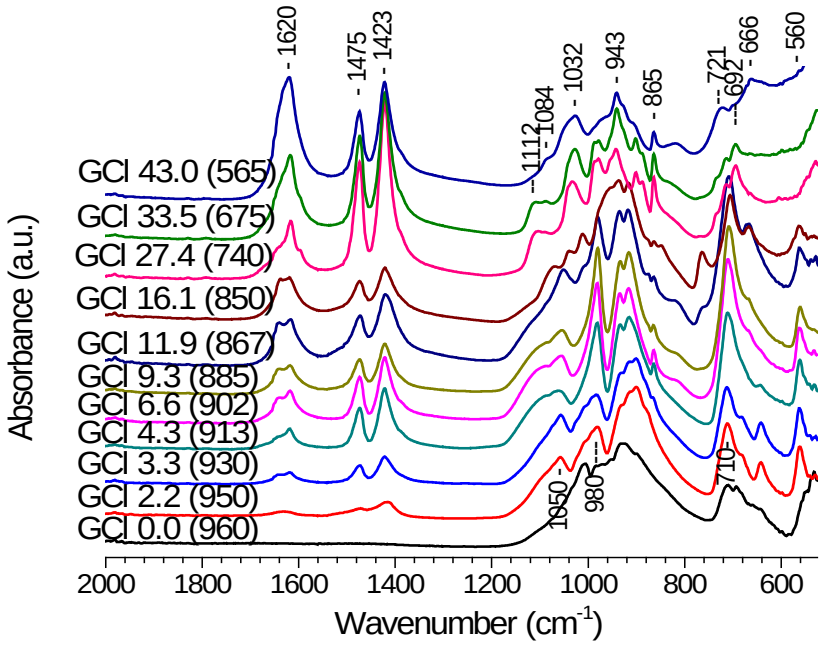

Figure 9.3.4 The FTIR Spectra of the heat treated GCl glass series. The numbers in the bracket represent the heat treatment temperature.

The main features of the FTIR spectra of heat treated GCl glass series are the appearance of peaks at 550-1200, 1400-1650 and 3000-3700 cm^{-1}, as shown in

Figure 9.3.4 and Figure 11.2.5 (in Appendix). The presence of bands at 560, 642, 666, 710, 903, 915 937, 980, 1050 and 1084 cm^{-1} in the spectra of those glasses samples with $CaCl_2$ equal or less than 10.5 mol% confirms the existence of the β-$CaSiO_3$ phase in the structure [177]. This is consistent with the XRD results. The bands at 3345 and 3412 cm^{-1} could be associated with the OH^- absorption bands. The vibration of O-H is also reflected at about 1620 cm^{-1}, indicating the presence of adsorbed water [175, 178]. The new bands emerge at 692, 721, 732 and 1112 cm^{-1} for glasses GCl 27.4, GCl 33.5 and GCl 43.0 are related to Si-O-Si vibration mode [176], suggesting the presence of a silicate crystalline phase upon heat treatment. The double peaks at 1423 and 1475 cm^{-1} match that of C-O stretching vibration band in CO_3^{2-} in the literature [175, 178, 179]. According to the XRD and FTIR results, the potential crystallisation phases of the GCl glass series upon heat treatment are summarised in the appendix.

Further Discussion

The existence of such a wide glass forming region in this ternary system has not been anticipated because there is practically no information in the literature on a maximum amount of chloride possible to incorporate into silicate glasses. The fact that the glass composition with nearly equal amounts of SiO_2, CaO and $CaCl_2$ has been synthesised is surprising and could not have been predicted especially taking into account chloride losses. Moreover, the composition GCl 53.1 did not crystallise, thus, implying that it still would be possible to extend glass formation further to higher $CaCl_2$ content. However, reactivity of the high chloride containing glasses is extremely high and the material would require a different quenching regime.

The glass transition temperature, first crystallisation temperature and glass density reduce significantly with an increase in $CaCl_2$ content, while the glass molar volume increases remarkably with increasing $CaCl_2$ content. It is worth noting that a break in behaviour in these properties occurs when the incorporated of $CaCl_2$ content is around 19.2 mol%. The presence of a break in behaviour is likely to be attributed to a change

of glass structure. In the glasses with relatively low $CaCl_2$ content (≤ 10.5 mol%), glass structure is dominated by the silica structure. With an increase of $CaCl_2$ content to over 19.2 mol%, the glass structure might be dominated by chloride clusters. ^{29}Si and ^{35}Cl MAS-NMR will be carried out to further investigate the glass structure.

The expansion of the glass volume arising from the presence of $CaCl_2$ aids glass degradation, the dissolution study in Tris buffer suggests the completion of glass degradation with 3 days immersion. Due to the absence of PO_4^{3-} in Tris, no apatite or other phase formation was detected after immersion. For this glass series, SBF solution might be more informative for the apatite formation study, as it provides phosphate although the composition of SBF is deficient in phosphate relative to the apatite stoichiometry. The Ca:P ratio of SBF is approximately 2.5 compared with 1.67 for apatite. However, the presence of P_2O_5 in the glass is not essential to achieve some bioactivity, as long as P can be provided from other sources, such as SBF and saliva. It was shown by Ebisawa *et al.* that P_2O_5 free glasses can also show some bioactivity in SBF [167].

The XRD patterns and FTIR spectra of the heat treated GCl glass series consistently indicate that β-$CaSiO_3$ is the main crystalline phases in the glasses with $CaCl_2$ content equal or less than 16.1 mol%. $CaSiO_3$ is the other crystalline phase in the glasses with $CaCl_2$ content no more than 11.9 mol%. The amount of $CaSiO_3$ formation reduced with increasing $CaCl_2$ content over 4.3 mol%. It seems that $CaSiO_3$ formation is favoured at high temperature. Multiple crystalline phases formed in the heat treated samples and the identification has proved to be very difficult as shown above.

DSC results show that the glasses (≥ 19.2 mol%) with T_{c1} less than 782 °C have the endothermic peak corresponding to $CaCl_2$ melting at around 782 °C; in other words, $CaCl_2$ is one of the potential crystalline phases for those three glasses. The XRD patterns of the heat treated glasses with high $CaCl_2$ content (≥ 19.2 mol%) did demonstrate new crystalline phases which differ from wollastonite, however, those

developed diffraction lines do not match that of $CaCl_2$. It seems to contradict to the DSC results shown above but it is necessary to note that those high chloride containing glasses have a strong tendency to react with atmospheric water during XRD data collection. Therefore it is possible that the obtained diffraction lines reflect the crystalline phase after reacting with atmospheric water, rather than the crystalline phase crystallised from the glass itself and calcium chloride is still thought to be the crystalline phase. To some extent, this suggests the possibility of forming Cl-Ca(n) species. The formation of $CaCl_2$ suggests that the glasses may contain Cl-Ca(n) species. This can be related to the fluoride glasses which have F-Ca(n) species crystallise upon heat treatment to CaF_2, $Ca_{10}(PO_4)_6F_2$ and $Ca_4(Si_2O_7)F_2$, which all have the F-Ca(n) species [111].

Summary

The wollastonite stoichiometry glasses with varying $CaCl_2$ content from 0.0 to 31.6 mol% were synthesised by a melt-quenched route. The XRD results of the as-quenched glasses indicate that the studied P free $CaCl_2$ containing glasses are amorphous; while the glass that only consists of CaO and SiO_2 (GCl 0.0) has partially crystallised to β-$CaSiO_3$. The significant reduction of glass transition temperature and first crystallisation temperature with $CaCl_2$ content suggest the possibility of forming Cl-Ca(n) species. A reduction in glass density and the increase in the glass volume with an increase in $CaCl_2$ content reveal that chloride expands glass volume. A break in behaviour in T_g, T_{C1}, D and V_m was observed when the $CaCl_2$ content is around 19.2 mol%. On immersion, glasses dissolved within 3 days immersion in Tris but no apatite formation was found. Upon heat treatment, the glasses with $CaCl_2$ content equal or less than 10.5 mol% that have T_{c1} higher than the melting temperature of $CaCl_2$ crystallised to wollastonite ($CaSiO_3$ and β-$CaSiO_3$). For the glasses with $CaCl_2$ content equal or higher than 19.2 mol%, which have T_{c1} lower than 782°C are likely to crystallise to $CaCl_2$.

10 Comparison of Halide Containing Bioactive Glasses

The objective of this chapter is to compare the data from the four series of glasses, including the retention of chloride, the glass transition temperature, density, molar volume, structure, glass degradation and apatite-like phase formation.

10.1 The Retention of Chloride

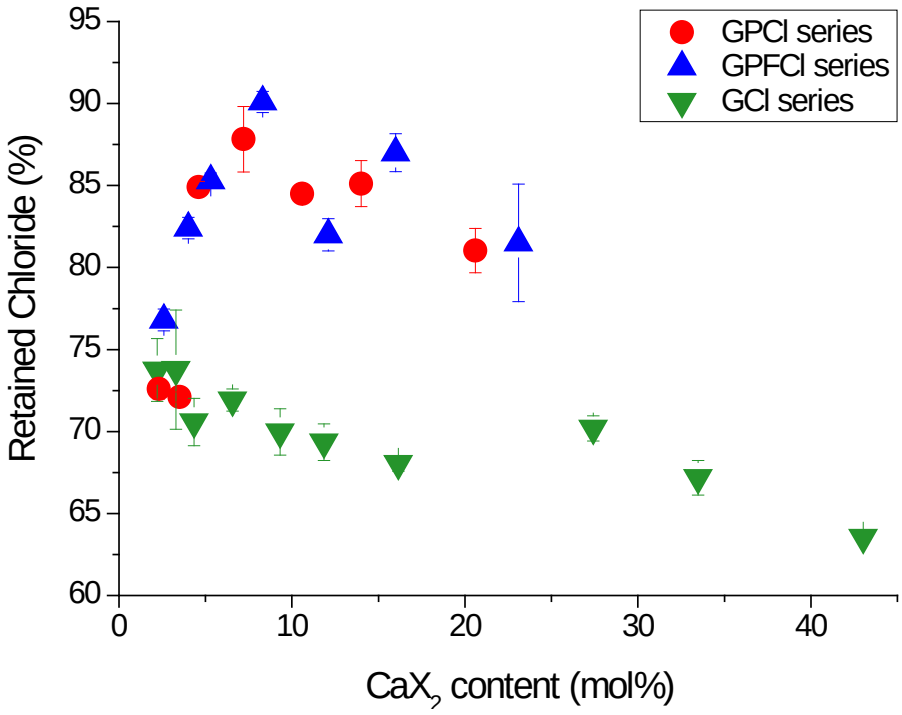

Figure 10.1.1 The percentage of the retained chloride in the initial glasses against the chloride content

The percentages of the retained chloride in the initial glasses after chloride loss are plotted against CaX_2 content for the three series of chloride glasses (GPCl, GPFCl and GCl series) in Figure 10.1.1. As mentioned in the previous chapters (Chapter 6,

Chapter 7 and Chapter 9), a large proportion (62 - 92%) of chloride was retained in the studied glasses which are predominantly Q^2 in structure confirmed by the ^{29}Si MAS-NMR (Figure 6.1.5). Although in all of these glasses the formation of the Cl-Ca(n) is assumed. It is clear that the phosphate free $CaCl_2$ containing glasses have a relatively lower chloride retention compared with the glasses with phosphate. To some extent, Cl-Ca(n) species might preferentially associates with orthophosphate tetrahedra. Thus, the absence of phosphate might lead to a higher amount of chloride loss. An unpublished molecular dynamics simulation study from Pedone [180] supports this. This indicates that the medium-range structure can influence retention of chloride and not just the immediate short-range local environment. To achieve a better understanding of the glass structure, future work i.e. ^{35}Cl MAS-NMR and a systematic molecular dynamics simulation study should be carried out.

10.2 The Glass Transition Temperature

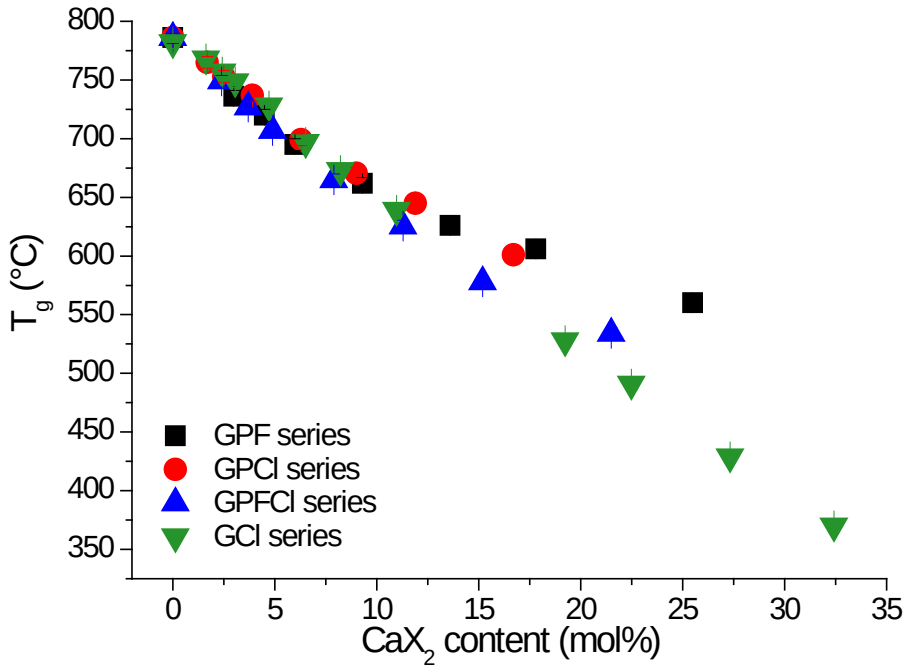

Figure 10.2.1 Glass transition temperature of the frit profiled as a function of CaX_2 content.

Figure 10.2.1 presents the glass transition temperature of the frit against CaX_2 (X=F/Cl/F+Cl) content for GPF, GPCl,GPFCl and GCl glass series. For each of glass series, there is a reduction in T_g with an increase in CaX_2 content. It is thought to be attributed to the formation of 'CaX^+' species, which behave in a similar fashion to Na^+ cations. Note that "CaX^+" represents as "CaF^+" for GPF glass series and "$CaCl^+$" for both GPCl and GCl glass series, while "CaX^+" could be "CaF^+" plus "$CaCl^+$" or "$Ca(F_a/Cl_{(1-a)})^+$" (0<a<1) for GPFCl glass series. As discussed previously in Chapter 5, the formation of 'CaX^+' species knock out the ionic bridge between two NBOs by divalent calcium ions and therefore disrupts the glass network, which accounts for the observed reduction behaviour in T_g.

Generally, T_g values for the P_2O_5 containing glasses with CaX_2 (X=F/Cl/F+Cl) content less than 10 mol% are pretty much identical between the series. Owing to the significant crystallisation of fluoride containing phases, a higher T_g of GPF glass series relative to GPCl glass series is observed when CaX_2 (X=F/Cl) content is higher than 10 mol%. As discussed in Chapter 5, the crystallisation of fluoride containing phases effectively removes fluoride from the glass matrix; therefore, T_g reduced less in the glasses with higher crystallinity. Instead of having intermediate values, the T_g of mixed CaF_2 and $CaCl_2$ glasses lie below those of the glasses with a single calcium halide. To some extent, this might be similar to the known mixed alkali effect shown for instance by Isard [181] and Brauer *et. al.* [182]; there could be a mixed halide effect. Comparing the T_g values for the GPCl series with the ones for GCl glass series, no significant difference was observed. This indicates that phosphate does not play a significant role in changing the T_g of in the studied glasses. Theoretically, $CaCl_2$ containing glasses should have a lower T_g reduce compared to CaF_2 containing glasses, since the chloride ion is larger than the fluoride ion. A large ion would be expected to result in a more expanded open glass network that may lead to a lower T_g [183]. Interestingly, almost identical T_g values of the amorphous glasses (< 10 mol% CaX_2) from both GPF

and GPCl glass series were found here. There is no certain answer about it at the moment. In the future, amorphous scattering studies may help here.

T_g is a significant parameter, which can be used to indirectly predict glass solubility, degradability and hardness of glasses within certain compositional ranges [6, 42]. The hardness measurement of bioactive glasses is challenging, because of their tendency to crystallise during casting and their tendency to surface react during sample preparation. However, both T_g and glass hardness are expected to be determined by the average bond strength in the glass structure, thus hardness and T_g might be expected to exhibit a strong correlation. O'Donnell [41] proposed that a strong linear correlation between T_g and the hardness of bioactive glass exists, where the glass with a lower T_g is expected to have a lower hardness. In addition, Farooq *et.al.* have found a reduction of the hardness with a decrease in T_g for the CaF_2 containing bioactive glasses when increasing the amount of Na_2O in the glass [6]. According to the strong relationship between T_g and CaX_2 content a glass with an optimised hardness can be designed for different applications. The glasses with a hardness lower than enamel are particularly of interest for desensitising toothpastes [41] and air abrasion polishing [6, 98].

10.3 Glass Density and Molar Volume

10.3.1 Glass Density

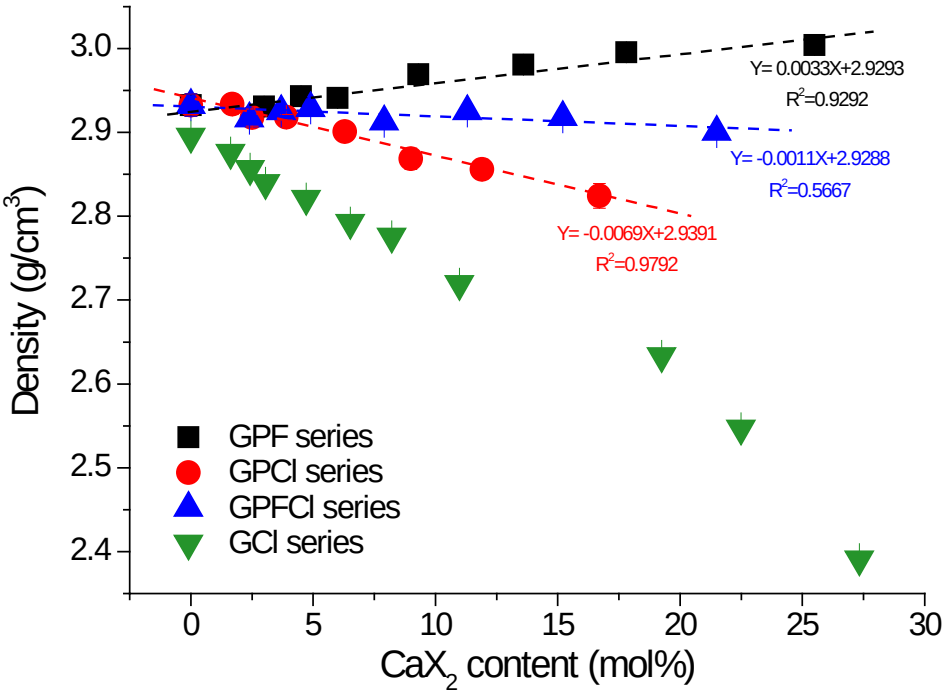

Figure 10.3.1 Glass density profiled as a function of CaX_2 (X=F/Cl/F+Cl) content. Linear relationships (Y=0.0033X+2.9293, R^2=0.9292 and Y=-0.0069X+2.9391, R^2=0.9792) between density and CaX_2 content are shown in GPF and GPCl glass series.

Glass density values of the GPF, GPCl, GPFCl and GCl glass series are plotted against CaX_2 content in Figure 10.3.1. A clear increase in density is visible with increasing CaF_2 content for the GPF glass series, conversely, the density of GPCl glass series decreases with an increase in $CaCl_2$ content. The presence of both CaF_2 and $CaCl_2$ is likely to neutralize the changes in density, which accounts for the fact that the density values of GPFCl glass series fall in between the equivalent of GPF glass series and GPCl glass series. The values fluctuate between 2.9 and 2.93 g/cm^3 and are practically independent of CaX_2 content, though clear linear relationships were found for the single calcium halide containing glass series (GPF and GPCl series).

The density estimated (D_c) from the individual series density values assuming an equal effect of fluoride and chloride (in Appendix, Table 11.2.3) are higher than the obtained experimentally (D_e) for the mixed series. Thus, for the most glasses (GPFCl 5.3, GPFCl 12.1, GPFCl 16.0 and GPFCl 23.1) from GPFCl series, chloride has a stronger effect than fluoride.

In the case of the GCl glass series, the density reduces with increasing in $CaCl_2$ content. A comparison of the density values of the GPCl series and GCl series shows that the $CaCl_2$ containing glasses with the absence of phosphate have lower density values.

As proposed by Brauer *et al.*[123], the density of CaF_2 containing glasses consists of a combination of both silicate glass and CaF_2-like phase. Chloride is thought to behave in the similar way to CaF_2, therefore, the density of chloride containing glasses would be composed of both silicate glass and $CaCl_2$-like species. For the GPCl glass series, the density of silicate glass part can be separated into silicate part (Q^3 and Q^2) and phosphate ($Ca_3(PO_4)_2$) part, ^{31}P MAS-NMR indicated that phosphate is present as orthophosphate in Chapter 6 (Figure 6.1.4). $Ca_3(PO_4)_2$ has a density of 3.14g/cm^3 which is higher than the equivalent silicate part (Q^3: 2.68g/cm^3 and Q^2:2.89g/cm^3). The P free GCl glasses have the NC equal to 2, therefore the glass density are expected to be lower than the GPCl glasses series, this agrees with the experimental data.

10.3.2 Glass Molar Volume

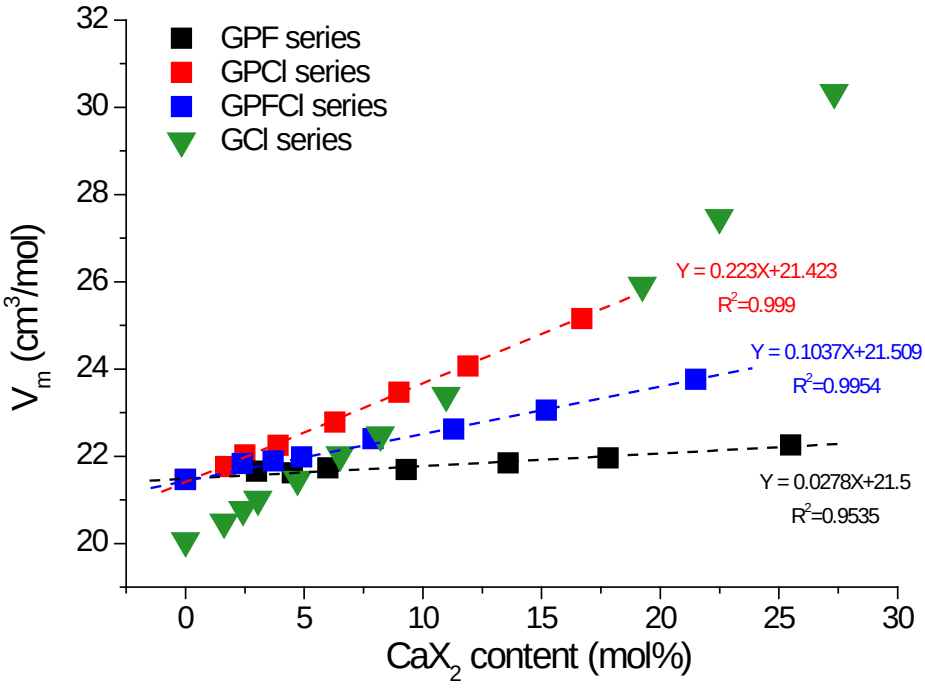

Figure 10.3.2 Glass molar volume profiled as a function of CaX_2 (X=F/Cl/F+Cl) content. Linear relationships (Y=0.223X+2.21.423, R^2=0.999, Y=0.1037X+21.509, R^2=0.9954 and Y=0.00278X+21.5, R^2=0.9535) between density and CaX_2 content are shown in GPF, GPCl and GPFCl glass series.

Figure 10.3.2 shows the glass molar volume of the four series of glasses plotted as a function of CaX_2 content. It is interesting to see that the glass molar volume increases linearly with an increase in CaX_2 content for all three series of phosphate containing glasses. The increased slope for GPCl series is more pronounced than the equivalent GPFCl series, which is much more significant than the equivalent GPF glass series. The dominating factor resulting in this difference is the fact that the chloride ion is substantially larger than the fluoride ion. Therefore the expansion of glass volume by incorporating chloride is much more pronounced than by incorporating fluoride alone, whilst, incorporating mixed fluoride and chloride lies in between. It is interesting to know how fluoride and chloride affect the glass molar volume in the mixed glass system. Do they have same strength of the effect? According to the proportion of CaF_2

content in CaX_2 (59.5 %-62.5%) and $CaCl_2$ in CaX_2 (37.5 %-40.5%) and the slopes in the linear relationships between V_m and CaX_2 content for GPF and GPCl series, the slope in the linear relationship for mixed series can be calculated. Suppose that the presence of CaF_2 and $CaCl_2$ show the same strength of the effect for the changes in glass molar volume, then the slope can be calculated by weighted sum model, which gives values between 0.101 to 0.1068. Compared these values to the slope (0.1037) from the experimental data, they are within 3% error. Thus, the conclusions can be drawn as that the presence of CaF_2 and $CaCl_2$ have same strength in affecting glass molar volume and it is possible to tailor the glass molar volume by changing the CaF_2 to $CaCl_2$ ratio.

By the comparison of the V_m from GCl series and GPCl series, it is clear that the V_m values for the GCl glass series are lower than the ones for the GPCl glass series when the $CaCl_2$ content is less than 19.2 mol%. This is in a good agreement with the result found by Doweidar [184] that V_m increases with an increase in P_2O_5 content.

The molar volume which was used to mirror the compactness of the glass can be also used to predict glass hardness [185]. On incorporation of CaX_2, the glass hardness would be expected to decrease, as a consequence of a reduced compactness of the glass by expanding the glass volume. This is in a good agreement with the reduction in T_g with increasing in CaX_2 content. Moreover, the glasses with larger molar volume are expected to have a lower crystallisation tendency and a faster glass degradation rate.

10.4 Crystallisation Tendency of the As-Quenched Glasses

The XRD patterns of the as-quenched glasses for the four glass series are summarized in Figure 10.4.1 (a)-(d) for convenient comparison purpose, although, they have been described and discussed in Chapter 5, 6, 7 and 9 in detail. Due to the fact that, chloride ion is bigger than fluoride ion, it is expected that within the four series of glasses, the fluoride containing glasses (GPF series) will crystallise most

readily, while the chloride containing glasses (GPCl and GCl series) will crystallise less readily and the mixed fluoride and chloride containing glasses (GPFCl series) will have an intermediate crystallisation tendency. The XRD patterns of the GPF glass series do suggest a high crystallisation tendency of this glass series. On incorporating $CaCl_2$ rather than CaF_2, the tendency of the glasses to crystallise is suppressed for both GPCl and GCl glass series. All the $CaCl_2$ containing glasses are largely amorphous, while the minor mixed hydroxy-chlorapatite detected by XRD is thought to form by reacting with atmospheric water on the surface of samples during the course of acquiring the XRD pattern for the GPCl glass series. Incorporating chloride as opposed to fluoride would be expected to result in a reduced tendency to crystallisation, since the lattice energies of the equivalent crystalline phase (ClAP) is likely to be smaller than FAP [186] and a large chloride ion is less likely to order calcium cations around itself than a smaller fluoride ion. A consequence of this is that larger amounts of $CaCl_2$ (up to 31.6 mol%) than CaF_2 can be incorporated into the glasses without significant crystallisation occurring during quenching. An intermediate crystallisation tendency in between GPF and GPCl glass series was not seen for the mixed CaF_2 and $CaCl_2$ glass series. In reality, the GPFCl glass series show a slightly increased tendency to crystallise compared to the equivalent GPF glass series but a lower crystallinity. As mentioned previously, the presence of chloride expands the glass volume effectively and therefore to some extent facilitates the arrangement of calcium cations around a fluoride ion. As a consequence, a higher tendency of crystallisation was observed for GPFCl series than GPF series.

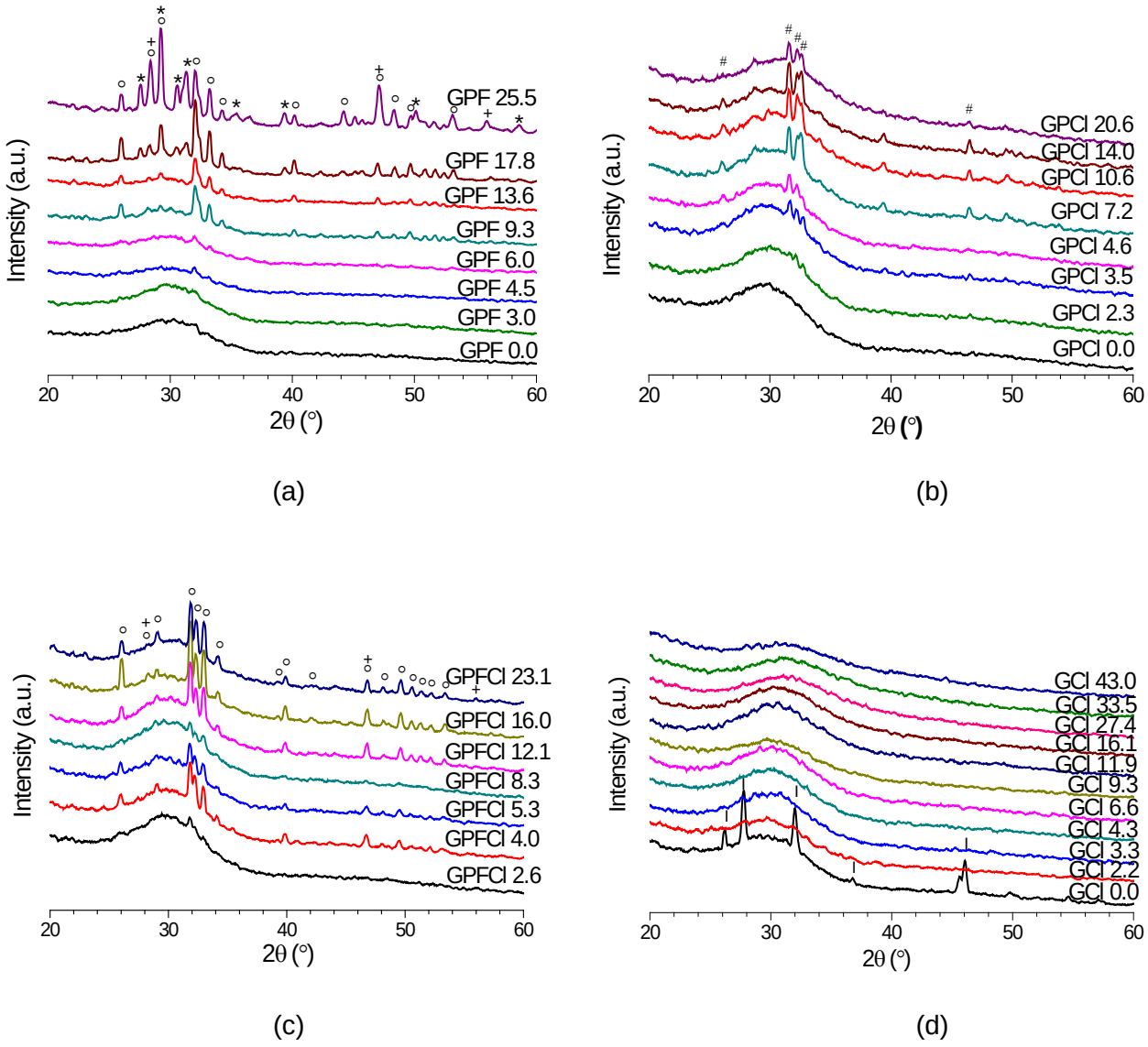

Figure 10.4.1 The XRD patterns of as-quenched (a) CaF_2 containing glasses; (b) $CaCl_2$ containing glasses; (c) mixed CaF_2 and $CaCl_2$ containing glasses; (d) P free $CaCl_2$ containing glasses (^{o}: $Ca_{10}(PO_4)_6F_2$; *: $Ca_4Si_2O_7F_2$; $^{+}$: CaF_2; $^{\#}$:$Ca_{10}(PO_4)_6(OH/Cl)_2$; ^{I}: β-$CaSiO_3$).

10.5 ^{31}P NMR Results of the As-Quenched Glasses

The ^{31}P MAS-NMR spectra of the as-quenched CaF_2 containing glasses, $CaCl_2$ containing glasses and mixed CaF_2 and $CaCl_2$ containing glasses suggest that phosphate is present as orthophosphate in the glasses. No evidence of Si-O-P bonds was found. The chemical shift of ^{31}P NMR spectra and the FWHM of ^{31}P MAS-NMR signal of those three glass series were estimated by using Bruker Top-Spin software

and is profiled as a function of CaX_2 (X=F/Cl/F+Cl) content in Figure 10.5.1 and Figure 10.5.2 respectively. Different glass series show different trends of the chemical shift. As a general observation, a constant chemical shift is shown in the GPF series, while a clear reduction of chemical shift is visible with incorporating $CaCl_2$ into the GPCl glass series. As explained in Chapter 6, this is likely to be a consequence of the shielding effect caused by the presence of high electron density chloride ion. In addition, a slight increase in chemical shift is seen with an increase in mixed CaF_2 and $CaCl_2$ content. It is probably arising due to the deshileding effect from the presence of both fluoride and chloride as discussed in detail in Chapter 7.

It is noteworthy that the FWHM of ^{31}P NMR MAS-NMR signals for the amorphous glasses are much larger than the equivalent crystallised glasses. The difference is particularly distinguishable in the GPF glass series. As we can see the amorphous glasses with CaF_2 content less than 9.3 mol% have FWHM values within the range of 1500-1700 Hz, while the FWHM for those crystallised glasses (CaF_2 content ≥ 9.3 mol%) reduce to the values below 950 Hz. Nevertheless, the difference of the FWHM for the amorphous glasses and the crystallised ones are less pronounced in the GPFCl glass series compared to the equivalent GPF series, as a consequence of a small fraction of crystallisation in the glasses with CaX_2 content higher than 2.4 mol% and the shielding effect by the high electron density chloride. Furthermore, the nearly identical FWHM are found for GPCl glass series, as these glasses are largely amorphous.

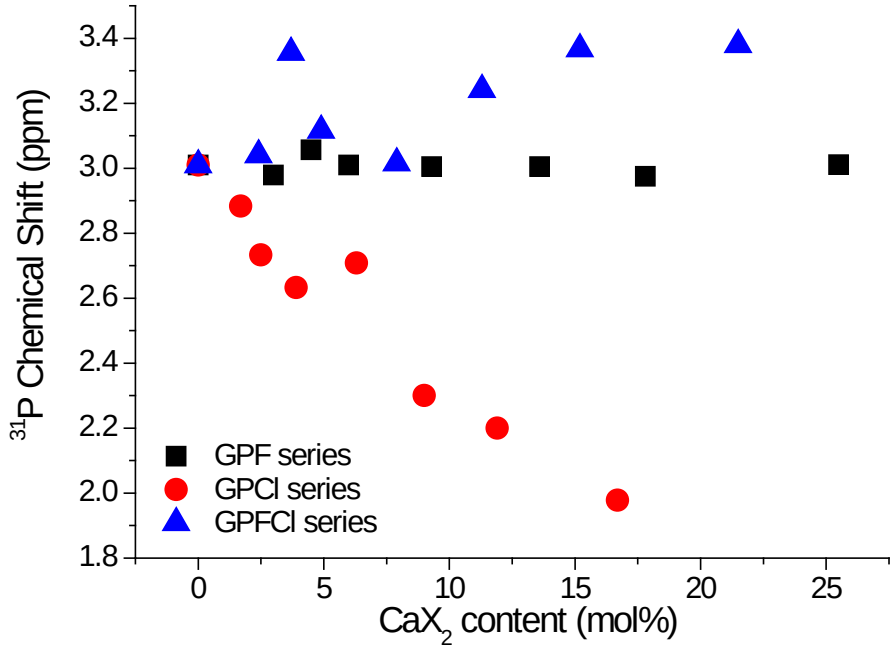

Figure 10.5.1 The chemical shift of ^{31}P MAS-NMR spectra against CaX_2 (X=F/Cl/F+Cl) content for all the calcium halide containing glasses.

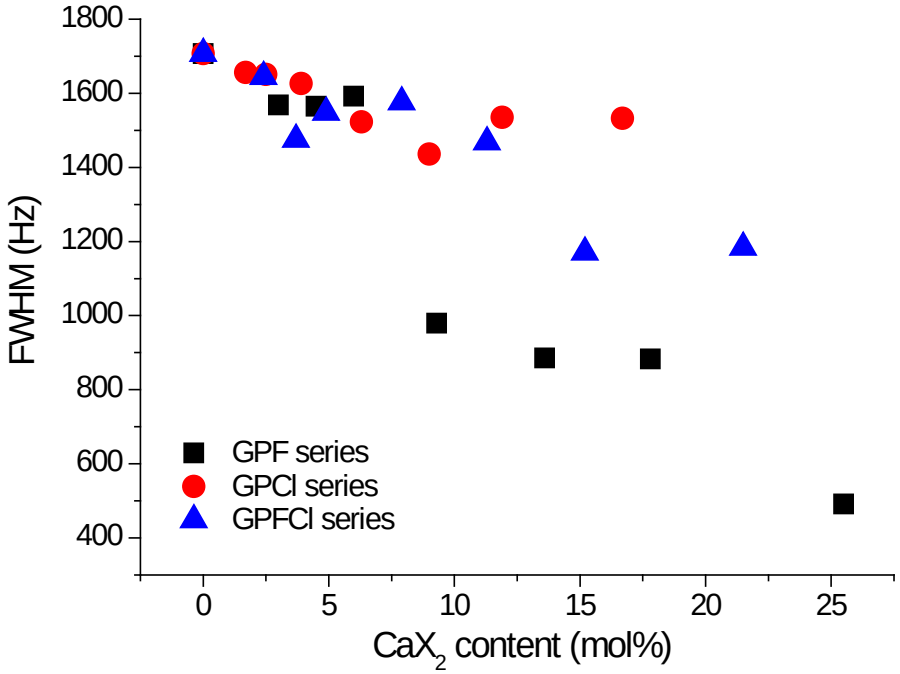

Figure 10.5.2 FWHM for ^{31}P MAS-NMR spectra plotted against CaX_2 (X=F/Cl/F+Cl) content for all the calcium halide containing glasses.

10.6 The Percentage of Calcium Release

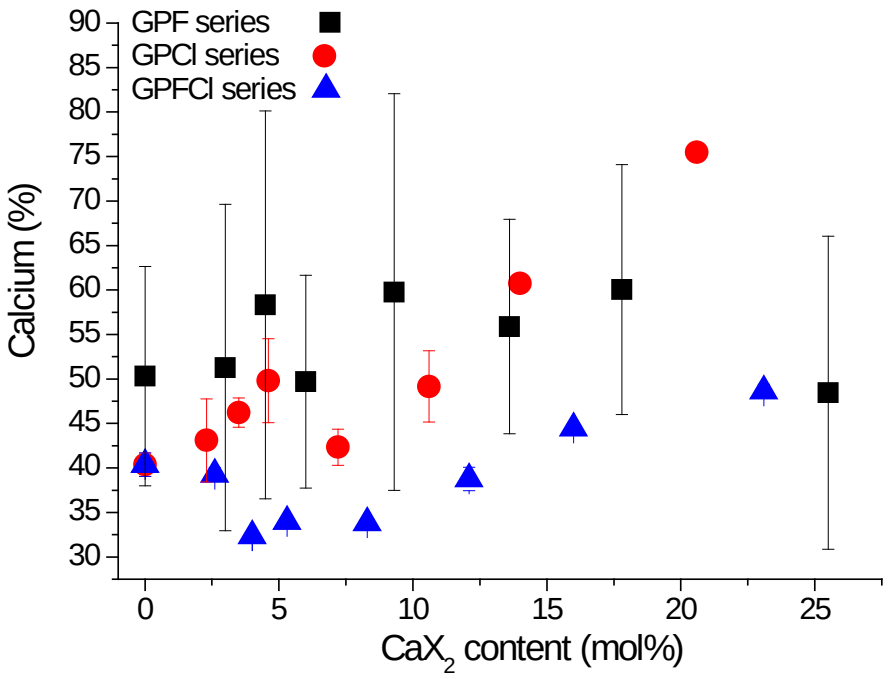

Figure 10.6.1 Ca concentration measured after 3 hours immersion in Tris buffer plotted as the percentage of the total calcium content in the original glass composition against the CaX_2 content for GPF, GPCl and GPFCl glass series.

Bioactive glasses degrade on immersion in buffer solution. The ion exchange between protons from buffer solution and Ca^{2+} ions from glasses leads to an increase of Ca^{2+} ion concentration in solution. Figure 10.6.1 shows the measured calcium concentration after 3 hours immersion in Tris buffer presented as a percentage of total amount of calcium in the nominal glass compositions for GPF, GPCl and GPFCl glass series. Large differences of the measured Ca^{2+} concentrations for the same composition were noticed for the GPF glass series. This is a consequence of the instrument calibration, which makes the data unreliable, although a relative small change of Ca% is seen through the whole GPF glass series. Consequently, only the data for GPCl and GPFCl glass series will be discussed below.

The main information delivered from Figure 10.6.1 is that the glass with a higher CaX_2 (X=Cl/F+Cl) content has a higher percentage of Ca released in buffer solution. This is

associated with a faster ion exchange between Ca^{2+} ions from glass and the protons from solution. As discussed in Chapter 6, the incorporation of chloride ion results in a dramatic expansion of glass molar volume and thereby effectively facilitates the diffusion of ions into and out of the glass. Note that the introduction of CaF_2 also expands glass molar volume (shown in Figure 10.3.2) but the effect is much smaller than $CaCl_2$. Therefore, the presence of chloride is the dominating factor controlling the rapid glass degradation and fast ion exchange.

10.7 The Measured pH after 3 and 24 Hours Immersion in Tris

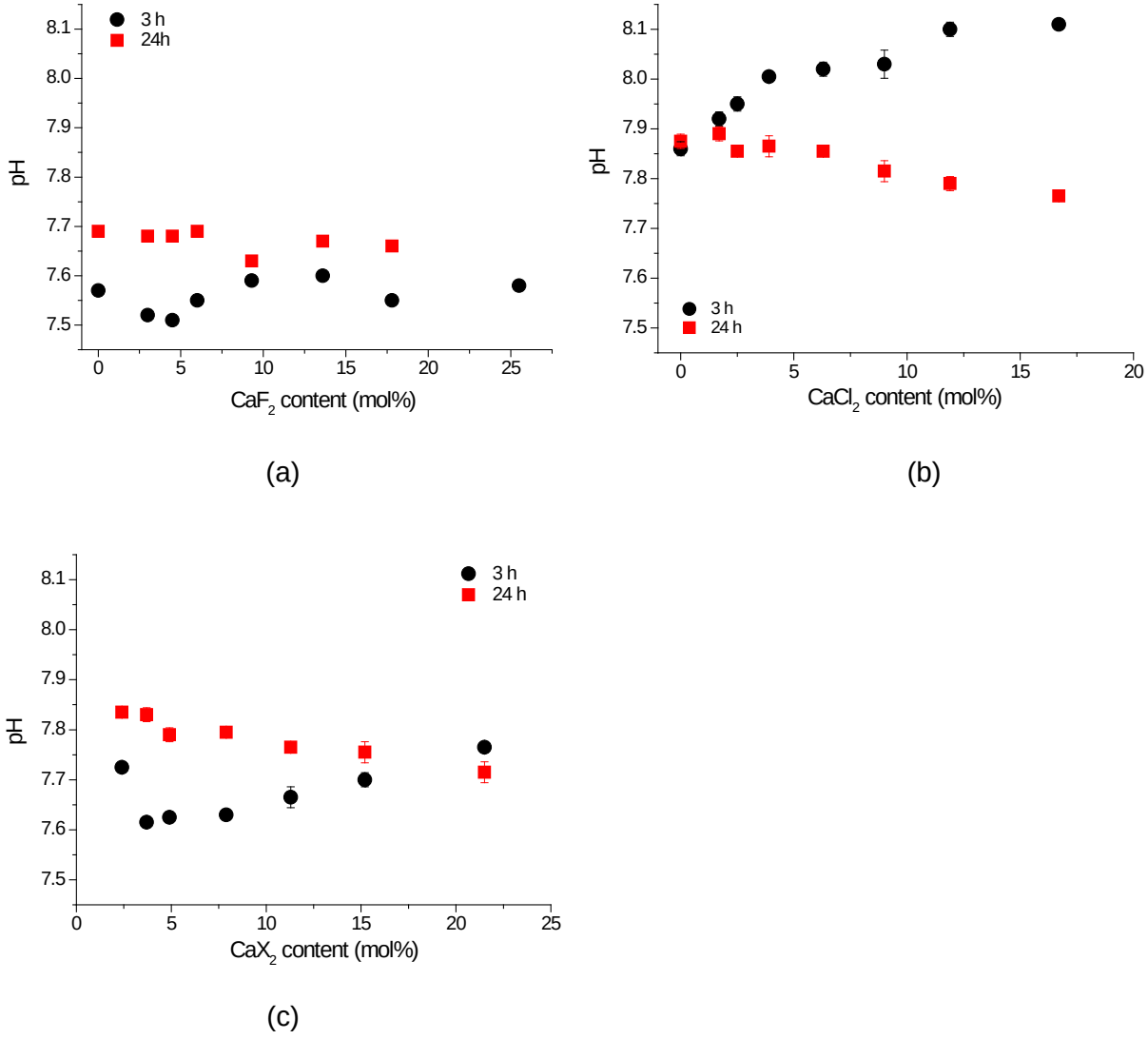

Figure 10.7.1 pH measured at the end of 3 and 24 hours immersion in Tris buffer plotted against CaX_2 (X=F/Cl/F+Cl) content (a) for GPF glass series, (b) for GPCl glass series and (c) GPFCl glass series .

Upon immersion, the degradation of glasses not only results in an increase in Ca^{2+} concentration, but also an increase in pH value, however, the apatite-like phase formation might result in a decrease in pH. The pH values measured at the end of 3 and 24 hours immersion in Tris buffer for the CaF_2 containing glasses are shown in Figure 10.7.1 (a). The equivalent results for $CaCl_2$ containing glasses and mixed CaF_2 and $CaCl_2$ containing glasses are shown in Figure 10.7.1 (b) and (c) respectively. Note that, the Tris buffer has an initial pH values within the range of 7.25-7.4, as a consequence of that the initial pH values for different glass series might vary slightly from batch to batch. However, for the same glass series even for different immersion time points the same batch of Tris buffer was used. Therefore, the direct comparison of pH values a cross a series is not precise but it is feasible for same glass series at different time points.

As shown in Figure 10.7.1 (a), (b) and (c), there are no clear trends of pH change with an increase in CaF_2 content after 3 or 24 hours for GPF glass series owing to the fact that high CaF_2 containing glasses (> 9.3 mol%) in GPF series are largely crystallised. Whilst an increase in pH after 3 hours and a decrease in pH after 24 hours with increasing CaX_2 content are found for both GPCl and GPFCl glass series. This less pronounced rise in pH of the GPCl and GPFCl glasses with more CaX_2 content after 24 hours is due to the decrease in non-bridging oxygen content with an increase in halide content in the one base sample (75 mg).

The studied glasses were designed by adding different amount of CaX_2 to the SiO_2-CaO-(P_2O_5) based glass, while reducing the amounts of all other components proportionally so in order to keep glass structure constant (predominantly Q^2 in structure). In a fixed weight of glass (75 mg) used for the bioactivity study in Tris buffer, the content of the silicate part of the glass (i.e. $Si\text{-}O^-$ $1/2Ca^{2+}$ bonds) allowing for exchange of modifier ions decreases with an increase in CaX_2 content in the glass. This could result in a reduction of the total amount of ion exchange occurring,

consequently, a less pronounced pH rise was observed for glasses with higher $CaCl_2$ contents after the completion of ion exchange.

Previous work on CaF_2 containing bioactive glasses by Brauer *et al.* [20]showed that the pH rise was less pronounced with increasing CaF_2 content in the glass, and this was originally interpreted as caused by another type of ion exchange occurring: hydroxyls (OH^-) from the solution exchanging for F^- from the glass in addition to H^+ for modifier cations. If this was the case, the same effect would be seen here, with an exchange of OH^- for Cl^- resulting in a lower pH with increasing $CaCl_2$ content in the glass, but in fact, the opposite trend was observed. This suggests that halides, such as CaF_2 or $CaCl_2$, presented in and released from bioactive glasses contribute only indirectly to pH changes in the dissolution medium. More detailed study [118] suggests that the pH rise typically observed for bioactive glasses is caused by the silicate part (i.e., by ion exchange between modifiers ionically connected to non-bridging oxygens and H^+) only, with contributions from the CaF_2 part being negligible.

Generally, the pH values measured by 24 hours are higher than the equivalent pH after 3 hours for both GPF and GPFCl glass series. However, the opposite trend is observed in GPCl glass series. This ascribes to the fact that fluorapatite is the predominant phase formed on immersion for the CaF_2 containing glasses (GPF and GPFCl glass series), while HAP is the dominating phase for the GPCl glass series. The consumption of OH^- group for HAP formation results in a reduction in pH.

Moreover, it is clear that the difference in pH by 3 and 24 hours is more distinct in a higher $CaCl_2$ containing glass (GPCl series), while it is less pronounced in a glass with higher mixed CaF_2 and $CaCl_2$ content (GPFCl series).

For GPCl glass series, if there is no consumption of OH^- for HAP formation, it would be expected to see a similar scenario of pH after 3 and 24 hours immersion as the equivalent ones for GPFCl glass series (Figure 10.7.1(c)). In reality, the OH^- ion is used to form HAP and the quantity of HAP formation relies upon the phosphate

content. Therefore, the glass with higher phosphate content forms more HAP and a more pronounced pH decrease is seen. Namely, the glass with lower $CaCl_2$ content has a more distinct reduction in pH. Thereby, a bigger difference in pH between 3 and 24 hours is found in the glass with a higher $CaCl_2$ content. In the case of GPFCl glass series, the increase in pH from 3 to 24 hours is more distinct in lower CaX_2 containing glasses. This can be also attributed to a slower ion exchange as a consequence of presenting less $CaCl_2$ and also the presence of a bigger content of the silicate part of the glass ($Si\text{-}O^-$ $1/2Ca^{2+}$ bonds).

10.8 Apatite-like Phase Formation in Tris Buffer Solution

The XRD patterns of the precipitates collected after 3 hours glass immersion in Tris for GPF, GPCl and GPFCl glass series are summarised in Figure 10.8.1 (a)-(c) for comparison purposes. The major diffraction lines developed after 3 hours immersion match with that of apatite for all the studied P containing glasses. However, additional diffraction lines corresponding to cuspidine and fluorite are also detected for the GPF glasses with CaF_2 content higher than 13.6 mol%. Due to the fact that the solubility of cuspidine and CaF_2 are much lower than the amorphous glass phase, for the glasses that initially crystallised to cuspidine and fluorite, on immersion those crystalline phases still existed while the amorphous glass phase largely dissolved. Furthermore, fluorite is also seen for the GPFCl 16.0 and GPFCl 23.1 glass compositions, which have 9.2 and 13.4 mol% CaF_2 respectively. It is interesting that less CaF_2 content was requested to see fluorite formation in the mixed CaX_2 series than the single CaF_2 containing series (9.2 VS 17.8 mol%). This could be contributed by the presence of chloride, which expands glass volume and facilitates the ordered arrangement of Ca^{2+} ions around fluoride ion.

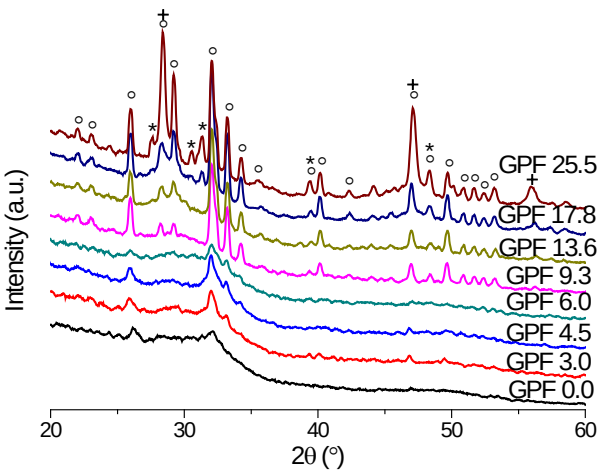

(a)

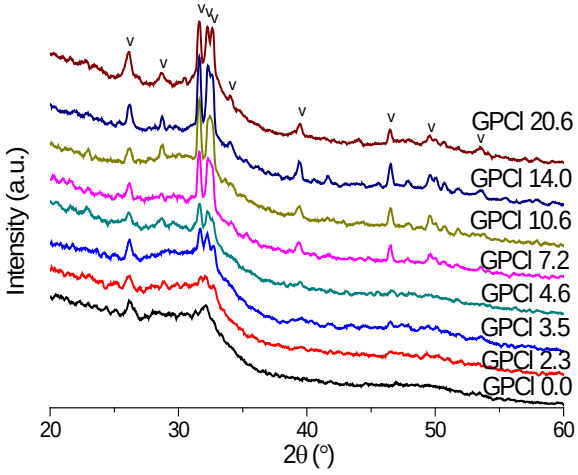

(b)

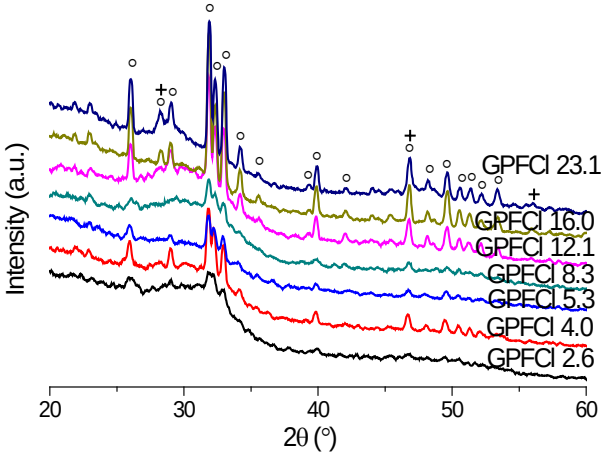

(c)

Figure 10.8.1 The XRD patterns of glass precipitates after 3 hours immerision in Tris for (a) CaF_2 containing glasses; (b) $CaCl_2$ containing glasses; (c) mixed CaF_2 and $CaCl_2$ containing glasses (^{o}: $Ca_{10}(PO_4)_6F_2$; *: $Ca_4Si_2O_7F_2$; $^{+}$: CaF_2; ^{v}:$Ca_{10}(PO_4)_6(OH)_2$).

It is interesting and worth comparing the apatite-like phase formation among the four series of glass. XRD, FTIR and NMR results consistently show rapid apatite-like phase formation within 3 hours immersion in Tris for all the high phosphate containing glasses (GPF, GPCl and GPFCl series). In the case of CaF_2 series, apart from forming apatite on immersion, additional fluoride containing phases were also detected in the high CaF_2 containing glasses (over 9.3 mol%). The formation of cuspidine and fluorite might reduce the bioactivity. In the case of $CaCl_2$ series, the apatite-like phase is the only phase formed on immersion. In addition, the increase of $CaCl_2$ content expands

glass volume and stimulates glass degradation, which therefore facilitates apatite-like phase formation. In the case of mixed CaF_2 and $CaCl_2$ containing glasses, apatite (mixed hydroxy-fluoapatite for GPFCl 2.6 and fluorapatite for GPFCl 4.0, GPFCl 5.3 and GPFGl 8.3) is the only phase formed for the glasses with CaX_2 content less than 12.1 mol%. CaF_2 appears when the CaX_2 content equal or above 12.1 mol% and the CaF_2 content increases with increasing CaX_2. ^{19}F MAS-NMR spectra (Figure 5.3.16 in Chapter 5 and Figure 7.3.7 in Chapter 7) reveal that clear FAP formation was found after 6 hours immersion for the amorphous glasses in GPF glass series (GPF 3.0, GPF 4.5 and GPF 6.0) but after 3 hours immersion for the amorphous glass (GPFCl 2.6) in GPFCl series. The observed faster FAP formation in GPFCl is thought to be caused by the presence of $CaCl_2$ that aids the glass degradation. In the case of P free $CaCl_2$ containing glasses (Figure 9.2.3), no apatite formation was detected after 3 days immersion in Tris, since both glasses and Tris buffer contain no source of phosphate. Thus, high phosphate content favours apatite-like phase formation, which is in a good agreement with the finding by Mneimne *et al.* [9] that high phosphate (> 6 mol% P_2O_5) glasses formed apatite within 6 hours, whilst the low phosphate glasses formed apatite in under 72 hours. In addition, O'Donnell *et al.* also demonstrated that higher P_2O_5 contents in the glass resulted in faster apatite formation and greater amounts of apatite being formed [50].

The formation of silica-gel is also considered important for bioactivity. Brauer *et al.* [20] suggested that the formation of silica-gel contributes to the nucleation of apatite, since phosphate concentration decreased when silicon concentration reached the solubility limit. However, as shown in Figure 6.2.5 in Chapter 6 and Figure 7.2.6 in Chapter 7, the silicon concentration reached the solubility limit (50-70 ppm) after 6 hours immersion for GPCl glass series and 9 hours for GPFCl glass series and were almost constant there afterwards, while phosphate decreased after 3 hours for GPCl glass series and 6 hours for GPFCl glass series. It seems that silica-gel forms after the

consumption of PO_4^{3-}, which suggests that apatite-like phases might not necessary to form on the surface of silica-gel.

11 Conclusions and Further Work

11.1 Conclusions

Bioactive silicate glasses based on SiO_2-P_2O_5-CaO-CaF_2/$CaCl_2$ and simple three component SiO_2-CaO-$CaCl_2$ glasses based on the wollastonite stoichiometry with increasing calcium halide contents have been successfully synthesised via a melt-quench route. To the best of our knowledge, the studied chloride glasses are the first chloride containing bioactive silicate glasses in the world.

The investigation of glass structure was carried out by MAS-NMR. The ^{19}F MAS-NMR spectra indicate the presence of F-Ca(n) species in fluoride containing glasses (GPF and GPFCl series), with no evidence of the presence of Si-F bonds. The ^{31}P MAS-NMR spectra suggest that phosphate is present as orthophosphate in the glasses rather than Si-O-P species. The ^{29}Si MAS-NMR spectra confirm that the studied glasses are predominantly Q^2 in structure.

Chemical analysis of the chloride content in the nominal glasses (in Chapters 6,7,9) reveals that the majority of chloride (up to 31.6 mol%) has been successfully retained in the Q^2 type silicate glasses. This contrasts with the glasses in the literature the highest of which contains less than 2 mol% $CaCl_2$.

The incorporation of CaX_2 leads to a significant decrease in the glass transition temperature by forming "CaX^+" species for all the studied glasses. However, the introduction of fluoride and chloride has different effects on glass density, which increases with increasing CaF_2 but decreases with $CaCl_2$. The mixed fluoride and chloride containing glass series have an intermediate density values. Moreover, the glass molar volume increases markedly with an increase in calcium halide content, suggesting that both fluoride and chloride expand the glass volume and dilute glass

network, therefore facilitate glass degradation. However, the expansion effect by fluoride is much smaller than the equivalent chloride as the fluoride ion is substantially smaller than the chloride ion.

The XRD, FTIR and NMR results consistently suggest that within the four series of glasses, the mixed fluoride and chloride containing glasses (GPFCl series) crystallised most readily, while the chloride containing glasses crystallise least readily (all the chloride containing bioactive glasses are largely amorphous) and the fluoride containing glasses have an intermediate crystallisation tendency. These are attributed to the fact that chloride ion is much bigger than fluoride ion (1.67 Å cf. 1.19 Å).

Glass degradation behaviour and apatite formation upon immersion were investigated in both Tris buffer and simulated body fluid. The study revealed that sodium-free, high phosphate containing glasses are highly degradable and formed an apatite-like phase (fluorapatite for GPF and GPFCl glass series and hydroxyapatite for GPCl glass series) within 3 hours immersion in Tris and 9 hours in SBF. Glass degradation rate increases with an increase in $CaCl_2$ content but not CaF_2. In the case of phosphate free $CaCl_2$ containing glasses, rapid glass degradation occurred within 3 days immersion but no apatite formation. Therefore, sodium is not an essential component in the bioactive glasses and high phosphate content favours apatite-like phase formation. The sodium-free, high phosphate calcium halide containing glasses are promising in dental and medical applications. Whilst, according to the known effects of CaF_2 and $CaCl_2$ on the glass bioactivity, the designable high phosphate chloride containing glasses with optimised fluoride content, which allow for rapid glass degradation, fast formation of a more durable FAP and providing a continuous release of F^- ion are particularly attractive for remineralising toothpastes.

Upon heat treatment, $CaCl_2$ is likely the crystallisation phase for the glasses without phosphate, indicating that in the chloride containing glasses the chlorine is likely to be present as a Cl-Ca(n) species in an analogous fashion to F-Ca(n) in fluoride containing

glasses. However, the halogen-free phosphate containing glass surface crystallised to pseudowollastonite and a hydroxyapatite. On incorporating a halide, the glasses exhibited largely bulk crystallization to a haloapatite. In the case of fluoride and mixed fluoride and chloride, the glasses primarily crystallised to fluorapatite. In the case of chloride, the glasses crystallised to chlorapatite. This is the first time that chlorapatite has been shown to crystallise from a glass. The obtained ClAP glass-ceramics are the first ClAP glass-ceramics ever.

11.2 Further work

- The structural role of chloride in the glasses should be further explored by ^{35}Cl MAS-NMR to obtain a direct evidence of forming Cl-Ca(n) species and address the arrangement of halide phase in the glass. A systematic molecular dynamics simulation study would be beneficial to achieve a better understanding of the glass structure, as ^{35}Cl NMR is quite difficult.
- Amorphous scattering on P free $CaCl_2$ containing glasses will be helpful for understanding the glass structure and interpreting the break in linear T_g, density, V_m and T_{c1} behaviours with increasing $CaCl_2$ content.
- ^{29}Si-enriched MAS-NMR on the as-quenched and heat treated P free $CaCl_2$ containing glasses should be carried out, in order to study the Q structure of the glasses and identify the crystallisation phase after heat treatment.
- The dissolution study of phosphate containing bioactive glasses (GPF, GPCl and GPFCl series) within a short time immersion period (< 1h) should be carried out, in order to determine the mechanism of glass degradation, transformation into apatite without releasing PO_4^{3-}?
- The comparison of bioactivity between the as-quenched glasses and the formed glass-ceramics upon heat treatment should be carried out, in order to establish a better understanding on how the crystalline phase affect glass

bioactivity. ^{1}H NMR should be carried out to determine the conversion of ClAP to HAP with the presence of water.

- In regard to chlorapatite glass-ceramics, the influence of heat treatment time and temperature on the crystal phases formed, microstructure, fracture toughness and strength should be investigated.
- The cytotoxicity study of the investigated bioactive glasses.

12 Reference

[1] Hench LL. The story of Bioglass (R). Journal of Materials Science-Materials in Medicine 2006;17:967-78.
[2] Hench LL, Paschall HA. Direct chemical bond of bioactive glass-ceramic materials to bone and muscle. Journal of biomedical materials research 1973;7:25-42.
[3] Jones JR. Review of bioactive glass: From Hench to hybrids. Acta Biomater 2013;9:4457-86.
[4] Brauer DS, Karpukhina N, Law RV, Hill RG. Structure of fluoride-containing bioactive glasses. Journal of Materials Chemistry 2009;19:5629-36.
[5] Pedone A, Charpentier T, Menziani MC. The structure of fluoride-containing bioactive glasses: new insights from first-principles calculations and solid state NMR spectroscopy. Journal of Materials Chemistry 2012;22:12599-608.
[6] Farooq I, Tylkowski M, Muller S, Janicki T, Brauer DS, Hill RG. Influence of sodium content on the properties of bioactive glasses for use in air abrasion. Biomedical materials (Bristol, England) 2013;8:065008.
[7] Brauer DS, Karpukhina N, Seah D, Law RV, Hill RG. Fluoride-containing bioactive glasses. In: Liska M, Galusek D, Klement R, Petruskova V, editors. Glass - the Challenge for the 21st Century2008. p. 299-304.
[8] Elliott JC. Monoclinic Space Group of Hydroxyapatite. Nature-Physical Science 1971;230:72.
[9] Mneimne M, Hill RG, Bushby AJ, Brauer DS. High phosphate content significantly increases apatite formation of fluoride-containing bioactive glasses. Acta Biomater 2011;7:1827-34.
[10] Lockyer MWG, Holland D, Dupree R. NMR Investigation of the structure of some bioactive and related glasses. Journal of Non-Crystalline Solids 1995;188:207-19.
[11] Hench LL, Jones JR, Sepulveda P. Bioactive Materials for Tissue Engineering Scaffolds. 2002.
[12] Liu X, Rahaman MN, Day DE. Conversion of melt-derived microfibrous borate (13-93B3) and silicate (45S5) bioactive glass in a simulated body fluid. Journal of Materials Science-Materials in Medicine 2013;24:583-95.
[13] Rahaman MN, Day DE, Bal BS, Fu Q, Jung SB, Bonewald LF, et al. Bioactive glass in tissue engineering. Acta biomaterialia 2011;7:2355-73.
[14] Gorustovich AA, Roether JA, Boccaccini AR. Effect of Bioactive Glasses on Angiogenesis: A Review of In Vitro and In Vivo Evidences. Tissue Engineering Part B-Reviews 2010;16:199-207.
[15] Fredholm YC, Karpukhina N, Law RV, Hill RG. Strontium containing bioactive glasses: Glass structure and physical properties. Journal of Non-Crystalline Solids 2010;356:2546-51.
[16] Gentleman E, Fredholm YC, Jell G, Lotfibakhshaiesh N, O'Donnell MD, Hill RG, et al. The effects of strontium-substituted bioactive glasses on osteoblasts and osteoclasts in vitro. Biomaterials 2010;31:3949-56.
[17] Lusvardi G, Malavasi G, Menabue L, Menziani MC. Synthesis, characterization, and molecular dynamics simulation of Na2O-CaO-SiO2-ZnO glasses. Journal of Physical Chemistry B 2002;106:9753-60.

[18] Aina V, Malavasi G, Pla AF, Munaron L, Morterra C. Zinc-containing bioactive glasses: Surface reactivity and behaviour towards endothelial cells. Acta Biomaterialia 2009;5:1211-22.
[19] Azevedo MM, Jell G, O'Donnell MD, Law RV, Hill RG, Stevens MM. Synthesis and characterization of hypoxia-mimicking bioactive glasses for skeletal regeneration. Journal of Materials Chemistry 2010;20:8854-64.
[20] Brauer DS, Karpukhina N, O'Donnell MD, Law RV, Hill RG. Fluoride-containing bioactive glasses: effect of glass design and structure on degradation, pH and apatite formation in simulated body fluid. Acta Biomater 2010;6:3275-82.
[21] Lusvardi G, Malavasi G, Cortada M, Menabue L, Menziani MC, Pedone A, et al. Elucidation of the structural role of fluorine in potentially bioactive glasses by experimental and computational investigation. Journal of Physical Chemistry B 2008;112:12730-9.
[22] Watts SJ, Hill RG, O'Donnell MD, Law RV. Influence of magnesia on the structure and properties of bioactive glasses. Journal of Non-Crystalline Solids 2010;356:517-24.
[23] De Aza PN, De Aza AH, Pena P, De Aza S. Bioactive glasses and glass-ceramics. Boletin De La Sociedad Espanola De Ceramica Y Vidrio 2007;46:45-55.
[24] Varila L, Lehtonen T, Tuominen J, Hupa M, Hupa L. In vitro behaviour of three biocompatible glasses in composite implants. Journal of Materials Science-Materials in Medicine 2012;23:2425-35.
[25] Goel A, Kapoor S, Rajagopal RR, Pascual MJ, Kim HW, Ferreira JM. Alkali-free bioactive glasses for bone tissue engineering: a preliminary investigation. Acta Biomater 2012;8:361-72.
[26] Vogel M, Voigt C, Gross UM, Muller-Mai CM. In vivo comparison of bioactive glass particles in rabbits. Biomaterials 2001;22:357-62.
[27] O'Donnell MD. Predicting bioactive glass properties from the molecular chemical composition: Glass transition temperature. Acta Biomaterialia 2011;7:2264-9.
[28] ASTM. Committee [Subcommittee 1, Committee C–14] Offers Definition of Glass. Glass Ind 1941;22:216.
[29] McMillan PW. "Glass Ceramic " second edition. New York: Academic Press 1979.
[30] Doremus RH. Glass science: Wiley; 1973.
[31] Shelby JE. "Introduction to Glass Science and Technology": The Royal Society of Chemistry; 2005.
[32] McMillan PW. "Glass Ceramic" Academic press; 1964.
[33] Turnbull D. Under what conditions can a glass be formed? Contemp Phys 1969;10:473.
[34] Angell CA. Perspective on the glass transition 1988.
[35] Moynihan C. The Glass Transition and the Nature of the Glassy State1976.
[36] Ediger MDA, C. A.; Nagel, Sidney R. . "Supercooled Liquids and Glasses". The Journal of Physical Chemistry 1996; 100.
[37] Holloway DG. The physical properties of glass: Wykeham publications LTD; 1973.
[38] Clare AG. The Unique Nature of Glass. Bio-Glasses: John Wiley & Sons, Ltd; 2012. p. 1-12.
[39] Zarzycki J. Glasses and the Vitreous State. Cambridge, New York, Port Chester, Melbourne, Sydney: Cambridge University Press; 1991.

[40] Jones GO. Glass. London: Methuen, Wiley; 1956.
[41] O'Donnell MD. Predicting bioactive glass properties from the molecular chemical composition: Glass transition temperature. Acta Biomaterialia 2011;7:2264-9.
[42] Hill RG, Brauer DS. Predicting the glass transition temperature of bioactive glasses from their molecular chemical composition. Acta Biomater 2011;7:3601-5.
[43] Hill R. An alternative view of the degradation of bioglass. J Mater Sci Lett 1996;15:1122-5.
[44] Hill RG, Brauer DS. Predicting the bioactivity of glasses using the network connectivity or split network models. Journal of Non-Crystalline Solids 2011;357:3884-7.
[45] O'Donnell MD, Hill RG. Influence of strontium and the importance of glass chemistry and structure when designing bioactive glasses for bone regeneration. Acta biomaterialia 2010;6:2382-5.
[46] Kokubo T, Kim HM, Kawashita M. Novel bioactive materials with different mechanical properties. Biomaterials 2003;24:2161-75.
[47] Hench LL, West J. Biological applications of bioactive glasses. Life Chemistry Reports 1996;13:187-241.
[48] Kallace K. Design of Bioactive Glass Compositions: University of Limerick; 2000.
[49] Edén M. The split network analysis for exploring composition-structure correlations in multi-component glasses: I. Rationalizing bioactivity-composition trends of bioglasses. Journal of Non-Crystalline Solids 2011;357:1595-602.
[50] O'Donnell MD, Watts SJ, Hill RG, Law RV. The effect of phosphate content on the bioactivity of soda-lime-phosphosilicate glasses. Journal of materials science Materials in medicine 2009;20:1611-8.
[51] Hill R. MAT420, Individual Project, Telsol Presentation. London: Queen Mary University of London; 2009.
[52] Hench LL. Bioceramics-from concept to clinic. Journal of the American Ceramic Society 1991;74:1487-510.
[53] Bingel L, Groh D, Karpukhina N, Brauer DS. Influence of dissolution medium pH on ion release and apatite formation of Bioglass® 45S5. Materials Letters 2015;143:279-82.
[54] Kokubo T, Takadama H. How useful is SBF in predicting in vivo bone bioactivity? Biomaterials 2006;27:9.
[55] Bohner M, Lemaitre J. Can bioactivity be tested in vitro with SBF solution? Biomaterials 2009;30:2175-9.
[56] Cerruti M, Greenspan D, Powers K. Effect of pH and ionic strength on the reactivity of Bioglass((R)) 45S5. Biomaterials 2005;26:1665-74.
[57] Al-Noaman A, Rawlinson SCF, Hill RG. The role of MgO on thermal properties, structure and bioactivity of bioactive glass coating for dental implants. Journal of Non-Crystalline Solids 2012;358:3019-27.
[58] Clark A, Hench LL, Paschall H. The influence of surface chemistry on implant interface histology: a theoretical basis for implant materials selection. 1976;10:161-74.
[59] Kokubo T, Takadama H. How useful is SBF in predicting in vivo bone bioactivity? Biomaterials 2006;27:2907-15.
[60] Hill RG. MAT420. Individual Project, Telsil Presentation London, Queen Mary University of London 2009.

[61] Sepulveda P, Jones JR, Hench LL. In vitro dissolution of melt-derived 45S5 and sol-gel derived 58S bioactive glasses. Journal of biomedical materials research 2002;61:301-11.
[62] Hench L, L,. Bioceramic. Journal of the American Ceramic Society 1998;81:1705-28.
[63] Ahsan MR, Uddin MA, Mortuza MG. Infrared study of the effect of P2O5 in the structure of lead silicate glasses. Indian J Pure Appl Phys 2005;43:89-99.
[64] Mysen BO, Ryerson FJ, Virgo D. The structural role of phosphorus in silicate melts. American Mineralogist 1981;66:106-17.
[65] O'Donnell MD, Watts SJ, Law RV, Hill RG. Effect of P_2O_5 content in two series of soda lime phosphosilicate glasses on structure and properties - Part I: NMR. Journal of Non-Crystalline Solids 2008;354:3554-60.
[66] Elgayar I, Aliev AE, Boccaccini AR, Hill RG. Structural analysis of bioactive glasses. Journal of Non-Crystalline Solids 2005;351:173-83.
[67] Tilocca A, Cormack AN. Structural effects of phosphorus inclusion in bioactive silicate glasses. Journal of Physical Chemistry B 2007;111:14256-64.
[68] De Aza PN, Guitian F, De Aza S. Bioactivity of Wollastonite ceramics-in vitro evaluation. Scripta Metallurgica Et Materialia 1994;31:1001-5.
[69] Ohura K, Nakamura T, Yamamuro T, Ebisawa Y, Kokubo T, Kotoura Y, et al. Bioactivity of CaO.SiO2 Glasses added with various ions. Journal of Materials Science-Materials in Medicine 1992;3:95-100.
[70] Palmer C, Wolfe SH. Position of the American Dietetic Association: The impact of fluoride on health. Journal of the American Dietetic Association 2005;105:1620-8.
[71] M. Grynpas, D. Chachra, limeback H. The action of fluoride on bone 2000.
[72] Grynpas MD, Rey C. The effect of fluoride treatment on bone-mineral crystals in the rat. Bone 1992;13:423-9.
[73] Aoba T. The effect of fluoride on apatite structure and growth. Critical Reviews in Oral Biology & Medicine 1997;8:136-53.
[74] Mousny M, Omelon S, Wise L, Everett ET, Dumitriu M, Holmyard DP, et al. Fluoride effects on bone formation and mineralization are influenced by genetics. Bone 2008;43:1067-74.
[75] Jin XQ, Xu H, Shi HY, Zhang JM, Zhang HQ. Fluoride-induced oxidative stress of osteoblasts and protective effects of baicalein against fluoride toxicity. Biological Trace Element Research 2007;116:81-9.
[76] Hayashi M, Nabeshima N, Fukuyama H, Nagata K. Effect of fluorine on silicate network for CaO-CaF2-SiO2 and CaO-CaF2-SiO2-FeOx glasses. Isij International 2002;42:352-8.
[77] Stebbins JF, Zeng Q. Cation ordering at fluoride sites in silicate glasses: a high-resolution F-19 NMR study. Journal of Non-Crystalline Solids 2000;262:1-5.
[78] Rabinovich EM. On the structural role of fluorine in silicate-glasses. Physics and Chemistry of Glasses 1983;24:54-6.
[79] Hill RG, Da Costa N, Law RV. Characterization of a mould flux glass. Journal of Non-Crystalline Solids 2005;351:69-74.
[80] Cocchi M, Durante C, Lusvardi G, Malavasi G, Menabue L. Evaluation of the behaviour of fluorine-containing bioactive glasses: reactivity in a simulated body fluid solution assisted by multivariate data analysis. Journal of Materials Science-Materials in Medicine 2012;23:639-48.

[81] Christie JK, Pedone A, Menziani MC, Tilocca A. Fluorine Environment in Bioactive Glasses: ab Initio Molecular Dynamics Simulations. The Journal of Physical Chemistry B 2011;115:2038-45.
[82] Hill R, Wood D, Thomas M. Trimethylsilylation analysis of the silicate structure of fluoro-alumino-silicate glasses and the structural role of fluorine. Journal of Materials Science 1999;34:1767-74.
[83] Lusvardi G, Malavasi G, Menabue L, Aina V, Morterra C. Fluoride-containing bioactive glasses: Surface reactivity in simulated body fluids solutions. Acta Biomaterialia 2009;5:3548-62.
[84] Sandland TO, Du L-S, Stebbins JF, Webster JD. Structure of Cl-containing silicate and aluminosilicate glasses: A 35Cl MAS-NMR study. Geochimica et Cosmochimica Acta 2004;68:5059-69.
[85] Stebbins JF, Du LS. Chloride ion sites in silicate and aluminosilicate glasses: A preliminary study by Cl-35 solid-state NMR. American Mineralogist 2002;87:359-63.
[86] Baasner A, Hung I, Kemp TF, Dupree R, Schmidt BC, Webb SL. Constraints on the incorporation mechanism of chlorine in peralkaline and peraluminous Na2O-CaO-Al2O3-SiO2glasses. American Mineralogist 2014;99:1713-23.
[87] Kiprianov AA, Karpukhina NG. Oxyhalide silicate glasses. Glass Phys Chem 2006;32:1-27.
[88] Poulsen S, Errobe M, Lescay MY, Glenny AM. Potassium containing toothpastes for dentine hypersensitivity. Cochrane Database Syst Rev 2006.
[89] Gupta AK, Sharma N, Bramta M. Dentin tubular occlusion with bioactive glass containing dentrifice gluma desensitizer - a comparative SEM Evaluation. Dental Journal of Advance Studies 2014:16-21.
[90] Lynch E, Brauer DS, Karpukhina N, Gillam DG, Hill RG. Multi-component bioactive glasses of varying fluoride content for treating dentin hypersensitivity. Dental Materials 2012;28:168-78.
[91] Gillam RHaDG. Dentine Hypersensitivity: Springer International Publishing; 2015.
[92] Jones JR, Lin S, Yue S, Lee PD, Hanna JV, Smith ME, et al. Bioactive glass scaffolds for bone regeneration and their hierarchical characterisation. Proceedings of the Institution of Mechanical Engineers Part H-Journal of Engineering in Medicine 2010;224:1373-87.
[93] Shah FA, Brauer DS, Desai N, Hill RG, Hing KA. Fluoride-containing bioactive glasses and Bioglass (R) 45S5 form apatite in low pH cell culture medium. Materials Letters 2014;119:96-9.
[94] Gentleman E, Stevens MM, Hill RG, Brauer DS. Surface properties and ion release from fluoride-containing bioactive glasses promote osteoblast differentiation and mineralization in vitro. Acta Biomaterialia 2013;9:5771-9.
[95] Elliott JC, Young RA. Conversion of Single Crystals of Chlorapatite into Single Crystals of Hydroxyapatite. Nature 1967;214:904-6.
[96] Banerjee A, Watson TF. Air abrasion: its uses and abuses. Dental update 2002;29:340-6.
[97] Banerjee A, Thompson ID, Watson TF. Minimally invasive caries removal using bio-active glass air-abrasion. Journal of dentistry 2011;39:2-7.
[98] Banerjee A, Hajatdoost-Sani M, Farrell S, Thompson I. A clinical evaluation and comparison of bioactive glass and sodium bicarbonate air-polishing powders. Journal of dentistry 2010;38:475-9.

[99] Metcalfe BL, Donald IW. Candidate wasteforms for the immobilization of chloride-containing radioactive waste. Journal of Non-Crystalline Solids 2004;348:225-9.
[100] Jantzen CM. First Principles Process-product Models for Vitrification of Nuclear Waste: Relationship of Glass Composition to Glass Viscosity, Resistivity, Liquidus Temperature, and Durability. 1992.
[101] Vance ER, Davis J, Olufson K, Chironi I, Karatchevtseva I, Farnan I. Candidate waste forms for immobilisation of waste chloride salt from pyroprocessing of spent nuclear fuel. Journal of Nuclear Materials 2012;420:396-404.
[102] Elliott JC. Structure and Chemistry of the Apatites and Other Calcium Orthophosphates. Second ed: Elsevier; 2003.
[103] Suchanek W. Processing and properties of hydroxyapatite-based biomaterials for use as hard tissue replacement implants. Journal of materials research 1998;13:94-117.
[104] Vallet-Regí M, González-Calbet JM. Calcium phosphates as substitution of bone tissues. Progress in Solid State Chemistry 2004;32:1-31.
[105] Kuo MC, Yen SK. The process of electrochemical deposited hydroxyapatite coatings on biomedical titanium at room temperature. Materials Science and Engineering: C 2002;20:153-60.
[106] Elliott JC, Mackie PE, Young RA. Monoclinic Hydroxyapatite. Science 1973;180:1055-7.
[107] Kreidler ER, Davis TS, Parodi JA. Luminescence of antimony in calcium halophosphates. Bulletin of the American Physical Society 1971;16:408.
[108] O'Donnell MD, Hill RG, Fong SK. Neutron diffraction of chlorine substituted fluorapatite. Materials Letters 2009;63:1347-9.
[109] Mackie PE, Young RA, Elliott JC. Monoclinic structure of synthetic Ca5(PO4)3Cl, Chlorapatite. Acta Crystallographica Section B-Structural Crystallography and Crystal Chemistry 1972;B 28:1840.
[110] Elliott J, Wilson R, Dowker S. Apatite Structures. International Centre for Diffraction Data , Advances in X-ray Analysis, 2002;46.
[111] Hill RG, Law RV, O'Donnell MD, Hawes J, Bubb NL, Wood DJ, et al. Characterisation of fluorine containing glasses and glass-ceramics by F-19 magic angle spinning nuclear magnetic resonance spectroscopy. Journal of the European Ceramic Society 2009;29:2185-91.
[112] Alia A, Ganapathy S, de Groot HJM. Magic angle spinning (MAS) NMR: a new tool to study the spatial and electronic structure of photosynthetic complexes. Photosynthesis Research 2009;102:415-25.
[113] Stamboulis A, Hill RG, Law RV. Structural characterization of fluorine containing glasses by F-19 Al-27 Si-29 and P-31 MAS-NMR spectroscopy. Journal of Non-Crystalline Solids 2005;351:3289-95.
[114] Brauer DS, Al-Noaman A, Hill RG, Doweidar H. Density-structure correlations in fluoride-containing bioactive glasses. Mater Chem Phys 2011;130:121-5.
[115] Moreno EC, Kresak M, Zahradni.Rt. Fluoridated hydroxyapatite solubility and caries formation. Nature 1974;247:64-5.
[116] Featherstone JDB. The science and practice of caries prevention The Journal of the American Dental Association 2000;131:887-99.
[117] Nanci A. Ten Cate's Oral Histology-Pageburst on VitalSource: Development, Structure, and Function: Elsevier Health Sciences; 2007.

[118] Brauer DS, Mneimne M, Hill RG. Fluoride-containing bioactive glasses: Fluoride loss during melting and ion release in tris buffer solution. Journal of Non-Crystalline Solids 2011;357:3328-33.
[119] LeGeros RZ, Trautz OR, Klein E, LeGeros JP. Two types of carbonate substitution in the apatite structure. Experientia 1969;25:5-7.
[120] Kim CY, Clark AE, Hench LL. Compositional dependence of calcium phosphate layer formation in fluoride Bioglasses. Journal of biomedical materials research 1992;26:1147-61.
[121] Hayashi M, Nabeshima N, Fukuyama H, Nagata K. Effect of Fluorine on Silicate Network for CaO-CaF2-SiO2and CaO-CaF2-SiO2-FeOx Glasses. ISIJ International 2002;42:352-8.
[122] Jager C, Welzel T, Meyer-Zaika W, Epple M. A solid-state NMR investigation of the structure of nanocrystalline hydroxyapatite. Magnetic resonance in chemistry : MRC 2006;44:573-80.
[123] Brauer DS, Al-Noaman A, Hill RG, Doweidar H. Density–structure correlations in fluoride-containing bioactive glasses. Materials Chemistry and Physics 2011;130:121-5.
[124] Chen QZ, Thompson ID, Boccaccini AR. 45S5 Bioglass®-derived glass–ceramic scaffolds for bone tissue engineering. Biomaterials 2006;27:2414-25.
[125] Jalota S, Bhaduri SB, Tas AC. Effect of carbonate content and buffer type on calcium phosphate formation in SBF solutions. Journal of Materials Science-Materials in Medicine 2006;17:697-707.
[126] Varila L, Fagerlund S, Lehtonen T, Tuominen J, Hupa L. Surface reactions of bioactive glasses in buffered solutions. Journal of the European Ceramic Society 2012;32:2757-63.
[127] Jabbarifar SE, Salavati S, Akhavan A, Khosravi K, Tavakoli N, Nilchian F. Effect of fluoridated dentifrices on surface microhardness of the enamel of deciduous teeth. Dent Res J (Isfahan) 2011;8:113-7.
[128] G M. Serum Chloride. In: Walker HK, Hall WD, Hurst JW, editors. Clinical Methods: The History, Physical, and Laboratory Examinations 3rd edition. Boston: Butterworths; 1990.
[129] Guidelines for drinking-water quality. Health criteria and other supporting information. 2nd ed. Genava: World Health Organization; 1996.
[130] Karim BFA, Gillam DG. The Efficacy of Strontium and Potassium Toothpastes in Treating Dentine Hypersensitivity: A Systematic Review. International Journal of Dentistry 2013;2013:13.
[131] Sandland TO, Du LS, Stebbins F, Webster JD. Structure of Cl-containing silicate and aluminosilicate glasses: A Cl-35 MAS-NMR study. Geochim Cosmochim Acta 2004;68:5059-69.
[132] Fagerlund S, Hupa L, Hupa M. Comparison of Reactions of Bioactive Glasses in Different Aqueous Solutions. Advances in Bioceramics and Biotechnologies: John Wiley & Sons, Inc.; 2010. p. 101-13.
[133] Penel G, Leroy G, Rey C, Sombret B, Huvenne JP, Bres E. Infrared and Raman microspectrometry study of fluor-fluor-hydroxy and hydroxy-apatite powders. Journal of Materials Science-Materials in Medicine 1997;8:271-6.
[134] O'Donnell MD, Hill RG, Law RV, Fong S. Raman spectroscopy, 19F and 31P MAS-NMR of a series of fluorochloroapatites. Journal of the European Ceramic Society 2009;29:377-84.
[135] Yi H, Balan E, Gervais C, Segalen L, Fayon F, Roche D, et al. A carbonate-fluoride defect model for carbonate-rich fluorapatite. American Mineralogist 2013;98:1066-9.

[136] Mason HE, McCubbin FM, Smirnov A, Phillips BL. Solid-state NMR and IR spectroscopic investigation of the role of structural water and F in carbonate-rich fluorapatite. American Mineralogist 2009;94:507-16.
[137] Arends J, Nelson, D.G.A, Dijkman, A.G, Jongebloed, W.L. Effects of various fluorides on enamel structure and chemistry. Cariology Today 1984:245-58.
[138] Kreinbrink AT, Sazavsky CD, Pyrz JW, Nelson DGA, Honkonen RS. Fast-magic-angle-spinning 19F NMR of inorganic fluorides and fluoridated apatitic surfaces. Journal of Magnetic Resonance (1969) 1990;88:267-76.
[139] White DJ, Nelson DGA, Faller RV. Mode of action of fluoride: application of new techniques and test methods to the examination of the mechanism of action of topical fluoride. Advances in dental research 1994;8:166-74.
[140] Gerhardt L-C, Boccaccini AR. Bioactive Glass and Glass-Ceramic Scaffolds for Bone Tissue Engineering. Materials 2010;3:3867-910.
[141] Gough JE, Boccaccini AR. Tissue Engineering Using Ceramics and Polymers 2007.
[142] Höland W. Glass-Ceramics. Bio-Glasses: John Wiley & Sons, Ltd; 2012. p. 97-105.
[143] Rawlings RD, Wu JP, Boccaccini AR. Glass-ceramics: Their production from wastes-a review. Journal of Materials Science 2006;41:733-61.
[144] Kokubo T. Bioactive glass ceramics: properties and applications. Biomaterials 1991;12:155-63.
[145] Calver A, Hill RG, Stamboulis A. Influence of fluorine content on the crystallization behavior of apatite-wollastonite glass-ceramics. Journal of Materials Science 2004;39:2601-3.
[146] Freeman CO, Brook IM, Johnson A, Hatton PV, Hill RG, Stanton KT. Crystallization modifies osteoconductivity in an apatite–mullite glass–ceramic. J Mater Sci: Mater Med 2003;14:985-90.
[147] Kokubo TS, Masazumi; Nagashima,, Yukihito; Tashiro MN, Takashi; Yamamuro,, Takao; Higashi S. Apatite- and Wollastonite-Containg Glass-Ceramics for Prosthetic Application. 1982;90.
[148] Rafferty A, Clifford A, Hill R, Wood D, Samuneva B, Dimitrova-Lukacs M. Influence of Fluorine Content in Apatite–Mullite Glass-Ceramics. Journal of the American Ceramic Society 2000;83:2833-8.
[149] Goodridge RD, Wood DJ, Ohtsuki C, Dalgarno KW. Biological evaluation of an apatite–mullite glass-ceramic produced via selective laser sintering. Acta Biomaterialia 2007;3:221-31.
[150] Brauer DS, Anjum MN, Mneimne M, Wilson RM, Doweidar H, Hill RG. Fluoride-containing bioactive glass-ceramics. Journal of Non-Crystalline Solids 2012;358:1438-42.
[151] Freeman CO, Brook IM, Johnson A, Hill RG, Hatton PV. Osseointegration of novel ionomeric glass-ceramics. Journal of Dental Research 2000;79:1184-.
[152] Holand W, Rheinberger V, Wegner S, Frank M. Needle-like apatite-leucite glass-ceramic as a base material for the veneering of metal restorations in dentistry. Journal of Materials Science-Materials in Medicine 2000;11:11-7.
[153] Chan JCC, Ohnsorge R, Meise-Gresch K, Eckert H, Höland W, Rheinberger V. Apatite Crystallization in an Aluminosilicate Glass Matrix: Mechanistic Studies by X-ray Powder Diffraction, Thermal Analysis, and Multinuclear Solid-State NMR Spectroscopy. Chemistry of Materials 2001;13:4198-206.

[154] Beall GH. Design and properties of glass-ceramics. Annual review of materials science 1992;22:91-119.
[155] Henry J, Hill RG. The influence of lithia content on the properties of fluorphlogopite glass-ceramics. I. Nucleation and crystallisation behaviour. Journal of Non-Crystalline Solids 2003;319:1-12.
[156] García-Tuñón E, Franco J, Dacuna B, Zaragoza G, Guitian F. Chlorapatite Conversion to Hydroxyapatite under High Temperature Hydrothermal Conditions. Materials science forum 2010:9-14.
[157] Garcia-Tunon E, Franco J, Eslava S, Bhakhri V, Saiz E, Giuliani F, et al. Synthesis and Optimization of the Production of Millimeter-Sized Hydroxyapatite Single Crystals by Cl--OH- Ion Exchange. Journal of the American Ceramic Society 2013;96:759-65.
[158] Mackie PE, Young RA. Fluorine-chlorine interaction in fluor-chlorapatite. Journal of Solid State Chemistry 1974;11:319-29.
[159] O'Donnell MD, Fredholm Y, de Rouffignac A, Hill RG. Structural analysis of a series of strontium-substituted apatites. Acta Biomater 2008;4:1455-64.
[160] Hill RG, Stamboulis A, Law RV, Clifford A, Towler MR, Crowley C. The influence of strontium substitution in fluorapatite glasses and glass-ceramics. Journal of Non-Crystalline Solids 2004;336:223-9.
[161] Paluszkiewicz C, Blażewicz M, Podporska J, Gumuła T. Nucleation of hydroxyapatite layer on wollastonite material surface: FTIR studies. Vibrational Spectroscopy 2008;48:263-8.
[162] Mihailova B, Konstantinov L, Dinolova E. Cluster-approximation modelling of infrared and Raman spectra of crystalline and vitreous CaSiO3. Journal of non-crystalline solids 1995;191:79-84.
[163] Bhatnagar VM. IR-spectra of fluorapatite and fluorchlorapatite. Experientia 1967;23:10-2.
[164] Watanabe.T, Hayashi.M, Hayashi.S, Fukuyama.H, Nagata.K a. Solid-state 19F NMR on CaO-SiO2-CaF2 glasses. VII International Conference on Molten Slags Fluxes and Salts2004.
[165] Stanton KT, Hill RG. Crystallisation in apatite-mullite glass-ceramics as a function of fluorine content. Journal of Crystal Growth 2005;275:E2061-E8.
[166] Garcia-Tunon E, Couceiro R, Franco J, Saiz E, Guitian F. Synthesis and characterisation of large chlorapatite single-crystals with controlled morphology and surface roughness. Journal of Materials Science-Materials in Medicine 2012;23:2471-82.
[167] Ebisawa Y, Kokubo T, Ohura K, Yamamuro T. Bioactivity of CaO·SiO2-based glasses:in vitro evaluation. J Mater Sci: Mater Med 1990;1:239-44.
[168] Ohura K, Nakamura T, Yamamuro T, Ebisawa Y, Kokubo T, Kotoura Y, et al. Bioactivity of CaO·SiO2 glasses added with various ions. J Mater Sci: Mater Med 1992;3:95-100.
[169] Hench LL, Spilman DB, Hench JW. Fluoride-containing Bioglass™ compositions. Google Patents; 1988.
[170] Hill RG, Stamboulis A, Law RV. Characterisation of fluorine containing glasses by 19F, 27Al, 29Si and 31P MAS-NMR spectroscopy. Journal of dentistry 2006;34:525-32.
[171] Christie JK, Pedone A, Menziani MC, Tilocca A. Fluorine Environment in Bioactive Glasses: ab Initio Molecular Dynamics Simulations. Journal of Physical Chemistry B 2011;115:2038-45.
[172] Nida Mahmud, Xiaojing Chen, Natalia Kapukhina, Hill R. Phosphate free, sodium-free, fluorine containing bioactive glasses. 2014.

[173] Srivastava AK, Pyare R. Characterization of ZnO Substituted 45S5 Bioactive glasses and glass-ceramics. Journal of Materials Science Research 2012;1:p207.
[174] Serra J, Gonzalez P, Liste S, Chiussi S, Leon B, Perez-Amor M, et al. Influence of the non-bridging oxygen groups on the bioactivity of silicate glasses. Journal of Materials Science-Materials in Medicine 2002;13:1221-5.
[175] Essien ER, Adams LA, Shaibu RO, Olasupo IA, Oki A. Economic route to sodium-containing silicate bioactive glass scaffold. Open Journal of Regenerative Medicine 2012;01:33-40.
[176] Peitl O, Dutra Zanotto E, Hench LL. Highly bioactive P2O5–Na2O–CaO–SiO2 glass-ceramics. Journal of Non-Crystalline Solids 2001;292:115-26.
[177] Atalay S, Adiguzel HI, Atalay F. Infrared absorption study of Fe2O3-CaO-SiO2 glass ceramics. Materials Science and Engineering a-Structural Materials Properties Microstructure and Processing 2001;304:796-9.
[178] Lin K, Chang J, Liu Z, Zeng Y, Shen R. Fabrication and characterization of 45S5 bioglass reinforced macroporous calcium silicate bioceramics. Journal of the European Ceramic Society 2009;29:2937-43.
[179] Ducheyne P, Radin S, King L. The effect of calcium-phosphate ceramic composition and structure on in vitro behavior. 1. dissolution. Journal of biomedical materials research 1993;27:25-34.
[180] Pedone A. MD-derived structures of Cl-containing bioactive glasses (Cl and O ions modelled as core-shell: Clc – Cls / Oc - Os). 2015.
[181] Isard JO. The mixed alkali effect in glass. Journal of Non-Crystalline Solids 1969;1:235-61.
[182] Tylkowski M, Brauer DS. Mixed alkali effects in Bioglass® 45S5. Journal of Non-Crystalline Solids 2013;376:175-81.
[183] Elgayar I. The influence of alkali metal content and network connectivity on bioactive glasses Imperial College London (University of London) 2004.
[184] Doweidar H. Density–structure correlations in Na2O–CaO–P2O5–SiO2 bioactive glasses. Journal of Non-Crystalline Solids 2009;355:577-80.
[185] Smedskjaer MM, Jensen M, Yue Y. Effect of thermal history and chemical composition on hardness of silicate glasses. J Non-Cryst Solids 2010;356:893-7.
[186] Cruz FJAL, Canongia Lopes JN, Calado JCG, Minas da Piedade ME. A Molecular Dynamics Study of the Thermodynamic Properties of Calcium Apatites. 1. Hexagonal Phases. The Journal of Physical Chemistry B 2005;109:24473-9.

13 Appendix I - Supplementary Results

Table 11.2.1 Particle size analysis results for GPF glass series

Glass Code	Volume Median Diameter (SD, µm)			Span
	D [v, 0.5]	D [v, 0.1]	D [v, 0.9]	
GPF 0.0	5.95 (0.07)	0.73 (0.01)	30.74 (0.17)	5.04 (0.08)
GPF 3.0	6.61 (0.09)	0.71 (0.02)	30.89 (0.12)	4.57 (0.08)
GPF 4.5	6.76 (0.07)	0.75 (0.01)	34.57 (0.07)	5.00 (0.06)
GPF 6.0	6.43 (0.29)	0.74 (0.03)	30.10 (0.46)	4.57 (0.15)
GPF 9.3	9.11 (0.08)	0.97 (0.03)	31.98 (0.07)	3.41 (0.03)
GPF 13.6	8.66 (0.11)	0.96 (0.04)	34.68 (0.1)	3.89 (0.06)
GPF 17.8	9.46 (0.1)	1.07 (0.1)	37.92 (0.67)	3.89 (0.04)
GPF 25.5	8.40 (0.09)	0.94 (0.01)	33.49 (0.18)	3.87 (0.03)

Table 11.2.2 P values obtained from Student's t-test to estimate the statistically significant difference between groups for the FWHM of ^{31}P MAS-NMR spectra; P<0.05 is considered as significant, p<0.0001 is considered to be extremely significant.

GPF 4.5 in Tris	0 h	3 h	6 h	9 h
0 h	-	P<0.0001	P<0.0001	P<0.0001
3 h	P<0.0001	-	P<0.0001	P<0.0001
6 h	P<0.0001	P<0.0001	-	P=0.0001
9 h	P<0.0001	P<0.0001	P=0.0001	-
GPF 4.5 in SBF	0 h	3 h	6 h	9 h
0 h	-	P<0.0001	P<0.0001	P<0.0001
3 h	P<0.0001	-	P=0.0010	P<0.0001
6 h	P<0.0001	P=0.0010	-	P<0.0001
9 h	P<0.0001	P<0.0001	P<0.0001	-
GPF 13.6 in Tris	0 h	3 h	6 h	9 h
0 h	-	P<0.0001	P<0.0001	P<0.0001
3 h	P<0.0001	-	P<0.0001	P<0.0001
6 h	P<0.0001	P<0.0001	-	P<0.0001
9 h	P<0.0001	P<0.0001	P<0.0001	-
GPF 13.6 in SBF	0 h	3 h	6 h	9 h
0 h	-	P<0.0001	P<0.0001	P<0.0001
3 h	P<0.0001	-	P<0.0001	P<0.0001

6 h	P<0.0001	P<0.0001	-	P=0.1361
9 h	P<0.0001	P<0.0001	P=0.1361	-

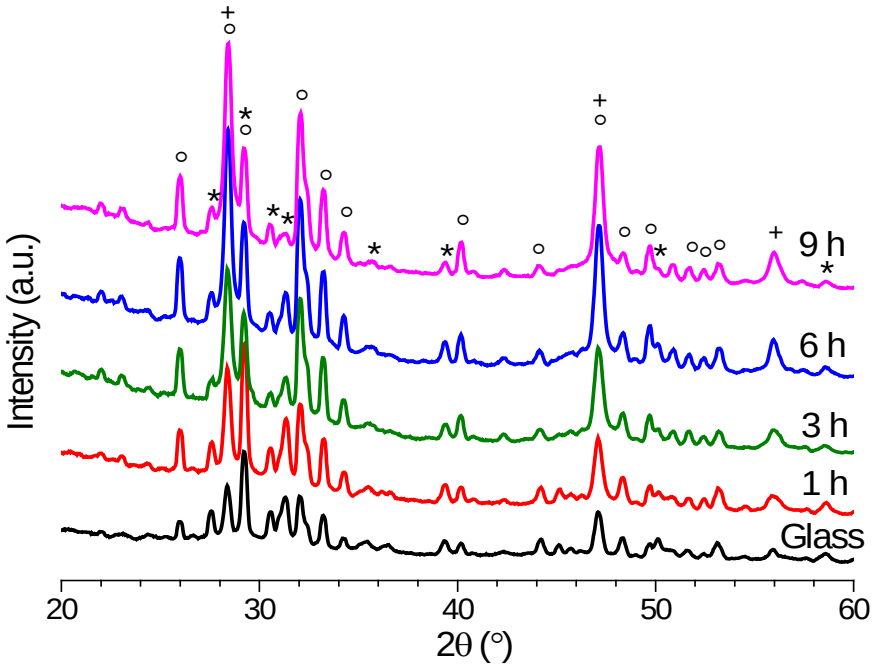

Figure 11.2.1 The XRD patterns of the glass precipitates with 25.5 mol% CaF_2 collected after immersion in Tris up to 1 week (°: $Ca_{10}(PO_4)_6F_2$; *: $Ca_4Si_2O_7F_2$; +: CaF_2).

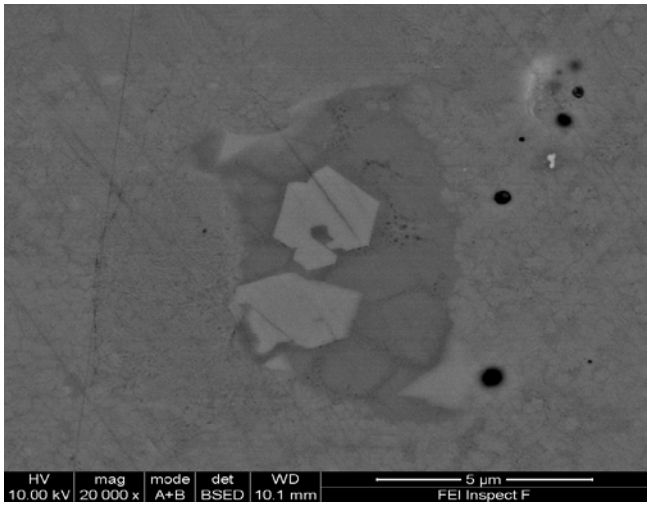

Figure 11.2.2 SEM images of the heat treated samples of GF 0.0 at 1030°C

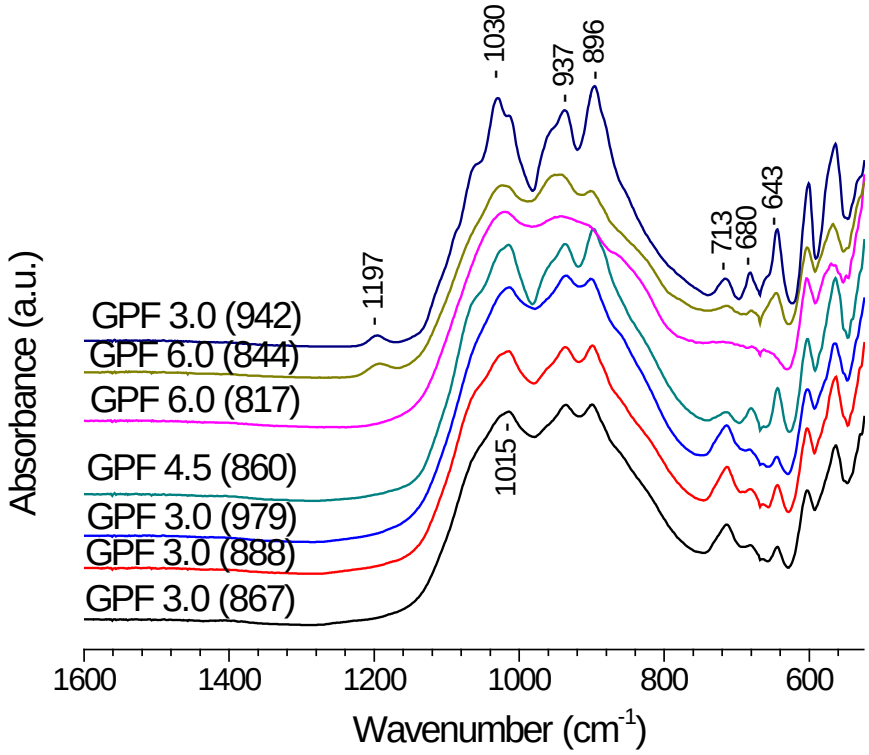

Figure 11.2.3 The FTIR Spectra of the heat treated with low CaF_2 content (≤ 6.0 mol%) in GPF series. The numbers in the bracket represent the heat treatment temperature

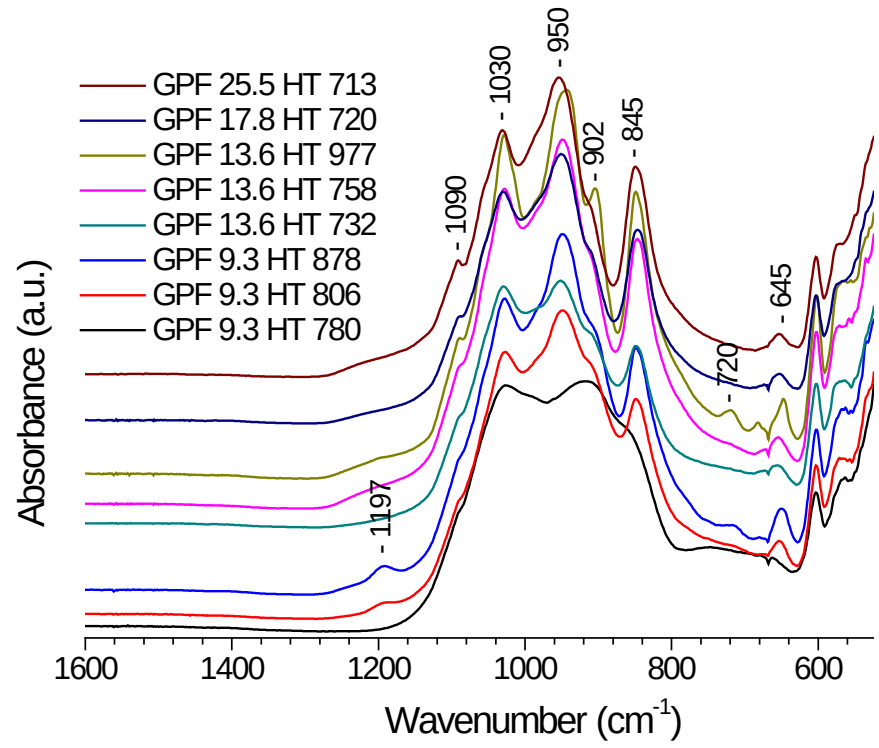

Figure 11.2.4 The FTIR Spectra of the heat treated with high CaF_2 content (≥ 9.3 mol%) in GPF series.

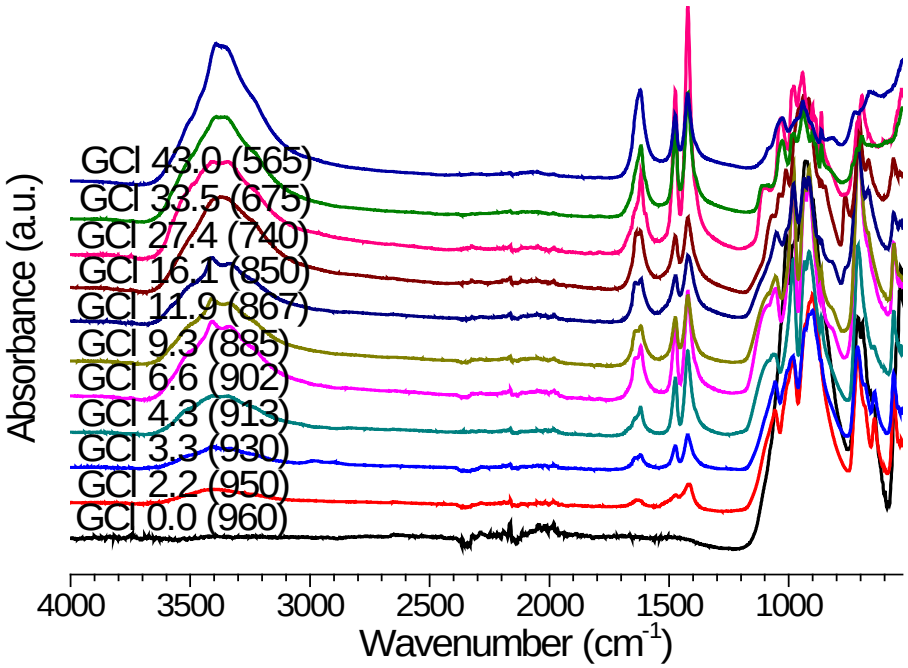

Figure 11.2.5 The FTIR Spectra of the heat treated GCl glass series. The numbers in the bracket represent the heat treatment temperature.

Table 11.2.3 The experimental density and the calculated density of GPFCl glass series. D_e represents the experimental density and Dc represents the calculated density

Glass Code	D_e	D_c
GPFCl 2.6	2.9166	2.9337
GPFCl 4.0	2.9252	2.9341
GPFCl 5.3	2.9287	2.9341
GPFCl 8.3	2.9129	2.9336
GPFCl 12.1	2.9251	2.9360
GPFCl 16.0	2.913	2.9352
GPFCl 23.1	2.9006	2.9395

14 Appendix II - Academic Achievements

Based on this PhD project, a world patent has been filed. Some of the results from this PhD work have been published in four peer-review papers and presented in different conferences and competitions.

14.1 World Patent

'Chlorine-containing Silicate Glasses and Glass Ceramics'. WO2014154874 A3

14.2 Peer-Reviewed Publications

1. X.J.Chen, N.Karpukhina and R.Hill, Chlorapatite Glass-Ceramics, International Journal of Applied Glass Science, 2014, 5: 207-16.
2. X.J.Chen, X.H.Chen, D.S.Brauer, R.M. Wilson, R.Hill and N.Karpukhina, Novel Alkali Free Bioactive Fluorapatite Glass-Ceramics, Journal of Non Crystalline Solid, 2014, 402: 172-7.
3. X.J.Chen, X.H.Chen, D.S.Brauer, R.M. Wilson, R.Hill and N.Karpukhina, Bioactivity Investigation of Sodium Free Fluoride Containing Glasses and Glass-ceramics, Materials, 2014, 7: 5470-87.
4. X.J.Chen, D.S.Brauer, N.Karpukhina and R.Hill, Novel Highly Degradable Chloride Containing Bioactive Glasses, Biomedical Glasses, 2015, 1:108-118.

14.3 Conference Presentations

Oral Presentations:

1. Glass can dissolve like sugar - Do you believe? X.J. Chen, 2015 Young Persons' Lecture Competition, February 2015, London, UK. (**The Runner up of the South East Heat of the 2015 Young Person's Lecture Competition)**
2. The Influence of Fluoride Content on the Crystallisation of Sodium Free Fluorapatite Glass-Ceramics, X.J.Chen, N.Karpukhina, D.Brauer and R.Hill, 5th International Congress on Ceramics, August 2014, Beijing, China.
3. Novel Halide Containing Bio-glasses for Dental Applications, X.J. Chen, The competition on British Federation of Women Graduates Academic Awards, July 2014, London, UK. (**British Federation of Women Graduates (BFWG) Academic Awards - The Margaret KB Day Scholarship)**
4. Mixed Fluoride-Chloride Containing Bioactive Glasses for Remineralising Toothpaste, X.J.Chen, N.Karpukhina and R.Hill, International Association for Dental Research General Sessions and Exhibitions, June 2014, Cape Town, South Africa.
5. Mixed Fluoride and Chloride Bioactive Glasses for Dental Applications, X.J.Chen, N.Karpukhina and R.Hill, PhD Day, April 2014, Barts and the London School of Medicine and Dentistry, London. (**Best Verbal Presentation Prize)**
6. Novel Halide Containing Bioactive Glasses for Dental Application, X.J.Chen, N.Karpukhina, and R.Hill, British Society for Oral and Dental Research 2013, September 2013, Bath, UK. **(Commendation VOCO Prize for Dental Biomaterials Prize)**
7. The Comparison between Novel Fluoride and Chloride Bioactive Glasses, X.J.Chen, N.Karpukhina, and R.Hill, The 'Living glass' Conference – Society of Glass Technology, September 2013, Cambridge, UK.
8. Crystallization of Chlorapatite from Chloride Containing Bioactive Glasses, X.J.Chen, N.Karpukhina, R.M.Wilson and R.Hill, 23rd International Congress on Glass, July 2013, Prague, Czech Republic.
9. Sodium-free Fluoride-Containing Bioactive Glasses, X.J.Chen, N.Karpukhina, X.H.Chen, D.S.Brauer and R.Hill, XIII International Conference on the Physics of Non-Crystalline Solids, September 2012, Wuhan, China.

Poster Presentations

1. Novel Highly Degradable Chloride Containing Bioactive Glasses, X.J.Chen, N.Karpukhina, R.M.Wilson and R.Hill, 12th International Conference on Structure of Non-Crystalline Materials, July 2013, Trento, Italy. **(Best Poster Award)**
2. Alkali-free Oxyhalide Silicate Bioactive Glasses and Bioceramics, X.J.Chen, N.Karpukhina, and R.Hill, PhD Day, March 2013, Barts and the London School of Medicine and Dentistry, London. **(Best Poster Award)**
3. Novel Bioactive Glasses for Drill Free Dentistry, X.J.Chen, N.Karpukhina, and R.Hill, William Harvey Day, October 2012, Barts and the London School of Medicine and Dentistry, London.

***A*bstract published for an oral presentation in the "2015 Young Persons' Lecture Competition", London, UK, February 2015**

14.3.1 Glass Can Dissolve Like Sugar - Do You Believe?

Xiaojing Chen

Dental Physical Sciences, Institute of Dentistry, Barts and The London School of Medicine and Dentistry, Queen Mary University of London, London, United Kingdom

Fluoride can prevent dental cavities and thus has been incorporated into bioactive glasses (BG) as mineralizing additives for toothpaste. Unlike un-dissolvable window glasses, fluoride containing BG dissolve rapidly in the mouth and form an acid resistant mineral on the tooth surface to reduce sensitivity.

Many People suffer from sensitive teeth, which is caused by the exposure of small tubes in the tooth as a result of receding gums, tooth decay and enamel loss, when taking hot or cold beverages or food into mouth.

There are regulatory issues with fluoride. Chlorine however behaves like fluorine in BG but results in chloride release. Chloride is naturally present in the body. In this talk we will discuss the first chloride-containing BG in the world. These can dissolve as fast as sugar and form acid resistant mineral very rapidly. They are attractive for toothpaste applications.


LMS
IPLC 2nd Prize
HAOTING CHEN
TH February 20

***A*bstract published for an oral presentation in the "The Competition on British Federation of Woman Graduates Academic Awards", London, UK, July 2014**

14.3.2 Novel Halide Containing Bio-glasses for Dental Applications

Xiaojing Chen

Dental Physical Sciences, Institute of Dentistry, Barts and The London School of Medicine and Dentistry, Queen Mary University of London, London, United Kingdom

Many People (8-35% of the adult population) experience sharp tooth pain when taking hot or cold beverages or food into mouth. This type of tooth pain is caused by the exposure of small tubes in the tooth (tubules) to the air as a result of receding gums, tooth decay and enamel loss.

Fluoride can prevent dental cavities as it inhibits enamel and dentine loss. It has been incorporated into bioactive glasses as remineralising additives for toothpaste. These glasses dissolve in the mouth and form an acid resistant tooth mineral on the tooth surface to reduce sensitivity. In addition, the small mineral particles can block the tubules, hence alleviate tooth pain.

However, fluoride is classified as a drug and excess fluoride might result in dental fluorosis, which appears as unnoticeable, tiny white streaks or specks in the enamel of the tooth. It is important to find an alternative for the excess of fluoride. Chloride is likely to behave like fluorine but no potential problem as fluoride. Salt (sodium chloride) has been taken every day and also presents naturally in the body. Chloride containing bioactive glasses can also dissolve fast and form minerals rapidly. Therefore they are attractive remineralising additive for toothpastes to treat tooth pain.

This awards the

British Federation of Women Graduates

2014 Margaret K B Day Scholarship

to

Xiaojing Chen

for her research on

Novel halide containing bio-glasses for dental applications

Gloria Bonner

President BFWG

BFWG Scholarships Committee

***A*bstract published for an oral presentation in the "British Society for Oral and Dental Research 2013", Bath, UK, September 2013**

14.3.3 Novel Halide Containing Bioactive Glasses for Dental Application

Xiaojing Chen*, Natalia Karpukhina, Robert Hill

Dental Physical Sciences, Institute of Dentistry, Barts and The London School of Medicine and Dentistry, Queen Mary University of London, London, United Kingdom

Objectives: Fluoride has often been incorporated into many glasses used in dentistry, for example, glass ionomer cements, apatite based glass-ceramics and more recently fluoride containing bioactive glasses. However, chloride containing glasses have rarely been investigated. The objective of this project is to investigate incorporation of chloride into sodium free bioactive glasses.

Methods: Sodium free glasses with varying amounts of fluoride and chloride were synthesised by a melt-quench route and characterised using X-ray Diffraction (XRD), Differential Scanning Calorimetry (DSC) and Fourier Transform Infrared Spectroscopy (FTIR). Glass powders were heat treated for the crystallisation study. Glass bioactivity was investigated by the immersion of glass powders in Tris buffer solution. The apatite formation was evaluated by XRD, FTIR and Magic Angle Spinning Nuclear Magnetic Resonance (MAS-NMR). The ion release and glass degradation were quantified by Inductively Coupled Plasma-Optical Emission Spectrometer (ICP-OES).

Results: The results show that glasses with high fluoride (>9.3 mol%) content are partially crystallised into fluorapatite, however, CaF_2 was found in 25.5 mol% CaF_2 containing glass. Similarly, partial crystallisation of chlorapatite has been observed in the chloride containing glasses. Both glass series showed high bioactivity, the glasses degraded primarily within the first hour of immersion in Tris buffer and formed apatite within 3 hours. Fluorapatite and chlorapatite formed in the heat treated glasses.

Conclusion: The presence of CaF_2 / $CaCl_2$ in sodium free bioactive glasses is beneficial for the fluorapatite/ chlorapatite formation. These highly bioactive halide glasses can be used for dental applications.

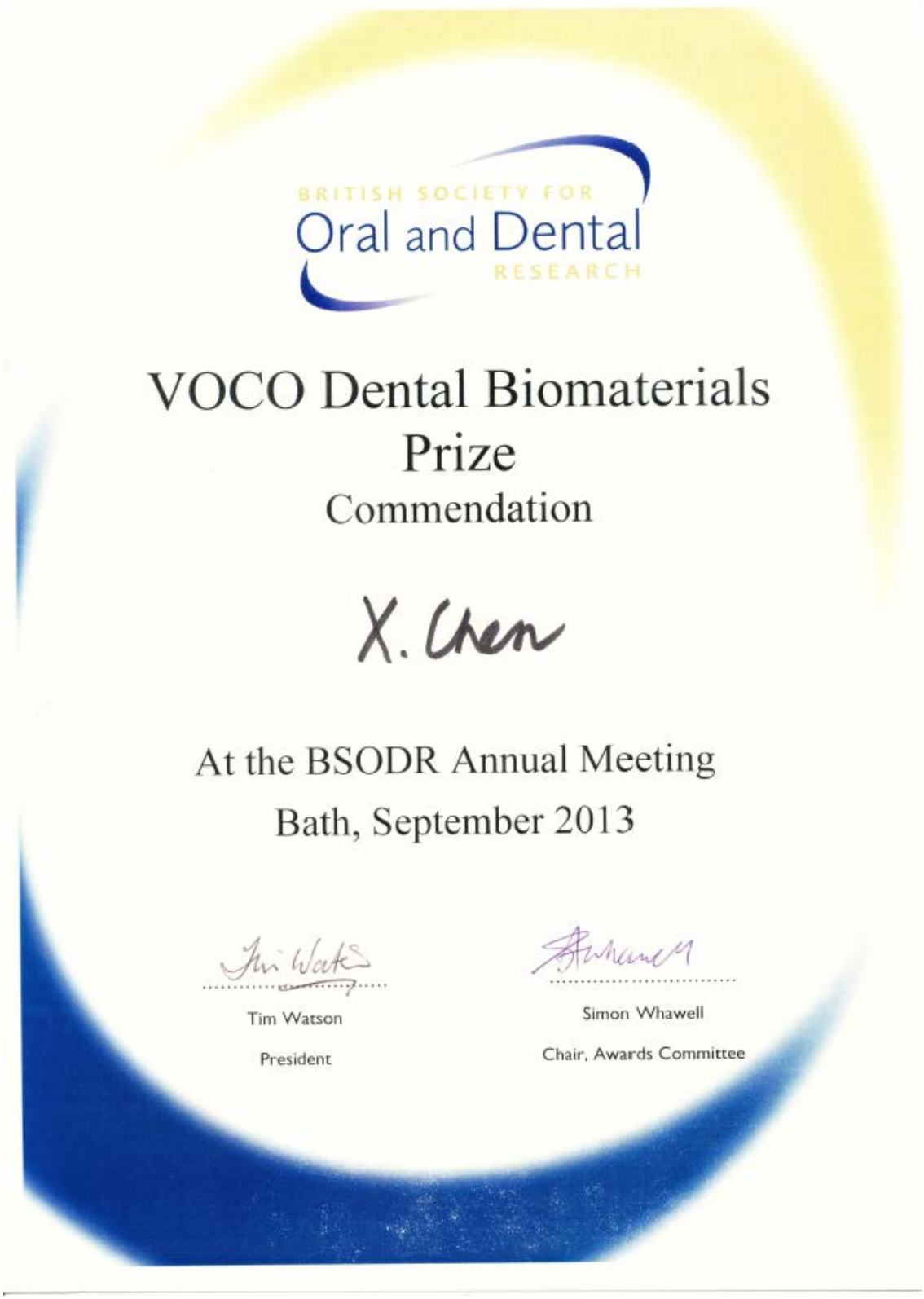

BRITISH SOCIETY FOR
Oral and Dental
RESEARCH

VOCO Dental Biomaterials Prize

Commendation

X. Chen

At the BSODR Annual Meeting

Bath, September 2013

Tim Watson

President

Simon Whawell

Chair, Awards Committee

Abstract accepted for a poster presentation for "12th International Conference on Structure of Non-Crystalline Materials", Trento, Italy, July 2013

14.3.4 Novel Highly Degradable Chloride Containing Bioactive Glasses

Xiaojing Chen[1]*, Natalia Karpukhina[1], Rory M. Wilson[2], Robert Hill[1]

[1]Dental Physical Sciences, Institute of Dentistry, Barts and The London School of Medicine and Dentistry, Queen Mary University of London, London, United Kingdom

[2]School of Engineering and Materials Science, Queen Mary University of London, London, United Kingdom

Addition of CaF_2 to a silicate glass typically reduces the glass transition temperature (T_g). The fluoride containing bioactive glasses investigated recently [4, 5] favour formation of fluoride substituted apatite which is less soluble in acidic conditions. In this paper we looked at the potential of chloride as an alternative to a fluoride addition to the bioactive glass. A slightly larger chloride ion can result in a more expanded glass network that may lead to a lower T_g, softer glasses and more rapid glass dissolution. In addition, chloride is naturally present in the human body, there is no restriction on chloride content in toothpastes and biomedical materials unlike with fluoride.

The series of bioactive glasses based on the quaternary system SiO_2-P_2O_5-CaO-$CaCl_2$ with varying $CaCl_2$ content were successfully synthesised via melt-derived route and characterised by differential scanning calorimetry (DSC). The bioactivity study of the investigated glasses was performed in Tris buffer solution and simulated body fluid. The apatite formation was characterised by Fourier transform infrared spectroscopy, X-ray diffraction (XRD) and nuclear magnetic resonance (NMR). Dissolution was followed by the ion release measurements.

The DSC results showed a dramatic reduction in T_g with an increase in $CaCl_2$ content. The results of the experiments in buffer solutions demonstrated that the designed chloride containing bioactive glasses are highly degradable and form apatite within 3 hrs in Tris and 9 hrs in SBF. The ^{31}P MAS NMR spectra of the glass powders before and after immersion in Tris indicate that phosphorus is present as orthophosphate. This study revealed that the chloride containing bioactive glasses that can be easily synthesized have the greatest innovative potential for novel applications in remineralising toothpaste and bone substitution.

UNIVERSITY OF TRENTO - Italy
Department of Physics

IFN
Institute for Photonics and Nanotechnologies

sponsored by
AGC
CORNING

NCM12 - 12th INTERNATIONAL CONFERENCE ON THE

STRUCTURE OF NON CRYSTALLINE MATERIALS

Best Poster Award

to

Xiaojing Chen

Trento, July 12, 2013

Giuseppe Dalba
NCM12 General Chairman

Francesco Rocca
NCM12 General Co-Chairman

International Journal of Applied Glass Science, 5 [3] 207–216 (2014)
DOI:10.1111/ijag.12082

INTERNATIONAL JOURNAL OF
Applied Glass
SCIENCE

Chlorapatite Glass-Ceramics

Xiaojing Chen, Robert Hill,* and Natalia Karpukhina

Dental Physical Sciences, Institute of Dentistry, Barts and the London School of Medicine and Dentistry, Queen Mary University of London, Mile End Road, London, E1 4NS, UK

Apatite glass-ceramics are attractive for medical and dental applications, and fluorapatite glass-ceramics based on aluminosilicate glasses have been extensively studied. This study is the first study of chlorapatite glass-ceramics based on calcium chloride-containing Q^2 bioactive phosphosilicate glasses. The crystallization behavior of oxychloride glasses is examined and compared with mixed oxychloride/fluoride and oxyfluoride glasses. The glass transition temperature decreased for all three series with increasing halogen content. On increasing the halogen content, there was an increasing tendency of the glasses to crystallize. The halogen-free glass surface crystallized to pseudowollastonite and an apatite. On incorporating a halide, the glasses exhibited largely bulk crystallization to a haloapatite. In the case of chloride, the glasses crystallized to chlorapatite. This is the first time to our knowledge that chlorapatite has been shown to crystallize from a glass. Chlorapatite is very attractive for medical applications because it converts to hydroxyapatite the mineral phase of tooth and bone on immersion in water.

Introduction

Apatite-based glass-ceramics are attractive for medical and dental applications, because the mineral phase of bone and tooth is thought to be based on hydroxyapatite. Kokubo *et al.* developed an apatite–wollastonite (AW) glass-ceramic.[1–3] This system exhibits excellent integration with bone and relatively good mechanical properties including high strength and fracture toughness. However, it has to be machined to shape using diamond tooling making it expensive to fabricate the complex shapes required for substitute bone parts. The AW glass-ceramic system developed by Kokubo *et al.*[1–3] exhibits surface nucleation, and the processing route involves crystallization and sintering to form a monolith, prior to machining. The option of direct casting to shape is not feasible because of the strong tendency of this system to exhibit surface crystal nucleation. The apatite phase present in the AW system is probably a mixed fluoro/oxyapatite.[4]

Hill and coworkers developed fluorapatite–mullite glass-ceramics[5–14] with even better mechanical properties than the AW system that bulk-nucleated via prior amorphous phase separation, giving rise to fluorapatite crystals with a needle-like habit. These systems could be cast to shape using loss wax casting. Compositions exhibited excellent osseo-integration.[15,16] However, fluorapatite is not very resorbable, mullite is almost completely inert, and concern was raised over the possibility of aluminum release, despite the aluminum being in the form of insoluble mullite.

Höland and coworkers[17–19] have also developed fluorapatite glass-ceramics that crystallize with a

*r.hill@qmul.ac.uk

needle-like habit and have developed them successfully for dental crowns. Numerous other workers[20–27] have studied fluorapatite-based glass-ceramic systems following the early studies of the groups led by Hill and Höland. It would be attractive to form hydroxyapatite, rather than fluorapatite in a glass-ceramic system for medical and dental applications, particularly where resorption and replacement by bone is desired, as hydroxyapatite is more readily dissolved under acidic conditions than fluorapatite. However, hydroxyl groups are volatilized readily during melting and are not retained in glass melts at sufficient concentrations to form hydroxyapatite. This is the reason for incorporating fluorides and making the fluoride analogue of hydroxyapatite. The substitution of fluoride for hydroxyls is used with a wide variety of glass-ceramics.[28–33] Höland and Beall have discussed such glass-ceramic systems in detail.[34]

Chlorine incorporation in glass forming systems has rarely been investigated relative to fluorine, because of more acute problems with chlorine volatilization. Kiprianov and Karpukhina[35] carried out a review of oxyhalide glasses and identified the key problems. Most chloride salts are appreciably volatile at glass melting temperatures unlike fluoride salts, which are not.

Chlorapatite glass-ceramics would be more attractive than fluorapatite glass-ceramics for medical and dental applications, because Elliott and Young[36] have shown that chlorapatite will convert completely to hydroxyapatite in the presence of water. The key factor controlling this property is the size of the ion. The chloride ion is larger than the hydroxyl ion, which is larger than the fluoride ion. The fluoride ion is small enough to fit in the space at the center of the Ca(II) triangle in the apatite crystal lattice, whereas the hydroxyl ion is too large and is displaced above the plane of the triangle. The chloride ion which is even larger is displaced even further above the plane of the Ca(II) triangle. This results in a move from a hexagonal space group toward a monoclinic space group and a less stable apatite.

Chlorapatite and fluorapatite exhibit extensive solid solution phase formation,[37–39] although the substitution of chlorine and fluorine in the lattice may not be completely random. Forming a mixed fluor/chlorapatite should enable the solubility of the apatite to be controlled. The solubility could be further optimized by substitution of strontium for calcium, which is known to occur in hydroxyapatite[40] and fluorapatite glass-ceramics.[41]

The starting point for this study is a previous study by Chen *et al.*[42] that investigated a sodium-free glass composition with CaF_2. Calcium chloride was added progressively to the fluorine-free version of this glass. This series was chosen for the following reasons:

1. The network connectivity was constant. This assumes that the chlorine forms Cl-Ca(n) species in an analogous fashion to F-Ca(n) species in fluoride-containing glasses.[43–45] This view is supported by a limited study by Sandland *et al.*[46]
2. The glasses contained no sodium and one of the possible routes to chlorine loss is thought to be loss as NaCl[35], and as these glasses contain no sodium, this is not a possibility.
3. This series of glasses crystallized to fluorapatite making them potentially attractive glass-ceramics. Assuming the possibility of chlorine forming the analogous Cl-M(n) species, these glasses would be expected to crystallize to chlorapatite. In oxyfluoride glasses, the fluorine speciation in the glass always reflects the speciation in the first crystalline phase to form.[30]

Experimental

Glass Synthesis

The glasses were produced by melting analytical grade silica (Prince Minerals Ltd., Stoke-on-Trent, UK), calcium carbonate, calcium fluoride, calcium chloride dihydrate (all from Sigma-Aldrich, St. Louis, MO), and diphosphorus pentoxide (AnalaR) in a 300 mL platinum/rhodium crucible at a temperature (T_m) of 1400°C to 1550°C for 1 h in an electrical furnace (EHF 17/3; Lenton, Hope Valley, UK). The resulting melts were rapidly quenched into deionized water to try and prevent crystallization. The granular glass frits produced were dried and then ground using a vibratory mill (Gy-Ro mill, Glen Creston Ltd., Twickenham, UK) for two sets of 7 min and sieved to give fine powder (<38 or <45 μm). The original frit (1–2 mm) and fine powder were used in the subsequent analysis.

The glasses synthesized were comprised of three series as given in Table 1. The CaF_2 glass series (B1-H1) were designed by introducing different amounts of CaX_2 into the E1 composition first studied by Mneimne *et al.*[47] The chloride glass series (B3-H3) were designed by replacing CaF_2 with $CaCl_2{\cdot}2H_2O$ and a

Table 1. Experimental Glass Compositions (in mol%)

Glass	SiO_2	CaO	P_2O_5	CaF_2	$CaCl_2$
A1/A2/A3	38.1	55.5	6.3	–	–
B1	37.0	53.9	6.1	3.0	–
C1	36.4	53.0	6.0	4.5	–
D1	35.9	52.2	6.0	6.0	–
E1	34.6	50.4	5.7	9.3	–
F1	32.9	48.0	5.5	13.6	–
G1	31.4	45.7	5.2	17.8	–
H1	28.4	41.4	4.7	25.5	–
B2	37.1	54.1	6.1	1.5	1.1
C2	36.6	53.4	6.0	2.3	1.7
D2	36.2	52.6	5.9	3.0	2.3
E2	35.0	51.0	5.8	4.7	3.6
F2	33.5	48.8	5.6	6.9	5.2
G2	32.1	46.7	5.3	9.1	6.9
H2	29.3	42.7	4.9	13.2	9.9
B3	37.3	54.3	6.2	–	2.3
C3	36.8	53.6	6.1	–	3.5
D3	36.4	53.0	6.0	–	4.6
E3	35.4	51.6	5.9	–	7.2
F3	34.1	49.6	5.7	–	10.6
G3	32.8	47.7	5.4	–	14.0
H3	30.3	44.1	5.0	–	20.6

The chemical compositions given here are the compositions assuming no volatilization or loss of halogens. Fluoride retention was typically 90–96%, while chloride retention was slightly lower at 77–93%. Generally lower halogen-containing glasses lost more halogen, and this is thought to be a result of reaction with water to form HCl or HF during melting. The analysis of the glasses was carried out by Lucideon (using XRF.

mixed $CaCl_2/CaF_2$ series (B2-H2) by replacing 50% of the CaF_2 by $CaCl_2{\cdot}2H_2O$.

X-ray Diffraction Analysis

An X'Pert Pro X-ray diffractometer (Panalytical, Almelo, the Netherlands) with a copper (Ni-filtered Cu-Kα, $\lambda_1 = 0.1541$ nm and $\lambda_2 = 0.1544$ nm) X-ray source was used to characterize the glass and heat-treated glass-ceramic samples. The powdered samples were recorded between 5 and 70° (2θ range) at a step size of 0.0334° and a step time of 200.03 sec. Calibration was carried out using NIST standard reference material 660a (lanthanum hexaboride). X-ray diffraction (XRD) data were analyzed using X'Pret HighScore Plus (v2.0; PANalytical) in conjunction with the ICDD database.

^{31}P Magic Angle Spinning–Solid-State Nuclear Magnetic Resonance

^{31}P magic angle spinning–solid-state nuclear magnetic resonance (MAS-NMR) experiments were carried out using 600 MHz (14.1T) Bruker solid-state nuclear magnetic resonance spectrometer. A spinning rate of 18K or 10K with the resonance frequencies of 249.2 MHz was employed. Sixty seconds was used as recycle delay time. The data were collected after 16 or 32 scans. All the spectra were referenced using 85% H_3PO_4.

Fourier Transform Infrared Spectroscopy

The glass powders and heat-treated samples were analyzed using Fourier transform infrared spectroscopy (Spectrum GX; Perkin-Elmer, Shelton, CT). The data were collected from 500 to 4000 cm^{-1} of wave number and presented between 500 and 1600 cm^{-1}.

Differential Scanning Calorimetry

A Stanton Redcroft DSC1500 (Rheometric Scientific, Epsom, UK) with matched pair platinum crucibles was used to determine the glass transition and peak crystallization (T_c) temperatures of the glasses. Fifty milligrams of fine (<38 μm) and frit (1–2 mm) glass powder was run against an alumina reference at a heating rate of 20°C/min in flowing nitrogen gas at 60 mL/min from 25°C to 1200°C. Two particle size fractions were run (fine and frit) to assess the tendency toward surface nucleation. Full-width half-maximum values (FWHM) were calculated from the differential scanning calorimetry (DSC) traces of frit samples for the first peak crystallization temperatures as a sharper peak is indicative of bulk nucleation.

Heat Treatment of the Glasses

The amorphous glasses were further investigated to identify the crystal phases formed on heat treatment. Glass powders (<38 μm, 1.0 g) were compacted into disks and heat-treated on a platinum foil in a porcelain and furnace (Ceram Press NEY Dental International, Yucaipa, CA) at a rate of 20°C/min from 400°C to

heat treatment temperatures (approximately 10°C above T_c) based on the observed exotherms from the DSC traces. Air quenching was applied after the heat treatments. Glass with 2.3 mol% $CaCl_2$ has also been held at 913°C for 30 minutes. The heat-treated glass-ceramics were ground into powder for XRD analysis. To study the morphology of the crystallization phases, frit specimens were embedded in resin, polished, gold coated, and viewed using a field emission scanning electron microscope (FEI Inspect F; Oxford Instruments, Buckinghamshire, UK) using a back-scattering mode.

Results and Discussion

All the glasses on quenching with the exception of the higher fluoride content (>9 mol%) glasses gave optically transparent glass frits. Figure 1 shows the XRD patterns of the $CaCl_2$-containing glasses. The XRD patterns of glasses exhibited some evidence of diffraction lines corresponding to apatite. In the case of the oxychloride glasses, this is probably chlorapatite or a mixed hydroxychlorapatite. In the case of the mixed oxychloride/oxyfluoride glasses, the diffraction lines could correspond to chlorapatite, fluorapatite, hydroxyapatite, or a mixed fluorochlorapatite. ^{31}P MAS-NMR showed a single broad peak for the $CaCl_2$ glasses corresponding to amorphous calcium phosphate (Fig. 2). There was no evidence of crystalline apatite in the synthesized glasses, and there was no evidence of apatite in the Fourier transform infrared spectroscopy (FTIR) spectra of the glasses. In contrast, the ^{31}P MAS-NMR spectra for the fluoride series (Fig. 3) showed a progressive sharpening of the calcium orthophosphate peak corresponding to crystalline apatite formation. The ^{31}P MAS-NMR spectra of the mixed series mainly gave broad amorphous spectra. The apatite detected by XRD in the chloride glasses is thought to arise through reaction of the fine glass powder with atmospheric water at the surface to form a mixed hydroxychlorapatite during the time the XRD pattern was collected.

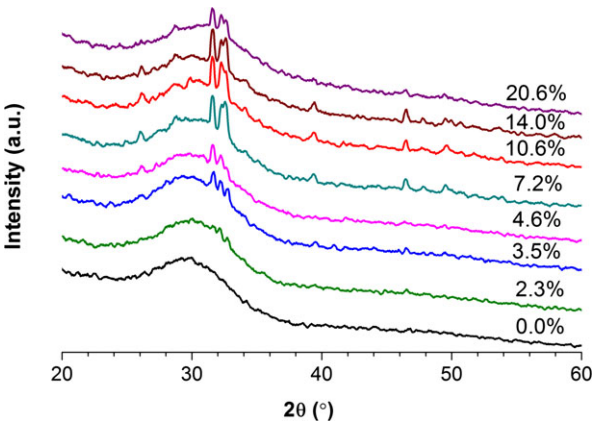

Fig. 1. XRD patterns of the $CaCl_2$ glasses. $CaCl_2$ content (mol%) for each composition is indicated. Diffraction lines correspond to apatite.

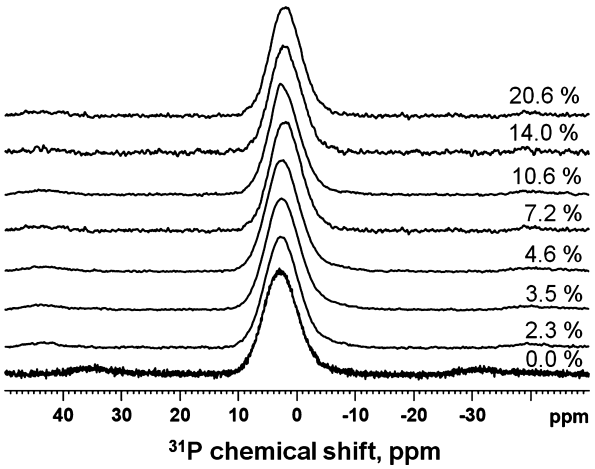

Fig. 2. ^{31}P MAS-NMR spectra of the $CaCl_2$-containing glasses, compositions A3-H3 from bottom to top, $CaCl_2$ content (mol%) is indicated.

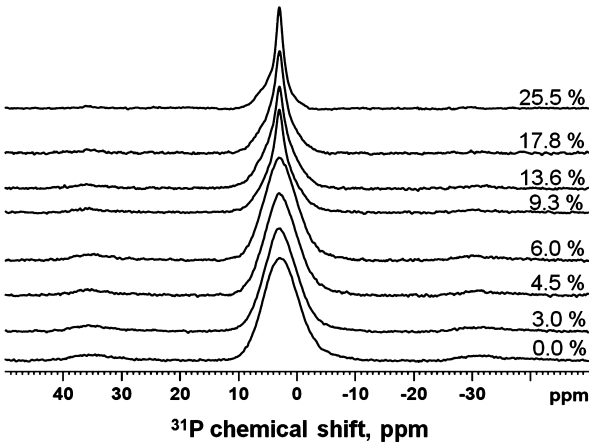

Fig. 3. ^{31}P MAS-NMR spectra for the CaF_2 series (A1-H1 compositions). The numbers indicate CaF_2 content (mol%) in glasses. The peak sharpens and FWHM reduces as fluorapatite crystallizes above 9.3 mol% CaF_2 (E1).

Table 2. Summary of the Crystallinity Analysis of as Quenched Glasses Based on XRD, FTIR, and ^{31}P MAS-NMR

Glass	CaF_2	$CaCl_2$	Crystal Phases
A1/A2/A3	–	–	Amorphous
B1	3.0	–	Amorphous
C1	4.5	–	Amorphous
D1	6.0	–	Amorphous
E1	9.3	–	$Ca_{10}(PO_4)_6F_2$ (trace)
F1	13.6	–	$Ca_{10}(PO_4)_6F_2$
G1	17.8	–	$Ca_{10}(PO_4)_6F_2$, $Ca_4Si_2O_7F_2$, CaF_2
H1	25.5	–	$Ca_{10}(PO_4)_6F_2$, $Ca_4Si_2O_7F_2$, CaF_2
B2	1.5	1.1	Amorphous
C2	2.3	1.7	Largely Amorphous
D2	3.0	2.3	Largely Amorphous
E2	4.7	3.6	Largely Amorphous
F2	6.9	5.2	$Ca_{10}(PO_4)_6F_2$ or HAP
G2	9.1	6.9	$Ca_{10}(PO_4)_6F_2$ or HAP
H2	13.2	9.9	$Ca_{10}(PO_4)_6F_2$ or HAP
B3	–	2.3	Amorphous
C3	–	3.5	Amorphous
D3	–	4.6	Amorphous
E3	–	7.2	Amorphous
F3	–	10.6	Amorphous
G3	–	14.0	Amorphous
H3	–	20.6	Amorphous

Table 2 summarizes the crystallinity of the glasses based on the XRD, FTIR, and ^{31}P MAS-NMR spectra. The hydroxyl groups in the apatite formed must come from surface reaction with atmospheric water as there is unlikely to be significant quantities of hydroxyl groups in the original glasses.

The glass transition temperature (T_g) values are plotted against $CaCl_2$ content in Fig. 4. The T_g of the equivalent CaF_2-containing glasses and mixed halogen glasses were plotted for comparison. The T_g values for the oxychloride glasses reduce by over 200°C with increasing $CaCl_2$ content and are typically about 30°C above those of the equivalent oxyfluoride glasses. The T_g of the mixed halide glasses lie below those of the oxyfluoride glasses, rather than having intermediate values. There is a break in the T_g behavior of the CaF_2 glasses (from 10 mol% CaF_2), which corresponds to crystallization of fluorapatite, which effectively removes

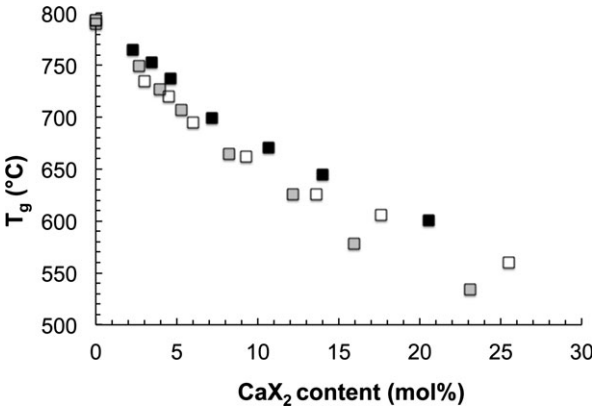

Fig. 4. T_g plotted against CaX_2 (X = Cl/F/Cl + F) content (mol%). ■ = Cl, □ = Cl/F, and □ = F.

fluoride from the glass phase and consequently T_g reduces less with increasing CaF_2 content.

Brauer *et al.*[44,45] and Mneimne *et al.*[47] have both shown previously that increasing the CaF_2 content of the glass reduces T_g. Brauer *et al.* proposed since fluoride ions complex calcium ions that this effectively converts a Ca^{2+} cation to a "CaF^+" species, which unlike a Ca^{2+} cation can no longer ionically bridge two nonbridging oxygens. This is supported by ^{19}F MAS-NMR spectroscopy[44,48] and the MD simulations of Christie *et al.*[49] On the basis that chloride incorporation gives very similar reductions in T_g, this suggests that Cl-Ca (n) species are forming in these glasses in an analogous fashion to the F-Ca(n) species found in fluoride-containing glasses. This is supported by the fact that Sandland *et al.*[46] found evidence of Cl-Ca(n) species in their study with glasses of very low chlorine content.

On incorporating $CaCl_2$ rather than CaF_2, the tendency of the glasses to crystallize during synthesis is suppressed and the T_g reduces more linearly with CaX_2 content. Incorporating chloride as opposed to fluoride would be expected to result in a reduced tendency to crystallization, as the chloride ion is substantially larger than the fluoride ion and the lattice energies of the equivalent crystalline phases are likely to be smaller, and furthermore, a large chloride ion is less likely to order calcium cations around itself than a smaller fluoride ion. A consequence of this is that larger amounts of $CaCl_2$ than CaF_2 can be incorporated into the glasses without significant crystallization occurring during quenching from the melt.

The mixed $CaCl_2/CaF_2$ glasses also have a reduced tendency to crystallize compared with the CaF_2 glasses,

and this effect is more pronounced at higher mol% of CaX_2. Fluorapatite forms in significant amounts in the CaF_2 series from 9.3 mol% CaF_2. Cuspidine ($3CaO\text{-}CaF_2\text{-}2SiO_2$ or $Ca_4Si_2O_7F_2$) and CaF_2 crystallize from the glass in increasing amounts during quenching as the CaF_2 content of the glass is increased.

Figure 5 plots the first peak crystallization temperature (T_{c1}) for the three glass series. It can be seen that T_{c1} reduces with increasing CaX_2 content mirroring the T_g behavior. Figure 6 plots the first peak crystallization temperature (T_{c1}) against $CaCl_2$ content for fine and frit (1–2 mm) particle sizes of the chloride series. The zero $CaCl_2$ content glass exhibits a marked temperature difference between the T_{c1} values for frit and fine powder. In addition, the full-width half-maximum (FWHM) increases markedly for the frit particles compared with the fine micrometer particles. This indicates pronounced surface nucleation. This halogen-free glass crystallizes largely to wollastonite and an apatite. Pseudowollastonite is a Q^2 ring silicate, which is known to strongly surface-nucleate. The apatite is thought to be a hydroxyapatite, but given the low hydroxyl content of silicate glasses, this is either thought to form as an oxyapatite, which subsequently reacts with water or more likely is a result of water vapor in the furnace atmosphere diffusing into the glass and enabling apatite formation from the glass surface.

On incorporating $CaCl_2$, the difference between the T_{c1} values for the different particle sizes reduces markedly to <20°C, and at about 6–9 mol% $CaCl_2$, the two values are equal (Fig. 6) with T_{c1} frit–T_{c1} fine going to approximately zero.

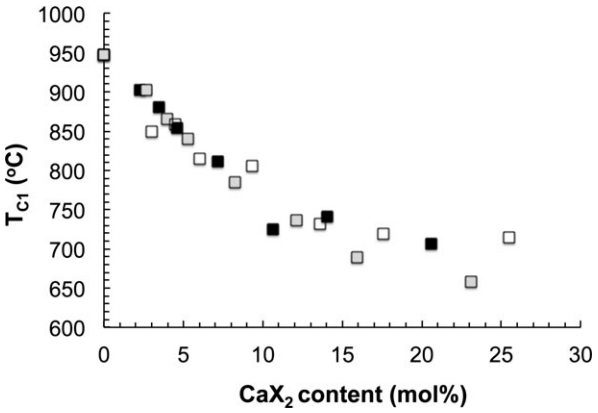

Fig. 5. T_{c1} for frit particles plotted against CaX_2 (X = Cl/F/Cl + F) content (mol%). ■ = Cl, ▩ = Cl/F, and □ = F.

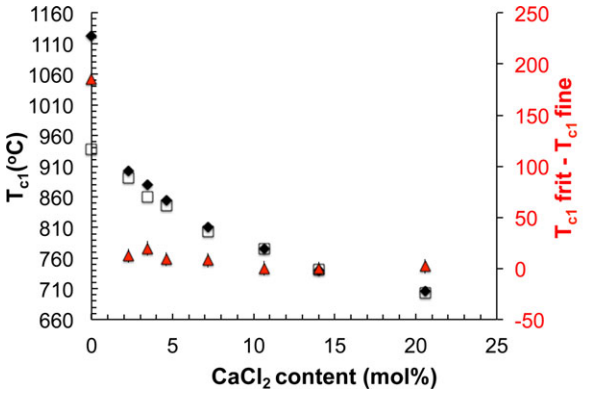

Fig. 6. First peak crystallization temperature (T_{c1}) for frit (▲) and fine (□) glass particles plotted against $CaCl_2$ content and T_{c1} frit–T_{c1} fine (▢). The error in the DSC measurements of T_{c1} is < 1°C which is smaller than the data points.

Figure 7 shows the FWHM of the first crystallization peak temperature for the three glass series. The FWHM decreases markedly with CaX_2 content for all three series and exhibits a minimum at about 6–9 mol % for the chloride and mixed halide glasses, but there is no distinct trend for the FWHM data for the fluoride glasses above 9 mol%, which reflects the fact that these glasses are significantly crystalline and also crystallize to cuspidine ($Ca_4Si_2O_7F_2$) and fluorite (CaF_2). Both cuspidine and fluorite have an F-Ca(4) structure with four Ca^{2+} cations surrounding each fluoride ion and might be expected to form at higher fluoride

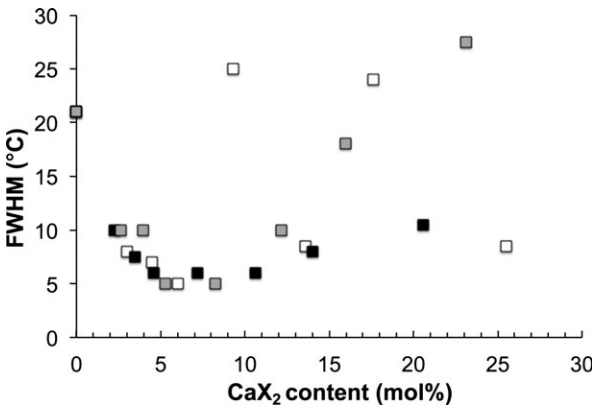

Fig. 7. FWHM for first crystallization exotherm (T_{c1}) plotted against CaX_2 (X = Cl/F/Cl + F) content (mol%). ■ = Cl, ▩ = Cl/F, and □ = F. The errors in determining the FWHM are estimated to be < 1°C, which is about the size of the data points.

contents relative to fluorapatite which has an F-Ca(3) speciation.[30] The minimum at 6–9 mol% CaX_2 content for the mixed halide and chloride glasses indicates that these glasses bulk-nucleate most readily making them most suitable for forming apatite glass-ceramics. The diffraction patterns of the heat-treated glasses for the mixed halide system are consistent with fluorapatite formation, rather than chloroapatite formation. The minimum corresponds to about 2–3 times the halide content in terms of crystallizing all the phosphate in the glass to a haloapatite. A degree of caution must be exercised with view to interpreting crystal nucleation mechanisms from particle size studies with bioactive glasses following Massera *et al.*[56] largely as a result of the fact that viscous flow sintering and crystallization can occur simultaneously. However, in the present glasses, the onset temperature for crystallization occurs <100°C above the T_g, consequently viscous flow sintering is unlikely to occur and the interpretation of the nucleation mechanisms is therefore valid. The ability to bulk-nucleate is important, as it enables the ability to cast the glass in the molten state and then heat-treated to convert the glass to the glass-ceramic.

XRD patterns of the heat-treated samples of the chloride glasses match that of chlorapatite although some hydroxyl substitution in the lattice cannot be ruled out and apatite is largely bulk nucleating. In contrast, T_{c2}, which corresponds to the crystallization of pseudowollastonite, still increases markedly on going from fine powder to frit indicating that pseudowollastonite still has a strong tendency toward surface nucleation. This is shown in Fig. 8a and b for DSC plots for the 2.3 and 10.6 mol% $CaCl_2$ glasses. The maximum in T_{c2} not only moves to higher temperatures for frit particles, but also reduces in amplitude and becomes broader again indicating evidence of strong surface nucleation. This becomes more pronounced with increasing $CaCl_2$ content. In contrast, T_{c1} peak is sharp for both fine and frit particles.

Figure 9 shows the XRD pattern of the 2.3 mol% $CaCl_2$ glass after heat treatment to 913°C slightly higher than the first crystallization peak temperature (T_{c1}) and to 1020°C slightly higher than the second peak crystallization temperature (T_{c2}). The XRD pattern shows the glass to have crystallized to a small amount of chlorapatite at 913°C and to a much larger amount at 1020°C, while the original glass is almost entirely amorphous. There is also a small amount of pseudowollastonite present.

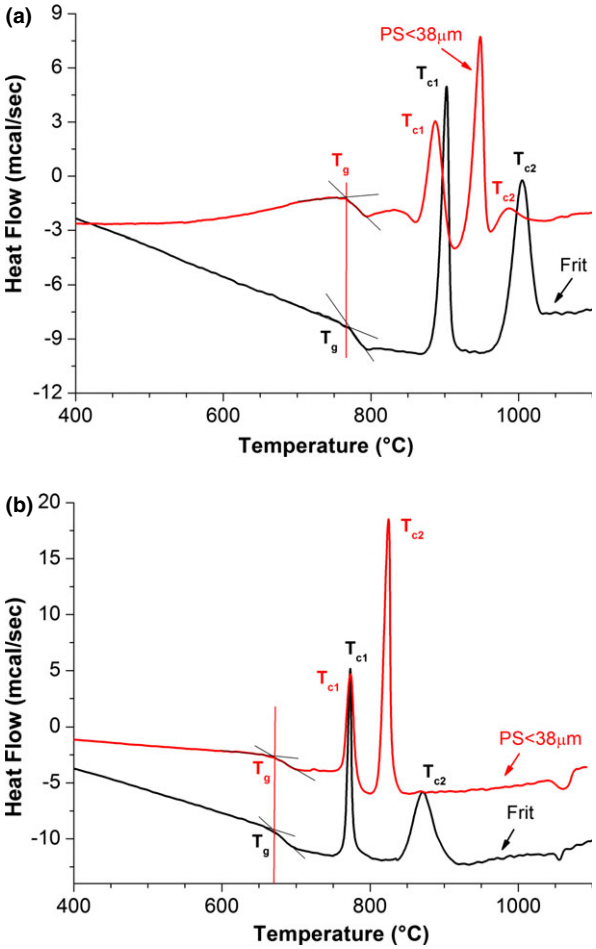

Fig. 8. DSC traces for frit and <38 μm powder of (a) 2.3 and (b) 10.6 mol% $CaCl_2$ glasses showing largely bulk nucleation of the first crystallization peak and surface nucleation of the second crystallization peak.

Figure 10 shows the equivalent FTIR spectra. The original glass shows a broad peak between 500 and 600 cm^{-1} corresponding to the bending mode of P-O^- in an amorphous calcium orthophosphate, and also a Si–O–Si bending vibration is seen in this region.[50–53] Around 720 cm^{-1} in the glass spectrum is the broad band due to Si–O bending vibrations.[54,55] The dominant bands at approximately 920 and 990 cm^{-1} can be attributed to Si–O^- (Q^2) and Si–O–Si stretching vibrations, respectively. On heat treatment, the broad band at 500 to 600 cm^{-1} is lost and two new peaks at 560 and 605 cm^{-1} appear corresponding to P-O bending in a crystalline orthophosphate and a peak at 1035 cm^{-1} corresponding to P-O stretching appear. In

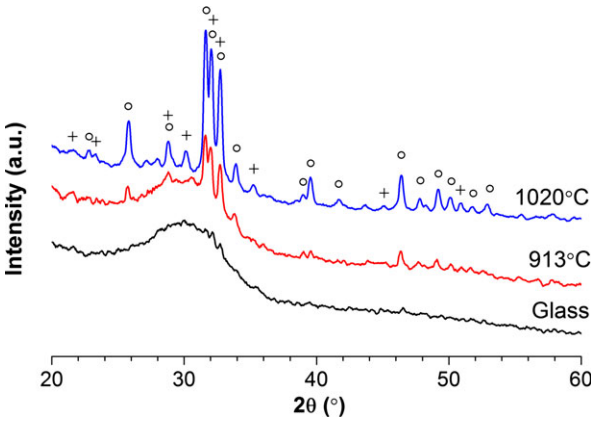

Fig. 9. XRD patterns of the 2.3 mol% $CaCl_2$ glass and heat-treated glasses of this initial composition. ○ = apatite, + = wollastonite/pseudowollastonite.

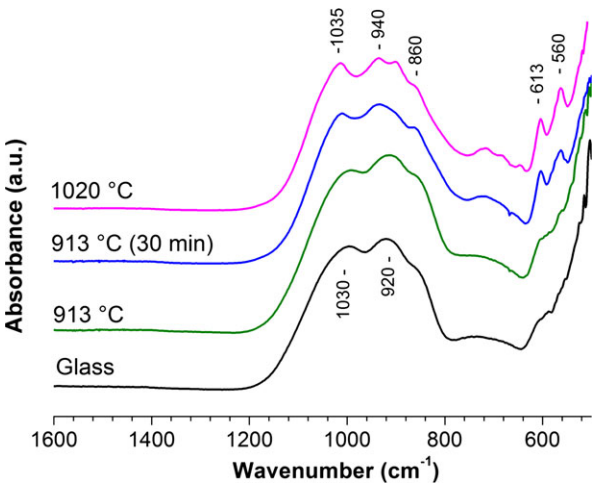

Fig. 10. FTIR spectra of the 2.3 mol% $CaCl_2$ glass and heat-treated glasses of this initial composition.

addition, the Si-O bending and stretching vibration becomes more pronounced after heat treatment at 1020°C. The presence of the sharp peaks at 560 and 605 cm^{-1} is indicative of apatite crystallization. The presence of sharper peaks at 920 and 980 cm^{-1} compared with the original glass in the sample heat-treated to 1020°C corresponding to T_{p2} indicates a much more ordered Q^2 calcium silicate environment. On the basis that following crystallization of chlorapatite, this glass will have a CaO/SiO_2 ratio close to the wollastonite stoichiometry, and it might be expected that T_{c2} might correspond to the crystallization of pseudowollastonite. The FTIR spectra following heat treatment at 1020°C are consistent with the formation of a crystalline Q^2 calcium silicate.

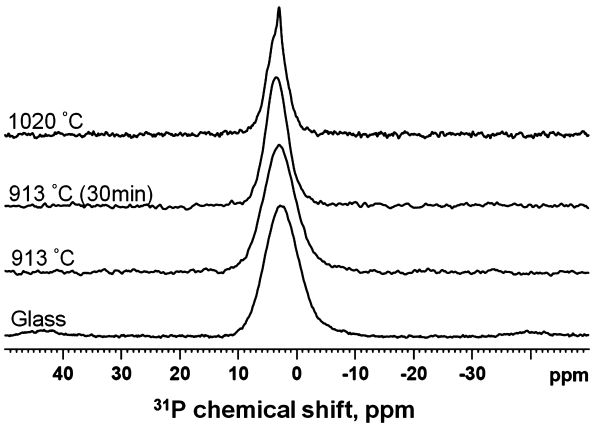

Fig. 11. ^{31}P MAS-NMR spectra of the 2.3 mol% $CaCl_2$ glass and heat-treated glasses.

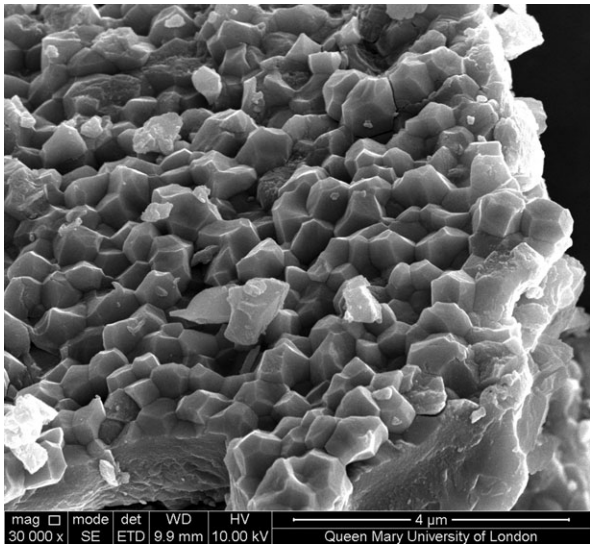

Fig. 12. SEM of the fractured surface of 2.3 mol% $CaCl_2$ glass-ceramic heat-treated at 913°C.

Figure 11 shows the ^{31}P MAS-NMR spectra of the 2.3 mol% $CaCl_2$ glass and the heat-treated samples. There is a progressive sharpening of the major peak upon crystallization. At 913°C, relatively little apatite is formed and most of the phosphorus in the glass has not crystallized. After heat-treating at 1020°C, most of the phosphorus in the glass has crystallized to chlorapa-

tite and consequently the peak sharpens and has a sharp maximum at about 2.6 ppm corresponding to apatite. The sample heat-treated to 913°C has a microstructure (Fig. 12) that consists of uniform equiaxed hexagonal crystals of chlorapatite. In contrast, the equivalent fluoride-containing glass formed hexagonal needle-like crystals of fluorapatite. Fluorapatite generally forms crystals with a needle-like habit when crystallized from oxyfluoride glasses,[10–13,18] while chlorapatite has a tendency to form equiaxed crystals[56].

Conclusions

The glass transition temperature for the three glass series reduced with increasing CaX_2 content. The reduction in the T_g is probably a result of the formation of X-Ca(n) species in the glass structure. The halogen-free glass surface crystallized to wollastonite and apatite. All the glasses with chloride or fluoride crystallized first to a haloapatite. Fluoride-containing glasses crystallized more readily and also tended to crystallize to additional phases, including cuspidine and fluorite. Glasses with 2.3 to 9.3 mol% CaX_2 had a reduced tendency to surface-nucleate to a haloapatite and are attractive for potential apatite glass-ceramics. The second crystallization process of the chloride glasses and mixed halide glasses was wollastonite, which always strongly surface-nucleated. The surface nucleation of wollastonite is undesirable and would probably eliminate the ability to produce apatite–wollastonite glass-ceramics by a direct casting route. However, it would be possible to crystallize these glasses to only apatite to form apatite glass-ceramics with a bioactive residual glass phase. Tailoring the fluorine/chlorine ratio should enable mixed haloapatites to be produced, enable the tailoring of the microstructure and *in vivo* resorbability of the glass-ceramics.

The chloride glasses studied here are very reactive and appear to react with atmospheric water, and further work is required to develop practical chloroapatite and mixed chloro/fluorapatite glass-ceramics and to study their *in vitro* and *in vivo* biocompatibility.

Further work is required to characterize these oxychloride glasses and chlorapatite glass-ceramics using the ^{35}Cl NMR to identify the chlorine speciation in the glass and ^{29}Si MAS-NMR to confirm that the Q speciation does not change with the addition of $CaCl_2$.

Acknowledgments

Xiaojing Chen was supported by China Scholarship Council (CSC)/ Queen Mary Joint PhD scholarships.

References

1. T. Kokubo "Bioactive Glass Ceramics: Properties and Applications," *Biomaterials*, 12 [2] 155–163 (1991).
2. T. Kokubo, S. Ito, M. Shigematsu, S. Sakka, and T. Yamamuro, "Mechanical-Properties of a New Type of Apatite-Containing Glass Ceramic for Prosthetic Application," *J. Mater. Sci.*, 20 2001–2004 (1985).
3. K. Ono, T. Yamamuro, T. Nakamura, and T. Kokubo, "Quantitative Study on Osteoconduction of Apatite Wollastonite Containing Glass Ceramic Granules, Hydroxyapatite Granules, and Alumina Granules," *Biomaterials*, 11 [26] 5–271 (1990).
4. A. Calver, R. G. Hill, and A. Stamboulis, "Influence of Fluorine Content on the Crystallization Behavior of Apatite-Wollastonite Glass-Ceramics," *J. Mater. Sci.*, 39 2601–2603 (2004).
5. R. Hill and D. Wood, "Apatite Mullite Glass-Ceramics," *J. Mater. Sci. Mater. Med.*, 6 311–318 (1995).
6. A. Clifford and R. Hill, "Apatite-Mullite Glass-Ceramics," *J. Non-Cryst. Solids*, 196 346–351 (1996).
7. A. Clifford, R. G. Hill, M. R. Towler, and D. J. Wood, "The Crystallisation of Glasses from the Ternary Caf2-Caal2si2o8-P2o5 System," *J. Mater. Sci.*, 36 3955–3961 (2001).
8. A. Johnson, M. Y. Shareef, J. M. Walsh, P. V. Hatton, R. van Noort, and R. G. Hill, "The Effect of Casting Conditions on the Biaxial Flexural Strength of Glass–Ceramic Materials," *Dent. Mater.*, 14 412–416 (1998).
9. K. Stanton and R. Hill, "The Role of Fluorine in the Devitrification of Sio2-Al2o3-P2o5-Cao-Caf2 Glasses," *J. Mater. Sci.*, 35 1911–1916 (2000).
10. K. T. Stanton, K. P. O'Flynn, S. Kiernan, J. Menuge, and R. Hill, "Spherulitic Crystallization of Apatite-Mullite Glass-Ceramics: Mechanisms of Formation and Implications for Fracture Properties," *J. Non-Cryst. Solids*, 356 1802–1813 (2010).
11. A. Rafferty, A. Clifford, R. Hill, D. Wood, B. Samuneva, and M. Dimitrova-Lukacs, "Influence of Fluorine Content in Apatite–Mullite Glass-Ceramics," *J. Am. Ceram. Soc.*, 83 2833–2838 (2000).
12. K. T. Stanton and R. G. Hill, "Crystallisation in Apatite-Mullite Glass-Ceramics as a Function of Fluorine Content," *J. Cryst. Growth*, 275 E2061–E2068 (2005).
13. R. Hill, A. Calver, A. Stamboulis, and N. Bubb, "Real-Time Nucleation and Crystallization Studies of a Fluorapatite Glass-Ceramics Using Small-Angle Neutron Scattering and Neutron Diffraction," *J. Am. Ceram. Soc.*, 90 763–768 (2007).
14. R. G. Hill, M. D. O'Donnell, R. V. Law, N. Karpukhina, B. Cochrane, and D. U. Tulyaganov, "The Early Stages of Nucleation and Crystallisation of an Apatite Glass-Ceramic: Evidence for Nano-Scale Crystallisation," *J. Non-Cryst. Solids*, 356 2935–2941 (2010).
15. C. O. Freeman, I. M. Brook, A. Johnson, P. V. Hatton, R. G. Hill, and K. T. Stanton, "Crystallization Modifies Osteoconductivity in an Apatite–Mullite Glass–Ceramic," *J. Mater. Sci. Mater. Med.*, 14 985–990 (2003).
16. R. D. Goodridge, D. J. Wood, C. Ohtsuki, and K. W. Dalgarno, "Biological Evaluation of an Apatite–Mullite Glass-Ceramic Produced Via Selective Laser Sintering," *Acta Biomater.*, 3 221–231 (2007).
17. R. Muller, L. A. Abu-Hilal, S. Reinsch, and W. Holand, "Coarsening of Needle-Shaped Apatite Crystals in Sio2 Center Dot Al2o3 Center Dot Na2o Center Dot K2o Center Dot Cao Center Dot P2o5 Center Dot F Glass," *J. Mater. Sci.*, 34 65–69 (1999).
18. W. Holand, V. Rheinberger, S. Wegner, and M. Frank, "Needle-Like Apatite-Leucite Glass-Ceramic as a Base Material for the Veneering of Metal Restorations in Dentistry," *J. Mater. Sci. Mater. Med.*, 11 11–17 (2000).

19. J. C. C. Chan, R. Ohnsorge, K. Meise-Gresch, H. Eckert, W. Holand, and V. Rheinberger, "Apatite Crystallization in an Aluminosilicate Glass Matrix: Mechanistic Studies by X-Ray Powder Diffraction, Thermal Analysis, and Multinuclear Solid-State Nmr Spectroscopy," *Chem. Mater.*, 13 4198–4206 (2001).
20. D. U. Tulyaganov, "Phase Equilibrium in the Fluorapatite-Anorthite-Diopside System," *J. Am. Ceram. Soc.*, 83 3141–3146 (2000).
21. K. P. O'Flynn and K. T. Stanton, "Nucleation and Early Stage Crystallization of Fluorapatite in Apatite-Mullite Glass-Ceramics," *Cryst. Growth Des.*, 10 1111–1117 (2010).
22. A. K. Swarnakar, A. Stamboulis, D. Holland, and O. Van der Biest, "Improved Prediction of Young's Modulus of Fluorine-Containing Glasses Using Mas-Nmr Structural Data," *J. Am. Ceram. Soc.*, 96 1271–1277 (2013).
23. T. Hoche, C. Moisescu, I. Avramov, C. Russel, and W. D. Heerdegen, "Microstructure of Sio2-Al2o3-Cao-P2o5-K2o-F- Glass Ceramics. 1. Needlelike Versus Isometric Morphology of Apatite Crystals," *Chem. Mater.*, 13 1312–1319 (2001).
24. K. T. Stanton, K. P. O'Flynn, S. Nakahara, J. F. Vanhumbeeck, J. M. Delucca, and B. Hooghan, "Study of the Interfacial Reactions between a Bioactive Apatite-Mullite Glass-Ceramic Coating and Titanium Substrates Using High Angle Annular Dark Field Transmission Electron Microscopy," *J. Mater. Sci. Mater. Med.*, 20 851–857 (2009).
25. S. Agathopoulos *et al.*, "Structural Analysis and Devitrification of Glasses Based on the Cao-Mgo-Sio2 System with B2o3, Na2o, Caf2 and P2o5 Additives," *J. Non-Cryst. Solids*, 352 322–328 (2006).
26. D. U. Tulyaganov, S. Agathopoulos, J. M. Ventura, M. A. Karakassides, O. Fabrichnaya, and J. M. F. Ferreira, "Synthesis of Glass-Ceramics in the Cao-Mgo-Sio2 System with B2o3, P2o5, Na2o and Caf2 Additives," *J. Eur. Ceram. Soc.*, 26 1463–1471 (2006).
27. I. Denry, J. A. Holloway, and P. K. Gupta, "Effect of Crystallization Heat Treatment on the Microstructure of Niobium-Doped Fluorapatite Glass-Ceramics," *J. Biomed. Mater. Res. Part B Appl. Biomater.*, 100B 1198–1205 (2012).
28. G. H. Beall, "Design and Properties of Glass-Ceramics," *Annu. Rev. Mater. Sci.*, 22 91–119 (1992).
29. J. Henry and R. G. Hill, "The Influence of Lithia Content on the Properties of Fluorphlogopite Glass-Ceramics. I. Nucleation and Crystallisation Behaviour," *J. Non-Cryst. Solids*, 319 1–12 (2003).
30. R. G. Hill *et al.*, "Characterisation of Fluorine Containing Glasses and Glass-Ceramics by F-19 Magic Angle Spinning Nuclear Magnetic Resonance Spectroscopy," *J. Eur. Ceram. Soc.*, 29 2185–2191 (2009).
31. S. Likitvanichkul and W. C. Lacourse, "Effect of Fluorine Content on Crystallization of Canasite Glass-Ceramics," *J. Mater. Sci.*, 30 6151–6155 (1995).
32. C. A. Miller, I. M. Reaney, P. V. Hatton, and P. F. James, "Crystallization of Canasite/Frankamenite-Based Glass-Ceramics," *Chem. Mater.*, 16 5736–5743 (2004).
33. G. H. Beall, "Chain Silicate Glass-Ceramics," *J. Non-Cryst. Solids*, 129 163–173 (1991).
34. W. Holand and G. H. Beall, *Glass Ceramic Technology*, Vol., 2nd Edition, Wiley, Hoboken, NJ, 2012.
35. A. A. Kiprianov and N. G. Karpukhina, "Oxyhalide Silicate Glasses," *Glass Phys. Chem.*, 32 1–27 (2006).
36. J. C. Elliott and R. A. Young, "Conversion of Single Crystals of Chlorapatite into Single Crystals of Hydroxyapatite," *Nature*, 214 904–906 (1967).
37. P. E. Mackie and R. A. Young, "Fluorine-Chlorine Interaction in Fluor-Chlorapatite," *J. Solid State Chem.*, 11 319–329 (1974).
38. M. D. O'Donnell, R. G. Hill, and S. K. Fong, "Neutron Diffraction of Chlorine Substituted Fluorapatite," *Mater. Lett.*, 63 1347–1349 (2009).
39. M. D. O'Donnell, R. G. Hill, R. V. Law, and S. Fong, "Raman Spectroscopy, 19f and 31p Mas-Nmr of a Series of Fluorochloroapatites," *J. Eur. Ceram. Soc.*, 29 377–384 (2009).
40. M. D. O'Donnell, Y. Fredholm, A. de Rouffignac, and R. G. Hill, "Structural Analysis of a Series of Strontium-Substituted Apatites," *Acta Biomater.*, 4 1455–1464 (2008).
41. R. G. Hill, A. Stamboulis, R. V. Law, A. Clifford, M. R. Towler, and C. Crowley, "The Influence of Strontium Substitution in Fluorapatite Glasses and Glass-Ceramics," *J. Non-Cryst. Solids*, 336 223–229 (2004).
42. X. J. Chen, X. H. Chen, D. S. Brauer, R. M. Wilson, R. G. Hill, and N. Karpukhina, "Bioactivity of Sodium Free Fluoride Containing Glasses and Glass-Ceramics," *J. Non-Cryst. Solids* (2013).
43. R. G. Hill, N. Da Costa, and R. V. Law, "Characterization of a Mould Flux Glass," *J. Non-Cryst. Solids*, 351 69–74 (2005).
44. D. S. Brauer, N. Karpukhina, R. V. Law, and R. G. Hill, "Structure of Fluoride-Containing Bioactive Glasses," *J. Mater. Chem.*, 19 5629–5636 (2009).
45. D. S. Brauer, M. N. Anjum, M. Mneimne, R. M. Wilson, H. Doweidar, and R. G. Hill, "Fluoride-Containing Bioactive Glass-Ceramics," *J. Non-Cryst. Solids*, 358 1438–1442 (2012).
46. T. O. Sandland, L.-S. Du, J. F. Stebbins, and J. D. Webster, "Structure of Cl-Containing Silicate and Aluminosilicate Glasses: A 35 cl Mas-Nmr Study," *Geochim. Cosmochim. Acta*, 68 5059–5069 (2004).
47. M. Mneimne, R. G. Hill, A. J. Bushby, and D. S. Brauer, "High Phosphate Content Significantly Increases Apatite Formation of Fluoride-Containing Bioactive Glasses," *Acta Biomater.*, 7 1827–1834 (2011).
48. A. Pedone, T. Charpentier, and M. C. Menziani, "The Structure of Fluoride-Containing Bioactive Glasses: New Insights from First-Principles Calculations and Solid State Nmr Spectroscopy," *J. Mater. Chem.*, 22 12599–12608 (2012).
49. J. K. Christie, A. Pedone, M. C. Menziani, and A. Tilocca, "Fluorine Environment in Bioactive Glasses: Ab Initio Molecular Dynamics Simulations," *J. Phys. Chem. B*, 115 2038–2045 (2011).
50. M. Vallet-Regí, A. M. Romero, C. V. Ragel, and R. Z. LeGeros, "XRD, SEM-EDS, and FTIR Studies of *in Vitro* Growth of an Apatite-Like Layer on Sol-Gel Glasses," *J. Biomed. Mater. Res.*, 44 416–421 (1999).
51. M. R. T. Filgueiras, G. Latorre, and L. L. Hench, "Solution Effects on the Surface-Reactions of 3 Bioactive Glass Compositions," *J. Biomed. Mater. Res.*, 27 1485–1493 (1993).
52. O. Peitl, E. D. Zanotto, and L. L. Hench, "Highly Bioactive P2o5-Na2o-Cao-Sio2 Glass-Ceramics," *J. Non-Cryst. Solids*, 292 115–126 (2001).
53. O. Peitl, G. P. LaTorre, and L. L. Hench, "Effect of Crystallization on Apatite-Layer Formation of Bioactive Glass 45s5," *J. Biomed. Mater. Res.*, 30 509–514 (1996).
54. D. M. Sanders, W. B. Person, and L. L. Hench, "Quantitative Analysis of Glass Structure with the Use of Infrared Reflection Spectra," *Appl. Spectrosc.*, 28 530–536 (1974).
55. J. Serra *et al.*, "Ftir and Xps Studies of Bioactive Silica Based Glasses," *J. Non-Cryst. Solids*, 332 20–27 (2003).
56. E. Garcıa-Tunon, R. Couceiro, J. Franco, E. Saiz, and F. Guitia, "Synthesis and characterisation of large chlorapatite single-crystals with controlled morphology and surface roughness," *J. Mater. Sci. Mater. Med.*, 23 2471–2482 (2012).

Journal of Non-Crystalline Solids 402 (2014) 172–177

Contents lists available at ScienceDirect

Journal of Non-Crystalline Solids

journal homepage: www.elsevier.com/ locate/ jnoncrysol

Novel alkali free bioactive fluorapatite glass ceramics

Xiaojing Chen [a], Xiaohui Chen [a,d], Delia S. Brauer [b], Rory M. Wilson [c], Robert G. Hill [a], Natalia Karpukhina [a,*]

[a] Dental Physical Sciences, Institute of Dentistry, Queen Mary University of London, Mile End Road, London E1 4NS, United Kingdom
[b] Otto-Schott-Institut, Friedrich-Schiller-Universität, Fraunhoferstr. 6, Jena 07743, Germany
[c] School of Engineering and Materials Science, Queen Mary University of London, Mile End Road, London E1 4NS, United Kingdom
[d] School of Dentistry, University of Manchester, Coupland 3 Building, Higher Cambridge Street, Machester M15 6FH, United Kingdom

ARTICLE INFO

Article history:
Received 1 April 2014
Received in revised form 15 May 2014
Available online 21 June 2014

Keywords:
Alkali/sodium free;
Fluorapatite;
Strontium;
Fluoride;
MAS–NMR bioactive glass/ceramics

ABSTRACT

Alkali free bioactive glasses with the presence of Ca/SrF_2 were synthesized and then characterised by Differential Scanning Calorimetry, X-ray Diffraction, Fourier Transform Infrared Spectroscopy and Magic Angle Spinning–Nuclear Magnetic Resonance Spectroscopy. The crystallisation of the glasses was explored by heat treatment. An increased crystallisation tendency of the as quenched glasses was evident with an increase in the Ca/SrF_2 content, where $Ca_{10}(PO_4)_6F_2$ (fluorapatite), $Ca_4Si_2O_7F_2$ (cuspidine) and CaF_2 crystallise in sequence for the Ca-containing system, and $Sr_{10}(PO_4)_6F_2$, $SrSiO_3$ and SrF_2 for the Sr-containing system. Upon heat treatment, $Ca_{10}(PO_4)_6F_2$ or $Sr_{10}(PO_4)_6F_2$, which is mainly nucleated from bulk is the primary crystalline phase. Although partially crystallised these sodium free fluorapatite glass ceramics are proposed to have enhanced bioactivity comparable to bioactive glasses.

1. Introduction

Bioactive glasses and glass ceramics with the ability to form apatite-like phases on heat treatment or on being exposed in physiological solution have been used extensively in medicine and dentistry [1,2]. Apatite glass ceramics are attractive as bone fillers and implant materials, as a result of their favourable biocompatibility and osteoconductivity arising from the presence of apatite [3,4]. Kokubo et al. [5] developed an apatite wollastonite (AW) glass ceramics system, which has high mechanical strength and shows good chemical bonding with living tissue. However, as this system surface nucleates, it has to be sintered and then machined to shape, which is unattractive commercially. In addition, the extremely low CaF_2 content (<1 mol%) used in AW formulations results in a restricted amount of fluoride substitution in apatite and mixed oxy-fluorapatite crystals formation [3].

The castable apatite mullite (AM) glass ceramics based on the CaO–Al_2O_3–SiO_2–P_2O_5–CaF_2 system synthesized by Rafferty et al. [6] predominantly bulk nucleate and crystallise to fluorapatite (FAP) and mullite crystals. These bioactive glass ceramics can have high fracture toughness and strength and as a consequence of exhibiting bulk nucleation can be readily cast to shape. Nevertheless, the possibility of toxicity caused by the release of aluminium in vivo is perceived as being problematic for AM glass ceramics.

Brauer and co-workers [7,8] successfully developed two glass ceramic series with different amounts of P_2O_5 in the system of Na_2O–CaO–SiO_2–P_2O_5–CaF_2. Mixed sodium calcium fluoride phosphate, FAP, and combeite ($Na_2Ca_2Si_3O_9$) were found as the main crystalline phases in the glasses with high P_2O_5 content (>4.7 mol%) [7], whilst no FAP crystallised from low P_2O_5 (<1.1 mol%) containing glasses [8]. Brauer et al. also found that a sodium free high P_2O_5 containing bioactive glass composition crystallised to FAP. Thus, it is clear that the crystallisation of apatite from glass is strongly influenced by the phosphate content. The presence of sodium is often considered to be essential for bioactive glasses to achieve bioactivity. However, recently, apatite formation in simulated body fluid was also found for glass and glass ceramics that contain no sodium [9–11]. Furthermore, sodium free formulations of bioactive sol–gel glasses have been known for a long time [12] in addition to recently developed hybrid materials [13]. This suggests that sodium is not an essential component for bioactive glasses and glass ceramics [14–16]. In fact high sodium content can cause undesirable rapid rise in pH and a cytotoxic effect.

Fluorapatite ($Ca_{10}(PO_4)_6F_2$) is analogous to hydroxyapatite ($Ca_{10}(PO_4)_6(OH)_2$; HAP), which is close to the main mineral component of bones and teeth [17,18]. However, FAP is much more stable in acidic environment (pH < 4) compared to HAP, this is extremely favourable in dentistry.

The Sr^{2+} cation is chemically similar to the Ca^{2+} cation but slightly larger in size (effective ionic radius: 1.16 vs 0.94 Å), and therefore it can potentially replace Ca^{2+} in the apatite crystal lattice to form strontium fluoride apatite ($Sr_{10}(PO_4)_6F_2$) [19]. Strontium has the capacity to facilitate enamel remineralisation [20], and the incorporation of strontium into bioactive glasses was reported to promote osteoblast proliferation and reduce osteoclast resorbtion [21,22]. Hence, the strontium containing bioactive glasses are attractive for dental remineralisation and bone regeneration.

* Corresponding author. Tel.: +44 2078825975; fax: +44 2078827089.
E-mail address: n.karpukhina@qmul.ac.uk (N. Karpukhina).

http://dx.doi.org/10.1016/j.jnoncrysol.2014.05.025
0022-3093/

To minimize the disadvantages caused by the presence of sodium and also leverage the benefits by introducing fluoride into glasses, the aim of this paper is to investigate the influence of CaF_2 and SrF_2 content on the crystallisation behaviour of the novel sodium free, high phosphate content bioactive glasses.

2. Materials and methods

2.1. Glass synthesis

Novel sodium free fluoride containing bioactive glasses were designed by introducing CaF_2/SrF_2 into the SiO_2–P_2O_5–CaO ternary glass system (Table 1). Glasses were synthesized by a melt–quench method with analytical grade silica (Prince Minerals Ltd., Stoke-on-Trent, UK), calcium carbonate, phosphorus pentoxide and calcium fluoride or strontium fluoride (all Sigma-Aldrich, Gillingham, UK). A 200 g batch was melted in a 300 ml platinum/rhodium crucible for 1 h in an electrical furnace (EHF 17/3, Lenton, UK). The melting temperature was 1550 °C for glasses with 0 and 3 mol% CaF_2 and 1500 °C for the rest. The melted glasses were quenched into cold deionised water to suppress crystallisation. The as quenched granular glass frit was dried overnight and ground into powder by a vibratory mill (Gyro mill, Glen Creston, UK) for 14 min. The resultant powder was sieved through a 45 μm test sieve (Endecotts Ltd, UK) to obtain fine powder.

2.2. Glass characterisation

2.2.1. X-ray diffraction (XRD)

The amorphous state of the glasses synthesised in the present study was characterised by an X'Pert Pro X-ray diffractometer (PANalytical, The Netherlands) with a copper (Ni-filtered Cu-Kα) X-ray source. The XRD patterns of the glasses were recorded between 5 and 70° 2θ with a step size of 0.0334° and a step time of 200.03 s. Phase identification was carried out by using X'Pert HighScore Plus (v2.0, PANalytical, The Netherlands) in conjunction with the ICDD PDF-4 database.

2.2.2. Fourier Transform Infrared Spectroscopy (FTIR)

Attenuated Total Reflectance–Fourier Transform Infrared Spectroscopy (Spectrum GX, Perkin-Elmer, USA) was used to analyse the chemical bonding in the glass powder and heat treated samples. Ten scans were performed for each sample, and the data were collected for wavenumbers from 500 to 1600 cm^{-1}.

2.2.3. Magic Angle Spinning–Nuclear Magnetic Resonance (MAS–NMR)

^{31}P and ^{19}F MAS–NMR were employed to investigate glass structure and crystalline phases by using a 600 MHz (14.1T) Bruker solid state NMR Spectrometer. Experiments were carried out at spinning rates of 18 or 21 kHz and resonance frequencies of 242.9 and 564.7 MHz for ^{31}P and ^{19}F MAS–NMR, respectively. Recycle delay time was 60 s for ^{31}P and 30 s for ^{19}F. Typically 16 or 32 scans were used for ^{31}P, whilst 32 or 64 scans were adopted for ^{19}F MAS–NMR. Chemical shift for ^{31}P and ^{19}F was referenced by using 85% H_3PO_4 and 1 M NaF solution; the latter signal was adjusted to –120 ppm relative to $CFCl_3$.

Table 1
Glass compositions in mol%. GF is used for CaO/CaF_2 series and SF for SrO/SrF_2 series.

Glass code	SiO_2	CaO/SrO	P_2O_5	CaF_2/SrF_2
GF/SF 0.0	38.1	55.5	6.3	0.0
GF/SF 3.0	37.0	53.9	6.1	3.0
GF/SF 4.5	36.4	53.0	6.0	4.5
GF/SF 6.0	35.9	52.2	5.9	6.0
GF/SF 9.3	34.6	50.4	5.7	9.3
GF/SF 13.6	32.9	48.0	5.5	13.6
GF/SF 17.8	31.4	45.7	5.2	17.8
GF/SF 25.5	28.4	41.4	4.7	25.5

2.2.4. Differential Scanning Calorimetry (DSC)

Differential Scanning Calorimetry (DSC) was used to characterise the thermal properties of the glasses. Glass frit or fine powder (50 ± 1 mg) were heated under Nitrogen (60 ml/min^{-1}) at a rate of 20 °C/min from room temperature up to 1100 °C against alumina using a differential scanning calorimeter (DSC 1500 Stanton Redcroft, Rheometric Scientific, UK). Glass transition temperature (T_g) and crystallisation peak temperatures (T_p) of each glasses were then obtained from the recorded DSC trace. The accuracy of all characteristic temperatures obtained and further presented in figures and tables was ± 5 °C.

2.3. Crystallisation behaviour

1 g of fine powder (<45 μm) was compacted into a disc, placed on a platinum foil and heated up at a rate of 20 °C/min from 400 °C to the heat treatment temperature (T_{HT}) in a porcelain furnace (CeramPress, NEY Dental International, USA) without holding. According to the width of the crystallisation peak from the DSC traces, T_{HT} was T_p or approximately 10 °C above T_p. After heat treatment, samples were immediately withdrawn from the furnace and air quenched.

The resulting sintered glass ceramics were then ground into powder and characterised by using XRD, FTIR and NMR. In order to investigate the morphology of the crystalline phases, the heat treated glass ceramics were embedded in resin, polished with a series of silicon carbide grinding paper and finished with 0.3 μm diamond paste (Met Prep Ltd., UK). The polished specimens were gold coated and viewed under a scanning electron microscope (FEI Inspect F, Oxford Instruments, UK) using back-scatter and secondary electron imaging modes.

3. Results

3.1. Glass formation

The XRD patterns of the as quenched sodium free Ca- and Sr-containing glasses are given in Fig. 1a and b. Amorphous halos at 30° 2θ were found in glasses with low CaF_2 content (less than 9.3 mol%), whereas clear diffraction peaks were noticed for higher CaF_2 containing glasses. With an increase in the CaF_2 content (up to 9.3 mol%), additional small features at 25.86°, 32.23° and 33.07° 2θ were evident. These peaks were matched to the major apatite (FAP: 00-034-0011) diffraction lines. However, a minor peak at 31.89° 2θ was seen for glasses with 4.5 and 6.0 mol% CaF_2. A further increase in the CaF_2 content up to 17.8 mol% resulted in the crystallisation of cuspidine ($Ca_4Si_2O_7F_2$, 00-011-0075) with diffraction lines at 26.5° and 29.1°. At the same time, additional lines at 28.28° and 47° 2θ corresponding to fluorite (CaF_2, 00-004-0864) were also found.

The SrF_2-based series demonstrated similar patterns (Fig. 1b). Amorphous halos were exhibited at 29° 2θ in the glass with SrF_2 contents less than 4.5 mol%, and sharp peaks at 26.5°, 27.85°, 30.5° and 31.7° 2θ were observed for glasses with SrF_2 content greater than 4.5 mol%, which were identified with the main diffraction lines of $Sr_{10}(PO_4)_6F_2$ (00-050-1744). With increasing SrF_2 content up to 13.6 mol%, peaks corresponding to $SrSiO_3$ (00-034-0099) appeared at 24.95° and 43.9° 2θ. Furthermore, additional peaks at 43.19° and 52.23° in the XRD patterns of 17.8 and 25.5 mol% SrF_2 glasses were matched to the characteristic diffraction peaks of SrF_2 (00-001-0644). The crystalline phases identified in both glass series are summarised in Table 2.

FTIR spectra of the as quenched CaF_2 containing glasses (Fig. 2a) show the typical non-bridging oxygen band and Si–O–Si stretch band at 920 and 1030 cm^{-1} for the whole series. In addition, a small band around 600 cm^{-1} was noticed in the glasses with CaF_2 content lower

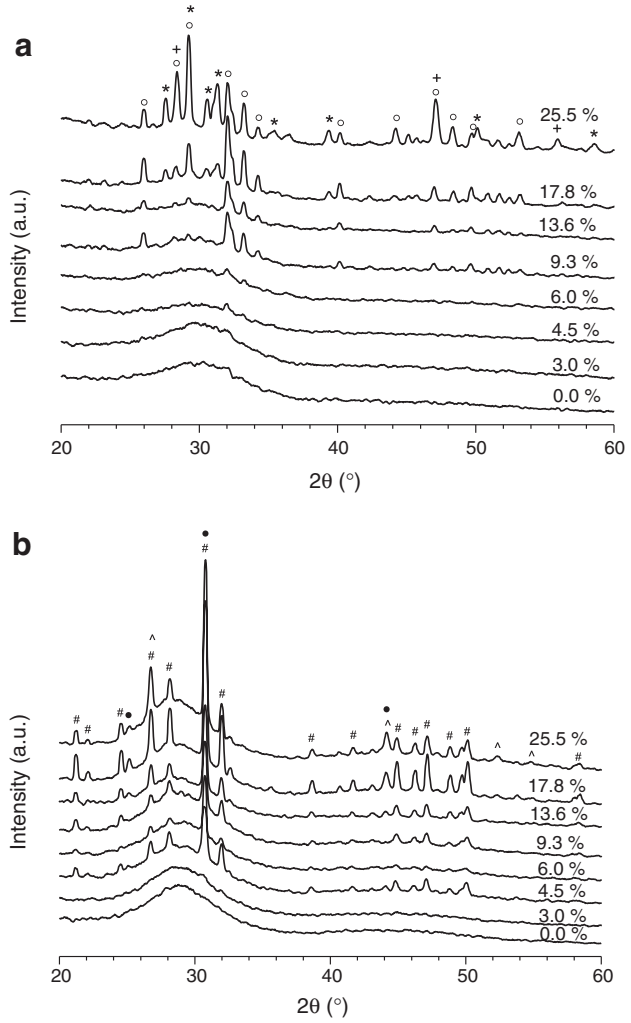

Fig. 1. XRD patterns of the as quenched glasses. (a) CaF_2-based glasses (°: $Ca_{10}(PO_4)_6F_2$; *: $Ca_4Si_2O_7F_2$; $^+$: CaF_2); (b) SrF_2 glasses ($^\#$: $Sr_{10}(PO_4)_6F_2$; ^: SrF_2; $^\bullet$: $SrSiO_3$). The numbers are nominal molar percentage of the CaF_2/SrF_2 in the compositions.

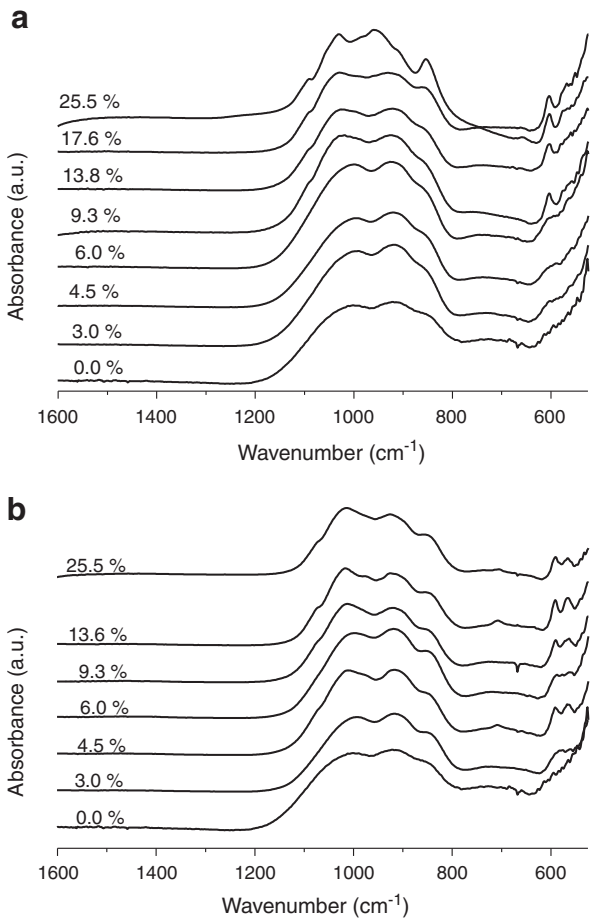

Fig. 2. FTIR spectra of the as quenched glasses. (a) CaF_2 glasses; (b) SrF_2 glasses. The numbers are nominal molar percentage of the CaF_2/SrF_2 in the compositions.

than 9.3 mol%, whilst the characteristic apatite split bands at 560 and 613 cm^{-1} were visible with an increase in CaF_2 content [23]. The spectrum of the Ca-containing glass with 25.5 mol% of CaF_2 was characterised with distinctly sharp band features in the region 800–1050 cm^{-1} indicating presence of silicate crystalline phase [24].

SrF_2 containing glasses demonstrated a similar trend as CaF_2 series (Fig. 2b). However, the typical apatite split bands at 595 cm^{-1} and 555 cm^{-1} were first recognised in the strontium series with 4.5 mol% SrF_2 content. At the same time the spectra of the glasses with high fluoride content clearly showed presence of a silicate crystalline phase.

^{31}P and ^{19}F MAS–NMR were used to characterise the atomic environment of phosphate and fluoride in the glasses. Fig. 3a shows the ^{31}P MAS–NMR spectra of CaF_2 containing bioactive glasses and glass ceramics. Broad peaks with a centre at 3 ppm, corresponding to amorphous calcium orthophosphate, are found in the spectra of low CaF_2 containing glasses. In addition, with an increasing amount of CaF_2 the linewidth of the peak reduced, but without changing the peak position. This suggests that glasses tend to partially crystallise to calcium orthophosphate of which, apatite is an example, which leads to a reduction in the linewidth of the ^{31}P NMR signal.

Three types of fluoride environment were presented by ^{19}F MAS–NMR spectra in Fig. 3b. The glasses with low CaF_2 content have broad peaks with a centre at about −96 ppm, whilst a tiny but sharp peak at −103 ppm, corresponding to fluorapatite is found on the shoulder of a broad glass signal in the glasses with CaF_2 content over 9.3 mol%. Furthermore, an asymmetric and sharp peak at −108 ppm of the chemical shift is obvious in the spectrum of the 25.5 mol% CaF_2 containing glass, indicating the crystallisation of CaF_2.

Table 2
The summary of crystalline phases identified from XRD patterns.

Glasses	Crystallisation phases	Glasses	Crystallisation phases
GF 0.0	Amorphous	SF 0.0	Amorphous
GF 3.0		SF 3.0	
GF 4.5		SF 4.5	
GF 6.0	$Ca_{10}(PO_4)_6F_2$	SF 6.0	$Sr_{10}(PO_4)_6F_2$
GF 9.3		SF 9.3	
GF 13.6		SF 13.6	$Sr_{10}(PO_4)_6F_2$, $SrSiO_3$
GF 17.8	$Ca_{10}(PO_4)_6F_2$, $Ca_4Si_2O_7F_2$, CaF_2	SF 17.8	$Sr_{10}(PO_4)_6F_2$, $SrSiO_3$, SrF_2
GF 25.5		SF 25.5	

3.2. Thermal properties

The glass transition temperature and crystallisation peak temperatures for both glass powder and frit are summarised and listed in Tables 3 and S1 (Supplemental material). Some of the compositions had more than one exotherm. The corresponding crystallisation peak temperatures, of the first (T_{p1}), second (T_{p2}), third (T_{p3}) and fourth (T_{p4}) exotherms were defined from the DSC traces. Particle size had no significant effect on T_g and some of the crystallisation temperatures, which result in close values for T_g, T_{p1} and some of the T_{p2} and T_{p3} values. However, some crystallisation peak temperatures of coarse

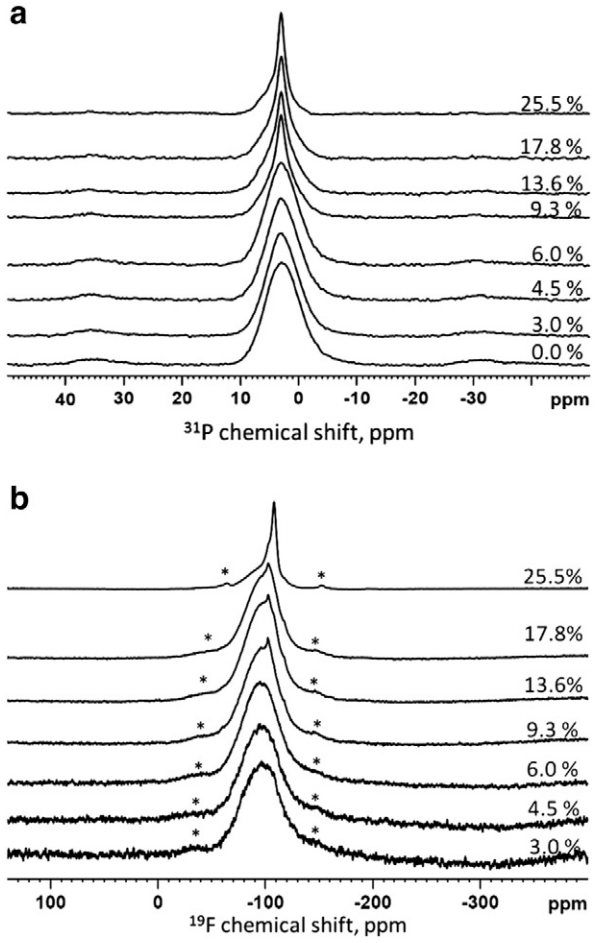

Fig. 3. (a) ^{31}P MAS–NMR and (b) ^{19}F MAS–NMR spectra of CaF_2-based glasses. The asterisk shows the spinning side bands. The numbers are nominal molar percentage of the CaF_2 in the compositions.

particles (frit) are higher than the equivalent fine powder, which were highlighted in Table 3.

As shown in Fig. 4, the glass transition temperature and first crystallisation peak temperature showed a similar trend, both reducing with increasing CaF_2 or SrF_2 content. Comparing T_g and T_{p1} of the two glass series, the T_{p1} values for the SrF_2 glasses are much lower (30–70 °C) than the equivalent ones for the CaF_2 series, though the T_g values were about the same.

3.3. Crystallisation behaviour

XRD results of heat treated glasses GF 3.0 and GF 25.5 are presented in Fig. 5. For GF 3.0 after heat treatment at T_{p1} (867 °C), sharp diffraction

Table 3
Characteristic temperature of glass powder (<45 μm) for fluoride containing glasses. The glasses mainly nucleated form surface are highlighted in bold.

XF_2 (mol%)	Glass powder (CaF_2 series)				Glass powder (SrF_2 series)				
	T_g (°C)	T_{p1}	T_{p2}	T_{p3}	T_g (°C)	T_{p1}	T_{p2}	T_{p3}	T_{p4}
GF 0.0	790	**925**	–	–	783	918	1042	–	–
GF 3.0	735	867	888	979	735	821	**862**	**955**	848
GF 4.5	722	860	–	–	706	801	**827**	**918**	–
GF 6.0	693	817	**844**	942	680	778	**795**	**859**	–
GF 9.3	655	780	**806**	**878**	657	744	–	862	–
GF 13.6	618	732	758	977	618	705	**716**	853	–
GF 17.8	601	720	–	–	–	–	–	–	–
GF 25.5	558	713	–	–	562	638	699	713	847

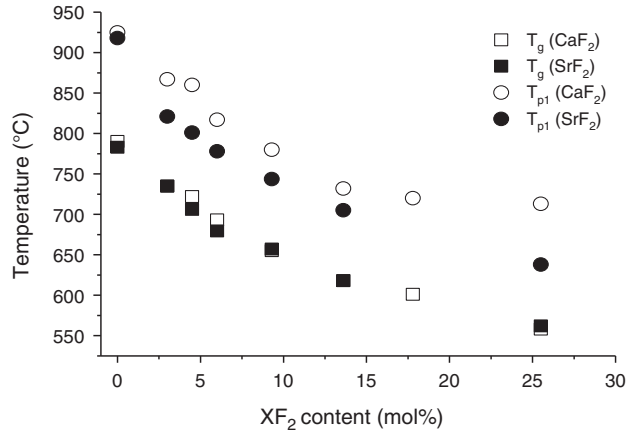

Fig. 4. Glass transition temperature (T_g) and first crystallisation peak temperature (T_{p1}) of fine powder against fluoride content. The accuracy of the defined temperature values is ±5 °C.

lines corresponding to apatite develop, and there is a trace of wollastonite present as well. Interestingly no new crystalline phases were found for the heat treatments at the higher temperatures. The partially crystallised glass GF 25.5, that already contains apatite, cuspidine and fluorite shows increase in diffraction line intensity of in particular cuspidine and fluorite indicating further crystallisation on heat treatment at 713 °C. The crystal phases formed on heat treatment of the glasses are presented in Table 4. Fig. S1 (Supplemental material) shows the XRD pattern of GF 0.0 heat treated at 1030 °C. Compared to

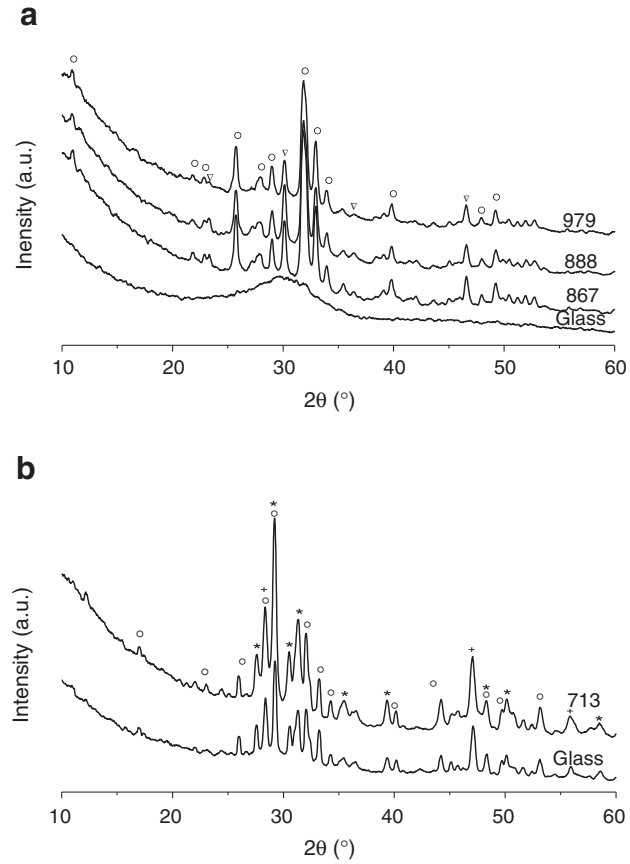

Fig. 5. XRD patterns of (a) GF 3.0 and (b) GF 25.5 as-quenched and heat treated at different temperatures. (∇: $CaSiO_3$, o: $Ca_{10}(PO_4)_6F_2$; *: $Ca_4Si_2O_7F_2$; +: CaF_2). The numbers are heat treatment temperature.

Table 4
Summary of phases crystallising on heat treatment. β-$CaSiO_3$: pseudowollastonite, $Ca_{10}(PO_4)_6(OH)_2$: hydroxyapatite, $Ca_{10}(PO_4)_6F_2$: fluorapatite, $CaSiO_3$: wollastonite-2M, $CaSiO_3$ (hexagonal): wollastonite-1A, $Ca_4Si_2O_7F_2$: cuspidine, CaF_2: fluorite, $SrSiO_3$: strontium silicate, $Sr_{10}(PO_4)_6F_2$: strontium phosphate fluoride and SrF_2: strontium fluoride.

Glasses	T_{HT} (°C)	Crystalline Phases
GF 0.0	1030	β-$CaSiO_3$ and $Ca_{10}(PO_4)_6(OH)_2$
GF 3.0	867	$Ca_{10}(PO_4)_6F_2$ and $CaSiO_3$
	888	
	979	
GF 4.5	860	
GF 6.0	817	
	844	
	942	$Ca_{10}(PO_4)_6F_2$ and $CaSiO_3$ (hexagonal)
GF 9.3	780	$Ca_{10}(PO_4)_6F_2$
	806	$Ca_{10}(PO_4)_6F_2$ and $Ca_4Si_2O_7F_2$
	878	
GF 13.6	732	
	758	
	977	
GF 17.8	720	$Ca_{10}(PO_4)_6F_2$, $Ca_4Si_2O_7F_2$ and CaF_2
GF 25.5	713	
SF 3.0	1040	$SrSiO_3$ and $Sr_{10}(PO_4)_6F_2$
SF 4.5	860	
	1000	
SF 6.0	830	$SrSiO_3$, $Sr_{10}(PO_4)_6F_2$ and SrF_2
	960	

the amorphous halo of the initial glass, distinct diffraction lines, which match with hydroxyapatite and pseudowollastonite are evidenced.

4. Discussion

4.1. Glass formation

XRD patterns, FTIR and NMR spectra all demonstrated that the low fluoride content glasses were amorphous, but the glasses with higher CaF_2 (≥9.3 mol%) and SrF_2 (≥4.5 mol%) content were partially crystallised to FAP ($Ca_{10}(PO_4)_6F_2$, and $Sr_{10}(PO_4)_6F_2$). The GF 13.6 glass crystallised to FAP and cuspidine. Crystalline CaF_2 and SrF_2 were found in addition on increasing the fluoride content to over 17.8 mol% CaF_2 and 13.6 mol% SrF_2, respectively. Interestingly, based on XRD results, the highest CaF_2 content (25.5 mol%) glass demonstrated a pronounced increase in the intensity of the diffraction lines corresponding to cuspidine, and this increase was at the expense of the intensity of the lines corresponding to FAP compared with the GF 17.8.

The SrF_2 containing glasses had a higher tendency to crystallise than CaF_2 ones. This can be attributed to the more expanded glass structure causing by the larger size of Sr^{2+} [22,25].

^{31}P MAS–NMR spectra suggest that in the sodium free fluoride containing bioactive glasses and glass ceramics, phosphorus is present as a calcium orthophosphate. ^{19}F MAS–NMR confirmed the presence of amorphous F–Ca(n) species and also identified spontaneous FAP (F–Ca(3)) crystallisation in the glasses with over 9.3 mol% CaF_2 content on quenching, whilst CaF_2 with a F–Ca(4) environment crystallised spontaneously from the glass with 25.5 mol% CaF_2.

Cuspidine has been found to crystallise from sodium and fluoride-containing bioactive glasses [8], glasses in the CaO–CaF_2–SiO_2 system [26,27] and mould-flux glasses [28]. Our study suggests that for glasses in the CaO–CaF_2–P_2O_5–SiO_2 system with a constant SiO_2:CaO:P_2O_5 molar ratio of 6:8.8:1, an increase in the CaF_2 content leads to an increased crystallisation tendency, where FAP, cuspidine and CaF_2 crystallise sequentially. At moderate fluoride content (at 9.3 mol%) only FAP forms in the as quenched glass, with increasing in fluoride content, two fluoride containing phases are present in the as quenched glass, i.e. FAP and cuspidine. The glasses with the highest fluoride content have all three fluoride containing phases.

The minute amount of apatite seen in the ground glass powders with the lowest fluoride content is due to the reaction with atmospheric moisture.

4.2. Thermal properties

Owing to fluoride complexing calcium, glass transition and crystallisation temperatures decreased markedly with increasing CaF_2/SrF_2 content (0 to 25.5 mol%) [8]. In the fluoride free glass (0 mol%), divalent calcium ions bind together silicate anions by electrostatic forces and the calcium ions effectively act as ionic bridges between two non-bridging oxygens (NBOs). When CaF_2/SrF_2 is added, hypothetical 'CaF^+'/'SrF^+' species are formed, and the electrostatic forces between NBOs are reduced considerably, resulting in a decrease in T_g [8,29]. The effect of CaF_2/SrF_2 on T_g was less pronounced at high fluoride content (Fig. 4). This could be attributed to the crystallisation of fluoride containing phases (such as FAP and CaF_2/SrF_2) in the as quenched glasses. However, as Sr^{2+} is larger in size compared to Ca^{2+}, it is thought to expand the glass network more [22,25], resulting in a less stable glass which crystallises more readily and at a lower temperature.

The glass transition temperature of the fluoride free glass (0 mol%, 790 °C) was considerably higher than that of the equivalent soda containing glass (ICSW9, 491 °C) studied by O'Donnell et al. [30]. This can be explained by differences in cross-linking. Owing to Ca^{2+} being replaced for two Na^+ (i.e. a reduced charge-to-size ratio of the modifier cation), ionic cross-linking between NBOs of neighbouring silicate chains is reduced, and as a consequence T_g increases. T_g is determined by the strength of the bonding in the glass and is also known to correlate with degradability and hardness of glasses [31]. In the absence of sodium, the addition of fluoride is particularly beneficial since fluoride decreases T_g and melting temperature in a similar fashion, facilitates melting and is expected to reduce glass hardness.

In Tables 3 and S1 (Supplemental material), the similar first crystallisation peak temperatures (T_{p1}) of powder and frit indicate that in the CaF_2 and SrF_2 containing glasses the first crystalline phases, which are believed to be $Ca_{10}(PO_4)_6F_2$ or $Sr_{10}(PO_4)_6F_2$, respectively, are mainly nucleated from bulk. Whilst T_{p1} of the frit is higher than fine powder for GF 0.0 (fluoride free), this is ascribed to wollastonite, which is a phase known to strongly surface nucleate. The second or third crystallisation phases of some compositions are also strongly nucleating from the surface. They are highlighted in Table 3. Compared with frit, fine powder has larger surface area, which provides more nucleation sites for crystallisation. Therefore fine powder is prone to crystallise at a lower temperature [32]. In contrast, when the crystallisation peak temperature is independent of particle size, then this may indicate bulk nucleation.

Crystallisation of a bioactive glass has been shown to reduce its bioactive properties [33] as the crystalline phases are generally more stable than the equivalent glass phase and generally crystallisation results in a residual glass phase with a higher network connectivity (NC). However, in the present glasses, crystals of FAP ($Ca_{10}(PO_4)_6F_2$ and $Sr_{10}(PO_4)_6F_2$) are able to serve as nuclei for the further growth of the apatite phase, which may therefore increase its bioactivity. In addition, the apatite formation will not result in a less reactive residual silicate glass since the NC of the glass will remain unchanged. The bioactivity of these glasses and glass-ceramics has been presented and discussed in a separate report [34].

4.3. Glass heat treatment

Two or three crystal phases were typically found upon heat treatment. The first was apatite, which is thought to be HAP, presenting as a hexagonal-like morphology in the fluoride free composition. Pseudowollastonite (β-$CaSiO_3$) also formed at the heat treatment temperature of 1030 °C (Fig. S1, Supplemental material). It is surprising that

an apatite was formed in the absence of fluoride since in AM glass ceramics, apatite only forms when fluoride is present [6]. It may be that the apatite formed is an oxyapatite which transforms to HAP by reaction with atmospheric water. The crystallisation peak observed for this composition was broad and is probably a result of the overlapping of apatite and pseudowollastonite crystallisation events.

GF 3.0 crystallised to FAP with an elongated and interlocking crystal structure (dendritic) (Fig. S2, Supplemental material) at 888 °C with coexisting FAP and wollastonite phases. All the heat treated samples of 4.5 and 6.0 mol% CaF_2 containing glasses crystallised to FAP and wollastonite. The heat treatment temperatures are too high to see the crystallisation of FAP without wollastonite. The wollastonite phase was expected on the grounds that the residual glass phase following crystallisation of FAP would have a Q structure close to Q^2 and also close to the stoichiometry of wollastonite.

FAP, cuspidine and CaF_2 are found as crystalline phases in the glasses with over 6 mol% CaF_2 following heat treatment. It is worth noting that in these series of glasses the Q structure did not change on crystallisation and remained at 2.08 (NC) irrespective of how much apatite crystallises. Cuspidine and CaF_2 are phosphate free crystalline phases and therefore should not restrict bioactivity. This is an attractive feature of these glasses and glass ceramics, since the essentially Q^2 speciation of the amorphous structure part will confer bioactivity. In addition, the presence of FAP is also extremely desirable and FAP glass ceramics have demonstrated excellent osseointegration [35]. The FAP may also provide seed crystals for the formation of more apatite as the Q^2 residual glass phase dissolves in body fluids. These glass ceramics combine the beneficial effects of a bioactive glass phase and the FAP crystals.

5. Conclusion

This study revealed that novel sodium free low fluoride content ($CaF_2 < 9.3$ mol% and $SrF_2 < 4.5$ mol%) bioactive glasses can be obtained in an amorphous state. Bioactive glasses with high fluoride content ($CaF_2 \geq 9.3$ mol% and $SrF_2 \geq 4.5$ mol%) crystallised spontaneously to fluorapatite during quenching, whilst CaF_2 and SrF_2 were found in the glasses with 17.8 and 25.5 mol% fluoride. Fluorapatite crystallised from all glasses upon heat treatment. An addition of fluoride into bioactive glasses leads to a dramatic reduction in T_g and T_{p1}. In order to obtain the glass ceramics for dental applications which show FAP as the only crystal phase, large crystallisation windows and optimised fluoride content (about 6.0 mol% CaF_2 and 4.5 mol% SrF_2) are required.

Appendix A. Supplementary data

Supplementary data to this article can be found online at http://dx.doi.org/10.1016/j.jnoncrysol.2014.05.025.

References

[1] L.L. Hench, Glass and glass-ceramic technologies to transform the world, Int. J. Appl. Glas. Sci. 2 (2011) 162–176.
[2] W. Höland, G.H. Beall, Glass-Ceramic Technology, 2nd ed. American Ceramic Society, 2012.
[3] A. Calver, R.G. Hill, A. Stamboulis, Influence of fluorine content on the crystallization behavior of apatite–wollastonite glass-ceramics, J. Mater. Sci. 39 (2004) 2601–2603.
[4] C.O. Freeman, I.M. Brook, A. Johnson, P.V. Hatton, R.G. Hill, K.T. Stanton, Crystallization modifies osteoconductivity in an apatite–mullite glass-ceramic, J. Mater. Sci. Mater. Med. 14 (2003) 985–990.
[5] T. Kokubo, M. Shigematsu, Y. Nagashima, M. Tashiro, T. Nakamura, T. Yamamuro, S. Higashi, Apatite- and wollastonite-containing glass-ceramics for prosthetic application, Bull. Inst. Chem. Res. Kyoto Univ. 60 (1982) 260–268.
[6] A. Rafferty, A. Clifford, R. Hill, D. Wood, B. Samuneva, M. Dimitrova-Lukacs, Influence of fluorine content in apatite–mullite glass-ceramics, J. Am. Ceram. Soc. 83 (2000) 2833–2838.
[7] D.S. Brauer, M.N. Anjum, M. Mneimne, R.M. Wilson, H. Doweidar, R.G. Hill, Fluoride-containing bioactive glass-ceramics, J. Non-Cryst. Solids 358 (2012) 1438–1442.
[8] D.S. Brauer, N. Karpukhina, R.V. Law, R.G. Hill, Structure of fluoride-containing bioactive glasses, J. Mater. Chem. 19 (2009) 5629–5636.
[9] X.J. Chen, R.G. Hill, M. Mneimne, D.S. Brauer, R.M. Wilson, R.V. Law, N. Karpukhina, Sodium is not essential for high bioactivity of glasses, 12th International Conference on the Structure of the Non-Crystalline Materials, Riva Del Garda - Italy, 2013, p. 72.
[10] M. Mneimne, R.G. Hill, A.J. Bushby, D.S. Brauer, High phosphate content significantly increases apatite formation of fluoride-containing bioactive glasses, Acta Biomater. 7 (2011) 1827–1834.
[11] D.S. Brauer, N. Karpukhina, M.D. O'Donnell, R.V. Law, R.G. Hill, Fluoride-containing bioactive glasses: effect of glass design and structure on degradation, pH and apatite formation in simulated body fluid, Acta Biomater. 6 (2010) 3275–3282.
[12] D. Arcos, M. Vallet-Regi, Sol–gel silica-based biomaterials and bone tissue regeneration, Acta Biomater. 6 (2010) 2874–2888.
[13] J.R. Jones, Review of bioactive glass: from Hench to hybrids, Acta Biomater. 9 (2013) 4457–4486.
[14] A. Goel, S. Kapoor, R.R. Rajagopal, M.J. Pascual, H.W. Kim, J.M. Ferreira, Alkali-free bioactive glasses for bone tissue engineering: a preliminary investigation, Acta Biomater. 8 (2012) 361–372.
[15] I. Kansal, A. Goel, D.U. Tulyaganov, R.R. Rajagopal, J.M.F. Ferreira, Structural and thermal characterization of CaO–MgO–SiO2–P2O5–CaF2 glasses, J. Eur. Ceram. Soc. 32 (2012) 2739–2746.
[16] D.S. Brauer, R.G. Hill, M.D. O'Donnell, Crystallisation of fluoride-containing bioactive glasses, Phys. Chem. Glasses Eur. J. Glass Sci. Technol. B 53 (2012) 27–30.
[17] K. Inoue, K. Sassa, Y. Yokogawa, Y. Sakka, M. Okido, S. Asai, Control of crystal orientation of hydroxyapatite by imposition of a high magnetic field, Mater. Trans. JIM 44 (2003) 1133–1137.
[18] A. Nanci, Ten Cate's Oral Histology-Pageburst on VitalSource: Development, Structure, and Function, Elsevier Health Sciences, 2007.
[19] R.G. Hill, A. Stamboulis, R.V. Law, A. Clifford, M.R. Towler, C. Crowley, The influence of strontium substitution in fluorapatite glasses and glass-ceramics, J. Non-Cryst. Solids 336 (2004) 223–229.
[20] T.T. Thuy, H. Nakagaki, K. Kato, P.A. Hung, J. Inukai, S. Tsuboi, H. Nakagaki, M.N. Hirose, S. Igarashi, C. Robinson, Effect of strontium in combination with fluoride on enamel remineralisation in vitro, Arch. Oral Biol. 53 (2008) 1017–1022.
[21] P.J. Marie, M. Hott, D. Modrowski, C. De Pollak, J. Guillemain, P. Deloffre, Y. Tsouderos, An uncoupling agent containing strontium prevents bone loss by depressing bone resorption and maintaining bone formation in estrogen-deficient rats, J. Bone Miner. Res. 20 (2005) 1065–1074 (Reprinted from vol 8, pg 607–615, 1993).
[22] Y.C. Fredholm, N. Karpukhina, D.S. Brauer, J.R. Jones, R.V. Law, R.G. Hill, Influence of strontium for calcium substitution in bioactive glasses on degradation, ion release and apatite formation, J. R. Soc. Interface 9 (2012) 880–889.
[23] D.S. Brauer, M. Mneimne, R.G. Hill, Fluoride-containing bioactive glasses: Fluoride loss during melting and ion release in tris buffer solution, J.Non-Cryst. Solids 357 (2011) 3328–3333.
[24] C. Paluszkiewicz, M. Blazewicz, J. Podporska, T. Gumula, Nucleation of hydroxyapatite layer on wollastonite material surface: FTIR studies, Vib. Spectrosc. 48 (2008) 263–268.
[25] Y.C. Fredholm, N. Karpukhina, R.V. Law, R.G. Hill, Strontium containing bioactive glasses: glass structure and physical properties, J. Non-Cryst. Solids 356 (2010) 2546–2551.
[26] T. Watanabe, M. Hayashi, S. Hayashi, H. Fukuyama, K. Nagata, Solid-state ^{19}F NMR on CaO–SiO2–CaF2 glasses, VII International Conference on Molten Slags Fluxes and Salts, The South African Institute of Mining and Metallurgy, 2004.
[27] T. Watanabe, H. Fukuyama, M. Susa, K. Nagata, Phase diagram cuspidine (3CaO center dot 2SiO(2) center dot CaF_2)–CaF_2, Metall. Mater. Trans. B Process Metall. Mater. Process. Sci. 31 (2000) 1273–1281.
[28] R.G. Hill, N. Da Costa, R.V. Law, Characterization of a mould flux glass, J. Non-Cryst. Solids 351 (2005) 69–74.
[29] M. Hayashi, N. Nabeshima, H. Fukuyama, K. Nagata, Effect of fluorine on silicate network for CaO–CaF_2–SiO_2 and CaO–CaF_2–SiO_2–FeOx glasses, ISIJ Int. 42 (2002) 352–358.
[30] M.D. O'Donnell, S.J. Watts, R.V. Law, R.G. Hill, Effect of P_2O_5 content in two series of soda lime phosphosilicate glasses on structure and properties – Part II: Physical properties, J. Non-Cryst. Solids 354 (2008) 3561–3566.
[31] M.D. O'Donnell, Predicting bioactive glass properties from the molecular chemical composition: glass transition temperature, Acta Biomater. 7 (2011) 2264–2269.
[32] A. Al-Noaman, S.C.F. Rawlinson, R.G. Hill, The role of MgO on thermal properties, structure and bioactivity of bioactive glass coating for dental implants, J. Non-Cryst. Solids 358 (2012) 3019–3027.
[33] O. Peitl, G.P. LaTorre, L.L. Hench, Effect of crystallization on apatite-layer formation of bioactive glass 45S5, J. Biomed. Mater. Res. 30 (1996) 509–514.
[34] X.J. Chen, X.H. Chen, D.S. Brauer, R.M. Wilson, R.G. Hill, N. Karpukhina, Bioactivity of sodium free fluoride containing glasses and glass-ceramics, Materials 7 (2014) (submitted for publication).
[35] C.O. Freeman, I.M. Brook, A. Johnson, R.G. Hill, P.V. Hatton, Osseointegration of novel ionomeric glass-ceramics, J. Dent. Res. 79 (2000) 1184-1184.

Materials **2014**, *7*, 5470-5487; doi:10.3390/ma7085470

OPEN ACCESS

materials

ISSN 1996-1944

www.mdpi.com/journal/materials

Article

Bioactivity of Sodium Free Fluoride Containing Glasses and Glass-Ceramics

Xiaojing Chen [1], Xiaohui Chen [1], Delia S. Brauer [2], Rory M. Wilson [3], Robert G. Hill [1] and Natalia Karpukhina [1,*]

[1] Dental Physical Science, Institute of Dentistry, Barts and the London School of Medicine and Dentistry, Queen Mary University of London, Mile End Road, London E1 4NS, UK; E-Mails: xiaojing.chen@qmul.ac.uk (Xiaoj.C.); xiaohui.chen@qmul.ac.uk (Xiaoh.C.); r.hill@qmul.ac.uk (R.G.H.)

[2] Otto-Schott-Institut, Friedrich-Schiller-Universität, Fraunhoferstr. 6, Jena 07743, Germany; E-Mail: delia.brauer@uni-jena.de

[3] School of Engineering and Materials Sciences, Queen Mary University of London, Mile End Road, London E1 4NS, UK; E-Mail: r.m.wilson@qmul.ac.uk

* Author to whom correspondence should be addressed; E-Mail: n.karpukhina@qmul.ac.uk; Tel.: +44-020-7882-5975; Fax: +44-020-7882-7089.

Received: 14 May 2014; in revised form: 16 July 2014 / Accepted: 18 July 2014 / Published: 25 July 2014

Abstract: The bioactivity of a series of fluoride-containing sodium-free calcium and strontium phosphosilicate glasses has been tested *in vitro*. Glasses with high fluoride content were partially crystallised to apatite and other fluoride-containing phases. The bioactivity study was carried out in Tris and SBF buffers, and apatite formation was monitored by XRD, FTIR and solid state NMR. Ion release in solutions has been measured using ICP-OES and fluoride-ion selective electrode. The results show that glasses with low amounts of fluoride that were initially amorphous degraded rapidly in Tris buffer and formed apatite as early as 3 h after immersion. The apatite was identified as fluorapatite by ^{19}F MAS-NMR after 6 h of immersion. Glass degradation and apatite formation was significantly slower in SBF solution compared to Tris. On immersion of the partially crystallised glasses, the fraction of apatite increased at 3 h compared to the amount of apatite prior to the treatment. Thus, partial crystallisation of the glasses has not affected bioactivity significantly. Fast dissolution of the amorphous phase was also indicated. There was no difference in kinetics between Tris and SBF studies when the glass was partially

crystallised to apatite before immersion. Two different mechanisms of apatite formation for amorphous or partially crystallised glasses are discussed.

Keywords: sodium-/alkali-free bioactive glass; bioactive glass-ceramics; fluorapatite; fluoride

1. Introduction

The bioactivity of glasses and ceramics is often investigated on immersion of the solid in a buffer solution simulating physiological fluids. Formation of an apatite-like layer on the surface of the solid as a result of the reaction with fluid is then evaluated. This laboratory procedure has a number of drawbacks and cannot be used directly for predicting the bioactivity of the same solid *in vivo* [1,2]. However, testing apatite formation in buffer solution is a useful inexpensive model for comparative evaluation of the bioactive glasses and bioceramics of different formulations in order to preselect compositions with potentially the most promising biological activity.

The earliest immersion time when apatite can be identified is typically used as a measure of bioactivity. However, the rate and ability of bioceramics to form apatite is dependent on the type of physiological buffer used even when the same formulation of bioceramics or glass is tested. In particular, concentrations of calcium and phosphate available in solution as well as the presence of other species affect the rate of apatite formation. The composition of the simulated body fluid (SBF) solution is close to the saturation level of apatite [2]. Therefore, potentially any surface exposed to SBF can aid precipitation of apatite irrespective of whether it is bioactive or not. On the other hand, only calcium- and phosphate-rich bioceramics and glasses can be tested for bioactivity in Tris buffer solution, owing to apatite precipitation following the initial release of these components from the solid into solution.

Alkali- or specifically sodium-containing bioactive glasses generate a high alkaline pH that can cause a cytotoxic cells response [3]. Although plenty of alkali-free bioceramics [4,5] based on calcium-rich crystalline phases have been studied including phosphates [6], carbonates [7] and silicates [8,9], there are only few reports on alkali-free bioactive glasses [10–16]. The majority of the available sodium-free bioactive glasses are of sol-gel origin [17–22], and the nominal composition of these glasses cannot be directly compared with melt-derived glasses owing to the presence of substantial amounts of, if not water, then hydroxyl groups in the glass. In a report where exclusively sodium-free melt-derived glasses were studied, the bioactivity of the glasses was clearly inhibited owing to the presence of significant amounts of MgO in the composition [12].

Typically, the rate of apatite formation is lower for ceramics than for amorphous glasses, as a crystalline solid has a lower dissolution rate and thus would be expected to exhibit lower bioactivity than an amorphous glass of a bioactive-type composition. For instance, sintered apatite bioceramics dissolves slower than apatite resulting from the degradation of bioactive glass [23]. Sintered glass exhibits a bioactivity lower than the one before sintering [24]. Moreover, partial crystallisation often occurs during sintering, for instance with 45S5, which will further decrease the reactivity of the glass [25–27].

Recent success in fluoride-containing bioactive glasses showed that there is a concentration limit for fluoride to be added to the glass before spontaneous crystallisation occurs [10,11,28–30]. This is owing to the known effect of fluoride destabilising glass against crystallisation [31]. It is also known that the type of the fluoride-containing crystalline phase is dependent on the composition of the glass. For example, in low phosphate content bioactive glasses, calcium fluoride crystallises out [32]. An increase in phosphate content caused formation of apatite in the glasses [33].

In the present study, the design of glasses is typical for bioactive compositions [34,35] and it is such that the silicate component is present mostly as chains [32,36,37], while fluoride is coordinated by calcium [38] and phosphate is present as orthophosphate [32,36]. Partial crystallisation of an apatite phase should not involve the silicate chain domains [32,33,38,39], and these will still remain amorphous, which means the silicate phase would still continue to dissolve rapidly. In addition, apatite crystals pre-formed in the system can minimise the nucleation energy via providing their surface for further precipitation and growth of the apatite crystals. Although apatite-containing systems have been known before, none of the bioactivity studies considered this in combination with a reactive glass phase. We propose that the bioactivity of these glasses will not be significantly affected by partial crystallisation of the glasses.

Thus, the aim of this paper is to investigate the bioactivity of sodium-free amorphous or partially crystallised glasses and compare the bioactivity of the two.

2. Results and Discussion

2.1. Apatite Formation

2.1.1. X-ray Diffraction (XRD) Results

XRD results of four compositions after immersion in Tris and SBF solutions are presented in Figure 1a–h. The compositions with 3 mol% CaF_2 and SrF_2 were amorphous as quenched, whereas compositions with 9.3 mol% CaF_2 and SrF_2 were partially crystallised upon quenching.

In Figure 1a,b, clear characteristic apatite peaks developed at 25.9° and 31.8° 2θ after short immersion times. The intensities of these diffraction lines increased with immersion time. However, it is seen that the intensities grew more rapidly in Tris buffer compared to SBF. The presence of significant amounts of apatite is revealed in the XRD patterns after immersion in Tris between 3 and 9 h, whereas a similar intensity of the apatite diffraction lines is seen after immersion in SBF for 3 days only. Immersions for durations longer than 9 h in Tris and 3 days in SBF did not reflect significant changes on the XRD patterns. Similar results were obtained for compositions with 0, 4.5, and 6 mol% CaF_2 (not shown).

Glasses with higher CaF_2 content that had partially crystallised to mainly fluorapatite (FAP) also exhibited bioactivity. As seen from Figure 1c,d, the intensity of apatite peaks increased after immersion compared to the non-immersed glass. However, there was no significant difference in the intensity of the apatite diffraction lines obtained after immersion in Tris and SBF for the same time period. It is clearly seen that the apatite diffraction lines are significantly broader for the compositions with low CaF_2 content (Figure 1a,b) than for the compositions with high CaF_2 content (Figure 1c,d) owing to the presence of crystalline FAP in the untreated glasses with high CaF_2 content.

Figure 1. XRD patterns of glasses after immersion in buffer solutions: (**a**) GF 3.0 in Tris; (**b**) GF 3.0 in SBF; (**c**) GF 9.3 in Tris; (**d**) GF 9.3 in SBF; (**e**) SF 3.0 in Tris; (**f**) SF 3.0 in SBF; (**g**) SF 9.3 in Tris; (**h**) SF 9.3 in SBF. Label Ap in CaF_2 series is fluorapatite $Ca_5(PO_4)_3F$ (00-034-0011), and strontium fluorapatite $Sr_5(PO_4)_3F$ in SrF_2 series (00-050-1744).

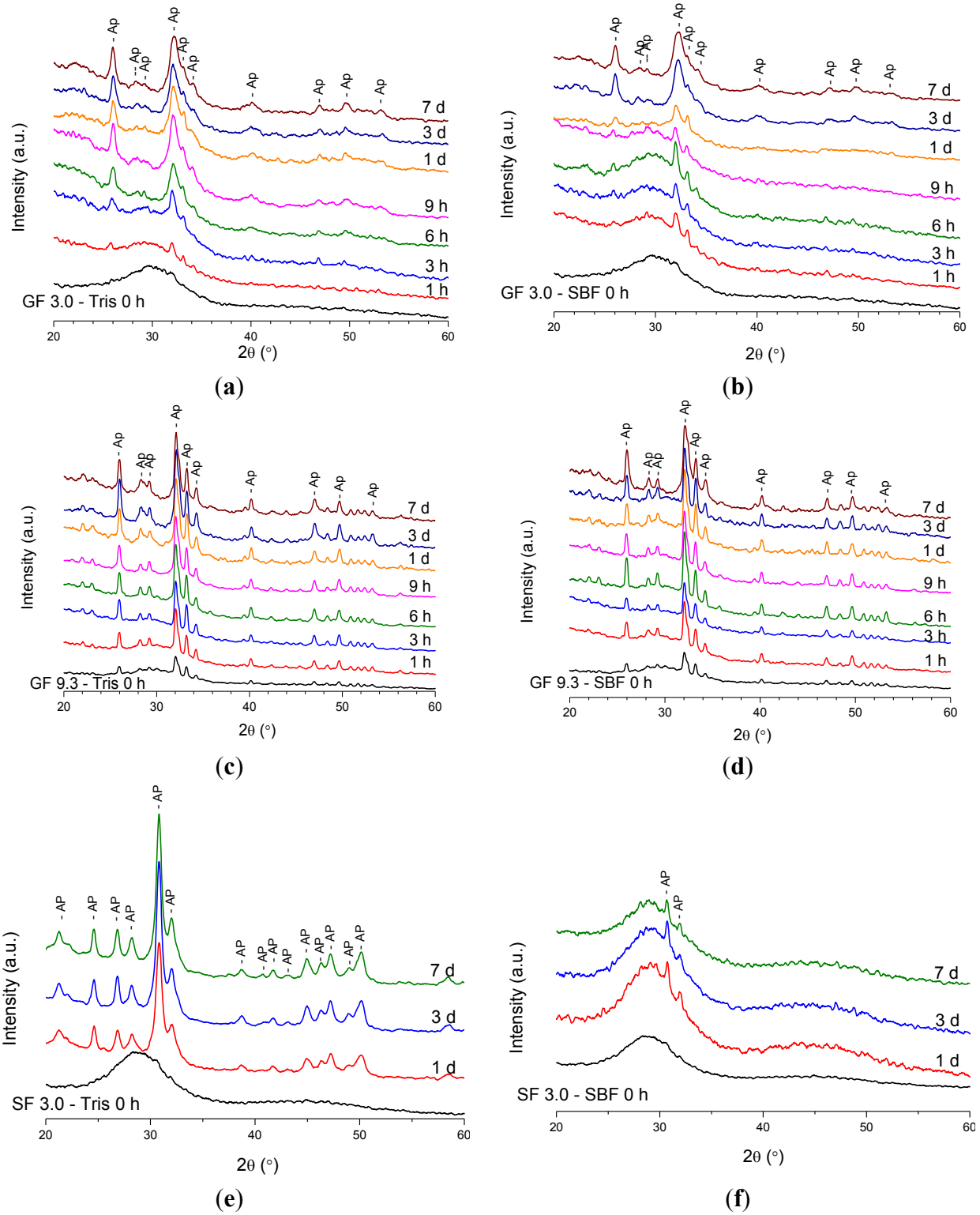

Figure 1. *Cont.*

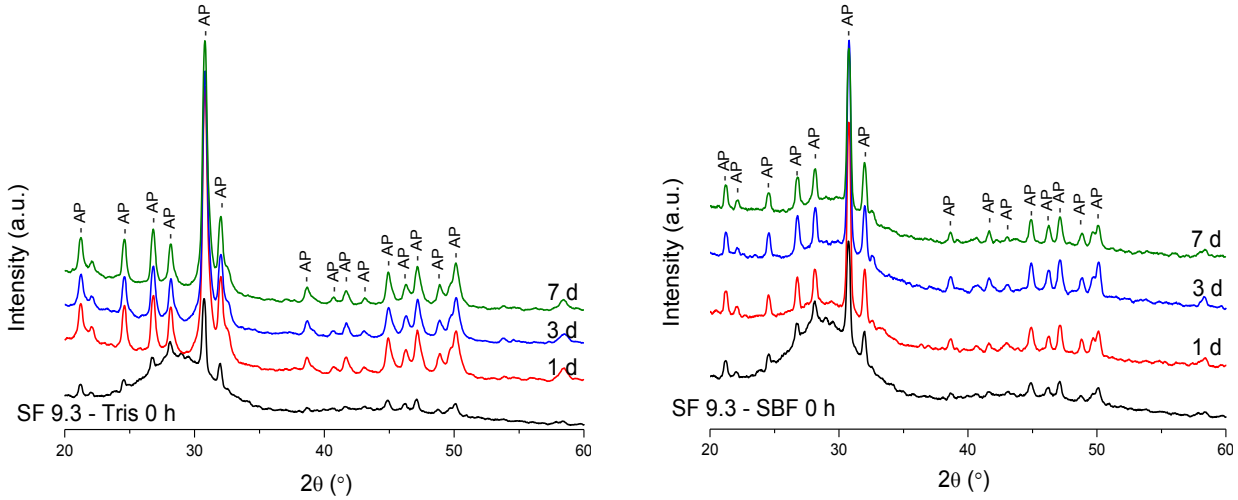

(g) **(h)**

Figure 1e,h show the XRD patterns of SrF_2-containing glasses after immersion, and the results are similar to those seen in the CaF_2 series. The diffraction peaks at 30.5° and 31.7° 2θ, which correspond to strontium phosphate fluoride ($Sr_{10}(PO_4)_6F_2$), developed after immersion of the composition with 3 mol% SrF_2 in Tris and SBF (Figure 1e,f). The intensity of the apatite diffraction lines after immersion in Tris is much stronger than after immersion in SBF. However, the difference in intensity after immersion in Tris or SBF is not significant when the SrF_2-containing glass contains crystalline fractions of apatite as observed for the composition with 9.3 mol% SrF_2 (Figure 1g,h).

Thus, for both the CaF_2 and SrF_2 series, the fraction of apatite detected from the XRD patterns grew faster during immersion in Tris than in SBF solution when the immersed glass powders were XRD amorphous before immersion. The higher initial intensity of the apatite lines for the partially crystallised glasses indicates that the apatite crystals present in the untreated glass served as nuclei for the apatite phase formed during immersion in buffer solution, and newly formed apatite crystals precipitated on the surface of the pre-existing crystalline phase.

2.1.2. Fourier Transform Infrared (FTIR) Spectroscopy Results

FTIR spectroscopy was used to monitor glass degradation and apatite formation upon immersion of glasses in buffer solution, and Figure 2a–h presents the FTIR results for the same four compositions shown in Figure 1. Each bottom spectrum in Figure 2 corresponds to the non-immersed glass powder mainly showing three strongly overlapped bands at about 1000, 920 and 870 cm^{-1}, which are known for bioactive type silicate glass and are assigned to the Si-O vibration modes, *i.e.*, Si-O-Si stretch, non-bridging oxygen $Si-O^-$ stretch and bend, respectively [10]. This assignment is consistent with the IR spectra computed by using accurate DFT calculations recently reported for phosphosilicate bioactive glasses [40,41]. The spectra of the samples collected after immersion reveal clear changes compared to the non-immersed glasses.

Figure 2. FTIR spectra of glasses after immersion in buffer solutions: (**a**) GF 3.0 in Tris; (**b**) GF 3.0 in SBF; (**c**) GF 9.3 in Tris; (**d**) GF 9.3 in SBF; (**e**) SF 3.0 in Tris; (**f**) SF 3.0 in SBF; (**g**) SF 9.3 in Tris; (**h**) SF 9.3 in SBF.

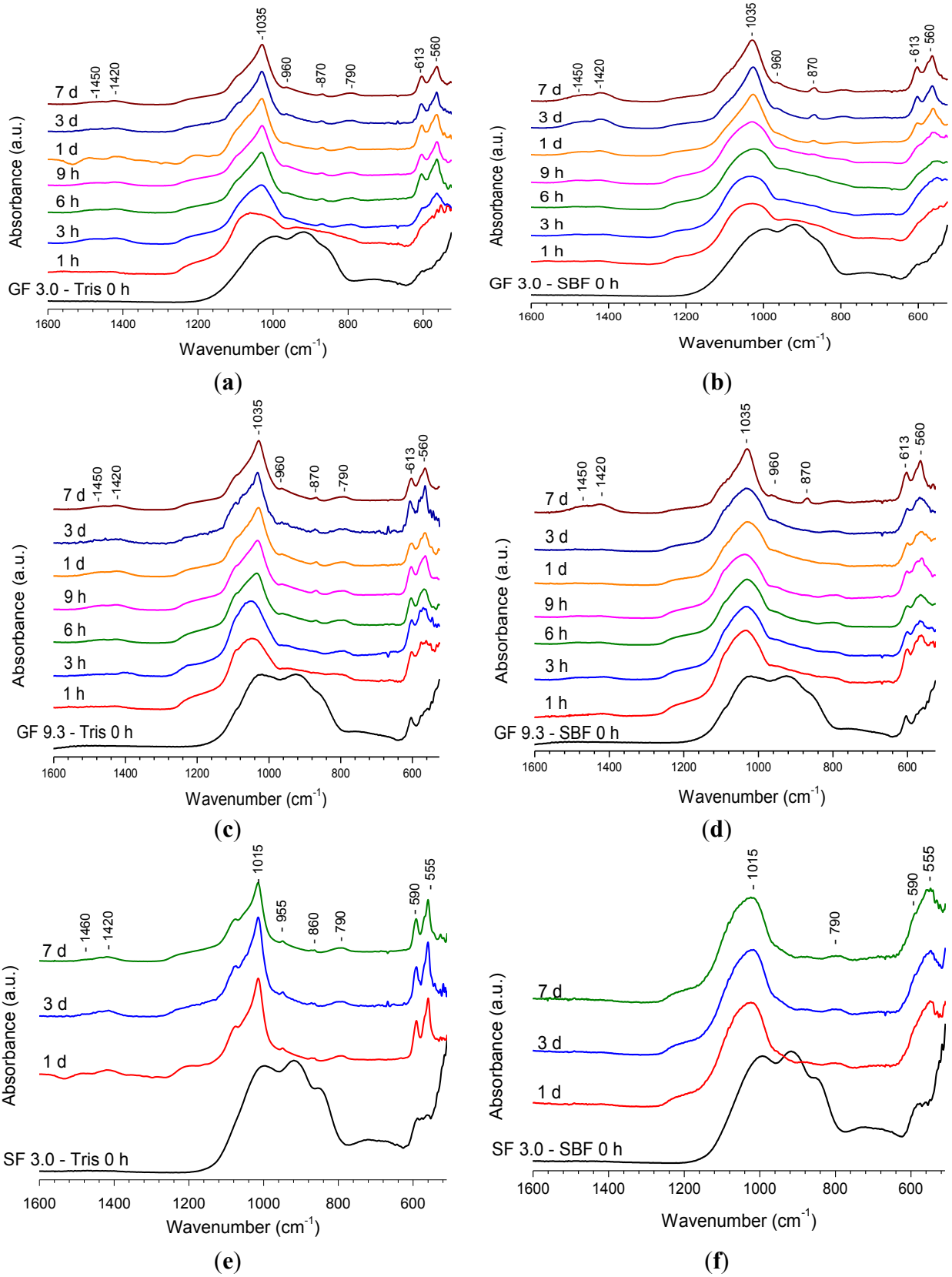

Figure 2. *Cont.*

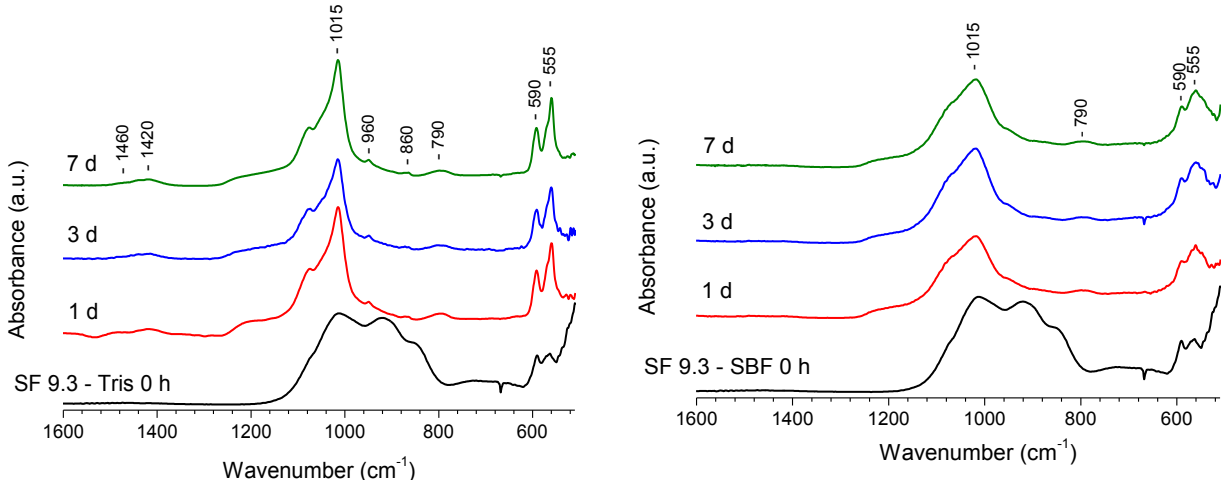

The non-bridging oxygen Si-O$^-$ band at 920 cm^{-1} decreased in intensity immediately upon immersion and disappeared at longer immersion times. All the spectra clearly show sharpening of the band at about 1035 cm^{-1} which is associated with both Si-O-Si and crystalline orthophosphate. The latter additionally accounts for the shoulder appearing at about 1100 cm^{-1} [10,11]. However, it is seen that the sharpening occurs more rapidly during immersion in Tris rather than SBF. Very clear changes can be seen in the region 500–600 cm^{-1}. The typical crystalline orthophosphate or apatite split bands at 560 cm^{-1} and 613 cm^{-1} are present for GF 3.0 glass at 3 h immersion in Tris (Figure 2a) and can be distinguished at 9 h of immersion in SBF (Figure 2b). The spectra indicating the presence of crystalline apatite have another band at about 960 cm^{-1} corresponding to the P-O stretch in the orthophosphate tetrahedron. The spectra for the samples collected after immersion contain bands at 1450, 1420 and 870 cm^{-1}, which are associated with the presence of carbonate substitution in the apatite. The band at 790 cm^{-1} appearing in the spectra after immersion is assigned to Si-O-Si between the two adjacent silicate tetrahedra [11,42]. This forms as a result of condensation reactions on glass degradation and essentially presents a silica-gel. Figure 2a shows that starting from 6 h of immersion the spectra are very similar to each other. No changes can be seen in the spectra at 24 h of immersion in SBF (Figure 2b).

The evolution of bands in the FTIR spectra for the GF 9.3 composition after immersion in Tris and SBF (Figure 2c,d) is similar to the one observed for glass GF 3.0. The spectrum of the original glass reveals signs of the presence of crystalline FAP in addition to the typical bands of Si-O vibration. On immersion, the spectra clearly reveal changes owing to glass dissolution. In addition, it is seen that the sharpening of the bands occurs at earlier time points after immersion in Tris than in SBF. Similar results were obtained for other compositions with CaF_2 contents higher than 9.3 mol% (not shown).

The FTIR spectra of SF 3.0 and SF 9.3 (Figure 2e–h) reveal similar results for the SrF_2-containing series. Upon immersion, non-bridging oxygen band disappeared, and a crystalline orthophosphate band develops. The position of the split bands characteristic for crystalline orthophosphate is slightly different from the CaF_2 series. These developed at 590 and 555 cm^{-1} which may be explained by the presence of strontium cations [39]. The FTIR spectra of SF 9.3 are similar to those of other

compositions with SrF_2 contents higher than 3.0 mol%. The differences in the rate of sharpening of the FTIR bands in Tris compared to SBF immersion is clearly seen in this series, too.

On comparison with the calcium series, it is seen that the spectrum of SF 3.0 immersed in Tris for 1 day (Figure 2e) displays sharper features than the spectrum of GF 3.0 at the same immersion time (Figure 2a), which indicates that the strontium-containing glass may dissolve and form apatite slightly faster than the calcium-containing one. FTIR spectroscopy characterises both amorphous and crystalline species present in solids unlike XRD, which reveals changes in the crystalline domains of a solid only. The presented FTIR results indicate that glass dissolution may occur faster in Tris buffer solution than in SBF for amorphous or partially crystallised bioactive silicate glasses.

2.1.3. Magic Angle Spinning-Nuclear Magnetic Resonance (MAS-NMR) Spectroscopy Results

Figure 3 displays the ^{31}P and ^{19}F MAS-NMR spectra of the calcium fluoride-containing series immersed for 6 h in Tris buffer; the spectra are plotted for increasing fluoride content from bottom to top. The ^{31}P MAS-NMR spectra in Figure 3a are very similar for the entire series and reveal a relatively sharp peak with the centre between 2.8 and 3.0 ppm, assigned to crystalline apatite [43]. Some of the spectra show an asymmetry of the signal indicating presence of multiple phosphorus species that can include the residual glass signal as well. The latter is expected to be around 3 ppm, though is broader than the signal assigned to apatite.

Figure 3. ^{31}P (**a**) and ^{19}F (**b**) MAS-NMR spectra of the samples collected after immersion in Tris buffer solution for 6 h.

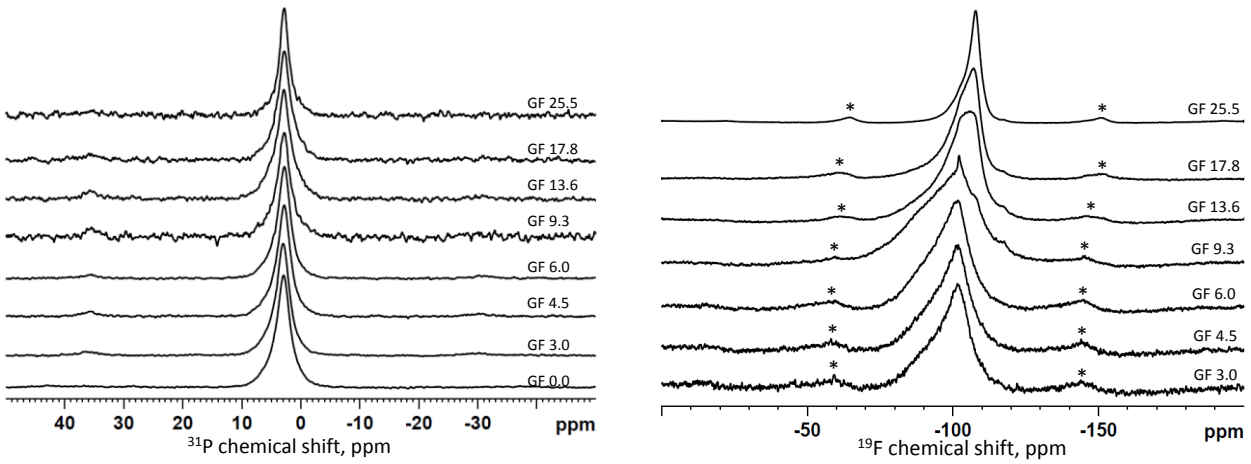

The ^{19}F MAS-NMR spectra shown in Figure 3b revealed multiple overlapping signals including the crystalline species of a fluoride-substituted apatite with a signal at about −103 ppm and calcium fluoride at about −108 ppm characterised by a sharp peak [11]. No crystalline calcium fluoride appears to be presence in the spectra of the compositions with low fluoride content (GF 3.0, GF 4.5 and GF 6.0); these glass compositions showed only formation of fluorapatite during immersion. The asymmetry of the signal is explained by the presence of fluoride species in the residual glass; the spectra of the initial glasses are characterised by a broad signal at about −95 ppm [39]. Starting from composition GF 9.3 the sharp feature at about −108 ppm corresponding to CaF_2 can be distinguished in the spectra

(Figure 3b), increasing in intensity at higher fluoride contents in the glass. Finally, in composition GF 25.5, most of the fluoride is present as crystalline calcium fluoride at 6 h immersion in Tris, although a crystalline fluorapatite in addition to calcium fluoride and fluorine in the glass phase was detected in the original glass before immersion.

The MAS-NMR results in Figure 3 indicate that 6 h immersion of the glass powders in Tris buffer produced a fluoride-substituted apatite as the major solid phase in most of the compositions. Although this result is consistent with those obtained from XRD and FTIR, the results from ^{19}F NMR in Figure 3b provide evidence that the apatite formed is fluoride-substituted. The ^{31}P MAS-NMR spectra of this glass series at 9 h of immersion were similar to the spectra in Figure 3a (6 h), although the line width decreased slightly at 9 h of immersion compared to 6 h. However, in the glass with the highest fluoride content most of the fluoride was detected as crystalline CaF_2 with only a small fraction of fluorapatite present. In addition, for the composition GF 25.5, the spectra of 6 and 9 h of immersion are practically identical. The latter is consistent with the XRD results, where the patterns were practically identical.

The ^{31}P NMR spectra of the partially crystallised glasses that contained an apatite phase before immersions (GF 9.3, GF 13.6, GF 17.8) were deconvolved [44], and the results show an increase in the apatite fraction at 9 h of immersion compared to the immersion for 6 h and the fraction of apatite in the untreated glass. A fraction of 20%–30% of the original phosphorus in GF 9.3, GF 13.6, GF 17.8 glasses was crystallised to an apatite; this increased up to 30%–40% at 6 h of immersion, which further increased to 40%–50% at 9 h of immersion in Tris. This indicates that the crystalline apatite formed in the glass spontaneously during quenching can serve as a seeding phase for the apatite precipitating during immersion in physiological solutions. This may also affect the morphology of the apatite formed on precipitation; the bigger apatite crystals of a more regular shape that formed spontaneously during glass quenching can further grow during immersion in buffer solution, whereas small nanometre-sized apatite crystals were formed when an amorphous bioactive glass powder was immersed in buffer solution [45].

2.2. Dissolution Study

2.2.1. pH Measurements Results

Figure 4 shows pH changes in Tris buffer solution during immersion of glass powders measured at the end of the immersion time. The general trend is similar for all compositions: pH increased on initial immersion, which is explained by substitution of protons from the solution for the cationic components of the glass, which increases the alkalinity of the solution. However, as the apatite phase starts precipitating, pH does not increase any longer and may even slightly decrease. It is seen that the highest increase in pH at the initial stage was observed for the fluoride-free glass GF 0.0. This is consistent with the effect of fluoride incorporated into a bioactive glass to reduce an increase in pH on initial dissolution which was previously seen and discussed [11,46]. However, overall, it is seen that the strontium-containing glasses gave a slightly lower pH during dissolution (mostly between 7.5 and 7.6) than the calcium-containing ones (mostly between 7.6 and 7.7).

Figure 4. pH measured at the end of the immersion time in Tris buffer. Open symbols are for the CaF_2 series (GF) and closed symbols are for the SrF_2 series (SF) with the same nominal fluoride content.

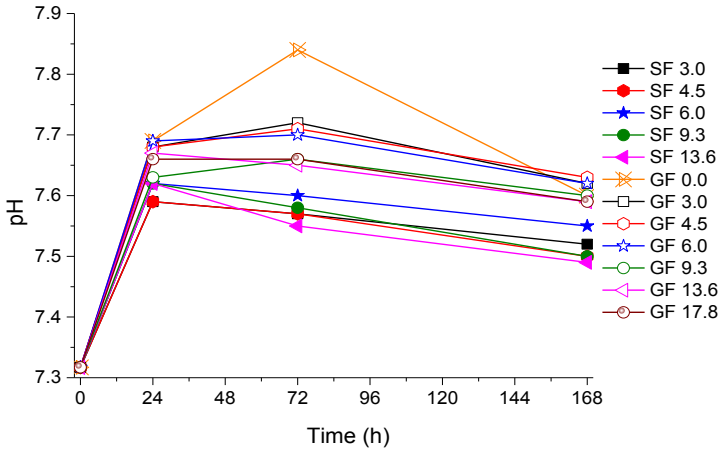

2.2.2. Ion Release Results

Figure 5a presents the relative phosphate concentration in Tris solution at 9 hours' immersion of glass powders of the calcium fluoride series, presented as a percentage of the phosphate in the nominal glass composition. It is seen that two different trends are observed depending on whether the original glass was amorphous or contained a crystalline phase. Amorphous glasses with low fluoride content show only presence of very small percentages (less than 2%) of phosphate in solution. By contrast, the partially crystallised glasses containing high amounts of fluoride show higher concentrations (up to 11% of phosphate) at early time points (1 h), followed by a decrease in phosphate concentration, which is consistent with the precipitation of an apatite phase during which phosphate is consumed. The higher the fluoride content in the glass, the higher the phosphate concentration at 1 h. However, the subsequent drop in the release was most pronounced for the GF 25.5 glass composition.

The concentrations of calcium and strontium from the glass powders upon immersion up to 1 week are presented in Figure 5b. It is seen that at 24 h of immersion 40%–50% of calcium and strontium are present in solution, and this concentration does not change significantly at the later time points. There seems to be no trend with fluoride content.

The percentage of fluoride present in Tris buffer is shown in Figure 5c for 3 and 6 h of immersion. It is seen that the highest concentration (over 35% of the nominal fluoride content in the glass) was observed for composition GF 9.3. However, the lowest concentration of fluoride (about 10%) is seen for the glass with the highest fluoride content, GF 25.5, although most of the fluoride in the original composition was in the crystalline phase as seen from its ^{19}F MAS-NMR spectrum. There was only a small difference between fluoride concentrations at 3 and 6 h of immersion, which is at the level of accuracy of the measurements. Thus, it is seen that fluoride concentrations increase with increase in fluoride content in the glass as long as fluoride remains in the amorphous glass. Once a fluoride-containing phase starts crystallising from the glass the fluoride concentrations decrease. This suggests that the amorphous fluoride-containing glass phase is the source of the fluoride release rather than the crystalline phase.

Figure 5. (**a**) The percentage of phosphate presented as concentration of elemental phosphorus in Tris for CaF_2-containing glasses; (**b**) The percentage of cations (Sr^{2+} or Ca^{2+}) concentration in Tris; (**c**) The percentage of fluoride concentration measured at 3 and 6 h in Tris for CaF_2-containing glasses.

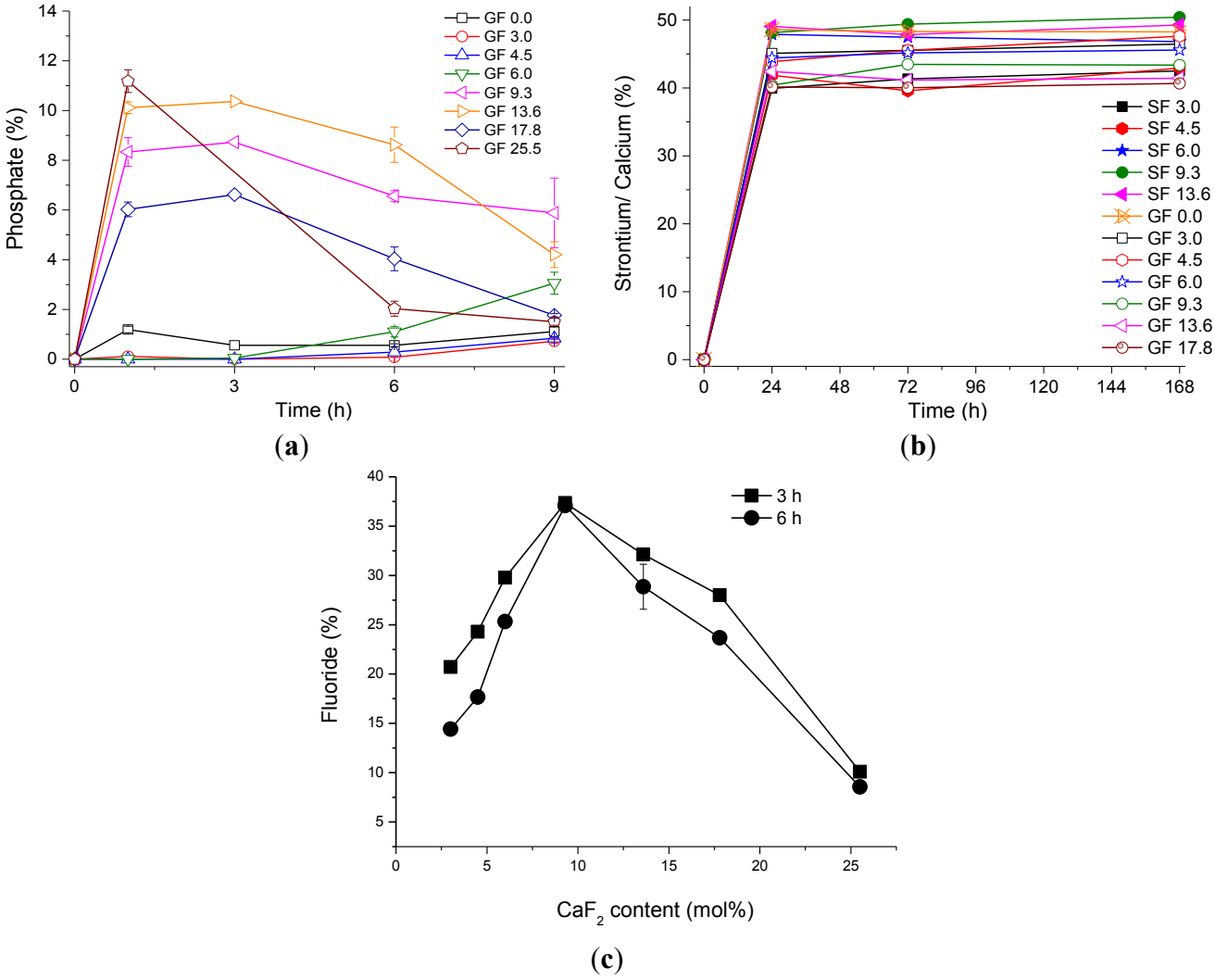

2.3. Final Discussion

This study presents bioactivity data for two fluoride-containing series of glasses that were either amorphous or partially crystallised. Those glasses which had partially crystallised can be considered as fluoride-containing glass-ceramics. All the glasses and glass-ceramics showed fast glass degradation and apatite formation upon immersion in buffer solutions. However, the results indicate that there is a clear difference in mechanism of bioactivity depending on whether the glass was amorphous or contained a fluoride-containing crystalline phase.

Based on FTIR, XRD and ^{31}P MAS-NMR data, the initially amorphous glasses containing relatively low amounts of fluoride (below 9% in Ca-containing and below 4.5% in Sr-containing series) degraded rapidly upon immersion in Tris buffer and formed apatite within 3 h. Results from ^{19}F MAS-NMR revealed that the apatite, which formed within 6 h in Tris, was fluorapatite. No crystalline CaF_2 phase was detected after immersion for glasses with low fluoride contents.

For dissolution studies in Tris buffer, the glass was the only source of phosphate for apatite formation. This proves that a high amount of phosphate present as orthophosphate in the bioactive glass is clearly beneficial for early apatite formation. The ionic concentration in solution confirm rapid glass degradation in Tris buffer. However, the results for phosphate were surprising, as concentrations observed for the initially amorphous glasses were very low, despite apatite having formed at very early immersion time points. This suggests that either phosphate was released at even earlier time points than the earliest investigated here (1 h), or apatite might form via a different mechanism than via dissolution-precipitation.

The kinetics of glass degradation and apatite formation was slower in SBF compared to Tris buffer for the initially amorphous glasses, as seen particularly from comparison of FTIR spectra. Apatite formation was noted in SBF by 24 h compared to 6 h in Tris. This delay can be explained by the higher ionic strength of the SBF solution, which alters the kinetics of glass degradation via inhibiting the dissolution of ionic species. The presence of Mg^{2+} in SBF is known to suppress apatite formation [47] and can additionally contribute to a delayed formation of apatite [48].

Fluorapatite was not the only crystalline phase found in the partially crystallised glasses. Strong presence of CaF_2 dominated in compositions with the highest fluoride contents starting from composition GF 13.6 with fluorapatite being present as a minor phase. However, the results presented above show that the fraction of crystalline apatite had grown in these bioceramics after immersion. The intensity of the signal assigned to apatite increased from XRD and FTIR. In addition, ^{31}P MAS-NMR suggested an increase of the apatite fraction after immersion in Tris.

The decrease in phosphate concentrations from 1 h in solution confirms a consumption of phosphate for apatite formation. The phosphate concentrations for the partially crystallised glasses was significantly higher than for the amorphous glasses, despite it being assumed that phosphate is released from the amorphous phase of the glass-ceramics rather than the crystalline. Despite this distinct difference, growth of the apatite fraction of the glass-ceramics is estimated to have occurred by 3–6 h, which is a similar time frame as for the amorphous glasses with low amounts of fluoride.

Presence of apatite crystals in the untreated materials, even in minor amounts compared to the amorphous part, clearly affected the bioactivity of the glass-ceramics during immersion. The observed increase in the apatite fraction with time indicates that the existing apatite crystals served as a seeding phase for further apatite crystal growth. As the amorphous phase of the glass-ceramics rapidly degraded with time in buffer solution, the additional apatite had precipitated from the solution via a dissolution-precipitation mechanism. Presence of a seeding phase reduces the energy required for formation of apatite nuclei, which is typically the limiting factor of apatite crystallisation. Comparison of apatite formation for (partially crystalline) glass-ceramics immersed in Tris and SBF showed that there was no significant difference in the kinetics between the two solutions unlike for the amorphous glasses. This is owing to elimination of the rate limiting stage of apatite nucleation for the partially crystallised glass-ceramics.

There was no significant difference between the Ca- and Sr-containing series, except for a higher tendency of the Sr-containing glasses to crystallise.

3. Experimental Section

3.1. Glass Preparation

A melt-quench method was employed to synthesise sodium-free, fluoride-containing bioactive glasses. The glasses were designed by introducing different amounts of CaF_2/SrF_2 into a SiO_2-P_2O_5-CaO/SrO glass system (Table 1). In order to preserve the predominantly Q^2 glass structure, calcium fluoride was added to the glasses with the ratios between other components kept constant.

Table 1. Glass compositions in mol%.

Glass code	SiO_2	CaO/SrO	P_2O_5	CaF_2/SrF_2
GF/SF 0.0	38.1	55.5	6.3	0.0
GF/SF 3.0	37.0	53.9	6.1	3.0
GF/SF 4.5	36.4	53.0	6.0	4.5
GF/SF 6.0	35.9	52.2	5.9	6.0
GF/SF 9.3	34.6	50.4	5.7	9.3
GF/SF 13.6	32.9	48.0	5.5	13.6
GF/SF 17.8	31.4	45.7	5.2	17.8
GF/SF 25.5	28.4	41.4	4.7	25.5

A 200 g batch of analytical grade silica (Prince Minerals Ltd., Stoke-on-Trent, UK), calcium carbonate, calcium fluoride and phosphorus pentoxide (Sigma-Aldrich, Gillingham, UK) were weighed out, mixed and transferred into a 300 mL platinum/rhodium crucible, melted at 1550 °C (glasses with 0 and 3 mol% CaF_2/SrF_2) and 1500 °C (all other glasses) for 1 h in an electrical furnace (EHF 17/3, Lenton, Hope Valley, UK). The melted glasses were quenched into cold deionised water to suppress crystallisation. The as-quenched granular glass frits were dried overnight and ground into powder by using a Gyro mill (Glen Creston, London, UK) for two sets of 7 min. A mesh analytical sieve (Endecotts Ltd., London, UK) with a size of 45 μm was applied to obtain fine powder.

3.2. Bioactivity Testing and Ion Release Measurements

Glass and glass-ceramics bioactivity was tested in Tris buffer solution and SBF. SBF was prepared following the recipe described by Kokubo and Takadama [2] for the corrected SBF (c-SBF). The preparation of Tris buffer solution was according to that described by Mneimne *et al.* [10]. The specimens were prepared in duplicate; 75 mg of glass powder was dispersed in 50 mL of buffer solution and transferred to a shaking incubator (KS 4000i Control, IKA, Staufen, Germany) at 37 ± 1 °C at an agitation rate of 60 rpm for 1, 3, 6, 9, 24, 72 and 168 h.

pH was measured using an Oakton® pH meter with 35811-71 pH electrode at the end of each immersion period. The solutions were filtered using the filter papers with pore size of 5–13 μm and precipitates were collected. The filtered solution was kept at 4 °C until further analysis.

The filtered solutions were acidified with 69% nitric acid to quantify ions concentrations using an inductively coupled plasma-optical emission spectroscopy (ICP-OES; Varian Vista-PRO, Yarnton, UK). The solutions were diluted by a factor 1:20 for measurements of the calcium and silicon content and no dilution was used for measurements of phosphate ion content. Calibrations were performed

using diluted multi-element stock solution. Fluoride content in solution was quantified using a fluoride ion selective electrode (Orion 9609BN, 710A meter, South Burlington, VT, USA) and NaF stock solution was used for preparation of the fluoride-containing calibration solutions.

3.3. Characterisation of Apatite Formation after Immersion

The precipitates collected after the immersion were dried and analyzed by X-ray Diffraction (XRD), Fourier Transform Infrared Spectroscopy (FTIR) and solid state Nuclear Magnetic Resonance (NMR).

An X'Pert Pro X-ray diffractometer (PANalytical, Eindhoven, The Netherlands) with a copper (Ni-filtered Cu-Kα) X-ray source was employed to characterise the glasses, glass-ceramics and the samples collected after immersion in buffer solutions. The patterns of powder samples were recorded between 5 and 70° 2θ at a step size of 0.0334°. Calibration was carried out using NIST standard reference material 660a (lanthanum hexaboride). XRD data were analyzed using X'Pert HighScore Plus (v2.0, PANalytical, Almelo, The Netherlands) in conjunction with the ICDD database.

The samples collected after immersion were assessed using Fourier Transform Infrared Spectroscopy (Spectrum GX, Perkin-Elmer, Cambridge, UK). The data were recorded from 500 to 1600 cm^{-1} of wavenumber.

Powders of the CaF_2-containing glasses after soaking in buffer solutions were investigated using solid state NMR on a 600 MHz (14.1T) Bruker NMR spectrometer (Bruker AV 600 NMR, Conventry, UK). ^{31}P MAS-NMR was run at the 242.9 MHz resonance frequency using a standard single resonance Bruker probe in a 4 mm rotor at spinning conditions of 8 and 10 kHz. Sixteen scans were run with a recycle delay of 60 s for each sample. The chemical shift was referenced using the primary reference, 85% H_3PO_4. ^{19}F MAS-NMR measurements were run at the 564.7 MHz resonance frequency using a standard double resonance Bruker probe with low fluorine background for a 2.5 mm rotor spinning at a speed of 18 kHz and 21 kHz. Typically, 32 or 64 scans were acquired with eight preliminary dummy scans and 30 s recycling delay. The chemical shift was referenced using the signal from 1M NaF solution scaled to −120 ppm relative to the CF_3Cl primary standard. The free *dmfit* software [44] was used for deconvolution of the NMR spectra.

4. Conclusions

Amorphous glasses with low amounts of fluoride (below 9 mol% CaF_2) degraded rapidly in Tris buffer solution and formed apatite within 3 h, which by 6 h could be identified as fluorapatite by ^{19}F MAS-NMR. Glass degradation and apatite formation were significantly slower in SBF compared to Tris buffer.

Partially crystallised glasses (containing crystalline phases such as fluorapatite or calcium/strontium fluoride) showed degradation of the amorphous phase and an increase in fraction of apatite by 3–6 h in Tris and SBF buffers, with no difference in kinetics observed for the two solutions. The increase in apatite fraction is thought to occur by precipitation of apatite onto the surface of apatite crystals already present within the glass-ceramics. High phosphate concentrations at 1 h followed by a decrease were observed for the glass-ceramics, which is in contrast to the amorphous glasses. It is proposed that two different mechanisms of apatite formation occur, depending on presence or absence of apatite crystals in the original glass.

Acknowledgments

Xiaojing Chen was supported by China Scholarship Council (CSC)/Queen Mary University of London Joint PhD scholarships. Laura Shotbolt is kindly thanked for conducting inductively coupled plasma-optical emission spectroscopy (ICP-OES) measurements.

Author Contributions

All the co-authors of the paper have contributed to the research and writing of the paper. Xiaojing Chen and Xiaohui Chen synthesised the glasses and performed the bulk of the studies. Delia Brauer contributed to the discussion of the experiments. Rory Wilson carried out the XRD. Robert Hill directed the research and Natalia Karpukhina codirected the research and performed the NMR study.

Conflicts of Interest

The authors declare no conflict of interest.

References

1. Bohner, M.; Lemaitre, J. Can bioactivity be tested *in vitro* with sbf solution? *Biomaterials* **2009**, *30*, 2175–2179.
2. Kokubo, T.; Takadama, H. How useful is sbf in predicting *in vivo* bone bioactivity? *Biomaterials* **2006**, *27*, 2907–2915.
3. Wallace, K.E.; Hill, R.G.; Pembroke, J.T.; Brown, C.J.; Hatton, P.V. Influence of sodium oxide content on bioactive glass properties. *J. Mater. Sci. Mater. Med.* **1999**, *10*, 697–701.
4. Hench, L.L. Glass and glass-ceramic technologies to transform the world. *Int. J. Appl. Glass Sci.* **2011**, *2*, 162–176.
5. Hench, L.; Wilson, J. *An Introduction to Bioceramics*; World Scientific Publishing: Singapore, Singapore, 1993; Volume 1.
6. Shirtliff, V.J.; Hench, L.L. Bioactive materials for tissue engineering, regeneration and repair. *J. Mater. Sci.* **2003**, *38*, 4697–4707.
7. Kasuga, T.; Maeda, H.; Kato, K.; Nogami, M.; Hata, K.; Ueda, M. Preparation of poly (lactic acid) composites containing calcium carbonate (vaterite). *Biomaterials* **2003**, *24*, 3247–3253.
8. Sainz, M.A.; Pena, P.; Serena, S.; Caballero, A. Influence of design on bioactivity of novel $CaSiO_3$-$CaMg(SiO_3)(2)$ bioceramics: *In vitro* simulated body fluid test and thermodynamic simulation. *Acta Biomater.* **2010**, *6*, 2797–2807.
9. De Aza, P.N.; Guitian, F.; de Aza, S. Bioactivity of wollastonite ceramics—*In vitro* evaluation. *Scripta Metall. Mater.* **1994**, *31*, 1001–1005.
10. Mneimne, M.; Hill, R.G.; Bushby, A.J.; Brauer, D.S. High phosphate content significantly increases apatite formation of fluoride-containing bioactive glasses. *Acta Biomater.* **2011**, *7*, 1827–1834.
11. Brauer, D.S.; Karpukhina, N.; O'Donnell, M.D.; Law, R.V.; Hill, R.G. Fluoride-containing bioactive glasses: Effect of glass design and structure on degradation, ph and apatite formation in simulated body fluid. *Acta Biomater.* **2010**, *6*, 3275–3282.

12. Goel, A.; Kapoor, S.; Rajagopal, R.R.; Pascual, M.J.; Kim, H.W.; Ferreira, J.M. Alkali-free bioactive glasses for bone tissue engineering: A preliminary investigation. *Acta Biomater.* **2012**, *8*, 361–372.
13. Kapoor, S.; Goel, A.; Pascual, M.J.; Ferreira, J.M.F. Thermo-mechanical behaviour of alkali free bioactive glass-ceramics co-doped with strontium and zinc. *J. Non-Cryst. Solids* **2013**, *375*, 74–82.
14. Kansal, I.; Goel, A.; Tulyaganov, D.U.; Rajagopal, R.R.; Ferreira, J.M.F. Structural and thermal characterization of CaO-MgO-SiO_2-P_2O_5-CaF_2 glasses. *J. Eur. Ceram. Soc.* **2012**, *32*, 2739–2746.
15. Pedone, A.; Charpentier, T.; Menziani, M.C. Multinuclear nmr of $CaSiO_3$ glass: Simulation from first-principles. *Phys. Chem. Chem. Phys.* **2010**, *12*, 6054–6066.
16. Fayon, F.; Duée, C.; Poumeyrol, T.; Allix, M.; Massiot, D. Evidence of nanometric-sized phosphate clusters in bioactive glasses as revealed by solid-state 31p nmr. *J. Phys. Chem. C* **2013**, *117*, 2283–2288.
17. Ma, J.; Chen, C.Z.; Wang, D.G.; Meng, X.G.; Shi, J.Z. *In vitro* degradability and bioactivity of mesoporous CaO-MgO-P_2O_5-SiO_2 glasses synthesized by sol-gel method. *J. Sol Gel Sci. Technol.* **2010**, *54*, 69–76.
18. Ma, J.; Chen, C.Z.; Wang, D.G.; Jiao, Y.; Shi, J.Z. Effect of magnesia on the degradability and bioactivity of sol-gel derived SiO_2-CaO-MgO-P_2O_5 system glasses. *Coll. Surf. B Biointerfaces* **2010**, *81*, 87–95.
19. Perez-Pariente, J.; Balas, F.; Vallet-Regi, M. Surface and chemical study of SiO_2 center dot P_2O_5 center dot cao center dot(mgo) bioactive glasses. *Chem. Mater.* **2000**, *12*, 750–755.
20. Saboori, A.; Rabiee, M.; Mutarzadeh, F.; Sheikhi, M.; Tahriri, M.; Karimi, M. Synthesis, characterization and *in vitro* bioactivity of sol-gel-derived SiO_2-CaO-P_2O_5-MgO bioglass. *Mater. Sci. Eng. C Biomim. Supramol. Syst.* **2009**, *29*, 335–340.
21. Yu, B.B.; Turdean-Ionescu, C.A.; Martin, R.A.; Newport, R.J.; Hanna, J.V.; Smith, M.E.; Jones, J.R. Effect of calcium source on structure and properties of sol-gel derived bioactive glasses. *Langmuir* **2012**, *28*, 17465–17476.
22. Lin, S.; Ionescu, C.; Baker, S.; Smith, M.E.; Jones, J.R. Characterisation of the inhomogeneity of sol-gel-derived SiO_2-CaO bioactive glass and a strategy for its improvement. *J. Sol Gel Sci. Technol.* **2010**, *53*, 255–262.
23. Kim, H.-M.; Himeno, T.; Kokubo, T.; Nakamura, T. Process and kinetics of bonelike apatite formation on sintered hydroxyapatite in a simulated body fluid. *Biomaterials* **2005**, *26*, 4366–4373.
24. Clupper, D.C.; Hench, L.L.; Mecholsky, J.J. Strength and toughness of tape cast bioactive glass 45S5 following heat treatment. *J. Eur. Ceram. Soc.* **2004**, *24*, 2929–2934.
25. Peitl, O.; Zanotto, E.D.; Hench, L.L. Highly bioactive P_2O_5-Na_2O-CaO-SiO_2 glass-ceramics. *J. Non-Cryst. Solids* **2001**, *292*, 115–126.
26. Moura, J.; Teixeira, L.N.; Ravagnani, C.; Peitl, O.; Zanotto, E.D.; Beloti, M.M.; Panzeri, H.; Rosa, A.L.; de Oliveira, P.T. *In vitro* osteogenesis on a highly bioactive glass-ceramic (biosilicate (r)). *J. Biomed. Mater. Res. Part A* **2007**, *82A*, 545–557.
27. Arstila, H.; Hupa, L.; Karlsson, K.H.; Hupa, M. Influence of heat treatment on crystallization of bioactive glasses. *J. Non-Cryst. Solids* **2008**, *354*, 722–728.

28. Pedone, A.; Charpentier, T.; Menziani, M.C. The structure of fluoride-containing bioactive glasses: New insights from first-principles calculations and solid state nmr spectroscopy. *J. Mater. Chem.* **2012**, *22*, 12599–12608.
29. Lusvardi, G.; Malavasi, G.; Tarsitano, F.; Menabue, L.; Menziani, M.C.; Pedone, A. Quantitative structure-property relationships of potentially bioactive fluoro phospho-silicate glasses. *J. Phys. Chem. B* **2009**, *113*, 10331–10338.
30. Lusvardi, G.; Malavasi, G.; Menabue, L.; Aina, V.; Morterra, C. Fluoride-containing bioactive glasses: Surface reactivity in simulated body fluids solutions. *Acta Biomater.* **2009**, *5*, 3548–3562.
31. Kiprianov, A.A.; Karpukhina, N.G. Oxyhalide silicate glasses. *Glass Phys. Chem.* **2006**, *32*, 1–27.
32. Brauer, D.S.; Karpukhina, N.; Law, R.V.; Hill, R.G. Structure of fluoride-containing bioactive glasses. *J. Mater. Chem.* **2009**, *19*, 5629–5636.
33. Brauer, D.S.; Anjum, M.N.; Mneimne, M.; Wilson, R.M.; Doweidar, H.; Hill, R.G. Fluoride-containing bioactive glass-ceramics. *J. Non-Cryst. Solids* **2012**, *358*, 1438–1442.
34. Edén, M. The split network analysis for exploring composition–structure correlations in multi-component glasses: I. Rationalizing bioactivity-composition trends of bioglasses. *J. Non-Cryst. Solids* **2011**, *357*, 1595–1602.
35. Hill, R.G.; Brauer, D.S. Predicting the bioactivity of glasses using the network connectivity or split network models. *J. Non-Cryst. Solids* **2011**, *357*, 3884–3887.
36. Pedone, A.; Charpentier, T.; Malavasi, G.; Menziani, M.C. New insights into the atomic structure of 45S5 bioglass by means of solid-state nmr spectroscopy and accurate first-principles simulations. *Chem. Mater.* **2010**, *22*, 5644–5652.
37. FitzGerald, V.; Pickup, D.M.; Greenspan, D.; Sarkar, G.; Fitzgerald, J.J.; Wetherall, K.M.; Moss, R.M.; Jones, J.R.; Newport, R.J. A neutron and X-ray diffraction study of bioglass with reverse monte carlo modelling. *Adv. Funct. Mater.* **2007**, *17*, 3746–3753.
38. Hayashi, M.; Nabeshima, N.; Fukuyama, H.; Nagata, K. Effect of fluorine on silicate network for CaO-CaF_2-SiO_2 and CaO-CaF_2-SiO_2-feox glasses. *ISIJ Int.* **2002**, *42*, 352–358.
39. Chen, X.; Chen, X.; Brauer, D.S.; Wilson, R.M.; Hill, R.G.; Karpukhina, N. Novel alkali free bioactive fluorapatite glass ceramics. *J. Non-Cryst. Solids* **2014**, *402*, 172–177.
40. Corno, M.; Pedone, A.; Dovesi, R.; Ugliengo, P. B3LYP simulation of the full vibrational spectrum of 45S5 bioactive silicate glass compared to v-silica. *Chem. Mater.* **2008**, *20*, 5610–5621.
41. Corno, M.; Pedone, A. Vibrational features of phospho-silicate glasses: Periodic B3LYP simulations. *Chem. Phys. Lett.* **2009**, *476*, 218–222.
42. Kim, C.Y.; Clark, A.E.; Hench, L.L. Early stages of calcium-phosphate layer formation in bioglasses. *J. Non-Cryst. Solids* **1989**, *113*, 195–202.
43. Fredholm, Y.C.; Karpukhina, N.; Brauer, D.S.; Jones, J.R.; Law, R.V.; Hill, R.G. Influence of strontium for calcium substitution in bioactive glasses on degradation, ion release and apatite formation. *J. R. Soc. Interface* **2012**, *9*, 880–889.
44. Massiot, D.; Fayon, F.; Capron, M.; King, I.; Le Calvé, S.; Alonso, B.; Durand, J.-O.; Bujoli, B.; Gan, Z.; Hoatson, G.; *et al.* Modelling one- and two-dimensional solid-state nmr spectra. *Magn. Reson. Chem.* **2002**, *40*, 70–76.

45. O'Donnell, M.D.; Watts, S.J.; Hill, R.G.; Law, R.V. The effect of phosphate content on the bioactivity of soda-lime-phosphosilicate glasses. *J. Mater. Sci. Mater. Med.* **2009**, *20*, 1611–1618.
46. Brauer, D.S.; Mneimne, M.; Hill, R.G. Fluoride-containing bioactive glasses: Fluoride loss during melting and ion release in tris buffer solution. *J. Non-Cryst. Solids* **2011**, *357*, 3328–3333.
47. Diba, M.; Tapia, F.; Boccaccini, A.R.; Strobel, L.A. Magnesium-containing bioactive glasses for biomedical applications. *Int. J. Appl. Glass Sci.* **2012**, *3*, 221–253.
48. Al-Noaman, A.; Rawlinson, S.C.F.; Hill, R.G. The role of mgo on thermal properties, structure and bioactivity of bioactive glass coating for dental implants. *J. Non-Cryst. Solids* **2012**, *358*, 3019–3027.

Research Article **Open Access**

Xiaojing Chen*, Natalia Karpukhina*, Delia S. Brauer, and Robert G. Hill

Novel Highly Degradable Chloride Containing Bioactive Glasses

DOI 10.1515/bglass-2015-0010
Received Apr 25, 2015; accepted Aug 20, 2015

Abstract: Addition of CaF_2 to a silicate bioactive glass favours formation of fluorapatite, which is less soluble in acidic environment than hydroxyapatite. However, excess CaF_2 in the glass is problematic, owing to the formation of crystalline calcium fluoride rather than fluorapatite on immersion. In this paper we investigate chloride as an alternative to fluoride in bioactive silicate glasses and in particular their bioactivity for the first time. Melt-derived bioactive glasses based on SiO_2-P_2O_5-CaO-$CaCl_2$ with varying $CaCl_2$ contents were synthesised and characterised by DSC. Chemical analysis of the chloride content was performed by using an ion selective electrode. Glass density was determined using Helium Pycnometry. The glass bioactivity was investigated in Tris buffer. Ion release measurements were carried out by using ICP-OES. The chemical analysis results indicated that the majority of the chloride is retained in the Q^2 type silicate glasses during synthesis. T_g and glass density reduced with increasing $CaCl_2$ content. Apatite-like phase formation was confirmed by FITR, XRD and ^{31}P MAS-NMR. The results of the in vitro studies demonstrated that the chloride containing bioactive glasses are highly degradable and form apatite-like phase within three hours in Tris buffer and, therefore, are certainly suitable for use in remineralising toothpastes. The dissolution rate of the glass was found to increase with $CaCl_2$ content. Faster dissolving bioactive glasses may be attractive for more resorbable bone grafts and scaffolds.

Keywords: chloride containing silicate glass; sodium free; highly degradable; bioactive glass; apatite

1 Introduction

Bioactive glasses are compelling for extensive use in medical and dental applications, for example bone grafts and toothpastes, due to their ability to degrade in physiological solutions and form a biomimetic apatite-like mineral layer [1–4]. Incorporation of various elements into the glass can tailor and improve the glass properties. For instance, zinc introduces an antibacterial effect [5], strontium stimulates bone regeneration [6, 7], magnesium facilitates processing [8] and fluoride enhances the bioactivity by forming fluorapatite (FAP) [9, 10].

FAP ($Ca_{10}(PO_4)_6F_2$), the fluoride analogue of hydroxyapatite (HAP, $Ca_{10}(PO_4)_6(OH)_2$), is chemically more stable in an acidic environment than HAP [11, 12]. In addition, fluoride is the key agent in preventing dental caries by encouraging remineralisation and inhibiting demineralisation [13, 14]. Moreover, fluoride is able to reduce the glass melting temperature, glass transition temperature and potentially reduces the glass hardness. Softer glasses with lower hardness are potentially less abrasive in toothpastes. The fluoride containing bioactive glasses are therefore particularly suitable for dental applications, especially for remineralising toothpaste.

Recently, Chen *et al.* [15] found that high fluoride contents in bioactive glasses result in the formation of crystalline calcium fluoride on quenching, rather than FAP. A high fluoride content in the toothpaste for children might result in dental fluorosis [16]. The regulatory authorities set a restriction on the fluoride content of toothpastes at 1500 ppm in Europe and 1200 ppm in the US. Hence, an alternative to fluoride component in bioactive glass that also potentially reduces the hardness and abrasivity of the glass is highly desirable.

Chlorine belongs to the same halogen group as fluorine and may have similar effects on the glass properties. However, chloride volatilisation is a significant problem during synthesis [17] and the incorporation of chloride into glasses has rarely been investigated compared to flu-

***Corresponding Author: Xiaojing Chen:** Dental Physical Sciences, Institute of Dentistry, Queen Mary University of London, Mile End Road, London E1 4NS, United Kingdom; Email: xiaojing.chen@qmul.ac.uk
***Corresponding Author: Natalia Karpukhina, Robert G. Hill:** Dental Physical Sciences, Institute of Dentistry, Queen Mary University of London, Mile End Road, London E1 4NS, United Kingdom; Email: n.karpukhina@qmul.ac.uk
Delia S. Brauer: Otto-Schott-Institut, Friedrich-Schiller-Universität Jena, Fraunhoferstr. 6, 07743 Jena, Germany

Table 1: Glass compositions in mol%. For each glass, the first row is the nominal composition as-designed and the second row is composition re-calculated based on the chloride component analysis.

Glass code	SiO_2	CaO	P_2O_5	$CaCl_2$
GPCl 0.0	38.1	55.5	6.3	0.0
	38.1	55.6	6.3	0.0
GPCl 2.3	37.3	54.3	6.2	2.3
	37.5	54.6	6.2	1.7
GPCl 3.5	36.8	53.6	6.1	3.5
	37.2	54.1	6.2	2.5
GPCl 4.6	36.4	53.0	6.0	4.6
	36.7	53.4	6.1	3.9
GPCl 7.2	35.4	51.6	5.9	7.2
	35.7	52.0	5.9	6.3
GPCl 10.6	34.1	49.6	5.7	10.6
	34.7	50.5	5.8	9.0
GPCl 14.0	32.8	47.7	5.4	14.0
	33.6	48.9	5.6	11.9
GPCl 20.6	30.3	44.1	5.0	20.6
	31.8	46.3	5.3	16.7

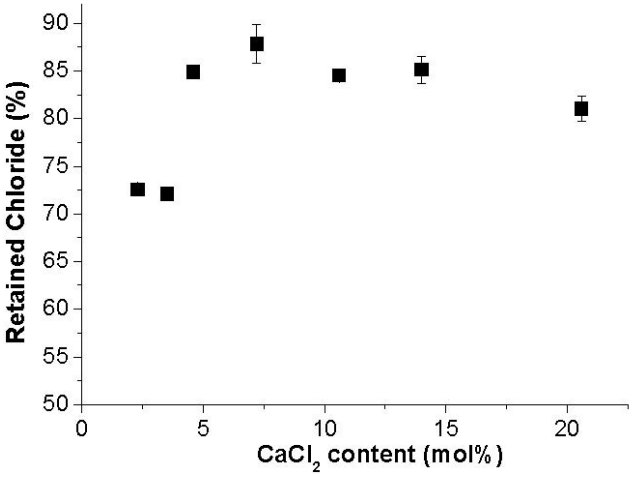

Figure 1: The percentage of the retained chloride in the initial glasses against the as-designed chloride content.

oride. The chloride ion is much larger than the fluoride ion (1.67 Å vs 1.19 Å) and when introduced into a glass, the chloride might expand the glass volume resulting in a more open and less compact glass structure. This could result in softer and less abrasive chloride containing bioactive glasses that can also dissolve faster and form apatite more rapidly. The larger size of the chloride ion compared to fluoride might also hinder crystallisation during synthesis.

Apatite stability follows the order FAP, HAP and chlorapatite (ClAP), with ClAP being the least stable [18]. We therefore would expect HAP to mainly form on dissolution of a chloride containing bioactive glass. Chloride is naturally present in the human body so is biologically acceptable and there is no restriction on the chloride content in toothpastes and biomedical materials unlike with fluoride.

This paper investigates the properties of chloride containing glasses free of sodium based on the SiO_2-P_2O_5-CaO-$CaCl_2$ system. Kiprianov *et al.* [17] proposed that chlorine might volatilise as NaCl. Hence, the absence of sodium would effectively minimise chlorine volatilization during melting. To the best of our knowledge, this study is the first ever investigation of the bioactivity of the chloride containing bioactive silicate glasses.

2 Materials and methods

2.1 Glass synthesis

The studied glasses were designed by incorporating various amounts of $CaCl_2$ into a sodium free calcium-silica-phosphate glass system and the ratio of CaO, SiO_2 and P_2O_5 was kept constant (Table 1). Analytical grade silica (Prince Minerals Ltd., Stoke-on-Trent, UK), calcium carbonate, phosphorus pentoxide and calcium chloride dihydrate (all Sigma-Aldrich, Gillingham, UK) were mixed and melted at high temperature (1550°C for GPCl 0.0 and GPCl 2.3; 1500°C for the rest glasses) for 1 hour in a platinum crucible in an electrical furnace (EHF 17/3, Lenton, UK). A

200 g batch was prepared. The molten glasses were rapidly quenched into deionised water to prevent crystallisation. The collected glass frit was dried overnight, ground into powder by a vibratory mill (Gyro mill, Glen Creston, UK) for 14 minutes and sieved through a 38 μm mesh sieve (Endecotts Ltd, UK).

2.2 Glass characterisation

2.2.1 Compositional analysis

The chloride contents in the initial glasses were quantified using a chloride ion selective electrode (ELIT Cl^- 2844, NICO 2000 UK). Glass powder (75 mg) with particle size smaller than 38 μm was dissolved in the 50 ml solution (48 ml deionized water, 1 ml 69% HNO_3 and 1 ml 5M $NaNO_3$ (ISA solution)). The samples were prepared in triplicate. The 1000 ppm Cl^- stock solution was prepared by dissolving 1.649 g NaCl (Sigma-Aldrich, Gillingham, UK) into 1 L distilled water and diluted to different concentrations to calibrate the electrode.

2.2.2 Differential Scanning Calorimetry (DSC)

The thermal properties of the glasses were evaluated by using a differential scanning calorimeter (DSC 1500 Stanton Redcroft, Rheometric Scientific, UK). The experiment was carried out under Nitrogen (60 ml min^{-1}). Both glass frit and glass powder with particle size less 38 μm (50 ± 0.1 mg) were heated from room temperature to 1100°C at a heating rate of 20°C/min using alumina as a reference. The glass transition temperature (T_g) was obtained from the DSC trace with an accuracy of ± 5°C.

2.2.3 Density Measurement

The density of each glass was determined by Helium Pycnometry (AccuPyc 1330-1000, Micromeritics, GmbH, Aachen, Germany). Two grams of glass powder (< 38 μm) was used and measured with the pressure at 1.6 bar. The density values reported are the mean of ten measurements performed during the experiment.

The experimental molar volume of the glasses is calculated by using the relation [19]:

$$V_m = \frac{M}{D} \quad (1)$$

Where M is the relative molecular mass of glass and D is the experimental density.

2.3 Bioactivity investigation

Glass bioactivity in terms of glass degradation and apatite formation was assessed in Tris buffer solution at pH=7.4 with concentration of tris(hydroxymethyl)aminomethane of about 0.06M. The buffer solution was prepared as described according to Mneimne *et al.* [9]. Glass powder (75 mg) with a particle size smaller than 38 μm was immersed in 50 ml buffer solution for different immersion periods (1, 3, 6, 9 and 24 hours). In order to simulate the human body environment, experiments were performed in a shaking incubator (KS 4000i Control, IKA, Germany) at an agitation rate of 60 rpm at 37°C. The samples were prepared in duplicate.

After the immersion periods, the pH values of the solution were measured immediately using a pH meter (Oakton®, Malaysia). The solution and deposit were separated by filtering using papers with a pore size of 5–13 μm.

An inductively coupled plasma-optical emission spectrometer (ICP-OES; Varian Vista-PRO, UK) was employed to determine the changes in concentration of calcium, silicon and phosphate in the filtered buffer solution after different immersion times. The diluted multi-element stock solutions were used to calibrate the machine.

2.4 Characterisation of apatite formation

Multi-techniques involving X-ray Diffraction (XRD), Fourier Transform Infrared Spectroscopy (FTIR) and Magic Angle Spinning-Nuclear Magnetic Resonance (MAS-NMR) were employed to characterise the precipitates.

The initial glass powder and the collected precipitates were analysed using an X'Pert Pro X-ray diffractometer (PANalytical, The Netherlands) with a copper (Ni-filtered Cu-Kα) X-ray source. The data were recorded from 5 to 70°2θ at a step size of 0.0334° and a step time of 200.03 s. XRD data were analysed using X'Pert HighScore Plus (v2.0, PANalytical, The Netherlands) in conjunction with the ICDD powder diffraction database.

The glass powders and the collected samples were also characterised using Fourier Transform Infrared Spectroscopy (Spectrum GX, Perkin-Elmer, USA) to study the chemical bonding in the materials. The data were presented from 500 to 1600 cm^{-1} wavenumbers.

In order to understand the evolution of glass after immersion, ^{31}P MAS-NMR was run using a 600 MHz (14.1T) Bruker NMR spectrometer (AV 600 NMR, UK). The spectra were acquired at the resonance frequencies of 242.9 MHz and spinning rate of 10 kHz in a 4 mm rotor. The experiments were set up using 30 s recycling delay and scan

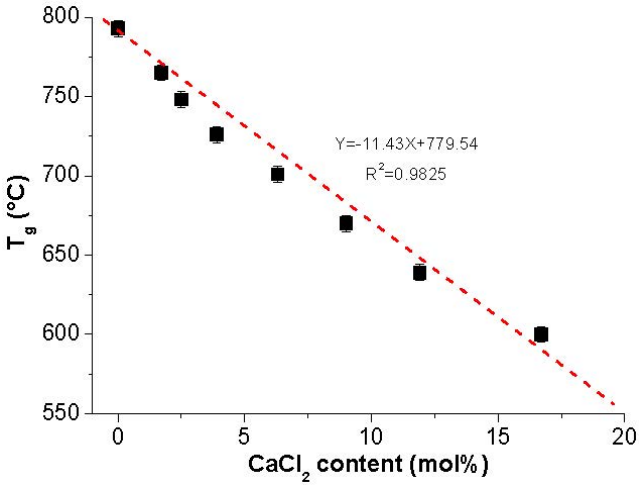

Figure 2: Glass transition temperature (T_g) of fine powder (< 38 µm) plotted against the actual $CaCl_2$ content.

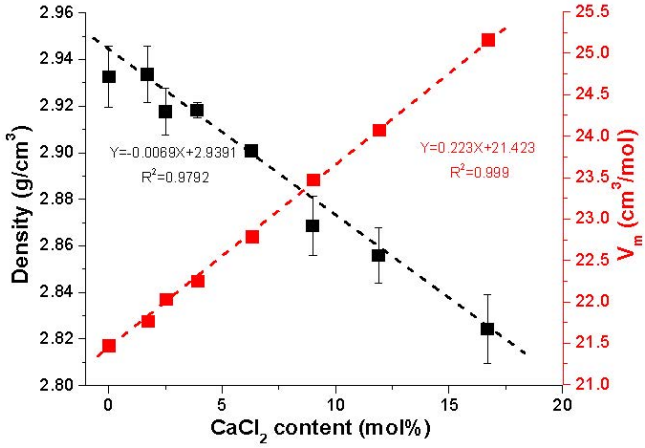

Figure 3: Glass density (T_g (■)) and molar volume of glasses (V_m (■)) profiled as a function of the actual $CaCl_2$ content.

number of 16 or 32. The chemical shift was referenced to the signal of 85% H_3PO_4 at 0 ppm.

3 Results

All the glass frits produced were optically clear. The higher chloride content glasses exhibited a small amount of crystallinity by XRD which is thought to be a result of the fine glass powder surface reacting with atmospheric water to form a mixed hydroxychloroapatite during the collection of the XRD data, since no evidence of crystallinity was found by either ^{31}P MAS-NMR or FTIR [18].

In Figure 1, the percentages of the retained chloride in the initial glasses after volatilization are plotted against the as-designed chloride content. A large fraction 73–87% of chloride has been successfully incorporated into the glasses.

In Figure 2, the glass transition temperature (T_g) of fine powder (< 38 µm) is plotted against $CaCl_2$ content; the data were first presented in [18]. It is clear that T_g values decrease dramatically and linearly (R^2 = 0.9825) with increasing $CaCl_2$ content.

Glass density and molar volume of glasses are also plotted as a function of the actual $CaCl_2$ content (Figure 3). The changes in glass density caused by increasing the $CaCl_2$ content are similar to the change of T_g as a result of increasing $CaCl_2$ content. A continuous reduction of glass density is observed with an increase in $CaCl_2$ content. While the molar volume of glasses increases linearly (R^2 = 0.999) with increasing $CaCl_2$.

Figure 4a shows the pH values measured after 3 and 24 hours immersion in Tris buffer solution for each glass. Interestingly, the glass with a higher $CaCl_2$ content has a higher pH value after 3 hours, while a relatively lower pH value after 24 hours, compared to the compositions with lower $CaCl_2$ content. Overall, a reduction of pH from 3 hours to 24 hours was found; the change was more significant at high $CaCl_2$ content in the glass.

The concentration of calcium in solution measured after 6 hours of immersion plotted as percentage of the total amount in the as-designed composition is presented in Figure 4b. There is a clear increase in the percentage of Ca concentration with an increase in $CaCl_2$ content. For example on increasing the $CaCl_2$ content from 0 to 16.7 mol% the percentage of Ca found in solution increases from 58.6% to 83.2%. The trend is practically linear.

The evolution of phosphate concentration measured in solution with increasing immersion time is shown in Figure 4c. In general, all the $CaCl_2$ containing glasses show similar trend of phosphate concentration with respect to time. The phosphate concentration increases in the first 3 hours and drops down afterwards.

The silicon concentration (mg/l) measured in solution is plotted as a function of immersion time in Figure 4d. It is seen that Si concentration increases up to 60–70 mg/l in the first 6 hours, with no significant change observed after longer immersion period. No substantial difference in measured silicon concentration between different glass compositions is observed.

The XRD patterns of each chloride containing bioactive glass on immersion up to 24 hours in Tris buffer are similar. The one for 1.7 mol% $CaCl_2$ containing glass (GPCl 2.3) is selected and presented as an example in Figure 5a. A broad amorphous halo centred at 30°2θ belongs to the untreated glass (0 h). After immersion for 3 hours, the halo broadens out and the peaks at 25.9°(002) and 32°(211) 2θ,

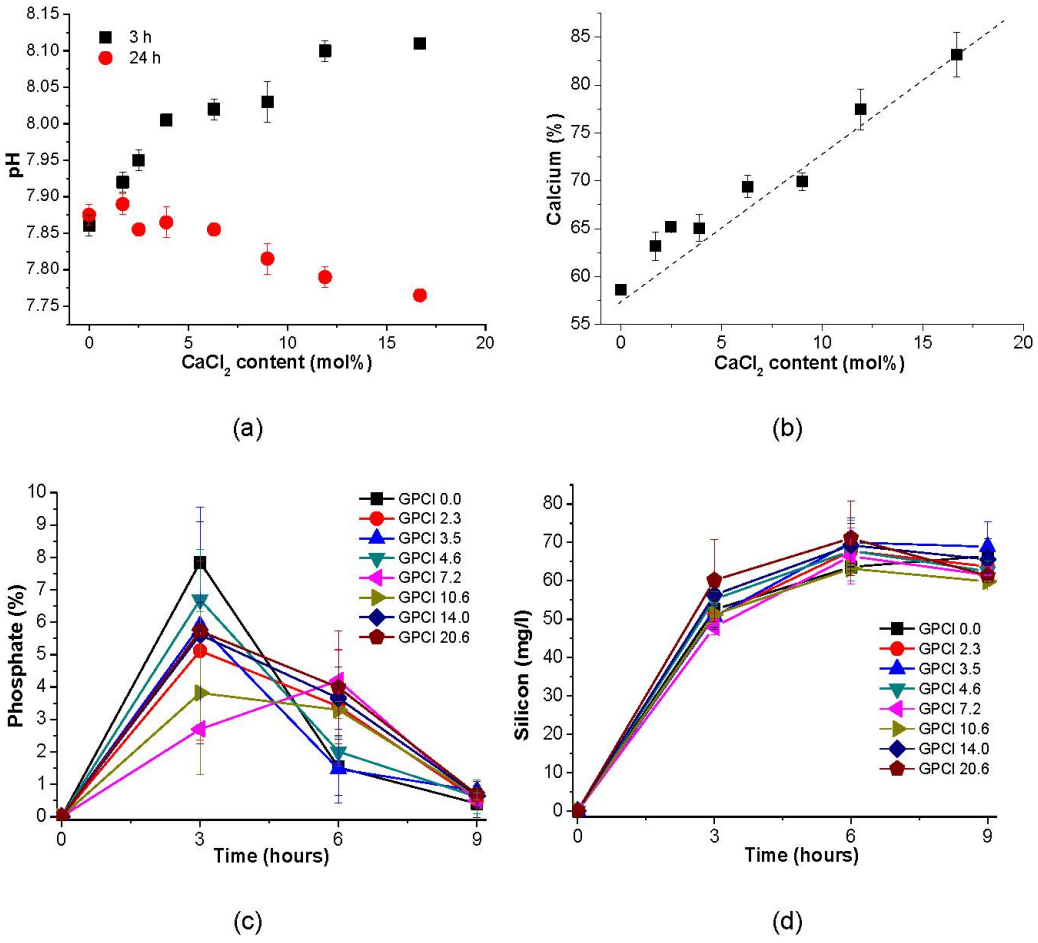

Figure 4: (a) pH value of solution after 3 and 24 hours immersion in Tris; (b) the Ca concentration measured after 6 hours immersion in Tris buffer solution plotted as the percentage of the total calcium content in the as-designed glass composition against the actual $CaCl_2$ content; (c) the concentration of phosphate measured after immersion in Tris buffer presented as the percentage of the total phosphorus content in the as-designed glass composition plotted as a function of immersion time; (d) the concentration in mg/l of silicon measured in Tris buffer plotted as a function of immersion time.

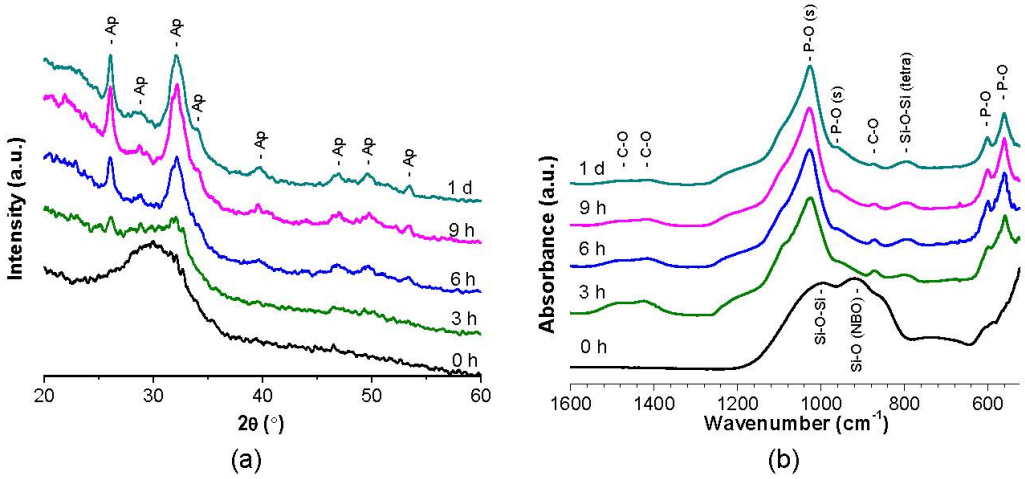

Figure 5: (a) The XRD patterns and (b) FTIR spectra of the 1.7 mol% $CaCl_2$ glass precipitate collected after the immersion in Tris up to 1 day. The numbers are immersion times.

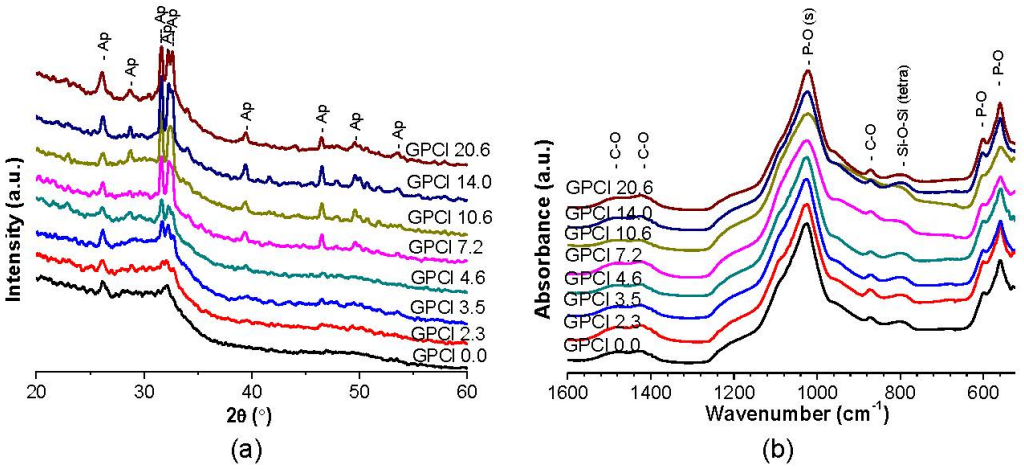

Figure 6: (a) The XRD patterns and (b) FTIR spectra of the glass precipitates collected after 3 hours immersion in Tris buffer solution.

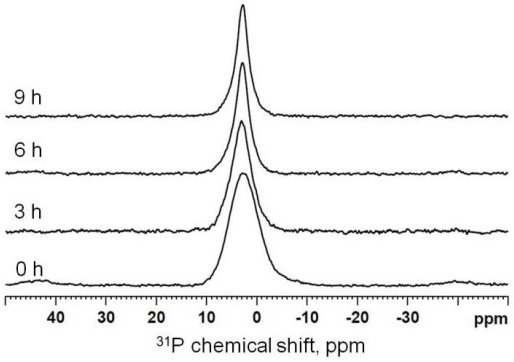

Figure 7: The ^{31}P MAS-NMR spectra of the glass precipitate with 1.7 mol% $CaCl_2$ collected after the immersion in Tris up to 9 hours. The numbers are immersion times.

which match the typical apatite diffraction lines, develop. The intensities of the peaks increase with immersion time up to 9 hours. Longer immersion times do not show any further change in the patterns. After 24 hours, the peak at 25.9°2θ is slightly narrowed down, suggesting the growth of apatite crystals. Similar results were obtained for the rest $CaCl_2$ containing glasses.

In addition, the XRD patterns of glass precipitates after 3 hours immersion are summarised in Figure 6a. It is clear that the peaks at 25.9°, 32° and 32.6°, corresponding to main diffraction lines of apatite appear after 3 hours immersion. The intensities of the diffraction peaks increased with $CaCl_2$ content of the glass. However, the diffraction lines are relatively broad, rather than sharp, indicating the formed apatite crystals are small.

Figure 5b shows the FTIR spectra of 1.7 mol% $CaCl_2$ containing glass precipitate after immersion up to 9 hours in Tris. The bands at 1028 and 920 cm^{-1}, which correspond to Si-O-Si stretching bands and non-bridging oxygen bands (Si-NBO$^-$) respectively, were seen in the spectrum of the untreated glass at the bottom. After 3 hours immersion the spectra change markedly, including the elimination of band at 920 cm^{-1}, the sharpening of band at 1030 cm^{-1}, the development of split peaks at 560 and 613 cm^{-1} and twin peaks at 1420 and 1450 cm^{-1} [9]. These changes suggest rapid glass degradation and apatite-like phase formation. Similar changes to the spectra were found for the rest of the $CaCl_2$ containing glasses as shown in Figure 6b.

^{31}P MAS-NMR was used to investigate phosphorus environment and identify apatite-like phase formation after immersion. The spectra of glass GPCl 2.3 before and after immersion are shown in Figure 7. In the spectrum of the untreated glass, a single peak at about 3 ppm, corresponding to amorphous calcium orthophosphate is visible. Upon immersion, the peaks narrow down, first after 3 hours and then further after 6 hours of immersion. However, the chemical shift remains constant. Similar changes in the spectra of the rest of the glass compositions were observed.

4 Discussion

The results of the chemical analysis of the chloride content indicate that between 70 and 90% of the chlorine is retained in the glasses after melting. Thus, the majority of the chloride is retained in the silicate glass during melting. In general, the higher amount of $CaCl_2$ losses is found in the lower $CaCl_2$ containing glasses. This can be attributed to a higher melting temperature of 1550°C for synthesis of the lower $CaCl_2$ containing glasses (GPCl 2.3 and GPCl 3.5).

Volatilisation of chloride is probable by two routes; direct volatilisation as $CaCl_2$ and loss as HCl by reaction with water vapour in the furnace atmosphere. If chloride volatilises as HCl, the CaO content in the actual glass composition would increase and the SiO_2 and P_2O_5 contents would decrease. Therefore, the glass network connectivity (NC) would decrease with an increase in $CaCl_2$ content and also the glasses would tend to crystallise. If chloride volatilises as $CaCl_2$, the CaO, P_2O_5 and SiO_2 would increase in proportion and the glass NC would remain constant.

The XRD patterns of the initial glasses suggest a very small fraction of glass crystallisation, which is probably caused by reaction with water on the glass surface during data collection rather than crystallisation on quenching [18]. In addition, the ^{29}Si MAS-NMR spectra (Figure S.1 (Supplemental material)) suggest that the obtained glasses have mainly the Q^2 structure and not a mixture of Q^1 and Q^2. Thereby, the chloride loss is likely to occur as $CaCl_2$ rather than HCl. The actual glass compositions have been calculated and summarised in Table 1.

It is important to note here that most chlorides with the notable exception of $CaCl_2$ have low boiling points and this has generally resulted in either no chloride remaining in the silicate glass or very little. Consequently chloride containing glasses have rarely been studied and those that have $CaCl_2$ content typically less than 2 mol%. This contrasts with the glasses here the highest of which contains 16.7 mol% $CaCl_2$.

This work reveals that the incorporation of $CaCl_2$ results in a very marked reduction in the glass transition temperature and density. It is proposed that in this $CaCl_2$ containing glass system, the Cl-Ca(n) species form in an analogous fashion to the F-Ca(n) species in the CaF_2 containing glasses [18, 20, 21]. The formation of Cl-Ca(n) species has been found in very low $CaCl_2$ (< 2 mol%) containing glasses by Sandland *et al.* [22].

The formation of hypothetical "$CaCl^+$" species, which has same field strength as Na^+ but lower than Ca^{2+}, will weaken the electrostatic force between two NBOs in the glass structure. Therefore, the more $CaCl_2$ is introduced into the glass composition, the weaker electrostatic forces between the two NBOs form and the lower is the glass transition temperature. T_g is a significant parameter, which can be used to indirectly predict glass solubility, degradability and hardness of glasses within certain compositional ranges [23–25]. The hardness measurement of bioactive glasses is challenging, because of their tendency to surface react during sample preparation. However, both T_g and glass hardness are determined by the average bond strength in the glass structure, thus hardness and T_g might be expected to exhibit a strong correlation. Farooq *et al.* found that the hardness of the CaF_2 containing bioactive glasses with different amounts of Na_2O reduces with decreasing T_g [25].

Additionally, the packing density which was used to mirror the compactness of the glass can be also used to predict glass hardness [26]. As shown in Figure 3, the glass density decreases with an increase in $CaCl_2$ content. This is due to the fact that the chloride ion is substantially large. Incorporation of chloride therefore increases the glass molar volume and results in a more open and less compact glass structure. Hence, to some extent the presence of chloride dilutes the glass network and expands the glass volume, which leads to a decrease in density and packing density of the glass. Moreover, the formation of large "$CaCl^+$" species in the glasses results in a weakening of the silicate glass network. The effect shown in this study is comparable with the effect on the replacement of Na_2O for CaO (replaced one Ca^{2+} ion by two Na^+ ions) and K_2O for Na_2O (K^+ is larger than Na^+, ion radius: 1.52 Vs 1.16 Å) in the glass. On incorporation of $CaCl_2$, the glass hardness would be expected to decrease, as a consequence of a reduced compactness of the glass. Therefore, the incorporation of $CaCl_2$ results in a reduction in T_g and probably the glass hardness.

The glasses with lower hardness are attractive for the desensitizing toothpastes for treating dentine hypersensitivity. A contributory cause of dentine hypersensitivity is loss of enamel at the cervical margins due to brushing with an abrasive toothpaste. Bioglass® 45S5 has been used in commercial toothpastes as NovaMin® technology for the remineralisation of teeth and for treating dentine hypersensitivity [27]. The hardness of the 45S5 composition is 4.68 GPa, whilst the enamel hardness is about 3.5 GPa only. In order to avoid enamel wear, a glass with a hardness value less than 3.5 GPa is attractive. Chloride containing bioactive glasses with their low T_g are one potential route to achieve this, since the hardness of a glass is expected to correlate to the glass transition temperature. The lower is the T_g, the softer the glass is likely to be. Thus chloride containing bioactive glasses could potentially reduce the abrasivity and enamel loss caused by tooth brushing. Moreover, rapid glass degradation and fast apatite formation found in this study make these chloride containing bioactive glasses also attractive for use in the remineralls-ing toothpastes.

According to the mechanism of dissolution of bioactive glasses proposed by Hench *et al.* [28, 29], the first step is the ion exchange of alkali ions (glass modifier cations) with protons (H^+) from body fluids. In the studied glasses, Ca^{2+} will be exchanged for protons in the Tris buffer during

glass degradation. The removal of protons from solution causes an accumulation of hydroxyl groups; hence, an increase in both Ca^{2+} release and the pH of the Tris buffer in the early period of glass immersion can be explained.

Previous work on CaF_2-containing bioactive glasses by D.S. Brauer *et al.* [20] showed that this pH rise was less pronounced with increasing CaF_2 content in the glass, and we originally interpreted this as caused by another type of ion exchange occurring: hydroxyls (OH^-) from the solution for F^- from the glass in addition to H^+ for modifier cations. If this was the case, however, we would observe the same effect here, with an exchange of OH^- for Cl^- resulting in a lower pH with increasing $CaCl_2$ content in the glass, but we do, in fact, observe the opposite trend. This suggests that halides, such as CaF_2 or $CaCl_2$, present in and released from bioactive glasses contribute indirectly only to pH changes in the dissolution medium. More detailed study [14] suggests that the pH rise typically observed for bioactive glasses is caused by the silicate part (i.e., by ion exchange between modifiers ionically connected to non-bridging oxygens and H^+) only, with contributions from the CaF_2 part being negligible.

The ion exchange process between modifier cations and protons in the present study is aided by incorporation of large chloride ions, which have the capacity to expand the glass network. This more open and expanded glass structure allows ions to diffuse much more easily into and out of the glass and therefore facilitates ion exchange, particularly for short immersion times. As a consequence there is a more rapid release of Ca^{2+} ions and a more rapid rise in pH in the glasses with higher $CaCl_2$ content during the first few hours of immersion. However after a longer immersion period (24 hours), a less pronounced rise in pH of the glasses with more $CaCl_2$ content was found. This can be attributed to a decrease of glass modifier content (here: CaO only), with an increase in $CaCl_2$ content.

The studied glasses were designed by adding $CaCl_2$ to glass, while reducing the amounts of all other components proportionally so as to keep glass structure constant (Q^2 glass structure). In a fixed weight of glass (75 mg) used for the bioactivity study in Tris buffer, the amount of the silicate part of the glass (i.e. $Si\text{-}O^- \; 1/2Ca^{2+}$ bonds) allowing for exchange of modifier ions decreased with an increase in $CaCl_2$ content in the glass. This could result in a reduction of the total amount of ion exchange occurring, therefore a less pronounced pH rise was observed for glasses with higher $CaCl_2$ contents. Additionally, the consumption of hydroxyl ions during the formation of hydroxycarbonated apatite and probably also the dissolution of atmospheric CO_2 lead to a reduction of pH after 24 hours immersion compared to 3 hours.

Rapid glass degradation and release of Ca^{2+} and PO_4^{3-} ions facilitate apatite-like phase formation. Apatite-like phase formation of these $CaCl_2$ containing bioactive glasses was evaluated in Tris Buffer. Unlike simulated body fluid (SBF) and artificial saliva (AS), Tris buffer contains no Ca^{2+} or PO_4^{3-} ions. The Ca and P detected in solution and any apatite detected therefore originate entirely from the glass composition. This considerably simplifies the analysis and interpretation of the degradation/dissolution of the glass. As discussed above, chloride promotes glass degradation as a result of expanding glass volume and the rapid glass degradation provides ions, such as Ca^{2+}, PO_4^{3-} and OH^- for apatite-like phase formation.

From the ion release data, the highest amount of phosphate was present in solution is around 7.85% after 3 hours immersion, this indicates a consumption of phosphate for apatite-like phase formation at an even earlier immersion time than 3 hours. The tests are done under phosphate deficient condition, as with the glass being only source of Ca^{2+} and PO_4^{3-}. The ratio of Ca:P ratio in glasses are 4.4:1, while the Ca:P ratio in apatite is 1.67:1. Therefore, the amount of apatite-like phase formation depends mainly on the phosphate content and high phosphate contents in bioactive glass are favourable for apatite-like phase formation, as also suggested by the earlier finding in paper by Mneimne *et al.* [9].

Brauer *et al.* [20] suggested that the formation of silica gel contributes to the nucleation of apatite, since phosphate concentration decreased when silicon concentration reached the solubility limit. However, as shown in Figure 3d, the silicon concentration reached the solubility limit (60–70 mg/l) after 6 hours immersion and was almost constant there afterwards, while phosphate decreased after 3 hours. This suggests that apatite-like phases might not be necessarily forming only on the surface of silica gel.

All the XRD, FTIR and NMR results suggest rapid apatite-like phase formation within 3 hours immersion in Tris, which is comparable to the equivalent CaF_2 containing bioactive glasses [30]. From the XRD patterns, the diffraction lines developed after 3 hours immersion matched those for the typical diffraction lines of hydroxyapatite, however, the intensities of the three main peaks between 31° to 33° 2θ are not completely identical with those for hydroxyapatite. This suggests the possibility of the presence of CO_3^{2-} or Cl^- in the apatite lattice.

In the apatite crystal lattice, the hydroxyl ion is too large to fit in the space at the centre of Ca(II) triangle and is displaced above the plane of the triangle. The chloride ion is larger than the hydroxyl ion, it displaces even further above the plane of the Ca(II) triangle. Therefore, chlorap-

atite is less stable than hydroxyapatite and is unlikely to form after immersion of the bioactive glass. Furthermore, chlorapatite is known to convert to hydroxyapatite with time in the presence of water [31].

The constant chemical shift (3 ppm) of the glass powders before and after immersion in Tris in the spectra of ^{31}P MAS-NMR indicates that almost all phosphorus is present as orthophosphate charge balanced by Ca^{2+} cations [20]. In the case of before immersion, the amorphous calcium orthophosphate results in a broad amorphous peak, since there are local variations in the local environment around the phosphorus. In the case of after immersion, the calcium orthophosphate peak gradually becomes sharper as the result of the formation of a crystalline calcium orthophosphate (apatite) and the amorphous calcium phosphate species in the glass dissolving. Thus, a progressive reduction in width of the ^{31}P peak was seen with an increase in immersion time.

It is worth comparing the chloride containing bioactive glasses studied here with the closely related fluoride containing glasses [30], both glass series show rapid apatite-like phase formation within 3 hours immersion in Tris. In the case of CaF_2 series, apart from forming fluorapatite on immersion, an additional phase of CaF_2 was also detected in the high CaF_2 containing glasses (over 9.3 mol%). Furthermore, CaF_2 is present as the main fluoride containing phase in the glass with 25.5 mol% CaF_2. The formation of CaF_2 might reduce the bioactivity in terms of the ability to bond to bone. However, in the case of $CaCl_2$ series, the apatite-like phase is the only phase formed after immersion for all $CaCl_2$ contents. In addition, the increase of $CaCl_2$ content stimulates glass degradation, which therefore facilitates apatite-like phase formation. The high bioactivity of the chloride containing glasses with their rapid dissolution rate are attractive for use in toothpastes and resorbable materials, especially bone grafts and scaffolds.

5 Conclusion

In this paper, the bioactive silicate glasses with chloride have been synthesised and studied for the first time. These novel chloride containing bioactive glasses contain up to 16.7 mol% of the chloride thus it is demonstrated that a significant retention of chloride is possible to achieve in this type of the silicate glass. This study has revealed that the chloride containing bioactive glasses are highly degradable and form an apatite-like phase within 3 hours immersion in Tris buffer. Glass degradation rate has been found to increase with $CaCl_2$ content. A reduction of density and an increasing of glass molar volume on increasing $CaCl_2$ suggest that chloride expands the glass volume and dilutes glass network, therefore, promoting ion exchange and glass degradation. The DSC results demonstrated a distinct reduction in the glass transition temperature (T_g) correlating linearly with an increase in chloride content. The decrease of T_g indicates a potential decrease in the glass hardness. These novel chloride containing bioactive glasses have outstanding potential for applications in remineralising toothpastes and resorbable bone substitutions.

Acknowledgement: Xiaojing Chen was funded by China Scholarship Council (CSC)/Queen Mary University of London Joint PhD scholarships. Dr. Rory Wilson is greatly appreciated for collecting X-ray diffraction data. Dr. Laura Shotbolt is kindly thanked for carrying out inductively coupled plasma-optical emission spectroscopy (ICP-OES) measurements.

Conflicts of Interest: The authors declare no conflict of interest.

References

[1] Hench L.L., Day D.E., Holand W., Rheinberger V.M., Glass and Medicine, Int. J. Appl. Glass Sci. 2010, 1, 104–117
[2] Hench L.L., The story of Bioglass (R), J. Mater. Sci. Mater. Med. 2006, 17, 967–978
[3] Jones J.R., Review of bioactive glass: From Hench to hybrids, Acta Biomater. 2013, 9, 4457–4486
[4] Tai B.J., Bian Z., Jiang H., Greenspan D.C., Zhong J., Clark A.E., et al., Anti-gingivitis effect of a dentifrice containing bioactive glass (NovaMin (R)) particulate, J. Clin. Periodontol. 2006, 33, 86–91
[5] Chen X., Brauer D.S., Karpukhina N., Waite R.D., Barry M., McKay I.J., et al., 'Smart' acid-degradable zinc-releasing silicate glasses, Mater. Lett. 2014, 126, 278–280
[6] Fredholm Y.C., Karpukhina N., Law R.V., Hill R.G., Strontium containing bioactive glasses: Glass structure and physical properties, J. Non-Cryst. Solids. 2010, 356, 2546–2551
[7] Gentleman E., Fredholm Y.C., Jell G., Lotfibakhshaiesh N., O'Donnell M.D., Hill R.G., et al., The effects of strontium-substituted bioactive glasses on osteoblasts and osteoclasts *in vitro*, Biomaterials 2010, 31, 3949–3956
[8] Al-Noaman A., Rawlinson S.C.F., Hill R.G., The role of MgO on thermal properties, structure and bioactivity of bioactive glass coating for dental implants, J. Non-Cryst. Solids. 2012, 358, 3019–3027
[9] Mneimne M., Hill R.G., Bushby A.J., Brauer D.S., High phosphate content significantly increases apatite formation of fluoride-containing bioactive glasses, Acta Biomater. 2011, 7, 1827–1834

[10] Lusvardi G., Malavasi G., Menabue L., Aina V., Morterra C., Fluoride-containing bioactive glasses: Surface reactivity in simulated body fluids solutions, Acta Biomater. 2009, 5, 3548–3562
[11] Montazeri N., Jahandideh R., Biazar E., Synthesis of fluorapatite-hydroxyapatite nanoparticles and toxicity investigations, Int. J. Nanomedicine 2011, 6, 197–201
[12] Wang C.J., Zhang Y.F., Wei J., Wei S.C., Effects of Different pH Conditions on Enamel Erosion Repair by Nano Fluorapatite Pastes, J. Nanosci. Nanotechnol. 2012, 12, 7346–7353
[13] Featherstone J.D.B., The science and practice of caries prevention, J. Am. Dent. Assoc. 2000, 131, 887–899
[14] Brauer D.S., Mneimne M., Hill R.G., Fluoride-containing bioactive glasses: Fluoride loss during melting and ion release in tris buffer solution, J. Non-Cryst. Solids. 2011, 357, 3328–3333
[15] Chen X., Chen X., Brauer D.S., Wilson R.M., Hill R.G., Karpukhina N., Novel alkali free bioactive fluorapatite glass ceramics, J. Non-Cryst. Solids. 2014, 402, 172–177
[16] Jabbarifar S.E., Salavati S., Akhavan A., Khosravi K., Tavakoli N., Nilchian F., Effect of fluoridated dentifrices on surface microhardness of the enamel of deciduous teeth, Dent. Res. J. (Isfahan) 2011, 8, 113–117
[17] Kiprianov A.A., Karpukhina N.G., Oxyhalide silicate glasses, Glass Phys. Chem 2006, 32, 1–27
[18] Chen X., Hill R., Karpukhina N., Chlorapatite Glass-Ceramics, Int. J. Appl. Glass Sci. 2014, 5, 207–216
[19] Brauer D.S., Al-Noaman A., Hill R.G., Doweidar H., Density-structure correlations in fluoride-containing bioactive glasses, Mater. Chem. Phys. 2011, 130, 121–125
[20] Brauer D.S., Karpukhina N., O'Donnell M.D., Law R.V., Hill R.G., Fluoride-containing bioactive glasses: Effect of glass design and structure on degradation, pH and apatite formation in simulated body fluid, Acta Biomater. 2010, 6, 3275–3282
[21] Hill R.G., Law R.V., O'Donnell M.D., Hawes J., Bubb N.L., Wood D.J., et al., Characterisation of fluorine containing glasses and glass-ceramics by 19F magic angle spinning nuclear magnetic resonance spectroscopy, J. Eur. Ceram. Soc. 2009, 29, 2185–2191
[22] Sandland T.O., Du L.S., Stebbins F., Webster J.D., Structure of Cl-containing silicate and aluminosilicate glasses: A Cl-35 MAS-NMR study, Geochim. Cosmochim. Acta 2004, 68, 5059–5069
[23] Hill R.G., Brauer D.S., Predicting the glass transition temperature of bioactive glasses from their molecular chemical composition, Acta Biomater. 2011, 7, 3601–3605
[24] Chen X., Chen X., Brauer D.S., Wilson R.M., Hill R.G., Karpukhina N., Novel alkali free bioactive fluorapatite glass ceramics, J. Nocryst. Solids 2014, 402, 172–177
[25] Farooq I., Tylkowski M., Muller S., Janicki T., Brauer D.S., Hill R.G., Influence of sodium content on the properties of bioactive glasses for use in air abrasion, Biomed. Mater. 2013, 8,
[26] Smedskjaer M.M., Jensen M., Yue Y., Effect of thermal history and chemical composition on hardness of silicate glasses, J. Non-Cryst. Solids. 2010, 356, 893–897
[27] Ananthakrishna S., Raghu T., Koshy S., Kumar N. Clinical evaluation of the efficacy of bioactive glass and strontium chloride for treatment of dentinal hypersensitivity, J. Interdiscip Dentistry. 2012, 2, 92–97
[28] Hench L.L., Bioceramics, J. Am. Ceram. Soc. 1998, 81, 1705–1728
[29] Hench L.L., Bioceramics - from concept to clinic, J. Am. Ceram. Soc. 1991, 74, 1487–1510
[30] Chen X., Chen X., Brauer D.S., Wilson R.M., Hill R.G., Karpukhina N., Bioactivity of Sodium Free Fluoride Containing Glasses and Glass-Ceramics, Materials 2014, 7, 5470–5487
[31] Elliott J.C., Young R.A., Conversion of Single Crystals of Chlorapatite into Single Crystals of Hydroxyapatite, Nature 1967, 214, 904–906

Supplementary Material

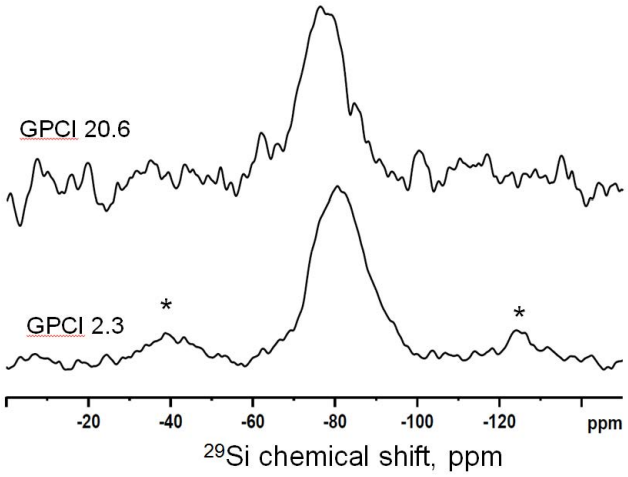

Figure S.1: ^{29}Si MAS-NMR spectra of the as-quenched 1.7 mol% and 16.7 mol% $CaCl_2$ containing glasses.